Scuola Internazionale Superiore di Studi Avanzati - Trieste

Doctoral Thesis

Search for Beyond Standard Model physics at high and low energy colliders

Candidate : Elena Venturini
Advisors : Prof. Aleksandr Azatov
Prof. Andrea Romanino

Opponents : Prof. Michael Spannowsky
Dr. Andrea Tesi

Academic Year 2018 – 2019

SISSA - Via Bonomea 265 - 34136 TRIESTE - ITALY

Abstract

In this thesis, different directions for the search for Beyond Standard Model physics are explored. Possible new physics effects in precision measurements are analyzed in both in the high and low energy regime of collider experiments.

The first part is dedicated to the study of electroweak *anomalous* Triple Gauge Couplings in diboson production at Large Hadron Collider, with an Effective Field Theory approach. In particular, the focus is on the λ_Z and $\tilde{\lambda}_Z$ parameters, associated to the contributions from $\mathcal{O}_{3W}$ and $\mathcal{O}_{3\tilde{W}}$ $d = 6$ operators. These deviations are quite hard to measure due to the suppression of their interference with the Standard Model amplitudes, in the inclusive cross section. Particular differential distributions are proposed, that can improve the sensitivity to the interference terms and the accuracy in the measurements of these interactions.

In the second part there is an analysis of the so-called charged current B *flavor anomalies*, which provide hints of Lepton Flavor Universality violation in semileptonic B meson decays. Data from Belle, BaBar and LHCb are considered. The study is performed making use of the Effective Field Theory language, at first in a model independent way and subsequently in a framework of Composite Higgs models, with Partial Compositeness as a mechanism to generate fermion masses.

Contents

Chapter 1

Introduction

The Standard Model (SM) of particle physics provides a very successful description of most of the observed phenomena, sanctioned eventually by the discovery of the Higgs boson. However there are some experimental hints and some theoretical issues suggesting that the SM is not a complete theory, but only the low energy limit of some larger scenario with new physics (NP) above a certain scale.

Indeed, within SM there are not explanations for neutrino masses and oscillations, for the existence of dark matter and for the large baryon asymmetry present in the Universe and, furthermore, the description of gravitational interactions, at quantum level, is not included. Then, there are theoretical puzzles related to the motivation for the number of flavor generations and for the pattern of masses and mixings for SM fermions, with a large hierarchy among Yukawa couplings. A deeper theoretical issue is the so-called naturalness (or hierarchy) problem associated to the physical size of the electroweak (EW) scale. In fact, in SM the Higgs scalar mass parameter is responsible for EW spontaneous symmetry breaking and, as any mass of a fundamental scalar field, receives radiative corrections that quadratically depend on any heavy scale of the theory. Therefore, in absence of NP, the natural value of the physical Higgs mass would be pushed up to the huge Planck scale, unless a large fine tuning in the EW sector is accepted. For this reason, some new physics explaining the stability of a low Higgs mass was expected, with a relatively low energy scale. This paradigm has motivated in the last decades a huge experimental effort for the direct search for Beyond Standard Model (BSM) effects at and slightly beyond the EW scale. Other fine tuning issues are the so-called strong CP problem, which is to say the non observation of charge-parity (CP) violation effects in strong interactions, and the cosmological constant problem, related to the smallness of the observed vacuum energy density compared to the value predicted once SM is coupled to gravity (in the latter case a complete understanding of gravity and of its QFT description would be necessary).

All these puzzles of the present Standard Model description motivate the experimental search for new physics. A NP discovery could come from direct searches of new degrees of freedom or might arise indirectly, through observed deviations from SM predictions in precision tests; in this thesis, an analysis that follows this second direction is displayed. Direct searches of NP are in general more model dependent and, despite the huge effort that has been done, so

far all such investigations have led to null results and many of the most commonly considered BSM models have been ruled out in large regions of their parameter spaces.

In view of this, one possible strategy is to analyze experimental data in a more model independent way, trying to understand the real pressure that they impose on any UV completion of SM. This means to perform a general study of precision measurements, looking for deviations from SM, and to describe any new physics effect making as few assumptions as possible about the specific UV completion. However, even in this kind of tests, so far there are very few hints of departure from Standard Model predictions; one of them is provided by the so-called *B flavor anomalies*, namely some effects of lepton flavor universality (LFU) violation in semileptonic B decays, which will be the main topic of Chapter 4.

Therefore, at the present moment, one of the main goal of particle physics phenomenology is a description as model independent as possible of any Beyond Standard Model effect that might be observed in the interactions among Standard Model fields at the energies accessible by collider experiments. In the case in which the new physics scale is above the energies that are relevant for the analyzed processes, a powerful method to perform this general analysis is provided by the Effective Field Theory approach, that will be explained in details in the following Chapter. This model independent procedure is widely used in this thesis.

However, a completely model independent description is not always the best way to account for precision test data, as will be shown in Chapter 4. In such cases, even without building a complete UV SM-extension, simplified models can be introduced, in which one assumes the presence of specific NP heavy degrees of freedom that mediate the effective interactions among standard fields (see Section 4.6). If it is possible to identify the heavy mediators that successfully explain experimental results, it can be interesting to embed them within consistent renormalizable models that provide UV completion for the SM, as will be done in Section 4.7.

The null result of the new physics searches performed so far encourages us to look for Beyond Standard Model effects in all possible ways. Even focusing on the analysis of precision tests, one could study possible deviations from SM predictions taking into account data from several experiments and various different observables, both in the high and low energy range.

This is indeed what I did during my PhD at SISSA: my work, described in this thesis, was dedicated to two different directions of NP search.

One ([1, 2]) is focused on the analysis of some BSM effects that could be seen at high energies at the Large Hadron Collider (LHC) or in other future collider experiments. In particular, we have studied the sensitivity to the electroweak *anomalous* Triple Gauge Couplings (aTGCs) λ_Z and $\tilde{\lambda}_Z$ in diboson production processes, namely $pp \to WZ$ and $pp \to W\gamma$. This analysis has been performed with an approach as model independent as possible, using Effective Field Theories as described in Chapter 2 and paying special attention to the range of validity of this method.

Then, I also explored ([3]) a different path to look for new physics: the study and interpretation of *B flavor anomalies*, with a particular focus on charged current interactions. This is motivated by the observation of a discrepancy between data and SM predictions, even if the

significance is not large enough to claim a discovery. Here, precision low energy measurements are taken into account: we are dealing with a completely different energy range, with respect to the aTGC analysis, and data from Belle, BaBar and LHCb experiments are used. In this work, we have used the EFT language, but the analysis has not been done only with a model independent approach. In fact, it is one of the cases, as anticipated, in which data, with the observed discrepancy, cannot be consistently explained without any assumption on the UV completion. We have thus considered a specific class of models, characterized by Composite Higgs and Partial Compositeness, as mechanism at the origin of fermion masses, trying to remain as general as possible.

This thesis is organized as follows. In Chapter 2, I present a general description of the Effective Field Theory approach, that has been used in the analyses that will be shown in the following. In Chapter 3 the study of anomalous Triple Gauge Coupling in diboson production at colliders is explained in details. Finally, in Chapter 4, I will describe our study of charged current B meson flavor anomalies.

Chapter 2

Effective Field Theories

Standard Model Effective Field Theory (SMEFT) is a theoretical framework developed in order to provide a rather model independent description of some new physics effects that can arise, because of the presence of non-SM heavy resonances, in interactions of low enough energy. It can be applied within the full energy reach of collider experiments under the hypothesis that the accessible energy spectrum is below the large mass scale, above which the new resonances might be produced on-shell. This assumption is quite well motivated by experimental results, that suggest that new physics, if there is any, should be at a scale with a moderate gap with the electroweak scale. A SMEFT should be compatible with a UV completion of SM, that must be recovered when the masses of new particles are sent to infinity. It is useful in order to probe SM couplings and their possible modifications due to new physics effects and also to study the presence of non standard interactions among SM particles, described by effective vertices having structure different from the Standard Model one.

Let us see now more in details the characteristics of the EFT approach.

An Effective Field Theory (EFT) is a theory that describes the interactions with a certain level of accuracy within a given energy regime, which means that it should be replaced by some more complete theory above a certain UV scale. Every theory, apart from an ultimate one, should be interpreted as an EFT, even the Standard Model itself, as discussed previously. In the effective description of physics below a given scale Λ, only light degrees of freedom, with masses smaller than this UV scale, are relevant and appear in the Lagrangian, since the heavy states with mass $M > \Lambda$ cannot be produced. Therefore, in order to get an EFT starting from a more complete theory, one should integrate out the heavy degrees of freedom. This, in the path integral language, means

$$e^{iS_{IR}(\varphi)} = \int \mathcal{D}\phi \, e^{iS_{UV}(\varphi,\phi)} \tag{2.0.1}$$

where φ and ϕ are the light and heavy degrees of freedom respectively and $S_{IR(UV)}$ stands for the IR (UV) action.
At tree-level, the integration out is equivalent with the substitution of the heavy d.o.f.s ϕ with their equations of motion $\phi(\varphi)$, as a function of the light fields. With this procedure, one

obtains a Lagrangian that is a function of light d.o.f.s φ only; it is a sum of the pure φ piece of the renormalizable UV Lagrangian and of a series of higher dimension operators involving light fields:

$$\mathcal{L}_{EFT}(\varphi) = \mathcal{L}_{ren}(\varphi) + \sum_{i,d>4} \tilde{c}_i^{(d)} \mathcal{O}_i^{(d)}(\varphi) \tag{2.0.2}$$

where an infinite sum is performed over all possible operators $\mathcal{O}_i$ of dimension $d > 4$, for all d. Thus, one ends up with a non renormalizable theory, but, as will be now explained, it is not an issue. This is also related to the fact that these non renormalizable terms are local operators, since only high energy (short range) effects have been integrated out; the low energy behaviors of the UV theory and of the EFT should coincide.

By naive dimensional analysis, the coefficient $\tilde{c}^{(d)}$ of an operator of dimension d is proportional to the $4 - d$ power of a quantity with the dimension of an energy, that is provided by the Λ scale characterizing the EFT:

$$\tilde{c}_i^{(d)} \sim \frac{c_i^{(d)}}{\Lambda^{d-4}} \tag{2.0.3}$$

where $c_i^{(d)}$ is adimensional and is the so-called Wilson Coefficients (WCs).
As a consequence, the EFT Lagrangian turns out to be a series of inverse powers of the UV cutoff; the zero order term is the renormalizable piece and the larger is the dimension d of an operator, the more the corresponding term in $\mathcal{L}_{EFT}$ is suppressed by the large size of Λ. Indeed, since we are dealing with local operators, the Lagrangian has a defined momentum expansion and an amplitude with insertion of an operator $\mathcal{O}_i^{(d)}$ scales as $\sim \left(\frac{E}{\Lambda}\right)^{d-4}$, where E is the (low) characteristic energy of the interaction (unless there is some non trivial suppression). Therefore, since $E \ll \Lambda$, according to the desired accuracy one might safely neglect all the contributions of order larger than a chosen one in $1/\Lambda$. This means that in Eq. (2.0.2) the expansion can be truncated at the level of operators of a given d dimension, obtaining a finite set of non renormalizable terms. Furthermore, in computing correlation functions within the EFT, pieces proportional to E/Λ powers larger than d should be neglected as well, which is to say that only quantum corrections up to a certain loop order are taken into account. Thus, the obtained EFT has only a finite number of divergences that should be regularized and non renormalizabilty is not an issue, as anticipated.

Then, what at the end is actually used to study low energy interactions, while neglecting contributions of order $(E/\Lambda)^{\bar{d}-4}$ and higher, is the following truncated EFT Lagrangian:

$$\mathcal{L}_{EFT}(\varphi) = \mathcal{L}_{ren}(\varphi) + \sum_{i,4<d<\bar{d}} \frac{c_i^{(d)}}{\Lambda^{d-4}} \mathcal{O}_i^{(d)}(\varphi)\,. \tag{2.0.4}$$

Assuming the presence of a specific renormalizable theory above the cutoff, one can express the WCs as a function of the parameters of the UV completion, by comparing the amplitudes obtained in the latter, in the low energy limit, with the ones that one gets in the EFT. This procedure is called *matching*; it should be done separately for each order in E/Λ, which means at a given loop level for certain considered higher dimensional operators. As we will see, this is useful to take advantage of the EFT approach in order to constrain different models.

Furthermore, with some small hypothesis about the kind of UV theory class that leads to the EFT, one can tell something more about the scaling and parametric dependence of the Wilson Coefficients. For example, for an operator $\mathcal{O}_i^{(d)}$, with n_i fields, that arises from a weakly coupled UV completion by a tree-level integration out procedure, following dimensional analysis the coefficient is $\sim \frac{g^{n_i-2}}{\Lambda^{d-4}}$, where g is the coupling of the full theory. If the effective operator comes out at L-loop level there is a further suppressing factor $(g/4\pi)^{2L}$. If the UV completion is strongly coupled and no perturbative expansion is possible, a correct size for the coefficients is obtained substituting g with 4π is the previous expression, namely $\sim \frac{(4\pi)^{n_i-2}}{\Lambda^{d-4}}$ [4]. These observations will be used in Section 3.2.3.

The key, and very much important, point of EFT approach is that the interactions below a certain UV cutoff, including possible effects deriving from the UV d.o.f.s, are described in terms of low energy fields and symmetry only, simply adding, to the renormalizable light field Lagrangian, all the allowed higher dimension operators with $d > 4$, till a certain chosen d value. It is a model independent procedure, that starts in principle without assumptions about the UV completion that originates the non renormalizable terms, even if the study of the validity of the EFT truncation is not completely model independent, as will be discussed.

One can parametrize in this way the observable effects of broad classes of UV theories. Exploiting experimental low energy data, it is possible to set constraints on the Wilson Coefficients and then, matching the EFT parameters with a possible underlying UV completion, bounds on couplings and masses for this full theory can be derived. In this way many different models could be probed using the same effective Lagrangian, which is therefore a very powerful tool. The EFT approach, thus, gives a consistent global picture of the low energy interactions and of all possible deviations from their description through a light d.o.f. renormalizable Lagrangian: this method might provide a guide in constructing UV completions. In the present work, the Effective Field Theory approach is indeed used to take advantage from this model independent feature, in order to embrace in one time a broader range of possible UV completions of the Standard Model.

We have seen that an Effective Field Theory depends on the degrees of freedom and the symmetries that survive in a low energy range, below a certain cutoff. For example, at energies smaller than the scale of electroweak spontaneous symmetry breaking (EW SSB), the only dynamical d.o.f.s are the photon, the gluons and all the SM fermions apart from the top quarks; the residual symmetries are only the electromagnetic $U(1)$ and the color $SU(3)$. It is not a $SU(2)_L \times U(1)_Y$ invariant theory and it is the so-called Weak Effective Theory (WET) that can be useful to describe B-meson interactions at the m_b scale, as will be done in Section 4.1. On the other hand, one can consider the Standard Model itself as an EFT, with an unknown UV completion. Above the scale of EW SSB, the theory is the full SM, with linearly realized $SU(3)_c \times SU(2)_L \times U(1)_Y$, plus a set of gauge invariant higher dimension operators that involve the SM fields. It is the so-called SMEFT, that will be the focus of Chapter 3 and Section 4.5. Any non zero value for some Wilson Coefficients corresponds to the presence of BSM physics. On the contrary, if no new physics effect is observed, data allow us to set upper bounds on the absolute values of the WCs of the SMEFT.

In principle, in a momentum expansion of the SMEFT Lagrangian, the leading contribution

to the non SM piece should come from dimension 5 operators. However, the only $d = 5$ gauge invariant operator is the Weinberg operator $\sim (H\, l_L)(H\, l_L)$, that violate lepton number conservation. Therefore, if one assumes that the lepton number accidental SM symmetry is maintained also in the SMEFT, the first non trivial EFT truncation is possible at the level of dimension 6 operators, for which a complete basis has been identified in [5, 6]. They are indeed the ones that will be studied in this thesis, in two different contexts: diboson production at LHC in Chapter 3 and B flavor anomalies in Chapter 4. Similarly, dimension 7 terms violate barion number conservation and thus, assuming L and B to be symmetries of the SMEFT, the leading effective Lagrangian involves $d = 6$ and $d = 8$ operators

$$\mathcal{L}_{SMEFT} = \mathcal{L}_{SM} + \sum_i \frac{c_i^{(6)}}{\Lambda^2}\mathcal{O}_i^{(6)} + \sum_i \frac{c_i^{(8)}}{\Lambda^4}\mathcal{O}_i^{(8)}\,. \tag{2.0.5}$$

One of the main goals of the current and High-Luminosity program of the LHC (HL-LHC), as well as of future High-Energy options (HE-LHC), is indeed the precise determination of the Wilson Coefficients of this SMEFT Lagrangian.

Above, all the terms that can give contributions to the cross section up to order $(E/\Lambda)^4$ are considered. Indeed, applying naive dimensional analysis, one can expect the following EFT expansion of the cross section, as a power series of E/Λ

$$\sigma \sim \sigma_{SM^2}\left[1 + \frac{E^2}{\Lambda^2}\frac{\sigma_{BSM_6\times SM}}{\sigma_{SM^2}} + \frac{E^4}{\Lambda^4}\frac{\sigma_{BSM_6^2} + \sigma_{BSM_8\times SM}}{\sigma_{SM^2}} + O\left(\frac{E^6}{\Lambda^6}\right)\right], \tag{2.0.6}$$

where σ_{SM^2} is the SM cross section, $\sigma_{BSM_d\times SM}$ is linear in the WC and is the term associated to the interference between SM and a BSM amplitude (where the latter has an insertion of a dimension d operator), $\sigma_{BSM_d^2}$ is the piece corresponding to the square of this BSM amplitude and is quadratic in $c_i^{(d)}$. Here, possible dynamical suppressions of anyone of these terms is neglected, while they will be discussed in Section 3.2 in presence of a specific set of dimension 6 operators.

A crucial point that must be underlined is that, based on dimensional analysis, the BSM contribution to the cross section has a more rapid growth with the relevant interaction energy E, with respect to the SM term. As a consequence, one can take advantage from the large energies explored at colliders in order to select a region of the spectrum in which the effects from higher dimension operators are clearly visible over the standard cross section, while remaining within the range of validity of the EFT: it means to study the energy range $\bar{E} < E < \Lambda$, where $\bar{E}$ stands for the threshold at which we start being sensitive to the BSM pieces of Eq. (2.0.5). In this way, one can apply SMEFT approach simultaneously improving the potential sensitivity to new physics. This will be one of the main topics of Chapter 3.

One can notice that, in the E/Λ expansion, at the same order there are both the contribution from the squared amplitudes with $d = 6$ operators and the interference between SM and amplitudes with $\mathcal{O}_i^{(8)}$ insertion. For this reason, in the case in which $\sigma_{BSM_6\times SM}$ term does not dominate over the $\sigma_{BSM_6^2}$ one, the validity of the EFT truncation at dimension 6 level is a delicate point and it is not completely model independent, as will be discussed in the following.

However, most of the analyses made using EFT approach are performed in presence of $d = 6$ operators only, as in the case of the present work.

2.1 General discussion about the validity of the Effective Field Theory approach

The EFT expansion is valid only below the UV cutoff above which the integrated out heavy degrees of freedom can be on-shell. Sometimes the effective Lagrangian is used to describe processes for which the characteristic energy scale is fixed, such as in the case of B-meson decays and mixings analyzed in Chapter 4. However, EFT approach can be applied also to the study of parton scattering interactions at hadron colliders, for which the center of mass energy is not fixed and even not experimentally measurable, e.g. in the case of diboson production at LHC discussed in Chapter 3. In these cases, one should pay attention and perform an analysis that takes into account only the part of spectrum below the cutoff Λ, in spite of the fact that, as previously underlined, it is interesting to focus on quite large energies, in order to improve the NP sensitivity exploiting the energy growth of BSM amplitudes.

This should be taken in mind in setting the Wilson Coefficients bounds, that are typically computed using the distributions of some kinematical variables related to the energy scale of the process. Usually, the setting of a maximum value for the relevant energy scale, for effective vertices, corresponds also to the imposition of cuts on the kinematical variables that are used to constrain the EFT: the obtained bounds depend on the choices for the cuts on the measurable kinematical scales. Thus, these cuts should be reported in presenting the results, in order to have the possibility to interpret them within a EFT framework, as will be done indeed in Section 3.6 and 3.7. The bounds found with this procedure are milder and more conservative than the ones that could be derived taking into account the full phase space; however only in this way the consistency of the EFT approach might be guaranteed. The issues related to EFT validity, in the case in which the total energy of effective interactions is not measurable, will be further discussed in Section 3.5, for the specific WZ production process.

Another issue about the EFT validity is related to the consistency of the chosen truncation, in the $1/\Lambda$ expansion, that many times is applied at the level of $d = 6$ effective operators. This is in some sense model dependent: it depends on the chosen power counting, which is the set of rules that allow to express the Wilson Coefficients as functions of the couplings and masses of the UV completion (see discussion in Section 3.2.3). Indeed, power counting provides an estimate of the ratio between terms of lower and higher order in the EFT expansion, which is not always given only by naive dimensional analysis and by the scaling with E/Λ. It may happen, indeed, that interactions with stronger couplings appear only at higher levels in the expansion, leading to the domination of $d = 6$ contribution over SM, but also possibly of $d = 8$ over $d = 6$ level. It can also occur that the low energy theory has some accidental symmetry, respected by Standard Model, that is not present in $d = 6$ effective operators but that can appear again at $d = 8$ level. In such cases, the contribution from $d = 6$ level in the SMEFT Lagrangian is suppressed by some small parameter associated to the symmetry breaking and

the $d = 8$ one can become more relevant. Another circumstance in which one should pay attention to the validity of EFT truncation is when the cross section terms associated to $d = 6$ operators vanish or are suppressed without any symmetry reason. In this category we have also the scenarios in which the BSM_6 amplitude does not interfere with SM, due for example to helicity selection rules: it is exactly the case of $2 \to 2$ scattering processes with two final transverse polarized gauge bosons, widely analyzed in Chapter 3.

In all the cases described above, a truncation of the EFT at the level of dimension 6 operators would be misleading, since it would neglect the $d = 8$ contribution that might be comparable or larger than the one from $d = 6$ level. However, to include complete sets of $d = 8$ operators is in general quite complicated; thus, usually SMEFT with only $d = 6$ effective operators is used, but paying attention case by case to possible failure of this truncation and possible relevant contribution to some $d = 8$ terms. This is what will be done also in the following Chapters.

Chapter 3

Anomalous Triple Gauge Couplings in Diboson Production

The analysis of interactions among electroweak gauge bosons offers a way to probe new physics (NP) that manifests as a deviation from the Standard Model (SM) predictions, in processes involving SM external states; thus, the SMEFT approach, described in Chapter 2, is used. They are particularly interesting also because they provide a key to study the interactions of Goldstone bosons, due to their high energy equivalence to longitudinally polarized gauge bosons. Thus they open a possibility to search Beyond Standard Model (BSM) effects related to electroweak symmetry breaking. Here, these gauge vector interactions are analyzed within diboson production processes $pp \to WV$, $V = W, Z, \gamma$. Generically, the leading contribution to BSM amplitudes for these processes has a ratio with the SM amplitude that grows with the center of mass energy of the interaction: the large energies explored at colliders, such as LHC, can be exploited to test the presence of new physics effects in diboson production.

This Chapter will be dedicated to the description of differential distributions and experimental searches that increase the sensitivity to some effective operators involved in WV production, by overcoming the suppression of the naively expected energy growth, which can occur in some cases.

3.1 Anomalous Triple Gauge Couplings (aTGCs)

The present analysis is focused on electroweak anomalous Triple Gauge Couplings (aTGCs), i.e. the deformation from the SM in the interaction between three electroweak vector bosons. In the SM the TGCs are described by $d = 4$ operators whose coefficients are fixed by the gauge symmetry in terms of only 2 independent parameters; they are given by

$$ig\, W^{+\,\mu\nu} W^-_\mu W^3_\nu + ig\, W^{3\,\mu\nu} W^+_\mu W^-_\nu \,, \tag{3.1.1}$$

where $W^3_\nu = c_\theta\, Z_\nu + s_\theta\, A_\nu$ is a linear combination of the Z and photon vector bosons, θ is the Weinberg angle and g is the $SU(2)_L$ coupling. The interaction in Eq. (3.1.1) is written

in the unitary gauge, so that the vector boson fields describe both longitudinal and transverse polarizations. There are only two types of CP-even anomalous triple gauge couplings (aTGCs) that modify the Lagrangian in Eq. (3.1.1), describing the low energy effects of some heavy new physics as described in Chapter 2. The first one consists in a deviation of the coefficients in (3.1.1) away from the SM point of parameter space

$$\mathcal{L}^{1st}_{aTGC} = \left(ig\, c_\theta\, \delta g_{1,Z}\, Z_\nu W^{+\,\mu\nu} W^-_\mu + h.c.\right) + ig\, (c_\theta\, \delta\kappa_Z\, Z^{\mu\nu} + s_\theta\, \delta\kappa_\gamma\, A^{\mu\nu}) W^+_\mu W^-_\nu \,. \tag{3.1.2}$$

Modifications of the coupling $W^{+\,\mu\nu} W^-_\mu A_\mu$ are forbidden by gauge invariance and the relation $\delta\kappa_Z = \delta g_{1,Z} - \tan^2\theta \delta\kappa_\gamma$ is satisfied if only dimension 6 operators are considered in the gauge invariant SMEFT (see Eq. (2.0.5)). The other type of deformations are obtained by adding new operators with extra derivatives to Eq. (3.1.1). This translates into higher powers of momentum in the amplitudes. In an expansion in momentum powers, the leading such deformation is given by the $d = 6$ (CP-even) operators

$$\mathcal{L}^{2nd}_{aTGC} = \frac{ig}{m_W^2} W^{+\,\mu_2}_{\mu_1} W^{-\,\mu_3}_{\mu_2} \left(\, \lambda_Z\, c_\theta\, Z^{\mu_1}_{\mu_3} \,+\, \lambda_\gamma\, s_\theta\, A^{\mu_1}_{\mu_3} \,\right) \,. \tag{3.1.3}$$

If only dimension 6 operators are taken into account in the BSM part of the SMEFT, gauge invariance implies $\lambda_Z = \lambda_\gamma$, which is to say that we have only one aTGC associated to CP-even terms with two extra derivatives with respect to the SM. Thus

$$\mathcal{L}^{2nd}_{aTGC} = \lambda_Z \frac{ig}{m_W^2} W^{+\,\mu_2}_{\mu_1} W^{-\,\mu_3}_{\mu_2} W^{3\,\mu_1}_{\mu_3} \,. \tag{3.1.4}$$

Therefore, we have, at $d = 6$ level, only three independent CP-even aTGCs $\{\delta g_{1,Z}, \delta\kappa_Z, \lambda_Z\}$. The latter have been the object of study for many tests on SM, as in [7, 8, 9] and in the more recent works [10, 11, 12, 13, 14, 15, 16, 17, 18]. The *anomalous* interactions in Eq. (3.1.2) and (3.1.4) were bounded with percent level accuracy at the LEP-2 experiment [19]:

$$\lambda_Z \in [-0.059, 0.017] \,, \quad \delta g_{1,Z} \in [-0.054, 0.021] \,, \quad \delta\kappa_Z \in [-0.074, 0.051] \,, \tag{3.1.5}$$

at 95% confidence level.

For a long period, it was considered that BSM modifications in diboson production could be described through 3 independent CP-even parameters, after imposing LEP-1 bounds, as said in [20, 21]. However, it has recently been shown (see [22]) that LHC can already improve the constraints on the quark couplings to gauge bosons, which means that LEP-1 bounds are no more strong enough to make the deformation of these couplings irrelevant while one is setting bounds on the aTGCs with LHC data. This correlation might lead to a 50% modification on $\delta\kappa_Z$ and $\delta g_{1,Z}$ constraints, while λ_Z bounds is almost independent from the presence of the qqV coupling in the fit. For this reason and for the sake of simplicity, this correlation will be neglected in the present analysis, that will be focused on λ_Z aTGC.

Moving away from the assumption of CP conservation, we can have also the CP-odd partners of the TGC operators described above. In particular, in this work the CP-odd $d = 6$ aTGC operator, related to the one in Eq. (3.1.4), is analyzed

$$\mathcal{L}^{2nd}_{aTGC-odd} = \tilde{\lambda}_Z \frac{ig}{m_W^2} W^{+\,\mu_2}_{\mu_1} W^{-\,\mu_3}_{\mu_2} \tilde{W}^{3\,\mu_1}_{\mu_3} \,. \tag{3.1.6}$$

where $\tilde{W}^{3\mu\nu}$ is the dual of the field strength tensor, namely $\tilde{W}^{3\mu\nu} = \frac{1}{2}\epsilon^{\mu\nu\alpha\beta}W^3_{\alpha\beta}$.

The CP-even aTGC Lagrangian can thus be obtained from only three independent gauge invariant $d = 6$ effective operators. The terms in $\mathcal{L}^{1st}_{aTGC}$, given by dimension 4 operators, can be derived via electroweak spontaneous symmetry breaking (EW SSB) from two independent $SU(2)_L \times U(1)_Y$ invariant $d = 6$ operators built with Higgs doublets and gauge boson fields. For example, we may consider, in SILH basis [23],

$$O_{HB} = ig'(D^\mu H)^\dagger D^\nu H\, B_{\mu\nu}\,,\ O_{HW} = ig(D^\mu H)^\dagger \sigma^a D^\nu H\, W^a_{\mu\nu} \tag{3.1.7}$$

where B_μ and W^a_μ are the $U(1)_Y$ and $SU(2)_L$ gauge bosons respectively. The contribution to the $d = 4$ operator, in broken phase, associated to $\delta g_{1,Z}$ can come only from O_{HW}, in which the field strength tensor $W^a_{\mu\nu}$ has charged components, while the aTGC $\delta\kappa_Z$ in $\mathcal{L}^{1st}_{aTGC}$ arises from both the $d = 6$ operators above. The following map holds

$$\delta g_{1,Z} = \frac{m_Z^2}{\Lambda^2} c_{HW}\ ,\quad \delta\kappa_Z = \frac{m_W^2}{\Lambda^2}\left(c_{HW} - \tan^2\theta\, c_{HB}\right)\ . \tag{3.1.8}$$

where c_{HB} and c_{HW} are the Wilson Coefficients of operators O_{HB} and O_{HW}. Analogously, the CP-odd partners are

$$O_{H\tilde{B}} = ig'(D^\mu H)^\dagger D^\nu H \tilde{B}_{\mu\nu}\,,\ O_{H\tilde{W}} = ig(D^\mu H)^\dagger \sigma^a D^\nu H \tilde{W}^a_{\mu\nu}\,, \tag{3.1.9}$$

$$\text{with}\quad \delta\tilde{g}_{1,Z} = \frac{m_Z^2}{\Lambda^2} c_{H\tilde{W}}\ ,\quad \delta\tilde{\kappa}_Z = \frac{m_W^2}{\Lambda^2}\left(c_{H\tilde{W}} - \tan^2\theta c_{H\tilde{B}}\right)\ . \tag{3.1.10}$$

The operators O_{HW} and O_{BW} contribute also to other effective vertices, involving not only gauge bosons, such as for example Zhh and ZZh couplings. Therefore, the Wilson Coefficients c_{HW} and c_{HB} are constrained also by measurements on Zh production; this has been recently studied in [24].

The dimension 6 CP-even aTGC operator in $\mathcal{L}^{2nd}_{aTGC}$ is obtained directly from a single gauge invariant $d = 6$ operator without passing through EW SSB:

$$O_{3W} = \frac{g}{3!}\epsilon_{abc} W^{a\,\nu}_\mu W^{b\,\rho}_\nu W^{c\,\mu}_\rho\ , \tag{3.1.11}$$

with the following map between the aTGC λ_Z and the Wilson Coefficient c_{3W} of O_{3W}

$$\lambda_Z = \frac{m_W^2}{\Lambda^2} c_{3W}\ . \tag{3.1.12}$$

Analogously, the CP-odd operator in $\mathcal{L}^{2nd}_{aTGC-odd}$ can be derived from

$$O_{3\tilde{W}} = \frac{g}{3!}\epsilon_{abc}\tilde{W}^{a,\mu\nu} W^b_{\nu\lambda} W^{c\lambda}{}_\mu \tag{3.1.13}$$

with the aTGC-WC map

$$\tilde{\lambda}_Z = \frac{m_W^2}{\Lambda^2} c_{3\tilde{W}}\,. \tag{3.1.14}$$

In principle one could use other sets of operators to parametrize deviations in the physics of $q\bar{q} \to WW/WZ$ production; though, as previously said, here the modifications to vector propagators and gauge boson couplings to fermions are neglected. Note that the commonly used SILH basis, apart from the operators of Eq. (3.1.7) and (3.1.11), also includes a further operator contributing to the aTGCs: $O_W = D^\mu W^\nu_\mu H D_\nu H + h.c.$. For the purposes of this work, however, it is enough to use (3.1.7) in order to capture the high energy behavior: the two $d = 6$ operators lead to triple boson interactions with the same helicity structure and the same number of derivatives. The results will be presented in terms of $\{\delta g_{1,Z}, \delta\kappa_Z, \lambda_Z\}$, which can be mapped into any other basis; for example in [10] this study is performed using different bases of dimension 6 operators.

3.2 Energy growth of helicity amplitudes and cross section

Generically, the cross section for any $2 \to 2$ scattering process, in the presence of dimension 6 BSM operators, can be expressed with the following EFT expansion, in a region with low enough energy, (see Chapter 2)

$$\sigma \sim \frac{g^4_{\rm SM}}{E^2}\left[\overbrace{\left(a_0^{\rm SM} + a_1^{\rm SM}\frac{M^2}{E^2} + ...\right)}^{\rm SM^2} + \overbrace{\frac{E^2}{\Lambda^2}\left(a_0^{\rm int} + a_1^{\rm int}\frac{M^2}{E^2} + ...\right)}^{\rm BSM_6\times SM} + \overbrace{\frac{E^4}{\Lambda^4}\left(a_0^{\rm BSM} + a_1^{\rm BSM}\frac{M^2}{E^2} + ...\right)}^{{\rm BSM_6}^{\,2}}\right], \tag{3.2.1}$$

where E is the typical energy of the interaction, M is the mass of the SM particles, where $M < E$, and ellipses stand for the smaller terms in the $\left(\frac{M^2}{E^2}\right)$ expansion. Here, higher order operators, with dimension $\geqslant 8$, have been neglected, as anticipated in Chapter 2. However, the possibility of having relevant contributions from them will be discussed in Section 3.2.2 and 3.2.3. Note that operators of dimension 7 necessarily violate either baryon or lepton number; in this work the scale of such symmetry violation is assumed to be very large and therefore irrelevant for diboson physics at the LHC. The interference terms between the SM and BSM as well as a pure BSM terms are indicated explicitly. In the high energy limit $E \gg M$ the leading contribution comes from the $a_0^{\rm SM,int,BSM}$ terms in the brackets corresponding to the zero mass limit of the SM particles, unless the a_0s are forced to be zero by some cancellation.

Indeed, within Standard Model a 4-point amplitude is dimensionless and thus we naively expect, in absence of specific peculiar cancellations, that it behaves as a constant in the interaction energy scale E. In particular, in the case of diboson production the total amplitude $\mathcal{M}(q\bar{q} \to WV)$ does not depend on the center of mass energy due to a cancellation that occurs between the E^2 terms in the s and t, u channels. Thus, any deviation from the SM values of the coefficients in front of the SM TGC operators $Z_\nu W^{+\,\mu\nu} W^-_\mu$, $Z^{\mu\nu} W^+_\mu W^-_\nu$ and $A^{\mu\nu} W^+_\mu W^-_\nu$, as in $\mathcal{L}^{1st}_{aTGC}$, spoils this cancellation and leads to a quadratic energy dependence of the 4-point amplitude, consistently with the fact that these aTGCs arise from dimension 6 gauge invariant operators.

Then, the aTGC operator in $\mathcal{L}^{2nd}_{aTGC}$ is absent in SM and, as noticed also previously, naturally brings an additional quadratic dependence on the 4-momentum with respect to Standard Model, due to the presence of two extra derivatives.

Thus, eventually we naively expect

$$\mathcal{M}_{\rm SM}\,(q\bar{q}\to WV)\sim E^0 \qquad \mathcal{M}_{\rm BSM}\,(q\bar{q}\to WV)\sim E^2 \tag{3.2.2}$$

where V can be any vector boson (W, Z or γ) and M_{BSM} is the diboson production amplitude in which the vertex among the three gauge bosons is modified adding dimension 6 operators in the SMEFT.

In the following the behavior with energy of this amplitudes will be more deeply discussed, in order to see whether there are deviations from the naive expectations.

3.2.1 Energy behavior of the helicity amplitudes in diboson production

In order to analyze the energy dependence of the terms in the cross section EFT expansion in presence of different aTGCs, it is useful to study the behavior of amplitudes for diboson production with fixed helicities for external states.

Diboson production at the LHC is dominated by the $2\to 2$ process with $q\bar{q}$ initial state. To neatly expose the leading energy growth of this helicity probability amplitudes one can use the Goldstone equivalence theorem, which is to say the parametrization where the transverse gauge bosons are massless and the would-be Goldstone bosons in the Higgs doublet describe the longitudinal components of the $W_\pm/Z$ gauge bosons. The total Standard Model Lagrangian is given by

$$\mathcal{L}_{\rm SM}=(D_\mu H)^\dagger D^\mu H+\mathcal{L}_{\rm gauge}+\mathcal{L}_\psi+V(H)\,, \tag{3.2.3}$$

where the $D_\mu H=(\partial_\mu-ig'YB_\mu-igT^aW^a_\mu)H$, with T the $SU(2)_L$ generators, $Y=1/2$ and $H^T=(\sqrt{2}\,G^+,v+h+iG_0)/\sqrt{2}$. As usual, the pure gauge sector is given by the field strengths $\mathcal{L}_{\rm gauge}=-\frac{1}{4}W^a_{\mu\nu}W^{a\mu\nu}-\frac{1}{4}B_{\mu\nu}B^{\mu\nu}-\frac{1}{4}G_{A\mu\nu}G^{A\mu\nu}$, the piece $\mathcal{L}_\psi$ involves the kinetic terms for the fermions and the Yukawa interactions, and $V(H)=-m^2|H|^2+\lambda|H|^4$. The Goldstone's equivalence theorem

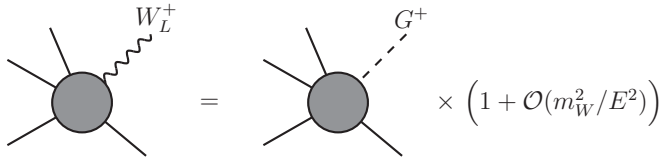

states that to get the leading large energy behavior of the amplitudes with massive gauge bosons in the final state, one can identify in Eq. (3.2.3) the transverse and longitudinal components of the physical gauge bosons as

$$\{W_L^+,\,W_T^+\} \;=\; \{G^+,\,(W^1-iW^2)/\sqrt{2}\}\,, \tag{3.2.4}$$

$$\{Z_L,\,Z_T\} \;=\; \{G_0/\sqrt{2},\,\cos\theta W_3-\sin\theta\,B\}\,, \tag{3.2.5}$$

where $\cos\theta = g/\sqrt{g'^2+g^2}$ is the cosine of the Weinberg angle.

Taking into account these results and parametrization, the SM triple gauge couplings arise from the gauge part of the Lagrangian but also from Higgs interactions, in the following way

$$\mathrm{tr}W_{\mu\nu}W^{\mu\nu} \supset \partial V_T V_T V_T \,, \tag{3.2.6}$$

$$(D_\mu H)^\dagger D^\mu H \supset \partial V_L V_T V_L + v V_T V_T V_L \,, \tag{3.2.7}$$

where SM coupling constants as well as $\mathcal{O}(1)$ numerical factors have been neglected. In Eq. (3.2.6) and (3.2.7) the Lorentz index contractions are understood; by V_L denotes either the W or Z longitudinal vector boson, while V_T could be also a photon. If the limit of massless light quarks is taken into account, so that these only couple to the transverse gauge bosons, the above TGCs lead to s channel amplitudes in which the leading energy dependence in the large energy regime $E \gg m_W$ is

$$\mathcal{M}\left(q\bar{q} \to V_T W_T^\pm\right) \sim E^0 \,, \quad \mathcal{M}\left(q\bar{q} \to V_L W_L^\pm\right) \sim E^0 \,, \quad \mathcal{M}\left(q\bar{q} \to V_T W_L^\pm / V_L W_T^\pm\right) \sim \frac{v}{E} \,, \tag{3.2.8}$$

where E is the center of mass energy of the diboson system. The subleading $\log(E)$ terms from loop corrections are neglected. The process $q\bar{q} \to V_T W_T$ is also mediated by t,u channel diagrams that have the same energy growth as the s channel, shown in Eq. (3.2.8).

The energy growth of tree-level amplitudes involving one insertion of the anomalous TGCs $\{\delta g_{1,Z}, \delta\kappa_Z, \lambda_Z\}$, defined in Eq. (3.1.2) - (3.1.4), depends on the structure of gauge bosons and Higgs doublet interactions within the $d = 6$ EFT operators that lead to these triple gauge couplings. The operators of the considered basis, in Eq. (3.1.7) and (3.1.11), include the following TGCs

$$O_{HB} \supset \partial W_L \partial V_T^0 \partial W_L + v W_T \partial V_T^0 \partial W_L + v^2 W_T \partial V_T^0 W_T + \dots \,, \tag{3.2.9}$$

$$O_{HW} \supset \partial V_L \partial V_T \partial V_L + v V_T \partial V_T \partial V_L + v^2 V_T \partial V_T V_T + \dots \,, \tag{3.2.10}$$

$$O_{3W} \supset \partial V_T \partial V_T \partial V_T + \dots \,, \tag{3.2.11}$$

where V_L and V_T are defined as previously, V_T^0 is an electrically neutral transverse boson (namely Z or γ) coming from $B_{\mu\nu}$ field strength tensor and ellipses denote interactions that are not of the triple gauge type. Note that in (3.2.9)-(3.2.11) we have neglected SM couplings as well as numerical $\mathcal{O}(1)$ factors. At large energies the leading contributions from the interactions in Eq. (3.2.9)-(3.2.11) to diboson production are

$$\mathcal{M}\left(q\bar{q} \to W_L^\mp W_L^\pm\right) \sim E^2/\Lambda^2 \; c_{HB} + E^2/\Lambda^2 \; c_{HW} \sim E^2/m_W^2 \; \delta g_{1,Z} + E^2/m_W^2 \; \delta\kappa_Z \tag{3.2.12}$$

$$\mathcal{M}\left(q\bar{q} \to Z_L W_L^\pm\right) \sim E^2/\Lambda^2 \; c_{HW} = E^2/m_Z^2 \; \delta g_{1,Z} \tag{3.2.13}$$

$$\mathcal{M}\left(q\bar{q} \to V_T W_T^\pm\right) \sim E^2/\Lambda^2 \; c_{3W} = E^2/m_W^2 \; \lambda_Z \tag{3.2.14}$$

where constant factors in front of the TGCs have been omitted and V_T can be W, Z or γ. As previously seen, the λ_Z/c_{3W} contributes only to processes with pure transverse polarized states. Instead, the other two aTGCs enter in all the three amplitudes, but in the cases not appearing

in (3.2.12)-(3.2.14) their contributions have an energy growth suppressed with respect to the naively expected behavior. In particular the $\delta\kappa_Z$ and $\delta g_{1,Z}$ pieces in the amplitude with two final transverse vectors are constant in the energy E and proportional to v^2/Λ^2, where v is the Higgs VEV. Interestingly, $\delta\kappa_Z/c_{HB}$ contributes at the order of E^2 only to the process in Eq. (3.2.12). The leading contribution of $\delta\kappa_Z$ to $q\bar{q} \to WZ$ appears for the polarizations $\mathcal{M}\left(q\bar{q} \to Z_T W_L^+\right)$ and scales as $\sim vE/\Lambda^2$. This follows from the fact that the expected quadratic dependence on energy in amplitudes with O_{HB} and O_{HW} insertions are obtained in diagrams with transverse polarization only for the intermediate vector (maximum number of derivatives and minimum number of Higgs VEVs in (3.2.9)) and in O_{HB} in such configuration this transverse boson must be a neutral one. Furthermore, one can notice that there aren't E^2/Λ^2 contributions in $\mathcal{M}\left(q\bar{q} \to V_T V_L\right)$ processes with one longitudinal and one transverse boson in the final state: the leading terms in such amplitudes suffer a linear suppression with respect to the naively expected behavior, they are $\sim Ev/\Lambda^2$. As a consequence, the leading contributions of $\delta\kappa_Z$ and $\delta g_{1,Z}$ to $W\gamma$ production grow only linearly in the energy of the diboson system and correspond to the case with longitudinal W; the amplitude with W and photon final state is dominated by the unsuppressed λ_Z term, having $\sim E^2/\Lambda^2$ behavior.

Therefore, one can notice that the $d = 6$ operator O_{3W} gives rise to unsuppressed amplitudes with the naively expected quadratic growth with energy, for any diboson final state. Furthermore, it involves only transverse polarizations and so there is no need of disentangling longitudinal and transverse final states. These are consequences of the fact that O_{3W} leads directly, without EW SSB, to the $d = 6$ TGC operator in $\mathcal{L}^{2nd}_{aTGC}$ that contains two extra derivatives. For these reasons, the aTGC λ_Z is peculiar; this work will be focus mostly on that.

The analysis of the CP-odd aTGCs is analogous and lead to similar results.

In Fig. 3.1, there are the results of a `MadGraph5` simulation of the $pp \to WV$ in presence of different CP-even aTGCs, for fixed $W\gamma$ (lower panel), WW and WZ (upper panel) final states. In the plot the ratio $\sigma_{\mathrm{BSM}_6^2}/\sigma_{\mathrm{SM}}$ is shown, as a function of the invariant mass m_{WV} of the WV final state, where BSM_6^2 is the pure non Standard Model contribution to the cross section within a EFT with dimension 6 operators, as in Eq. (3.2.1), and it is normalized to value 1 of the aTGC. Thus, this ratio has the same energy behavior as the squared amplitude with insertion of either O_{HW}, O_{HB} or O_{3W} operators, since the SM cross section in the high energy limit is dominated by the energy independent contribution and the g^4_{SM}/E^4 factor in (3.2.1) cancels. The results confirm what discussed in this Section. Indeed, all the lines present a quartic energy growth, apart from the cases of WZ production with $\delta\kappa_Z$ insertion and $W\gamma$ production with $\delta\kappa_Z$ or $\delta g_{1,z}$ insertion, in which, as explained above, the leading contributions to the amplitudes are linear in energy and associated to $Z_T W_L$ or γW_L productions.

3.2.2 Energy behavior of the SM-BSM interference term in the cross section for diboson production

The analysis of the energy dependence of diboson production amplitudes in presence of different TGCs is interesting in order to study the behavior of the various terms in the EFT expansion

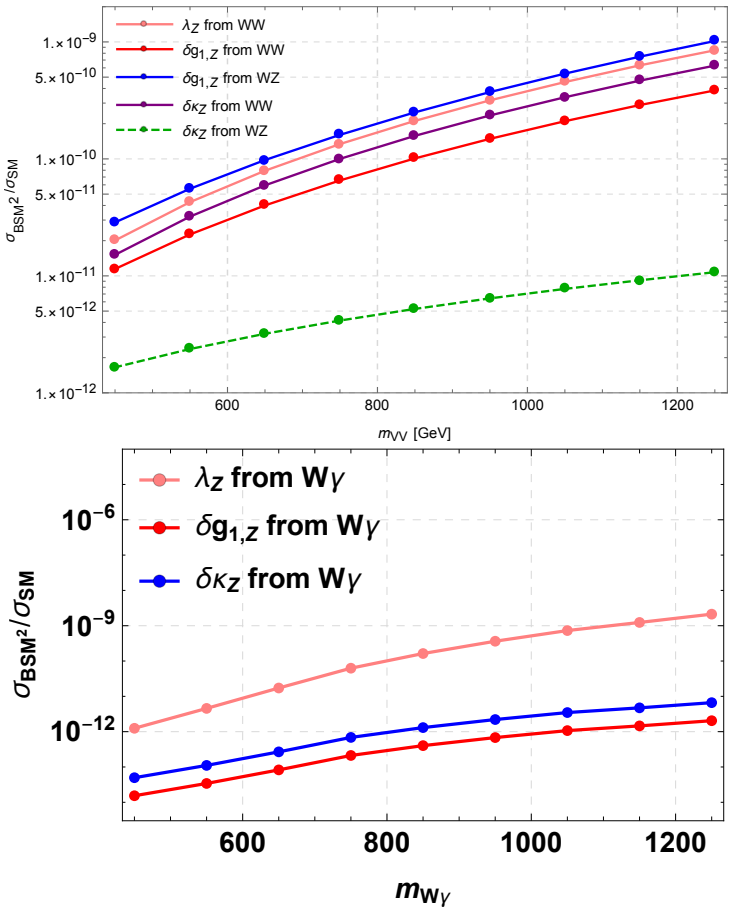

Figure 3.1: Results from a `MadGraph5` simulation of the $pp \to WV$, $V = W, Z$ process (upper panel) and $pp \to W\gamma$ process (lower panel) mediated by anomalous TGCs. The error bars of both plots due to statistical errors is within the width of the plotted lines.

of the cross section for these processes (see (3.2.1)). The discussion of the BSM_6^2 piece has been already done in the previous Section, since it follows straightforwardly from the energy growth of single amplitudes.

For the analysis of the $\mathrm{BSM}_6 \times \mathrm{SM}$ interference terms, one has to pay attention to the fact that interfering diagrams must have same helicity structure for external states. Thus, in presence of O_{HB} and O_{HW} the naively expected quadratic energy growth of the interference might be realized only for processes with pure longitudinal final states (therefore, also, only in cases without final photons), in which it is possible to avoid suppression both of the BSM and SM amplitudes

$$\mathcal{M}^{\mathrm{BSM}}\left(q\bar{q} \to W_L^{\mp} W_L^{\pm}\right)^* \mathcal{M}^{\mathrm{SM}}\left(q\bar{q} \to W_L^{\mp} W_L^{\pm}\right) + c.c. \sim E^2/\Lambda^2 \; c_{HB} + E^2/\Lambda^2 \; c_{HW} \tag{3.2.15}$$

$$\sim E^2/m_W^2 \; \delta g_{1,Z} + E^2/m_W^2 \; \delta\kappa_Z \tag{3.2.16}$$

$$\mathcal{M}^{\mathrm{BSM}}\left(q\bar{q} \to Z_L W_L^{\pm}\right)^* \mathcal{M}^{\mathrm{SM}}\left(q\bar{q} \to Z_L W_L^{\pm}\right) + c.c. \sim E^2/\Lambda^2 \; c_{HW} = E^2/m_Z^2 \; \delta g_{1,Z} \tag{3.2.17}$$

For all the other final states $V_T W_L$, $Z_L W_T$ and $V_T V_T$, involving one or more transverse W, Z or γ, the BSM$_6$ $\times$ SM interference has not any energy growth, it behaves like a constant, in presence of these two $d = 6$ effective operators. Indeed, for $V_T V_L$ final states both the BSM and the SM amplitudes suffer a linear suppression of the naively expected energy growth, while for pure transverse diboson production the diagrams with $\delta\kappa_Z$ and $\delta g_{1,Z}$ insertions undergo a quadratic suppression. This also means that for all the processes with photon production the interference has a flat energy behavior.

The analysis of λ_Z aTGC is less naive. Indeed the leading contribution to amplitudes in the high energy limit comes from pure transverse final state, but the helicity of a $V_T V_T$ state is not fixed. We can have the different configurations

$$V_T^{\pm} V_T^{\mp}\,, \qquad V_T^{\pm} V_T^{\pm} \tag{3.2.18}$$

In principle, both in SM and with insertion of O_{3W} the production of two transverse polarized gauge bosons does not suffer any suppression in the naively expected energy growth, reason for which this kind of aTGC is very interesting.

However, the operator O_{3W} (i.e. the λ_Z deformation) is special because the interference between the amplitude $\mathcal{M}\left(q\bar{q} \to V_T W_T^{\pm}\right) \sim E^0$ in Eq. (3.2.8) and $\mathcal{M}\left(q\bar{q} \to V_T W_T^{\pm}\right) \sim c_{3W} E^2$ in (3.2.14) is suppressed and the scaling of the BSM$_6$ $\times$ SM piece is softer. This is a consequence of the helicity selection rules shown in [25] and discussed in the following (see [26] for a pioneering discussion of this effect in the context of QCD).

The non-interference of the diboson production amplitude through O_{3W} and the SM can be understood by first taking the limit where the masses of the electroweak gauge bosons are zero and we have transverse polarizations only; this makes sense since we are focused on the high energy regime. In this limit the tree-level SM process $q\bar{q} \to VV$ is only non zero if the transverse helicities of the vector bosons are opposite $(\pm, \mp)$. This follows from the Maximally Helicity Violation (MHV) helicity selection rules, see for instance [27]. At the same time though, the operator O_{3W} in (3.1.7) leads to a triple gauge vertex where all three gauge bosons have the same helicity. A quick way to check this is to write the field strength in terms of spinor indices $W_{\mu\nu}\sigma^{\mu}_{\alpha\dot{\alpha}}\sigma^{\nu}_{\beta\dot{\beta}} = w_{\alpha\beta}\bar{\epsilon}_{\dot{\alpha}\dot{\beta}} + \bar{w}_{\dot{\alpha}\dot{\beta}}\epsilon_{\alpha\beta}$, where as usual the tensors ϵ and $\bar{\epsilon}$ are used to raise α and $\dot{\alpha}$ indices, respectively. Then, O_{3W}, once written in terms of the w and $\bar{w}$ fields, is given by

$$O_{3W} \propto w_{\alpha}{}^{\beta} w_{\beta}{}^{\gamma} w_{\gamma}{}^{\alpha} + \bar{w}_{\dot{\alpha}}{}^{\dot{\beta}} \bar{w}_{\dot{\beta}}{}^{\dot{\gamma}} \bar{w}_{\dot{\gamma}}{}^{\dot{\alpha}}\,. \tag{3.2.19}$$

Each antisymmetric tensor field $w/\bar{w}$ can create a massless particle of spin $+1/-1$, respectively, and therefore diboson production through the operator above leads to vector bosons with helicity $(\pm, \pm)$. Thus, at tree level we have that

$$q\bar{q} \;\longrightarrow\; V_{T_\pm} V_{T_\mp} \quad \text{(in the SM)}\,, \tag{3.2.20}$$

$$q\bar{q} \;\longrightarrow\; V_{T_\pm} V_{T_\pm} \quad \text{(with } O_{3W} \text{ insertion)}\,. \tag{3.2.21}$$

Since the final diboson states in (3.2.20) and (3.2.21) are different, there is no interference between those amplitudes. This statement is exactly true in the massless limit. However, two mass insertions $m_W \partial_\mu G^+ W^{-\mu}$ and $m_Z \partial_\mu G^0 Z^\mu$ can be used to flip the helicity of the final states,

leading to a non zero interference between the processes in (3.2.20) and (3.2.21). Flipping the helicity costs a factor m_W^2/E^2. Then, the leading cross section for diboson production in the limit $E \gg m_W$ is given by

$$\sigma(q\bar{q} \to V_T V_T) \sim \frac{g_{\rm SM}^4}{E^2}\left[1 + c_{3W}\frac{m_V^2}{\Lambda^2} + c_{3W}^2\frac{E^4}{\Lambda^4}\right]. \tag{3.2.22}$$

The important point to notice is that the second term of the expression above has a suppressed energy scaling with respect to the general expectation shown in Eq. (3.2.1).

Concerning the CP-odd aTGCs, the inclusive interference between a CP-odd BSM amplitude and the CP-even SM one should go to zero; thus, in this case, interference is strongly suppressed for all the couplings and final states.

In Fig. 3.2, there are the results of a `MadGraph5` simulation of the $pp \to WV$ in presence of different CP-even aTGCs, for fixed $W\gamma$ (lower panel), WW and WZ (upper panel) final states. In the plot the ratio $\sigma_{\rm int}/\sigma_{\rm SM}$ is shown, where $\sigma_{\rm int}$ is the $\text{BSM}_6 \times \text{SM}$ term of the cross section within a EFT with dimension 6 operators, as in (3.2.1), and it is normalized to value 1 of the aTGC. This quantity is expressed as a function of the invariant mass m_{WV} of the WV final state system. Similarly to the case of Fig. 3.1, this ratio has the same energy behavior as the interference term of the cross section itself, which is described in Eq. (3.2.16) and (3.2.17). The results confirm what discussed in this Section. Indeed, the $\delta\kappa_Z$ contribution to interference term in WW production is growing quadratically with m_{WW}, as well as the $\text{BSM}_6 \times \text{SM}$ pieces proportional to $\delta g_{1,Z}$ with generic WV final state. The dashed green line shows no growth as a function of the energy, this confirms the discussion after (3.2.17). Namely, for the final state WZ, the leading energy growth is mediated by $\delta g_{1,Z}$ (blue line) but not by $\delta\kappa_Z$. Furthermore, on the same upper plot we show that $\sigma_{\rm int}/\sigma_{\rm SM}$ mediated by λ_Z has no energy growth, confirming Eq. (3.2.22). This later measurement comes from WW production, but a similar result for λ_Z is obtained for WZ final state. The lower panel of the Figure shows how the interference is always suppressed in processes of $W\gamma$ production, for all the three aTGC contributions, confirming what has been previously discussed.

This behavior makes EFT consistent measurements of the c_{3W} difficult. Indeed, at the level of the dimension 6 operators the signal from the O_{3W} will be subdominant compared to the contributions of the other TGCs, which will require further disentanglement of the transverse and longitudinal final state polarizations. But even more, assuming an ideal separation of the longitudinal polarizations we need to remain in the EFT validity range, namely in the parameter space where the contributions from the dimension 8 operators can be safely ignored. We are in one the circumstances, discussed in Section 2.1, when the $d = 6$ truncation can fail, due to a cancellation that is not related to symmetry reasons. For the process $q\bar{q} \to V_T V_T$ the dimension 8 contribution to the cross section can be schematically written as

$$\Delta\sigma_{\rm dim=8}(q\bar{q} \to V_T V_T) \sim \frac{g_{\rm SM}^4}{E^2}\left[\overbrace{c_8\frac{E^4}{\Lambda^4}}^{\text{BSM}_8\times\text{SM}} + \overbrace{c_8^2\frac{E^8}{\Lambda^8}}^{\text{BSM}_8{}^2} + \dots\right]. \tag{3.2.23}$$

Note that the $\text{BSM}_8 \times \text{SM}$ piece scales as the BSM_6^2 contribution, i.e. as E^4/Λ^4, under the assumption that there is an interference between the SM and the new physics contributions at

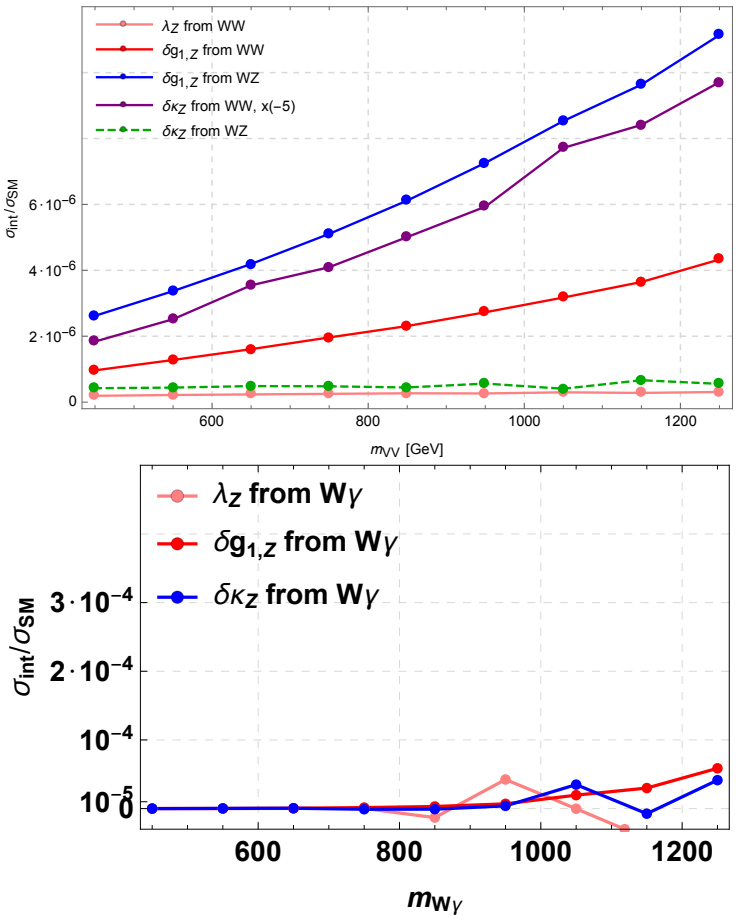

Figure 3.2: Results from a `MadGraph5` simulation of the $pp \to WV$, $V = W, Z$ process (upper panel) and $pp \to W\gamma$ process (lower panel) mediated by anomalous TGCs.

the level of the dimension 8 operators. For the process $q\bar{q} \to V_T V_T$ this is indeed the case; in fact one can consider for instance

$$gD^\nu W^{\sigma\tau} W_{\nu\tau} D^\mu W_{\mu\sigma} \sim D^{\dot{\alpha}\alpha} \omega_{\alpha\beta} \bar{\omega}_{\dot{\alpha}\dot{\gamma}} D^{\dot{\gamma}\sigma} \omega_\sigma^\beta - D^\alpha_{\dot{\gamma}} \bar{\omega}^{\dot{\beta}\dot{\gamma}} \omega_{\alpha\gamma} D^\sigma_{\dot{\beta}} \omega_\sigma^\gamma + D^\alpha_{\dot{\gamma}} \omega^{\beta\gamma} \omega_{\alpha\gamma} D^{\dot{\sigma}}_\beta \bar{\omega}^{\dot{\gamma}}_{\dot{\sigma}} + \dots \,, \quad (3.2.24)$$

where ellipses denote terms with helicity configurations other than $\sim \omega\omega\bar{\omega}$. There is also the operator (written again in terms of spinor indices)

$$g^2 \, (\bar{q}\gamma^\rho q) W_{\rho\nu} D^\mu W_\mu^\nu \sim q^\alpha \bar{q}_{\dot{\beta}} w_\alpha^{\ \beta} D_\beta^{\ \dot{\alpha}} \bar{w}_{\dot{\alpha}}^{\ \dot{\beta}} + \dots \,. \quad (3.2.25)$$

The latter operator is a contact interaction contributing to $q\bar{q} \to VZ$ while the one in Eq. (3.2.24) is a modification of the TGCs in the Lagrangian of Eq. (3.1.4). Note that both of them lead to final state bosons of helicities $(\pm, \mp)$, like in the SM.

Then, assuming that contributions of operators of dimension higher than eight are even smaller, the truncation at the dimension 6 level, that leads to a EFT expansion of the cross section as in Eq. (3.2.22), is valid only if

$$\max\left(c_{3W}\frac{m_V^2}{\Lambda^2}, c_{3W}^2\frac{E^4}{\Lambda^4}\right) > \max\left(c_8\frac{E^4}{\Lambda^4}, c_8^2\frac{E^8}{\Lambda^8}\right). \quad (3.2.26)$$

Suppose one can get rid of the interference suppression, then this condition is replaced by

$$\max\left(c_{3W}\frac{E^2}{\Lambda^2}, c_{3W}^2\frac{E^4}{\Lambda^4}\right) > \max\left(c_8\frac{E^4}{\Lambda^4}, c_8^2\frac{E^8}{\Lambda^8}\right), \tag{3.2.27}$$

which is less restrictive if $c_{3W}E^2/\Lambda^2 < 1$ (given that at LHC $E > m_V$).

Another advantage of having a large interference term is that it leads to the better measurement of the sign of the Wilson Coefficient, otherwise very weakly constrained. The importance of the improvement in Eq. (3.2.27) depends on the actual values of the Wilson Coefficients or in other words on some properties of the UV completions of the given EFT. This will be discussed more concretely, with a few examples, in the next Subsection.

3.2.3 Power counting examples

The strength of the Wilson Coefficients can be estimated using a given set of power counting rules characterizing a possible UV completion, as anticipated in Section 2.1. Power counting schemes are useful to incorporate particular biases towards the kind of BSM physics we would like to prove. This is a perfectly legitimate strategy and it is the point of using an Effective Field Theory approach, allowing to parametrize altogether broad classes of models. Particular examples are weakly coupled renormalizable UV completions, Minimal Flavor Violation (MHV) [28], the Strongly Interacting Light Higgs (SILH) [23], flavor universal BSM physics (see e.g. [29]), etc. The power counting schemes commonly used are imposed through arguments based on the symmetries or dynamics of the Action, such that possible radiative corrections violating the assumed power counting scheme are kept small or understood.

For example, we may assume that the UV completion is a renormalizable and weakly coupled QFT. Then, the power counting consists in classifying those operators that are loop generated v.s. those that are generated at tree-level, as explained in [30, 20]. The latter are expected to be bigger because the former are suppressed by $1/(16\pi^2)$ factors. Then, for example, considering models with heavy vector-like fermions, one expects

$$c_{3W} \sim \mathcal{O}(1) \times g^2/(4\pi)^2\,, \quad c_{(3.2.24)} \sim \mathcal{O}(1) \times g^2/(4\pi)^2\,, \tag{3.2.28}$$

where $c_{(3.2.24)}$ refers to the Wilson Coefficient of the dimension 8 operator in Eq. (3.2.24); the contribution to $c_{(3.2.25)}$ has a stronger loop suppression and thus is here neglected. This setup is somewhat pessimistic since the extra loop suppression makes it hard to prove c_{3W} with the LHC sensitivity. In any case, in this scenario the validity of EFT with truncation at $d = 6$ level receives an improvement if there is the possibility to overcome the suppression of $O_{3W} \times$ SM interference, since the latter is dominant over the term quadratic in the WCs:

$$E^2 < \Lambda m_W \;\longrightarrow\; E < \Lambda\,. \tag{3.2.29}$$

As another power counting instance, one may envision a scheme where, for each extra field strength added to the dimension 4 SM Lagrangian, we pay a factor $g_* \lesssim 4\pi$. With this power counting one obtains

$$c_{3W} \sim g_*/g\,, \quad c_{(3.2.24)} \sim g_*/g\,, \quad c_{(3.2.25)} \sim g_* g/(16\pi^2)\,, \tag{3.2.30}$$

where the $1/g$ factor is due to the normalization of O_{3W} in Eq, (3.1.7). This power counting, called *pure Remedios*, was introduced in [31]. The construction is based on the fact that the SM effective Lagrangian $\mathcal{L}_{EFT} = \mathcal{L}_{\text{Higgs}} + \mathcal{L}_{\psi} + \frac{\Lambda^4}{g_*^2} L(\hat{F}_{\mu\nu}/\Lambda^2, \partial_\mu/\Lambda)$, where the gauge field strengths $\hat{F}_{\mu\nu}$ are not canonically normalized, is seen as a functional that is expanded in inverse powers of Λ. Then, it is technically natural to set $g_* \gg g$ in $\mathcal{L}_{EFT}$ because as $g \to 0$ the $SU(2)_L$ gauge symmetry acting on $\mathcal{L}_{\text{EFT}}$ is deformed into $SU(2)_L^{\text{global}} \rtimes U(1)^3_{\text{gauge}}$ (see [31] for details). This power counting is more optimistic regarding possible LHC signals, since g_* can be naturally large. However, in this scenario there is no improvement from Eq. (3.2.26) to Eq. (3.2.27), and in both cases the energy range in which the $d = 6$ truncation is valid is the full EFT spectrum:

$$E < \Lambda\,. \tag{3.2.31}$$

Lastly, the one scale one coupling power counting (see [23]) predicts

$$c_{3W} \sim c_{(3.2.24)} \lesssim \frac{g_*}{g}, \quad c_{(3.2.25)} \lesssim \frac{g_*^2}{g^2}. \tag{3.2.32}$$

In this case the improvement from (3.2.26) to (3.2.27) would be

$$E < \left(\frac{g\Lambda^2 m_W^2}{g_*}\right)^{1/4} \longrightarrow E < \Lambda\sqrt{\frac{g}{g_*}}\,. \tag{3.2.33}$$

In general, EFT validity discussion needs some assumptions on power counting (see for a recent discussion [4]). In the following analysis, however, none of the aforementioned power counting rules will be used. Perturbative, but otherwise arbitrary, Wilson Coefficients will be assumed, taking for granted that the validity of the EFT expansion at dimension 6 level.

3.3 Resurrecting interference with angular modulation

The goal of the work explained in this Chapter is to find strategies to enhance the interference term in the EFT expansion of the cross section, in the cases in which it turns out to be suppressed. In particular, the focus is on scenarios with the O_{3W} and $O_{3\tilde{W}}$ dimension 6 aTGC operators only, since their interference with Standard Model amplitudes suffers, in the high energy limit $E \gg m_W$, the absence of the naively expected energy growth for any diboson production process.

The first way to overcome the interference suppression is by noting that in reality $pp \to WV$ are not $2 \to 2$ diboson production processes, but $2 \to 3$ or $2 \to 4$ scatterings, since the massive vector bosons decay into fermions: $q\bar{q} \to VW \to 4\psi$ if $V = W, Z$ and $q\bar{q} \to \gamma W \to \gamma 2\psi$. Thus, there can be interference between amplitudes in which the polarizations of an unstable weak gauge boson are different, provided that the helicity of the final fermions in which it decays are the same. The helicity selection rule shown in Section 3.2.2 holds for 4-point amplitudes, in the high energy massless limit, and it can therefore be circumvented by considering 5 or 6-point amplitudes.

3.3.1 Angular modulation in helicity amplitudes

The crucial point of this method for interference resurrection is the dependence on angular variables for the decay amplitudes of polarized weak gauge bosons. Given a massive vector V ($V = W, Z$) with mass m_V and energy E_V, the decays of its polarized states into ψ_1 and ψ_2 fermions, with energies E_{ψ_1} and E_{ψ_2}, are described by

$$M(V_+ \to \psi_1\psi_2) \sim \sqrt{2E_{\psi_1}E_{\psi_2}}\cos^2\frac{\theta_V}{2}e^{+i\phi_V} \tag{3.3.1}$$

$$M(V_- \to \psi_1\psi_2) \sim \sqrt{2E_{\psi_1}E_{\psi_2}}\sin^2\frac{\theta_V}{2}e^{-i\phi_V} \tag{3.3.2}$$

$$M(V_L \to \psi_1\psi_2) \sim \frac{E_V}{m_V}\sqrt{E_{\psi_1}E_{\psi_2}}\cos\frac{\theta_V}{2}\sin\frac{\theta_V}{2} = 2\frac{E_V}{m_V}\sqrt{E_{\psi_1}E_{\psi_2}}\sin\theta_V \tag{3.3.3}$$

where $V_\pm$ and V_L are the transverse and longitudinal polarized bosons. The variables θ_V and ϕ_V are respectively the polar and azimuthal angle of the $V \to \psi_1\psi_2$ decay plane, with respect to the momentum of the vector. The azimuthal angle is evaluated taking the decay plane normal direction $\hat{n}_{decay}$ as given by the helicities of final fermions: $\hat{n}_{decay} \parallel \vec{p}_{l,-} \times \vec{p}_{l,+}$, where $\vec{p}_{l,-}$ and $\vec{p}_{l,+}$ are the momenta of the left handed and right handed fermion respectively.

One can notice that the contributions to the cross section that keep an azimuthal dependence can only arise from products of decay amplitudes for bosons with different polarizations, i.e. from the interference of processes with different helicities for the intermediate unstable vectors.

3.3.2 Angular modulation in $\sigma^{\mathbf{int}}$ in presence of $\lambda_{\mathbf{Z}}$

When the decay of W and Z gauge boson is allowed, the helicity selection rule that forbids a non zero $O_{3W}\times$SM or $O_{3\tilde{W}}\times$SM term in Eq. (3.2.1) at 4-point amplitudes level, in the high energy limit, is avoided because it is possible to have interference among diagrams in which unstable intermediate vectors have different polarizations. The result is an interference term that is different from zero in certain regions of the final fermion phase space, in such a way that integrating over it, thus going back to the 4-point interaction, the suppression is reobtained. These regions in which a non zero interference growing with energy is restored can be built exploiting the amplitude dependence on the azimuthal angles of vector decay planes, described in (3.3.1)-(3.3.3).

For simplicity, let us consider the process $q\bar{q} \to WZ$, with production of a transverse polarized W_+ and lepton decay of Z boson only, in particular $Z \to l_-\bar{l}_+$. The differential cross section is given by

$$\frac{d\sigma(q\bar{q} \to W_+ l_-\bar{l}_+)}{d\text{LIPS}} = \frac{1}{2s}\frac{\left|\sum_i(\mathcal{M}^{\text{SM}}_{q\bar{q}\to W_+Z_i} + \mathcal{M}^{\text{BSM}}_{q\bar{q}\to W_+Z_i})\mathcal{M}_{Z_i\to l_-\bar{l}_+}\right|^2}{(k_Z^2 - m_Z^2)^2 + m_Z^2\Gamma_Z^2}, \tag{3.3.4}$$

where $d\text{LIPS} \equiv (2\pi)^4\delta^4(\sum p_i - p_f)\prod_i d^3p_i/\left(2E_i(2\pi)^3\right)$ is the Lorentz Invariant differential Phase Space and there is a sum over intermediate Z polarizations. The Z-boson propagator is factored out, thanks to the fact that all Z polarizations have the same mass and width.

Since the aim is the analysis of the SM interference with amplitudes having insertion of O_{3W} and $O_{3\tilde{W}}$, contributions from the intermediate longitudinal Z_L bosons may be neglected, at first approximation. Indeed, these $d = 6$ operators involve only transverse vectors and, furthermore, it is well known that, at LHC, the SM diboson production is dominated by the transverse polarizations [9].

Then, in the narrow width approximation, namely in the limit of on-shell Z, the leading contribution to the interference, i.e. the cross term $\mathrm{BSM}_6 \times \mathrm{SM}$ in (3.3.4), is given by:

$$\frac{\pi}{2s}\frac{\delta(s-m_Z^2)}{\Gamma_Z m_Z}\mathcal{M}^{\mathrm{SM}}_{q\bar{q}\to W_+Z_-}\left(\mathcal{M}^{\mathrm{BSM}}_{q\bar{q}\to W_+Z_+}\right)^*\mathcal{M}_{Z_-\to l_-\bar{l}_+}\mathcal{M}^*_{Z_+\to l_-\bar{l}_+} + h.c.\,. \tag{3.3.5}$$

There is a scaling with the function $\mathcal{M}_{Z_-\to l_-\bar{l}_+}\mathcal{M}^*_{Z_+\to l_-\bar{l}_+}$; this in turn is modulated by the azimuthal angle ϕ_Z spanned by the plane defined by the Z decay leptons and the scattering plane (formed by collision axis and Z boson momentum), see Fig. 3.3. Then, using Eq. (3.3.1) and (3.3.2), one can see that

$$\mathcal{M}_{Z_-\to l_-\bar{l}_+}\mathcal{M}^*_{Z_+\to l_-\bar{l}_+} \propto e^{-i2\phi_Z}\,. \tag{3.3.6}$$

Then, the actual ϕ_Z modulation of the interference depends on the relationship between the phase factors of the involved amplitudes with the ones of their hermitian conjugates. As explicitly shown in [32], the phase of the factor $\mathcal{M}^{\mathrm{SM}}_{q\bar{q}\to W_+Z_-}\left(\mathcal{M}^{\mathrm{BSM}}_{q\bar{q}\to W_+Z_+}\right)^*$ can be identified using the optical theorem and its properties under CP transformations. Let's consider an arbitrary amplitude $A(a \to b)$. Then the optical theorem (if there are no strong phases, i.e. contributions of nearly on-shell particles) fixes

$$A(a \to b) = A^*(b \to a). \tag{3.3.7}$$

At the same time the transformation under CP implies

$$A(a \to b) = \eta_{CP}A(b \to a) \tag{3.3.8}$$

where $\eta_{CP} = 1(-1)$ for interactions respecting (violating) CP symmetry. By combining Eq. (3.3.7) and Eq. (3.3.8) we can infer

$$A(a \to b)^* = \eta_{CP}A(a \to b). \tag{3.3.9}$$

Applying this result to the $qq \to WZ$ process, one obtains that

$$\mathcal{M}^{\mathrm{SM}}_{q\bar{q}\to W_+Z_-}\left(\mathcal{M}^{\mathrm{BSM}}_{q\bar{q}\to W_+Z_+}\right)^* = \eta_{CP}(\mathrm{BSM})\left[\mathcal{M}^{\mathrm{SM}}_{\mathrm{q\bar{q}}\to \mathrm{W_+Z_-}}\left(\mathcal{M}^{\mathrm{BSM}}_{\mathrm{q\bar{q}}\to \mathrm{W_+Z_+}}\right)^*\right]^*. \tag{3.3.10}$$

From the results in the Eq. (3.3.10) and Eq. (3.3.6), it is evident that, in the differential cross section, the $\mathrm{BSM}_6 \times \mathrm{SM}$ interferences arising from the insertion of the $d = 6$ aTGC O_{3W} and $O_{3\tilde{W}}$ operators have the following form

$$\begin{aligned} O_{3W}: &\quad \frac{d\sigma_{\mathrm{int}}(q\bar{q}\to W_+Z\to W_+l_-\bar{l}_+)}{d\phi_Z} \propto \mathcal{M}_{Z_-\to l_-\bar{l}_+}\mathcal{M}^*_{Z_+\to l_-\bar{l}_+} + h.c. \propto \cos(2\phi_Z) \\ O_{3\tilde{W}}: &\quad \frac{d\sigma_{\mathrm{int}}(q\bar{q}\to W_+Z\to W_+l_-\bar{l}_+)}{d\phi_Z} \propto \mathcal{M}_{Z_-\to l_-\bar{l}_+}\mathcal{M}^*_{Z_+\to l_-\bar{l}_+} - h.c. \propto \sin(2\phi_Z). \end{aligned} \tag{3.3.11}$$

At this point, one has to take also into account the decay of the W gauge boson, i.e. to consider the realistic process $q\bar{q} \to ZW \to 4\psi$. The ϕ_W dependence is analogous to the case of the ϕ_Z azimuthal variable: the previous analysis applies to any interaction with decay of an unstable vector. Since only one pair of the intermediate vector bosons, either the Ws or the Zs, has opposite helicities in the two interfering amplitudes, the modulations with respect to the two different angles arise in two independent terms of a sum and read

$$\begin{aligned} O_{3W}: \quad & \frac{d\sigma_{\rm int}(q\bar{q} \to WZ \to l\nu ll)}{d\phi_W d\phi_Z} \propto \frac{E^2}{\Lambda^2} \left(\cos(2\phi_W) + \cos(2\phi_Z)\right) \\ O_{3\tilde{W}}: \quad & \frac{d\sigma_{\rm int}(q\bar{q} \to WZ \to l\nu ll)}{d\phi_W d\phi_Z} \propto \frac{E^2}{\Lambda^2} \left(\sin(2\phi_W) + \sin(2\phi_Z)\right). \end{aligned} \tag{3.3.12}$$

where the quadratic growth with energy comes from the fact that with the considered helicity structures neither the SM nor the BSM_6 amplitude is suppressed.

The case of WW production processes is completely analogous.

Similarly, in the $W\gamma$ production there is a modulation of the interference term of the differential cross section with respect to the azimuthal angle ϕ_W, that describes the decay plane orientation for the single unstable boson present in this process. Therefore, one obtains

$$\begin{aligned} O_{3W}: \quad & \frac{d\sigma_{\rm int}(q\bar{q} \to W\gamma \to l\nu\gamma)}{d\phi_W} \propto \frac{E^2}{\Lambda^2} \left(\mathcal{M}_{W_- \to l\nu} \mathcal{M}^*_{W_+ \to l\nu} + h.c.\right) \propto \frac{E^2}{\Lambda^2} \cos(2\phi_W) \\ O_{3\tilde{W}}: \quad & \frac{d\sigma_{\rm int}(q\bar{q} \to W\gamma \to l\nu\gamma)}{d\phi_W} \propto \frac{E^2}{\Lambda^2} \left(\mathcal{M}_{W_- \to l\nu} \mathcal{M}^*_{W_+ \to l\nu} - h.c.\right) \propto \frac{E^2}{\Lambda^2} \sin(2\phi_W). \end{aligned} \tag{3.3.13}$$

These results tell us that by exploiting the azimuthal modulations of Eq. (3.3.13) and Eq. (3.3.12) it is possible to individuate regions of the final fermion phase space in which the $\mathrm{BSM}_6 \times \mathrm{SM}$ interference terms of the differential cross sections are different from zero. With this method, one can increase the precision on the determination of the Wilson Coefficients associated with the O_{3W} and $O_{3\tilde{W}}$ operators by overcoming the suppression of the interference, suppression that is recovered with no ambiguity by performing a complete integration over the ϕ_i angles that characterize the final state, in order to study the full diboson production cross section. Furthermore, it is worthy to notice that, due to the two $2\phi_i$ arguments in Eq. (3.3.13) and Eq. (3.3.12), the asymmetry is not washed out by the ambiguity in the direction of quark-antiquark initial state.

So far, the contributions from longitudinal polarizations in the SM amplitudes have been neglected, but, in the case of WW and WZ production, there is also another effect of interference between amplitudes that display the naively expected unsuppressed energy dependence. It involves SM amplitudes with intermediate longitudinal bosons and diagrams with O_{3W} and $O_{3\tilde{W}}$ effective vertices, where the latter involve only transverse vectors. The form of the modulation is different from the one in Eq. (3.3.12) and for $q\bar{q} \to WZ$ is proportional to $\cos(\phi_W + \phi_Z)$ or $\sin(\phi_W + \phi_Z)$, for the CP-even and CP-odd BSM_6 interaction respectively. It is a consequence of the fact that the decay amplitude of a longitudinal vector has not any azimuthal dependence, differently from the case of transverse bosons (see Eq. (3.3.3)). However, this modulation effect

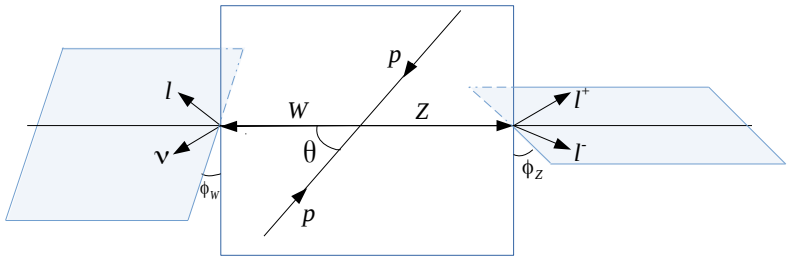

Figure 3.3: Angles for $2 \to 4$ scattering.

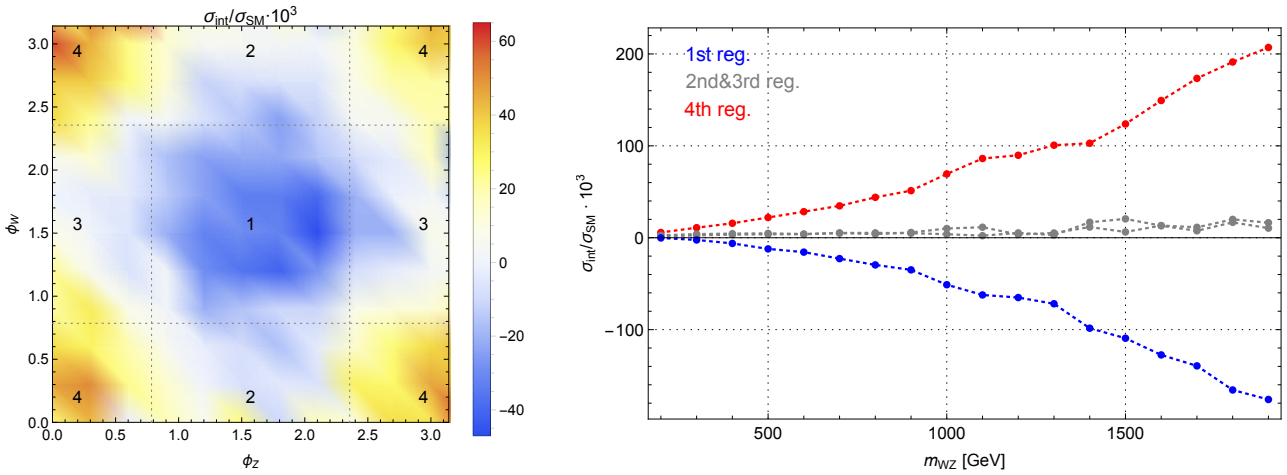

Figure 3.4: Left: Differential interference cross section over SM one as a function the azimuthal angles $\phi_{W,Z}$ for the events with WZ invariant mass $m_{WZ} \in [700, 800] GeV$. **Right:** same quantity as a function of the m_{WZ} binned according in the four bins defined in the left plot.

cancels out if we integrate the differential distribution over one of the azimuthal angles and is not invariant under the ambiguity in the direction of quark-antiquark initial states. Thus, it cannot be detected. Even in an ideal scenario in which there was the possibility to observe this kind of modulation, it would be absent in $W\gamma$ production. In fact, in such a process there isn't the possibility of a fully longitudinally polarized diboson state.

The contributions from the interference with SM amplitudes having one longitudinal and one transverse gauge boson are neglected. Indeed, as can be seen in Eq. (3.2.8), these helicity amplitudes are suppressed, in the high energy limit. These interference terms would present azimuthal modulations given by cosines and sines of ϕ_V or $2\phi_{V_1} - \phi_{V_2}$: they would be affected by the ambiguity in the versus of the initial quark and antiquark and in some cases cancelled by an integration over one angular variable.

Note that, naively, if the vector bosons are produced on-shell one would expect that vector

bosons with different helicity contributions should not interfere (or be suppressed by their width) even if we look at the decay products. Namely, one may expect that the interference is further suppressed than if the same $2 \to 4$ or $2 \to 3$ amplitude was mediated by a $2 \to 2$ sub-process $q\bar{q} \to VW$ that does lead to a cross section containing an interference term. However, this is not true, due to the basic fact that all the helicities have the poles of the propagators at exactly the same energies. Note that in the hypothetical case where the $2 \to 2$ process $\mathcal{M}^{\rm BSM}_{q\bar{q}\to W_+Z_-} \sim E^2/\Lambda^2$ was not suppressed, we would had gotten a $\Gamma_Z/m_Z \to 0$ limit as in Eq. (3.3.5), but where the amplitude would be instead controlled by the function $\mathcal{M}_{Z_-\to l_-\bar{l}_+}\mathcal{M}^*_{Z_-\to l_-\bar{l}_+}$, in which there is not any azimuthal modulation, but that has the same unsuppressed energy growth.

Also the squared SM or BSM amplitudes are modulated functions of the azimuthal angles, since they receive contributions from processes with different helicities of the intermediate diboson states. However, in the $\rm SM^2$ and $\rm BSM_6^2$ pieces of Eq.(3.2.1) there are also unsuppressed leading contributions whose differential distribution with respect to the azimuthal angles is a constant. Beside this, the $\rm BSM_6^2$ term includes the interference of diagrams with V_+V_+ and V_-V_- intermediate state, that in the case of WZ production is modulated as $\cos(2\phi_W + 2\phi_Z)$ or $\sin(2\phi_W + 2\phi_Z)$ in presence of O_{3W} and $O_{3\tilde{W}}$ respectively. One can notice that these modulating factors cancel out once an integration over even one single azimuthal angle is performed. In the case of $W\gamma$ production there are terms with the same angular dependence as in Eq. (3.3.13), together with unmodulated unsuppressed contributions. The case of the SM cross section is similar, with leading contributions that do not present azimuthal dependence but also $\sim E^0$ terms, in WZ production, with modulating factors proportional to $\cos(2\phi_W - 2\phi_Z)$ or $\cos(\phi_W - \phi_Z)$, for a scenario with the CP-even $d = 6$ aTGC operator. The extension to the CP-odd case or to $W\gamma$ production is straightforward.

In [1], we have performed a `MadGraph5` numerical simulation to test our theoretical expectations. The results are shown in Fig. 3.4 and are obtained in presence of the O_{3W} CP-even aTGC operator for a process of WZ production. In the left plot there is the interference differential cross section over the SM cross section as a function of ϕ_Z and ϕ_W. As explained in the previous paragraph, the modulated term within the SM cross section is subdominant with respect to the constant term. In fact, the shape of the function is as predicted by (3.3.12). This suggests that we should bin the events into four categories depending on whether $\phi_i \in [\pi/4, 3\pi/4]$, where the angles are shifted in such a way that they belong to $[0, \pi]$. The results are shown on the right plot of Fig. 3.4. The upper red line and the lower blue line correspond to the categories with $\phi_{W,Z} \in [0, \pi/4] \cup [3\pi/4, \pi]$ and $\phi_{W,Z} \in [\pi/4, 3\pi/4]$. We can see that there is a strong cancellation between these two contributions, however individually both of them grow with energy. So binning in azimuthal angles will increase dramatically the sensitivity to the interference.

3.3.3 Angular modulation in σ^{int} in presence of $\delta g_{1,z}$ and $\delta\kappa_z$

This work is focused on the analysis of the λ_Z and $\tilde{\lambda}_Z$ anomalous triple gauge couplings, but in this Section there is an analysis of the possible angular modulations in the $\rm BSM_6{\times}SM$ interference in presence of $\delta g_{1,z}$ and $\delta\kappa_z$ deviations or of their CP-odd partners.

As seen in Section 3.2.2, in a scenario with $\delta g_{1,z}$ aTGC the interference in WW and WZ production is not suppressed and the same occurs for $\delta\kappa_z$ in WW production. Within the leading contributions to this interference, there are unmodulated terms, but also pieces that display a dependence on the azimuthal angles, since they come from products of SM and BSM Feynman diagrams with transverse and longitudinal polarized intermediate bosons respectively. The shape of the angular modulation is determined by the azimuthal dependence in the decay amplitude of polarized vectors, shown in (3.3.3), and by the fact that the dominant contribution to amplitudes with insertion of the aTGCs $\delta g_{1,z}$ and $\delta\kappa_z$ comes from processes with purely longitudinal diboson states. Taking into account Eq. (3.2.20) and (3.3.9), one obtains

$$\begin{aligned}
\delta g_{1,z} \; : \quad & \frac{d\sigma_{\text{int}}(q\bar{q} \to WV \to 4\psi)}{d\phi_W \, d\phi_V} \propto \frac{E^2}{\Lambda^2} \left(\text{const} + \cos(\phi_W - \phi_V)\right) \\
\delta \tilde{g}_{1,z} \; : \quad & \frac{d\sigma_{\text{int}}(q\bar{q} \to WV \to 4\psi)}{d\phi_W \, d\phi_V} \propto \frac{E^2}{\Lambda^2} \left(\text{const} + \sin(\phi_W - \phi_V)\right).
\end{aligned} \tag{3.3.14}$$

where V can be either a W or a Z. The same energy and angular behavior occurs for interactions with $\delta\kappa_z$ and its CP-odd partner in WW production. The modulation of the CP-even interference is one of the kinds present also within the SM cross section. As previously discussed, it cannot be seen if we build the differential distribution with respect to a single azimuthal variable. Furthermore, it is in some way affected by the ambiguous determination of the initial quark and antiquark propagation versus, even if it is not completely washed out by this uncertainty, due to the difference in the parton distribution functions.

The case of $\delta\kappa_z$ contribution to WZ production is intrinsically different. Indeed, the suppression does not arrive only at the interference level, but it is already present in the BSM_6 amplitude, as depicted also in Fig. 3.1, in which the dominant term has a ratio with the SM amplitude that grows only linearly with the energy of the interaction and is associated to the production of a trasverse polarized Z and a longitudinal W. Thus, given the flat suppressed behavior of the interference shown in Fig. 3.2, we could at most restore a $\sim E/\Lambda$ growth, not a quadratic one; the corresponding contribution to the cross section would remain generally more subdominant. The modulations, in any case, would have form of $\cos(\phi_V)$ or $\cos(2\phi_{V_1} - \phi_{V_2})$ for the CP-even effective operator, as for the contribution of SM cross section with one transverse and one longitudinal boson. The CP-odd scenario is similar but with a sine shape of the angular dependence.

Analogously, for $W\gamma$ production, we have not amplitudes with $\delta g_{1,z}$ and $\delta\kappa_z$ contribution that grow quadratically with energy. Exploiting azimuthal differential distribution we have the possibility to give rise to $\sim E/\Lambda$ terms in the interference, with a $\cos(\phi_W)$ or $\sin(\phi_W)$ shape of modulation, for CP-even and odd interactions respectively.

One can consider also the differential distribution with respect to the polar angles associated to the vector decay products, as done in [32] in the case of diboson production and also in [24] for Zh emission. In the latter, invariant mass and angular differential distributions are used to constrain individually the 4 anomalous couplings involved in $pp \to hZ$, i.e. in Higgs Strahlung

processes. The azimuthal modulated interferences of Eq. (3.3.14) become

$$\delta g_{1,z}: \quad \frac{d\sigma_{\rm int}(q\bar{q}\to WV\to 4\psi)}{d\phi_W\, d\phi_V\, d\theta_W\, d\theta_V} \propto \tag{3.3.15}$$
$$\propto \frac{E^2}{\Lambda^2}\left(M^{SM}_{+-}\cos^2\tfrac{\theta_W}{2}\sin^2\tfrac{\theta_V}{2}+M^{SM}_{-+}\sin^2\tfrac{\theta_W}{2}\cos^2\tfrac{\theta_V}{2}\right)\sin\theta_W\sin\theta_V\cos(\phi_W-\phi_V).$$

$$\delta \tilde{g}_{1,z}: \quad \frac{d\sigma_{\rm int}(q\bar{q}\to WV\to 4\psi)}{d\phi_W\, d\phi_V\, d\theta_W\, d\theta_V} \propto \tag{3.3.16}$$
$$\propto \frac{E^2}{\Lambda^2}\left(M^{SM}_{+-}\cos^2\tfrac{\theta_W}{2}\sin^2\tfrac{\theta_V}{2}+M^{SM}_{-+}\sin^2\tfrac{\theta_W}{2}\cos^2\tfrac{\theta_V}{2}\right)\sin\theta_W\sin\theta_V\sin(\phi_W-\phi_V).$$

where θ_W and θ_V are the polar angles of emission for the fermions arising in the decays of W and $V=W,Z$. M^{SM}_{+-} (M^{SM}_{-+}) is the SM amplitude for production of W_+Z_- (W_-Z_+). In this way, we will avoid the washing out of modulation effects and interference resurrection that can emerge due to ambiguities in the angle determination, as we will see in the following Section.

In [24], angular modulation effects are analyzed also for contributions to the interference cross section that grows linearly and not quadratically with the energy of the interaction, while here only leading $\sim E^2/\Lambda^2$ terms are considered.

3.3.4 Visible angular modulation

In the previous Section we have discussed an ideal situation, assuming that the azimuthal angles between the plane spanned by the vector bosons decaying products and the scattering plane can be exactly determined. However the azimuthal angle determination suffers from a twofold degeneracy as pointed out in [32]. Let us recall the definitions of the ϕ angles which can be used experimentally. First we define two normals

$$\begin{aligned}\hat{n}^i_{\rm decay} &\parallel \vec{p}_{l^i,+}\times\vec{p}_{l^i,-}\\ \hat{n}^i_{\rm scat.} &\parallel \hat{z}_{\rm lab.}\times\vec{p}_{V^i}\end{aligned} \tag{3.3.17}$$

where the index i refers to the first or the second vector boson, l^i are the leptons from its decay and $\pm$ indicate the lepton helicities. The azimuthal angle ϕ between the two planes orthogonal to the normals is thus defined as

$$\phi_V = \text{sign}\left[(\hat{n}^i_{\rm scat.}\times\hat{n}^i_{\rm decay})\cdot\vec{p}_{V^i}\right]\arccos(\hat{n}^i_{\rm scat.}\cdot\hat{n}^i_{\rm decay}). \tag{3.3.18}$$

One cannot experimentally have access to the helicities of the final state leptons. As a consequence, the normal vector $\hat{n}^Z_{\rm decay}$ is defined only up to an overall sign, associated to the exchange of lepton helicities, once the electric charge is fixed instead. Remembering that positive helicity corresponds to positive charge in the case of LH leptons and to negative charge for RH leptons and using the definition of Eq. (3.3.18), this translates into an ambiguity

$$\phi_Z \leftrightarrow \phi_Z - \pi. \tag{3.3.19}$$

None of the modulations of the Eq. (3.3.12) are however affected by this ambiguity, since they are functions of $2\phi_Z$. On the contrary, other modulation factors are not left invariant by this ambiguity, such as cosine or sine functions of ϕ_Z or of $\phi_Z - \phi_W$, as we have for example in the interference with $\delta g_{1,z}$ contribution. What we actually measure is the azimuthal angle ϕ_Z^c of the decay plane for which the versus of the normal direction is fixed by the charges of final lepton, not by helicities. In the case of WZ production, the modulation described in Eq. (3.3.14), once expressed in terms of this visible angular variable becomes

$$\begin{aligned} \delta g_{1,z} \; : \quad & \sim (g_L^2 - g_R^2)\cos(\phi_W - \phi_Z^c) \\ \delta \tilde{g}_{1,z} \; : \quad & \sim (g_L^2 - g_R^2)\sin(\phi_W - \phi_Z^c) \end{aligned} \tag{3.3.20}$$

where g_L and g_R are the Z couplings to LH and RH lepton currents respectively and are quite similar in values: $g_L \sim T_{3,L} - Q_L s^2_{\theta_w} \approx -0.28$ and $g_R \sim T_{3,R} - Q_R s^2_{\theta_w} \approx -0.22$. Therefore, this azimuthal modulated contributions to interferences are very small and difficult to be seen, being proportional to the very small factor $g_L^2 - g_R^2$. The same occurs for every modulation with ϕ_Z argument and not $2\phi_Z$.

Now let us look at the azimuthal angle of the leptons from the W boson decay. Differently than for the Z boson, in this case the helicities of the final state leptons are fixed by the pure left handed nature of the EW interactions. However in this case the azimuthal angle determination suffers from a twofold ambiguity on the determination of the longitudinal momentum of the invisible neutrino, arising from the quadratic equation determining the on-shellness of the W boson. All together, for boosted W bosons this leads to the approximated ambiguity

$$\phi_W \leftrightarrow \pi - \phi_W . \tag{3.3.21}$$

This is illustrated in Fig. 3.5, where we plot the ϕ_W angle reconstructed assuming a randomly chosen p_z^ν solution against the same angle where the real, but experimentally unaccessible, value of p_z^ν has been used. The ambiguity of Eq. (3.3.21) clearly washes away the $\sin(2\phi_W)$ modulations of Eq. (3.3.12) and Eq. (3.3.13). Also all the other modulation factors different from $\sin(\phi_W)$ and $\cos(2\phi_W)$ are not invariant under this ambiguity, such as for example the angular functions in Eq. (3.3.14). The latter, in a WZ production process, would be in any case washed out by the indetermination that affects ϕ_Z. In the case of WW production through CP-even interactions associated to $\delta g_{1,z}$ aTGC, when we sum over W azimuthal angle ambiguities, the $\cos(\phi_{W_1} - \phi_{W_2})$ modulated term is modified but does not vanish; one gets

$$\delta g_{1,z} \; :\sim \sin(\phi_{W_1}^{rec})\sin(\phi_{W_2}^{rec}) \, . \tag{3.3.22}$$

Therefore, in a scenario with $\delta g_{1,z}$ aTGC, for a process with WW emission and decay, one could be able to exploit the differentiation with respect to fermion azimuthal angles in order to observe a contribution to the BSM$_6$×SM interference that would otherwise vanish in the inclusive cross section. The shape of the angular function, though, is different with respect to the one ideally expected in the case in which there were not ambiguities in the determination of the ϕ_Ws. However, this is not the case in a scenario with the CP-odd aTGC $\delta\tilde{g}_{1,z}$: the impossibility to measure the neutrino longitudinal momentum leads to a cancellation in the azimuthal dependent term of the interference, shaped as $\sin(\phi_{W_1} - \phi_{W_2})$.

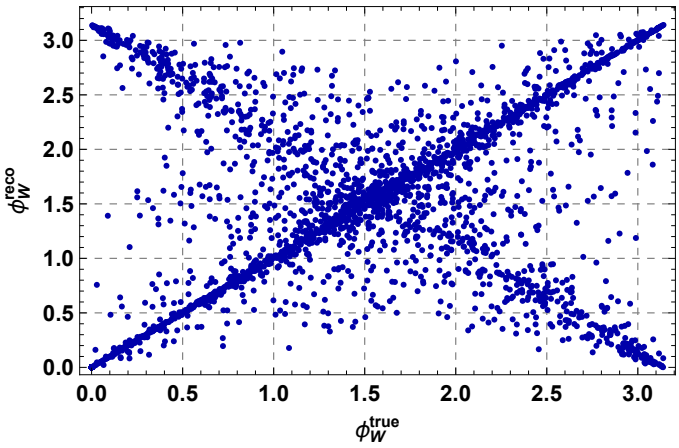

Figure 3.5: Parton level values of the ϕ_W angle defined in Eq. (3.3.18) built assuming a randomly chosen p_z^ν solution against the same angle where the real, but experimentally unaccessible, value of p_z^ν has been used. The ambiguity $\phi_W \leftrightarrow \pi - \phi_W$ is manifest.

If we consider the interference between SM and $d = 6$ amplitudes with $\delta g_{1,z}$ and $\delta \tilde{g}_{1,z}$ insertions, in order to have the possibility to observe angular modulated terms we can take the differential distribution with respect to a polar angle too, as also done in [32] and [24]. The polar angle associated to W decay products is not affected by the indetermination on the neutrino longitudinal momentum. On the other hand, the polar angle describing the emission of leptons from the Z is not invariant under the uncertainty on the fermion helicity, but it changes as

$$\theta_Z \leftrightarrow \pi - \theta_Z. \tag{3.3.23}$$

Thus, the angular function within Eq. (3.3.15) and (3.3.16), once expressed in terms of visible angles by summing over the ambiguities shown above, in the case of WZ productions becomes

$$\begin{aligned}
\delta g_{1,z} \; : \quad & \frac{d\sigma_{\rm int}(q\bar{q} \to WZ \to 4\psi)}{d\phi_W^{rec}\, d\phi_Z^c\, d\theta_W\, d\theta_Z^c} \propto \frac{E^2}{\Lambda^2} \sin\theta_W \sin\theta_Z^c \sin\phi_W^{rec} \sin\phi_Z^c \\
& [g_L^2 \left(M_{+-}^{SM} \cos^2\tfrac{\theta_W}{2} \sin^2\tfrac{\theta_Z^c}{2} + M_{-+}^{SM} \sin^2\tfrac{\theta_W}{2} \cos^2\tfrac{\theta_Z^c}{2} \right) + \\
& - g_R^2 \left(M_{+-}^{SM} \cos^2\tfrac{\theta_W}{2} \cos^2\tfrac{\theta_Z^c}{2} + M_{-+}^{SM} \sin^2\tfrac{\theta_W}{2} \sin^2\tfrac{\theta_Z^c}{2} \right)] \\
\delta \tilde{g}_{1,z} \; : \quad & \frac{d\sigma_{\rm int}(q\bar{q} \to WZ \to 4\psi)}{d\phi_W^{rec}\, d\phi_Z^c\, d\theta_W\, d\theta_Z^c} \propto \frac{E^2}{\Lambda^2} \sin\theta_W \sin\theta_Z^c \sin\phi_W^{rec} \cos\phi_Z^c \\
& [g_L^2 \left(M_{+-}^{SM} \cos^2\tfrac{\theta_W}{2} \sin^2\tfrac{\theta_Z^c}{2} + M_{-+}^{SM} \sin^2\tfrac{\theta_W}{2} \cos^2\tfrac{\theta_Z^c}{2} \right) + \\
& - g_R^2 \left(M_{+-}^{SM} \cos^2\tfrac{\theta_W}{2} \cos^2\tfrac{\theta_Z^c}{2} + M_{-+}^{SM} \sin^2\tfrac{\theta_W}{2} \sin^2\tfrac{\theta_Z^c}{2} \right)] .
\end{aligned} \tag{3.3.24}$$

where g_L and g_R are the coupling of the Z with left handed and right handed leptons.

One can notice that the azimuthal modulation that can be observe are not the $\cos(\phi_W - \phi_Z)$ and $\sin(\phi_W - \phi_Z)$ that we would have if we were able to determine without any ambiguity the emission angles for all the final helicity fermion states.

Integrating over the Z polar angle θ_Z^c in $[0,\pi]$, we end up with

$$\begin{aligned}\delta g_{1,z}\ : &\quad \sim \sin\theta_W \sin\phi_W^{rec} \sin\phi_Z^c \left(M_{+-}^{SM}\cos^2\tfrac{\theta_W}{2}(g_L^2-g_R^2)+M_{-+}^{SM}\sin^2\tfrac{\theta_W}{2}(g_L^2-g_R^2)\right)\\ \delta\tilde{g}_{1,z}\ : &\quad \sim \sin\theta_W \sin\phi_W^{rec} \cos\phi_Z^c \left(M_{+-}^{SM}\cos^2\tfrac{\theta_W}{2}(g_L^2-g_R^2)+M_{-+}^{SM}\sin^2\tfrac{\theta_W}{2}(g_L^2-g_R^2)\right).\end{aligned} \tag{3.3.25}$$

Since it holds that $g_L^2 - g_R^2 \sim 0$, the modulated terms above provide a very small contribution to the total interferences and are very hard to be observed.

On the other hand, if we integrate over the W polar angle θ_W in $[0,\pi]$, the factors depending on polar angles within the interference contributions of Eq. (3.3.24) are given by

$$\begin{aligned}&\sim \sin\theta_Z^c \left[M_{+-}^{SM}\left(g_L^2\sin^2\tfrac{\theta_Z^c}{2}-g_R^2\cos^2\tfrac{\theta_Z^c}{2}\right)+M_{-+}^{SM}\left(g_L^2\cos^2\tfrac{\theta_Z^c}{2}-g_R^2\sin^2\tfrac{\theta_Z^c}{2}\right)\right]\sim\\ &\sim \sin\theta_Z^c g_L^2\left(-M_{+-}^{SM}\cos\theta_Z^c+M_{-+}^{SM}\cos\theta_Z^c\right)=g_L^2\sin(2\theta_Z^c)\left(M_{-+}^{SM}-M_{+-}^{SM}\right)\end{aligned} \tag{3.3.26}$$

where the second equality assumes $g_L^2 \sim g_R^2$. Thus, we have in general a non zero result for the term of interference that is modulated in ϕ_W^{rec}, ϕ_Z^c and θ_Z^c, i.e. in the observable azimuthal angles and Z polar angle. Though, such term is suppressed proportionally to the cancellation between M_{+-}^{SM} and M_{-+}^{SM}, that however is only partial.

Moreover, in the case of WW production, the azimuthal and polar modulation of Eq. (3.3.15) might be visible in the form

$$\delta g_{1,z}\ : \qquad \frac{d\sigma_{\rm int}(q\bar{q}\to WW\to 4\psi)}{d\phi_{W_1}^{rec}\,d\phi_{W_2}^{rec}\,d\theta_{W_1}\,d\theta_{W_2}}\propto \tag{3.3.27}$$

$$\propto \frac{E^2}{\Lambda^2}\sin\theta_{W_1}\sin\theta_{W_2}\sin\phi_{W_1}^{rec}\sin\phi_{W_2}^{rec}\left(M_{+-}^{SM}\cos^2\tfrac{\theta_{W_1}}{2}\sin^2\tfrac{\theta_{W_2}}{2}+M_{-+}^{SM}\sin^2\tfrac{\theta_{W_1}}{2}\cos^2\tfrac{\theta_{W_2}}{2}\right).$$

Integrating over one polar angle or even both, we can still obtain a non vanishing contribution to the interference, displaying an azimuthal dependence, as already discussed in Eq. (3.3.22)

$$\delta g_{1,z}\ : \qquad \frac{d\sigma_{\rm int}(q\bar{q}\to WW\to 4\psi)}{d\phi_{W_1}^{rec}\,d\phi_{W_2}^{rec}\,d\theta_{W_1}\,d\theta_{W_2}}\propto\frac{E^2}{\Lambda^2}\sin\phi_{W_1}^{rec}\sin\phi_{W_2}^{rec}\left(M_{+-}^{SM}+M_{-+}^{SM}\right). \tag{3.3.28}$$

On the contrary, for the CP-odd interaction mediated by the aTGC $\delta\tilde{g}_{1,z}$ the angular dependent term of the interference, coming from product the BSM_6 amplitude with the transverse boson contribution to SM amplitude (see Eq. (3.3.15)), is cancelled out by the ambiguity on the W decay azimuthal angles.

Before concluding this Section a comment is in order. The definition of the diboson scattering plane of Eq. (3.3.17) strictly assumes a $2\to 2$ scattering process, where the two vector bosons are produced back to back in the center of mass frame of the initial partons. In the case of real radiation emission, as in the case of the presence of initial state radiation jets, the diboson scattering plane should be defined directly through the momenta of the two vector bosons. However in the case of the WZ and $W\gamma$ processes the determination of this plane will be again affected by the neutrino reconstruction ambiguities. Here, the definition of Eq. (3.3.17) is used in building the azimuthal angles of Eq. (3.3.18) throughout the analysis. This is a good approximation, since only processes with a hard jet emissions, which are kinematically suppressed, can lead to significant differences between the planes orientations.

3.3.5 Modulation from kinematic cuts

A partial restoration of the interference between the SM and the BSM_6 amplitudes, the latter with insertion of λ_Z or $\tilde{\lambda}_Z$ aTGC, can arise from the imposition of certain kinematic cuts, which we will see in Section 3.6.5. Let's consider for example the cut on the W boson transverse mass which is imposed in the experimental analyses [33] and [34]. This observable, M_W^T, can be defined only through W decay and in the case of $W \to e\nu$ it is

$$(M_W^T)^2 = (p_T^e + \not{p}_T)^2 - (\vec{p}_T^{\,e} + \vec{\not{p}}_T)^2 \tag{3.3.29}$$

where $\vec{\not{p}}_T \approx \vec{p}_T^{\,\nu}$, namely the missing transverse momentum approximately comes only from the neutrino. By looking at the dependence of the azimuthal angle ϕ_W on the transverse mass M_W^T illustrated in the two panels of Fig. 3.6, that refers to simulation of $pp \to W\gamma \to e\nu\gamma$, we observe that there is a strong correlation between the two variables. In the left panel all events within the detector kinematic acceptance are shown, while in the right panel the $p_T^\gamma > 100$ GeV cut is additionally imposed. In both plots we see that a small M_W^T is in correspondence with a value of 0 or π for ϕ_W. On the other side, for large p_T^γ, a cut on the W boson transverse mass automatically selects events in the azimuthal bin $[\pi/4, 3\pi/4]$. These two behaviors can easily be understood analytically.

Let's consider first the $M_W^T \sim 0$ case. In this limit the transverse momenta of the decay products of the W boson are parallel:

$$M_W^T = 0 \quad \Rightarrow \quad \vec{p}_T^{\,e} \parallel \vec{p}_T^{\,\nu} \parallel \hat{v} \tag{3.3.30}$$

where $\hat{v}$ is a unit vector in the transverse plane. The momenta of the W boson and the charged lepton can be decomposed in a transverse and longitudinal part as

$$\begin{aligned} \vec{p}_W &= \alpha_W \hat{v} + \beta_W \hat{z} \\ \vec{p}_e &= \alpha_e \hat{v} + \beta_e \hat{z} \end{aligned} \tag{3.3.31}$$

where $\hat{z}$ is a unit vector parallel to the beam line and $\alpha_{W,e}$ and $\beta_{W,e}$ are two real coefficients. Then Eq. (3.3.30) fixes the normals to the scattering plane and the decay planes, see Eq. (3.3.17), to be parallel

$$\begin{aligned} &\vec{n}_{\text{decay}} \propto \vec{p}_\nu \times \vec{p}_e \propto \vec{p}_W \times \vec{p}_e \parallel \hat{v} \times \hat{z} \\ &\vec{n}_{\text{scat.}} \propto \vec{p}_W \times \hat{z} \parallel \hat{v} \times z \end{aligned} \tag{3.3.32}$$

so that the azimuthal angle can only take the values of 0 or π (mod 2π). In the high energy regime one can also understand the correlation shown in the right panel of Fig. 3.6 in the $M_W^T \sim M_W$ limit. Indeed, assuming that the W boson is strictly on-shell, the condition $M_W^T = M_W$ leads to

$$\frac{|\vec{p}_T^{\,e}|}{|\vec{p}_T^{\,\nu}|} = -\frac{p_z^e}{p_z^\nu}. \tag{3.3.33}$$

Let us consider the limit $p_T^W \gg p_z^W$, which is equivalent to requiring $p_T^V \gg p_z^V$, where V is the vector boson produced in association with the W under analysis, i.e. $V = Z, \gamma$. This limit

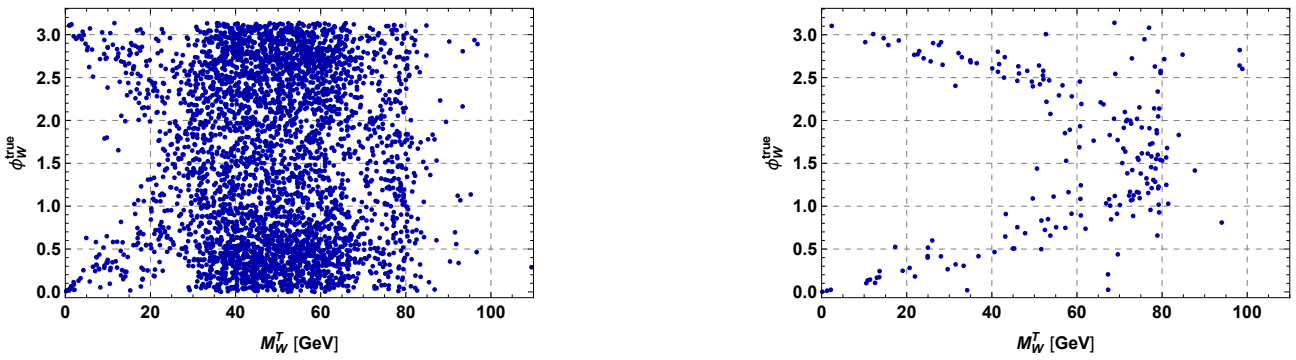

Figure 3.6: Distribution of the azimuthal angle ϕ_W vs transverse mass of the W bososn M_W^T. **Left**: no other cuts are imposed. **Right**: additional cut on the $p_T^\gamma > 100$ GeV is required.

in combination with the condition in Eq. (3.3.33) forces $p_T^{e,\nu} \gg p_z^{e,\nu}$. Hence in this case the normal to the decay plane will be always almost along the $\hat{z}$ direction, so that the azimuthal angle will take a value equal to $\pi/2$. All together we see that a high M_W^T cut, together with the requirement of a large photon transverse momentum, in the case of $W\gamma$ production, leads to the automatic selection of a preferred azimuthal angle bin. In the analysis that will follow, events will be binned in function of the transverse mass of the WZ and $W\gamma$ systems. However for a $2 \to 2$ scattering there is a one to one correlation between the W boson transverse momentum and the one of the other vector V produced in association. Hence, by selecting bins with high m_{WV}^T we automatically select events with high-p_T^V which, as shown above, lead to the selection of events where $\phi_W \sim \pi/2$.

It is important to stress that a cut on the W boson transverse mass, as discussed above, is imposed in the experimental analysis that we consider [33] and [34]. This kinematic selection is used to suppress backgrounds arising from processes without genuine missing transverse momentum, such as, for $W\gamma$ production, the overwhelming QCD γj background where a jet is misidentified as a lepton. Hence this *modulation from cuts* behavior is always present when performing a real experimental analysis. This is an important effect which has been overlooked in similar studies in the literature previous to [2] and that leads to an enhanced sensitivity with respect to what is naively expected. In the following, it will be quantitatively shown that this effect is more important in the $W\gamma$ case than in the WZ one.

3.4 Going beyond LO

The non-interference in diboson production, through λ_Z contribution, in the $2 \to 2$ process applies at tree-level only, at which Eq. (3.2.20) and Eq. (3.2.21) hold. Higher order corrections, either in the form of loops or radiation, overcome the interference suppression and lead to a $\text{BSM}_6 \times \text{SM}$ cross section piece that does grow with energy. This was first noticed in the context of QCD for the gluon operator $\sim G_\mu{}^\nu G_\nu{}^\rho G_\rho{}^\mu$ [26]. Here, as in [1], this idea is applied to the electroweak sector. The corrections from the virtual gluon will introduce the BSM×SM interference, however this effect will be suppressed by $\sim \frac{\alpha_s}{4\pi}$ compared to the angular modulation discussed in the previous Section. Another possibility is to consider $2 \to 3$ processes, namely

the production of the pair of the electroweak bosons with a hard QCD jet $VV + j$. Then, using Eq. (3.2.19), the BSM amplitudes have the following helicity configuration

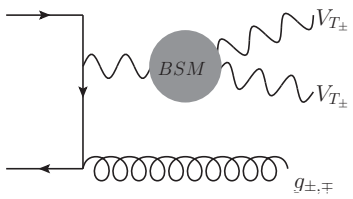

where the gluon g can take any polarization. In the SM the same process has necessarily the helicity configuration

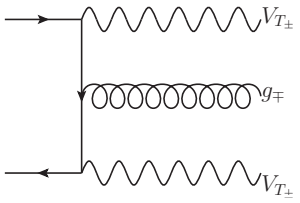

i.e. it can not be of the Maximally Helicity Violating type. Thus, the extra gluon radiation helps in sucking helicity allowing the same final state as in $VV + j$ mediated by O_{3W} (in the CP-even case). Thus, the simple requirement of extra radiation qualitatively changes the cross section behavior and provides a better handle on the interference terms. Note also that the solution advocated in this Section is complementary to the analysis presented in the Section 3.3, in addition to the binning in the azimuthal angle there is just the requirement of an extra hard jet. The consequences of going to complete next-to-leading order are analogous and even stronger.

The interference effect becomes small both in the soft and collinear jet limits [26]. This is expected since interfering SM amplitudes $A(q\bar{q} \to V_{T_\pm} V_{T_\pm} g_\mp)$ cannot be generated from $A_{SM}(q\bar{q} \to VV)$ by splitting quark (anti-quark) line into $q(\bar{q}) \to q(\bar{q})g$, due to the change of the helicity structure. So there will be no usual soft and collinear singularities corresponding to the poles of the splitting functions, which has been checked by explicit calculation. Then, the interference term in these limits, even if growing with energy, will be completely buried inside the SM contribution.

In [1], we have cross-checked the theoretical expectations with a `MadGraph5` simulation of $pp \to WZ + j$ in presence of the CP-even aTGC operator O_{3W}. In Fig. 3.7, the ratio $\sigma_{\rm int}/\sigma_{\rm SM}$ for WZ production is plotted as a function of the invariant mass m_{WZ}, making various requirements on the extra gluon. In blue we ask for no extra radiation which corresponds to the non-interference effect discussed in Fig. 3.2. In red and magenta we require a hard gluon which takes a significant fraction of the diboson phase-space, $m_{WZ}/10$ and $m_{WZ}/5$ respectively. Importantly, the simulation shows the expected energy growth of the interference term. On the other hand, the purple curve does not show a steady growth of the energy. This is also

expected since that curve is obtained by imposing a fixed lower cut on the jet p^T. As the energy of the diboson is increased the extra jet becomes relatively soft and the energy growth is lost. Numerical simulations (see Fig. 3.7) tell that one should require something like $p_j^T \gtrsim \frac{m_{WZ}}{5}$ to have a quadratic growth with energy. Error bars are due to the statistical treatment of the Monte Carlo (MC) simulation; they are small enough to observe the discussed effect.

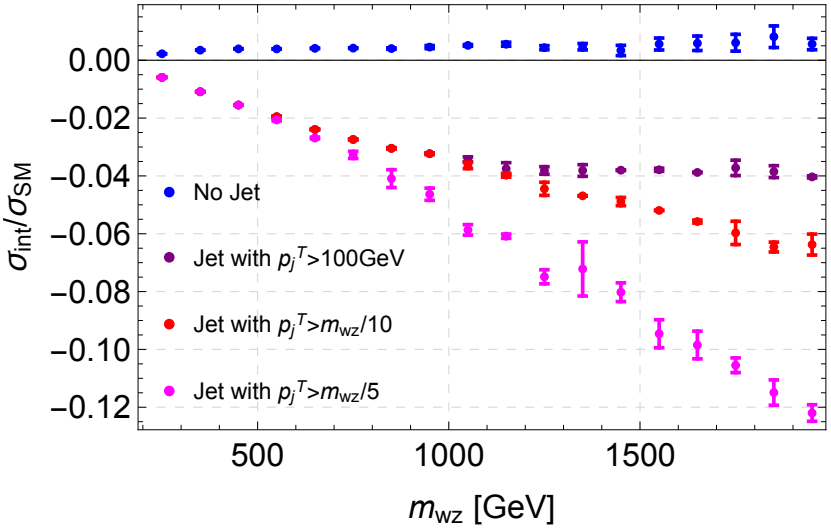

Figure 3.7: $\sigma_{\text{int}}/\sigma_{\text{SM}}$ as a function of m_{WZ} for the process $pp \to WZ$ (blue) and the process $pp \to VW + j$, with $p_j^T > m_{WZ}/5$ (magenta), $p_j^T > m_{WZ}/10$ (red), and $p_j^T > 100$ GeV (purple).

In the following, an analysis at NLO will be performed: this, as it has now been shown, intrinsically resurrects the $\text{BSM}_6\times\text{SM}$ interference that is suppressed for the interactions with λ_Z aTGC contribution.

3.5 EFT validity

In the previous Sections, methods to enhance the sensitivity to the $\text{BSM}_6\times\text{SM}$ interference, in presence of aTGCs λ_Z and $\tilde{\lambda}_Z$, have been shown. They can help to enlarge the region in which we might more safely neglect the contribution from operators of dimension 8 or higher, depending on the power counting as explained in Section 3.2.3. However, this is not enough to ensure the validity of the EFT interpretation of diboson production at the LHC, as seen also in Section 2.1. The convergence of the EFT expansion is controlled by the ratio of the invariant mass of the diboson system over the new physics scale and thus $m_{VW}/\Lambda \ll 1$ should be satisfied. However at hadron colliders it is hard to keep m_{VW}/Λ fixed. Firstly, the precise collision energy is unknown and not fixed, leading to an imprecise knowledge of m_{VW} from event to event. Secondly and more importantly, experimentalists only reconstruct the visible decay products. Namely, we cannot consider the full diboson invariant mass in presence of W bosons decaying leptonically, due to the final neutrino. We instead analyze the WZ or $W\gamma$

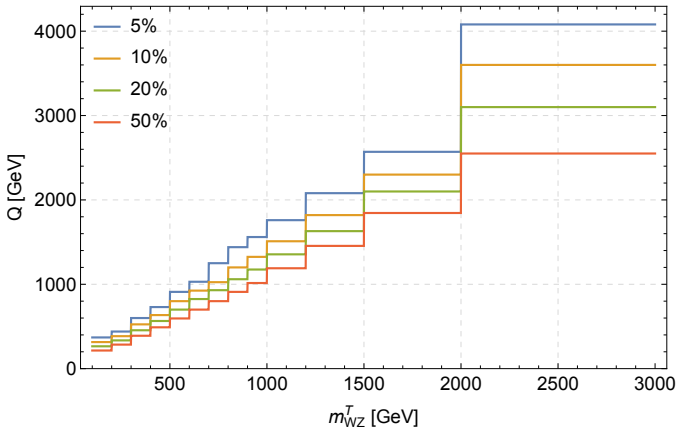

Figure 3.8: *Leakage*, for the process $q\bar{q} \to WZ$ with λ_Z turned on, as a function of m^T_{WZ}.

transverse masses

$$m^T_{WZ} = \sqrt{(E^W_T + E^Z_T)^2 - (p^W_x + p^Z_x)^2 - (p^W_y + p^Z_y)^2} \tag{3.5.1}$$

$$m^T_{W\gamma} = \sqrt{(E^W_T + p^\gamma_T)^2 - (p^W_x + p^\gamma_x)^2 - (p^W_y + p^\gamma_y)^2} \tag{3.5.2}$$

$$\text{with} \quad E^W_T = \sqrt{m^2_W + \sum_{i=x,y} (p^e_i + \not{p}_i)^2} \tag{3.5.3}$$

in the WZ and $W\gamma$ production respectively, where p^e is the momentum of the electron and $\not{p}$ the missing momentum approximately given by the neutrino. In processes with WW intermediate state we would have considered the visible dilepton invariant mass

$$m_{ll} = \sqrt{(p_{l^-} + p_{l^+})^2}\,. \tag{3.5.4}$$

The invariant mass m_{VW} of the diboson system is always greater or equal than these visible masses $m_{VW} \geqslant m_{ll}, m^T_{WV}$. This implies that binning and cutting the distributions in terms of m_{ll}/m^T_{WV} variables does not allow to ensure $m_{VW}/\Lambda \ll 1$. As an illustration of this point, in Fig. 3.8, what here is called *leakage* is shown, for WZ production. This is defined as the percentage of the number of events in a given m^T_{WV} (or m_{ll}) bin with invariant mass m_{VW} larger than a certain scale Q:

$$\text{Leakage} = \frac{N_i(m_{VW} > Q)}{N_i} \times 100\,, \tag{3.5.5}$$

where N_i is the total number of events in the given m^T_{WV} (or m_{ll}) bin. For instance, the red line in the bin $m^T_{WZ} \in [1500, 2000]$ GeV is interpreted as follows. Of all the events in that bin, 50% of them have an invariant mass $m_{WZ} \gtrsim 1800$ GeV. These numbers have been calculated conservatively using only the BSM^2_6 term of the cross section (see Eq. (3.2.1)) which is indeed the term giving the largest leakage.

Naively, we can use the information in Fig. 3.8 to set consistent bounds on the EFT. For example, if we require $\Lambda = 2$ TeV and the precision of the measurement $\lesssim O(1) \times 5\%$ we should

keep the transverse mass bins only up to 1.5 TeV. This would work under the assumption that the leakage calculated using the dimension 6 operator squared provides a conservative estimate compared to the full UV complete model, namely that we do not have a very large number of events for some value of invariant mass $M_* > 2$ TeV. This assumption is for example spoiled in the presence of the narrow Bright-Wigner resonances and the calculation with dimension 6 operators underestimates the cross section and leakage by the factor of

$$\frac{\sigma^{full}}{\sigma^{d=6}} \sim \frac{\pi\Lambda^2}{\Gamma^2}, \tag{3.5.6}$$

which becomes very large for narrow resonances (Λ and Γ are the mass and the width of the resonance). At the same time in the more strongly coupled theories, the quantity in Eq. (3.5.6) is only of order one $O(1)$. Thus, under the assumption $\sigma^{full}/\sigma^{d=6} \lesssim O(1)$, we can use the Fig. 3.8 to find the correspondence between the transverse and invariant mass cut-offs once the precision of the measurement is specified.

The leakage can be made arbitrarily small by simply assuming a large enough value of Λ in the EFT interpretation. Then there would be obviously no danger of narrow Breit-Wigner peaks, since the new particles would be too heavy to be produced at LHC. However, in that case the collider sensitivity would allow us only to prove Wilson Coefficients that are on the verge of non-perturbativity, in order to compensate the large value of Λ. In fact, in [35] bounds on the TGCs Wilson Coefficients are of order $c_i \lesssim [-2.5, 2.5]$, once rescaled to the normalization used here, with the cut-off $\Lambda = 1$TeV. This is done by analyzing the whole range of $m^T_{WV} \in [50, 650]$ GeV and thus there is probably a large number of events having invariant mass $m_{WV} \gtrsim 1$ TeV. Then, for the proper EFT interpretation we should set $\Lambda \gtrsim 2$ TeV, thus implying that the bound gets loosened roughly as $c_i \lesssim [-2.5, 2.5] \longrightarrow c_i \lesssim 4 \times [-2.5, 2.5]$, which pushes the EFT even further on the verge of non-perturbativity.

In the following paragraphs, another possible approach to perform a consistent EFT analysis is discussed. Without spoling the accuracy of the analysis, as it may happen through the *leakage* method in the case of low cut-off, it allows to lower Λ, and hence in principle be sensitive to theories less close to the non-perturbative regime, at least when the statistics is enlarged in the upcoming future.

The idea consists in comparing the observed cross section with the new physics expectation only in the constrained phase space satisfying the EFT validity requirements. This approach was originally suggested for the Dark Matter searches at LHC in [36] and later applied for the anomalous TGCs measurements in [11]. In the standard analysis, for every bin, e.g. in $m^T_{WZ} \in [m^T_1, m^T_2]$, one would compare the observed number of events $n_{\rm obs}$ with the theory prediction $M_{\rm th}$, which in presence of the $d = 6$ effective operators O_{3W} and $O_{3\tilde{W}}$ is

$$M_{\rm th} = n_{\rm SM} + n^e_{\rm int} c_{3W} + n^o_{\rm int} c_{3\tilde{W}} + n^e_{\rm BSM^2} c^2_{3W} + n^o_{\rm BSM^2} c^2_{3\tilde{W}} + n^{e-o}_{\rm BSM^2} c_{3W} c_{3\tilde{W}}\,, \tag{3.5.7}$$

where $n_{\rm SM}$ is the SM prediction and $n_{\rm int}$, $n_{\rm BSM^2}$ come from the $\mathrm{BSM}_6\times\mathrm{SM}$ and BSM_6^2 pieces in Eq. (3.2.1). The comparison, with the number $n_{\rm obs}$ of observed events, is performed by evaluating the likelihood in a given bin using the Poisson distribution $p(n_{\rm obs}|M_{\rm th}) = \frac{1}{n_{\rm obs}!} e^{-M_{\rm th}} M^{n_{\rm obs}}_{\rm th}$. Note however that if we took this procedure we would be comparing $M_{\rm th}$ with $n_{\rm obs}$ for events

were the effective expression of $M_{\rm th}$ in the equation above is not valid any more, due to a not sufficiently small ratio between the energy of the interaction and the cut-off scale Λ.

Instead, safety of the EFT approach is granted if we compare the observed number of events with the quantity $N_{\rm th}$, which we define as follows:

$$N_{\rm th} = \begin{cases} \widetilde{N}_{\rm th} & \text{if} \quad \widetilde{N}_{\rm th} > n_{\rm SM} \\ n_{\rm SM} & \text{otherwise} \end{cases} , \tag{3.5.8}$$

where $\widetilde{N}_{\rm th} = \tilde{n}_{\rm SM} + \tilde{n}^e_{\rm int} c_{3W} + \tilde{n}^o_{\rm int} c_{3\tilde{W}} + \tilde{n}^e_{\rm BSM^2} c^2_{3W} + \tilde{n}^o_{\rm BSM^2} c^2_{3\tilde{W}} + \tilde{n}^{e-o}_{\rm BSM^2} c_{3W} c_{3\tilde{W}}$ is as $M_{\rm th}$ but with $\tilde{n}_i$ defined as $n_i|_{m_{VV}<\Lambda_{\rm MC}}$, i.e. the expected number of events in the EFT is evaluated with the restriction of invariant mass m_{WV} below a certain fixed cut-off scale $\Lambda_{\rm MC}$. The latter is a scale set in the MC simulation and is different from the true value of Λ in the SMEFT, which is of course an unknown constant of nature. Also note that $\Lambda_{\rm MC}$ is analog to the scale Q introduced in Eq. (3.5.5). Thus, in practice the likelihood is modeled by $p(n_{\rm obs}|N_{\rm th}) = \frac{1}{n_{\rm obs}!} e^{-N_{\rm th}} N_{\rm th}^{n_{\rm obs}}$.

The key question is whether the bounds obtained using (3.5.8) lead to more conservative estimates than the ones which could come from the knowledge of full theory. The number of events in the full theory is

$$N_{\text{full theory}} = \widetilde{N}_{\rm th} + [N_{\text{full theory}}]_{m_{VV}>\Lambda_{MC}} , \tag{3.5.9}$$

where the theory below $\Lambda_{\rm MC}$ is approximated by the EFT expansion. Note that both terms in (3.5.9) are positive, since they are actually physical numbers of events. Then, the bounds from (3.5.8) are conservative only if

$$|n_{SM} - N_{\rm th}| \leqslant |n_{SM} - N_{\text{full theory}}| , \tag{3.5.10}$$

condition that is always fulfilled with the definition of $N_{\rm th}$ in (3.5.8).

Finally, let us note that in [11], in presence of O_{3W} only, the choice of the theory is $N_{\rm th} = n_{\rm SM} + \tilde{n}_1 c_{3W} + \tilde{n}_{\rm BSM^2} c^2_{3W}$, instead of the one in Eq. (3.5.8). This is equivalent to modify the BSM amplitudes by the following *form factor*

$$\mathcal{M}_{BSM} \to \mathcal{M}_{BSM} \times \theta(\Lambda_{\rm MC} - m_{VV}) , \tag{3.5.11}$$

where the $\theta(x)$ is the Heaviside step function or any close function like $(1 + e^{\alpha[\Lambda_{\rm MC} - m_{VV}]/m_{VV}})^{-1}$ with $\alpha \gg 1$, non analytic in $\Lambda^{-1}_{\rm MC}$. Then, Eq. (3.5.10) is fulfilled only if one assumes that the deviations from the SM below and above $\Lambda_{\rm MC}$ have the same signs, namely $\text{sign}(\Delta\sigma_{\rm BSM})|_{m_{VV}>\Lambda_{\rm MC}} = \text{sign}(\Delta\sigma_{\rm BSM})|_{m_{VV}<\Lambda_{\rm MC}}$. In terms of the variables in Eq. (3.5.8) it means

$$\text{sign}(N_{\text{full theory}} - n_{\rm SM} - \tilde{n}_1 c_{3W} - \tilde{n}_{\rm BSM^2} c^2_{3W}) \quad = \quad \text{sign}(\tilde{n}_1 c_{3W} + \tilde{n}_{\rm BSM^2} c^2_{3W}) . \tag{3.5.12}$$

This condition is trivially satisfied when BSM^2 dominates the non-SM piece of the cross section; however it is not true once interference term is of the same size, which is the case of interest for this work.

Commonly, in the experimental studies, such as in [37], a different form factor for the new physics contribution is used:

$$\mathcal{M}_{\rm BSM} \to \mathcal{M}_{\rm BSM} \times \frac{1}{\left(1 + \frac{m^2_{VV}}{\Lambda^2_{\rm MC}}\right)^2} . \tag{3.5.13}$$

The different form factors would lead to identical results for $\Lambda_{\rm MC} \gg m_{VV}$, but there will be order one differences for the events with invariant mass close to the cut-off $\Lambda_{\rm MC}$. Also, note that while the UV assumptions are very clear when using (3.5.11) they are somewhat more obscure in (3.5.13). The reason being that the fall-off of the form factor in (3.5.13) is not steep enough and its validity requires some discussion or assumptions on the leakage, similarly to what discussed below Eq. (3.5.6).

In [1], we have checked that the various methods described above lead to similar bounds: sticking to one of them is sufficient to provide quite general results. Thus, in the numerical analysis that will follow, bounds on the aTGCs are set using fixed cuts on the visible transverse masses m^T_{WZ} and $m^T_{W\gamma}$. One has to keep in mind that, using Fig. 3.8 or similar ones, it is possible to individuate a certain scale Q such that under a desired accuracy we might neglect events with invariant mass larger than Q, for the relevant interaction.

3.6 Analysis and results: $pp \to WZ$ process

The goal of the work described in this Chapter is to estimate the improvement that can be reached in the sensitivity to the aTGCs λ_Z and $\tilde{\lambda}_Z$ at hadron colliders, such as LHC, thanks to the differential distributions on angular variables or to NLO effects, as explained in Section 3.3 and 3.4. We will study the $pp \to WZ$ and $pp \to W\gamma$ processes at the LHC, focusing on the first one in this Section. The fully leptonic channels will be taken into account, since they are the cleanest ones.

Firstly, in what follows, a description of the simulation environment will be provided.

3.6.1 Details on the event simulation

In [2], we have simulated, via the `MadGraph5_aMCNLO` platform [38]) the hard scattering fully leptonic $pp \to WZ$ process. The presence of the BSM operator O_{3W} and $O_{3\tilde{W}}$, defined in Eq. (3.1.11) and (3.1.13), is introduced using the `HELatNLO_UFO` model that have been implemented in the `FeynRules` package [39] and exported under the `UFO` format [40] by the authors of [41]. The study is performed at NLO in QCD commenting, when relevant, the differences with respect to the results obtained at leading-order as well as NLO with an extra jet radiation in the matrix-element (hereafter NLO+j), which partially mimics the next-to-next-to-leading-order (NNLO) accuracy. Parton showering and hadronization of partons are performed with `PYTHIA8` [42]. Matching and merging between hard-scattering and parton shower have been performed through `PYTHIA8` for the NLO case and `PYTHIA8` + `FxFx` algorithm as described in [43] for the NLO+j case. In Table 3.1 there is a summary of the tools used for each level of the perturbative expansions. When analyzing the events, jets are reconstructed via the anti-κ_T algorithm [44] with $\Delta R = 0.4$ and a p_T threshold of 20 GeV through the `MadAnalysis5` package [45] as implemented in `MadGraph5_aMCNLO`.

In the simulated $pp \to W^{\pm}Z$, the Z boson is forced to decay into a muon pair and the W

boson into an electron and the associated neutrino and a final combinatorial factor is applied to take into account all possibile final state flavor configurations involving the first two generations. LO and NLO diboson productions are simulated, generating events with only the CP-even or CP-odd operator different from zero, as well as events where both the operators are present, so as to determine the contribution to the cross section due to the interference of the two deformations. The ATLAS experimental analysis of [33] is closely followed and the signal region is defined imposing the following set of cuts: $p_T^e > 20$ GeV, $p_T^\mu > 15$ GeV, $|\eta^{\mu,e}| < 2.5$, $\Delta R(\ell,\ell) > 0.2$, $\Delta R(\ell, j) > 0.4$, where $\ell = e, \mu$ and the p_T threshold for jets is 20 GeV. The same flavor opposite charge lepton pair, in particular muon pair in our simulations, is required to reconstruct the Z boson asking $|m_{\mu^+\mu^-} - m_Z| < 20$ GeV and a cut of 30 GeV on the W boson transverse mass, defined in Eq. (3.3.29), is imposed. The events are binned with respect to the WZ system transverse mass, which is define as

$$(m_{WZ}^T)^2 = \left(\sqrt{m_W^2 + \sum_{i=x,y}(p_i^e + \not{p}_i)^2} + \sqrt{m_Z^2 + \sum_{i=x,y}(p_i^{\mu^+} + p_i^{\mu^-})^2}\right)^2 - \sum_{i=x,y}(p_i^e + \not{p}_i + p_i^{\mu^+} + p_i^{\mu^-})^2, \tag{3.6.1}$$

where $\not{p}_i$ is the i^{th} component of the missing transverse momentum of the event. Finally, the ϕ_Z and ϕ_W azimuthal angles are built as defined in Eq. (3.3.18) and the events are categorized with respect to ϕ_Z and ϕ_W, both defined in the range 0 to π.

While the event generation has been performed at the parton level, we wish to mimic (at least partially) detector smearing effects when building the angular variables used for the analysis, without performing a dedicated detector simulation for all the event samples. The used procedure is the following. For one chosen event sample we compar, on an event by event basis, the values of the ϕ_Z and ϕ_W variables before and after having applied detector effects, which are evaluated through the `Delphes 3` package [46]. The latter then approximated with a three rectangles shape and the parton level values of the azimuthal angles are dressed with a $\Delta\phi_{Z,W}^{\text{smear}}$ evaluated with the computed probability. For concreteness, taking the angle deviation due to the smearing within the interval $[-\frac{\pi}{2}, \frac{\pi}{2}]$ due to the 2ϕ periodicity of the modulation terms, the following functions are used to reproduce detector effects:

$$\phi_Z^{\text{smear}} = \phi_Z \pm \Delta\phi_Z^{\text{smear}}, \quad \Delta\phi_Z^{\text{smear}} = \begin{cases} [0, 0.2] \text{ with probability } 0.68 \\ [0.2, \pi/2] \text{ with probability } 0.32\,, \end{cases}$$

$$\phi_W^{\text{smear}} = \phi_W \pm \Delta\phi_W^{\text{smear}}, \quad \Delta\phi_W^{\text{smear}} = \begin{cases} [0, \pi/4] \text{ with probability } 0.66 \\ [\pi/4, \pi/2] \text{ with probability } 0.34\,. \end{cases} \tag{3.6.2}$$

3.6.2 Comparison of perturbative expansions for the SM

The first test of reliability of the analysis and the results is the comparison of the simulation framework with the existing literature for the case of the SM. In [2] we have performed such check, considering the $pp \to WZ \to lll\nu$ processes for W^+ and W^- separately at LO, NLO and NLO+j order for the LHC with a center of mass energy of 14 TeV. By applying only a

Order	Hard-scattering	Parton Shower	Jet Merging
LO	MadGraph5_aMCNLO	PYTHIA8	/
NLO			PYTHIA8
NLO+j			PYTHIA8+FxFx

Table 3.1: Summary of the tools used for the event generations at each order in the QCD perturbative expansion.

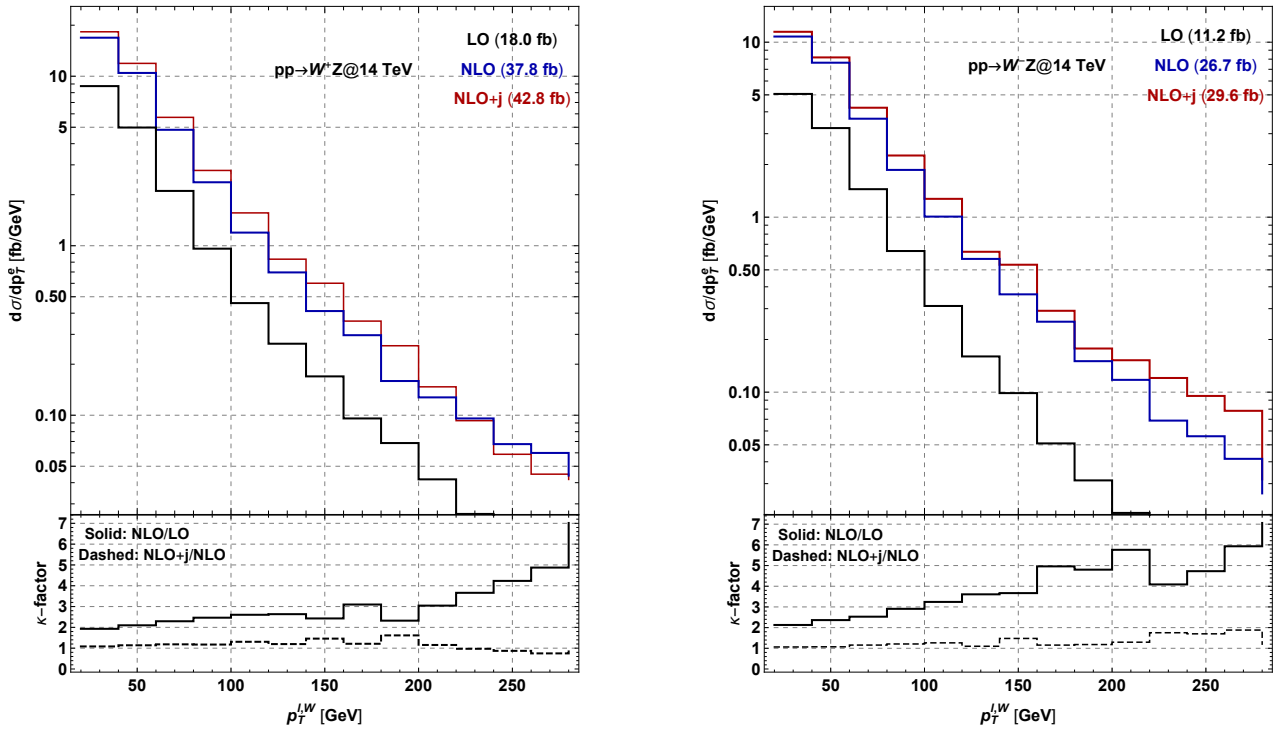

Figure 3.9: Differential distributions as a function of the transverse momentum of the lepton arising from the W^+ (left) and W^- (right) decay at the LO, NLO and NLO+j accuracy for the SM fully leptonic $pp \to W^{\pm}Z$ process. In the lower panels the NLO/LO and NLO+j/NLO differential cross section ratios are shown.

20 GeV cut on the transverse momenta of all visible leptons we obtain a cross section value at NLO and LO of 37.8 fb and 18.0 fb for the W^+ case and of 26.7 fb and 11.2 fb for the W^- case. The addition of an extra jet in the matrix element increases these value of an extra $\sim 10\%$. These findings nicely agree with the latest results of [47], computed for $\sqrt{s} = 13$ TeV. For the same processes we then compare the differential cross sections in function of the transverse momentum of the charged lepton from the W decay, also reported in [47] for $\sqrt{s} = 8$ TeV. By taking into account the parton luminosity rescaling factor between our and their center of mass energy (which is ~ 2 for the $q\bar{q}$ scattering of proton's valence quarks for $\sqrt{\hat{s}} =$ 300 GeV) we find an overall good agreement in the distributions shapes between our LO and NLO results and the ones of [47], thus further validating our simulation framework. Again, we observe that there is a small difference between the NLO and NLO+j calculations. Given the larger

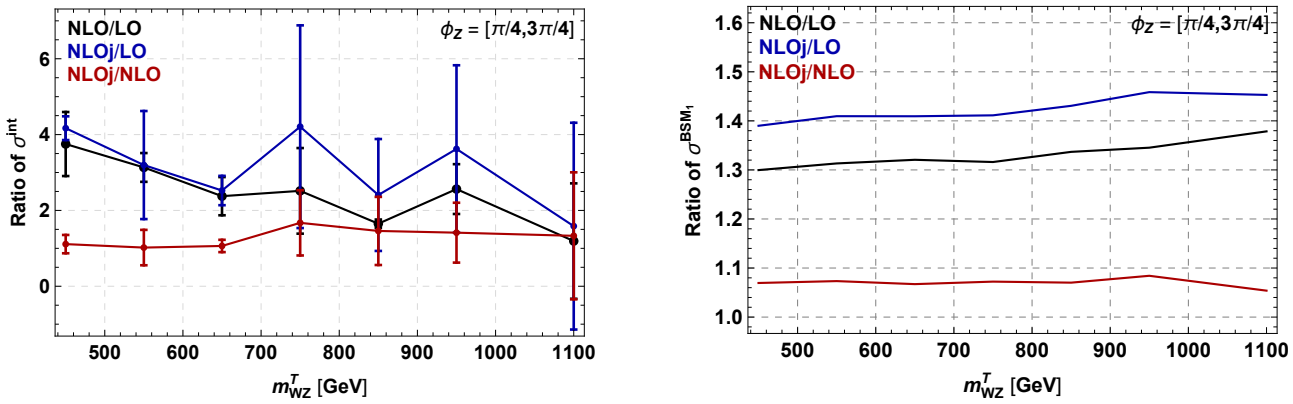

Figure 3.10: Differential distribution for the NLO/LO, NLO+j/LO and NLO+j/NLO ratios of $\sigma^{\rm int}$ (left panel) and $\sigma^{\rm BSM_1}$ (right panel) as a function of the WZ transverse mass.

computation time needed for the latter simulation, the results will be presented only at NLO accuracy in QCD.

3.6.3 Comparison of perturbative expansions for BSM scenario

Turning on the BSM operator O_{3W} and $O_{3\tilde{W}}$, we simulate LO and NLO events with the same strategy as for the SM case described in Section 3.6.2, in order to estimate the ratio between cross sections evaluated at different orders of accuracy in the perturbative expansion. The tools and cuts described in Section 3.6.1 are used.

Now one can proceed to the analysis of the various BSM contributions. Generically the production cross section in presence of the operators O_{3W} and $O_{3\tilde{W}}$ can be parametrized by

$$\sigma = \sigma_0 + \sigma^{\rm int} c_{3W} + \tilde{\sigma}^{\rm int} c_{3\tilde{W}} + \sigma^{\rm BSM_1} c_{3W}^2 + \sigma^{\rm BSM_2} c_{3\tilde{W}}^2 + \sigma^{\rm BSM_3} c_{3W} c_{3\tilde{W}}. \tag{3.6.3}$$

In Fig. 3.10 there is the comparison of the LO, NLO and NLO+j interference, $\sigma^{\rm int}$, (left) and quadratic, $\sigma^{\rm BSM_1}$, (right) terms of the cross section in presence of the CP-even operator O_{3W} in the angular region $\phi_Z \in [\frac{\pi}{4}, \frac{3\pi}{4}]$, as a function of the m^T_{WZ}. For the pure BSM term the κ-factor between NLO and LO turns out to be $\sim$ 1.3, only mildly growing with the parton energy of the process, and the addition of an extra jet in the matrix element only provides a small increase, around 5%, with respect to the NLO process, similarly to what has been found for the inclusive process in the SM case. On the other side, for the interference case, the κ-factor shows a slightly decreasing pattern with the energy of the system, reaching a value of $\sim$ 2 for $m^T_{WZ} \sim$ 1 TeV. Furthermore helicity selection rules are not applicable at NLO level leading to a mild restoration of the interference effects between the SM and BSM contributions (see Section 3.4 and [1, 48]). Additionally the off-shellness of the vector bosons also leads to the restoration of the interference, with the strength of the effect scaling as g^2 [49], similarly to the effect of the one loop electroweak corrections, which are ignored in the present study. One can notice that the statistical error in the determination of the NLO+j/LO and NLO+j/NLO ratios for $\sigma^{\rm int}$ can be quite large, almost around 50%, due to bigger uncertainties in the analysis of the interference at NLO+j accuracy. However, these statistical fluctuations do not affect

the precision on the results that will be shown for the c_{3W} and $c_{3\tilde{W}}$ bounds: they are obtained at NLO, without an extra jet emission, and at such level the uncertainty on the interference is smaller, around 10%.

3.6.4 Preliminary analysis at LO

Before moving to the more complete and accurate combined study of λ_Z and $\tilde{\lambda}_Z$ at NLO, done in [2], we firstly follow the analysis of [1], in which the focus is on the aTGC operator O_{3W} alone, with simulations performed at LO without taking into account detector effects on the angle smearing. It is useful in order to develop a qualitative idea of how much it is possible to improve the sensitivity to the $\text{BSM}_6\times\text{SM}$ interference term of the cross section by exploiting azimuthal angle distributions or by moving from the LO diboson production described with 4-point amplitudes. In this Section, effects of the virtual gluons are ignored. The $pp \to WZ \to lll\nu$ process is studied following the signal selection procedure presented in the experimental work [37] and using, for simulations, `MadGraph5` [38] with the model `EWdim6` [50] at LO. The results will be reported for the 14 TeV LHC collision energy and two benchmark luminosities, 300 and 3000 fb^{-1}.

It has been checked that the parton level simulation reproduces the acceptance at the particle level $A_{WZ} = 0.39$, for the experimental analysis at 8 TeV, done in [37]; it is defined with the ratio of the fiducial to the total cross section

$$\sigma^{tot}_{W^\pm Z} = \frac{\sigma^{fid}_{W^\pm Z\to l'\nu ll}}{B_W B_Z A_{WZ}}\,. \tag{3.6.4}$$

The fiducial cross section is

$$\sigma^{fid}_{W^\pm Z\to l'\nu ll} = \frac{N_{data} - N_{bkg}}{\mathcal{L}\, C_{WZ}} \times \left(1 - \frac{N_\tau}{N_{all}}\right)\,, \tag{3.6.5}$$

where the factor C_{WZ} simulates the detector efficiency, namely $C_{WZ} = N^{detector}_{events}/N^{particle}_{events} \approx 0.6$ [37], and it is approximate to be flavor universal. In Eq. (3.6.4) B_i denote the corresponding branching fractions; while the factor N_τ/N_{total} in (3.6.5) is the contribution of the leptons from τ decays, which is estimated to be of $\sim 4\%$ in [37] and thus might be neglected. $\mathcal{L}$ is the integrated luminosity; results will be calculated for $\mathcal{L} = 300$ fb^{-1} and 3 ab^{-1}.

The events, as in the final analysis described in Section 3.6.5, are binned according to their transverse mass m^T_{WZ} (bins of 100 GeV between $m^T_{WZ} = 100$GeV and $m^T_{WZ} = 1000$GeV, a bin $m^T_{WZ} \in [1000, 1200]$GeV and a bin $m^T_{WZ} \in [1200, 1500]$GeV). Furthermore, the emission of an extra hard jet is added, as discussed in Section 3.4, and a binning in the transverse momentum p^T_j of the jet is built as

$$p^T_j \in [0, 100],\ [100, 300],\ [300, 500],\ [500, \infty]\ \text{GeV}\,. \tag{3.6.6}$$

In this preliminary analysis, the coefficients in Eq. (3.5.7)-(3.5.8) are determined with parton level simulations. For the bin $p^T_j \in [0, 100]$ GeV we sum parton level simulations without jet

and with a single jet with $p_j^T \in [20, 100]$ GeV; for the SM input this approximation agrees well with the results obtained with `Madgraph5` together with `PYTHIA8` interface with showering and jet matching. For the events with soft jet, i.e. $p_j^T < 100$ GeV, the azimuthal angle ϕ_Z, defined in Eq. (3.3.18), is also binned, in order to resurrect a non vanishing interference term of the cross section with the effect described in Section 3.3. In particular, two categories are considered

$$\phi_Z \in [\pi/4, 3/4\pi] \quad \text{and} \quad \phi_Z \in [0, \pi/4] \cup [3\pi/4, \pi] \,. \tag{3.6.7}$$

These two bins correspond to negative and positive signs respectively for the $\cos(2\phi_Z)$ factor, that describes the ϕ_Z azimuthal modulation of the considered $O_{3W}\times$SM interference. One should notice that it is an angular function that is left unchanged under the ϕ_Z ambiguity shown in Eq. (3.3.19), that can thus be neglected. One may worry whether emission of a QCD jet can spoil the azimuthal angle modulation, however it has been checked that even for relatively hard jets $p_j^T \lesssim 100$ GeV the angular modulation remains an important effect and this makes these parton simulation results robust. On the other hand, for the higher p_j^T bins the binning in azimuthal angle gives only little improvement of the bounds, because the modulation effect becomes subdominant compared to energy growth due to additional hard jet. This is also the reason why for the analysis at NLO that will be shown in the following Sections the weight of the angular differential distribution decreases.

For each bin defined above, the cross section in the presence of the CP-even aTGC c_{3W} deformation is calculated. At first, we estimate the theory prediction according to the *leakage* method described in Section 3.5: a cut on WZ transverse mass is imposed in order to have the *leakage* defined in Eq. (3.5.5) below a certain desired precision for a chosen EFT cut-off. The coefficients $n_{SM}, n^e_{BSM^2}$ are calculated by switching off BSM and SM contributions respectively. For the interference term n^e_{int} this is not possible, since it is not a positive definite contribution. So in order to avoid any issues with the negative values of cross section, it has been fitted while keeping both SM and BSM contributions. This procedure generically can lead to large errors on the determination of the n^e_{int} coefficient, but the uncertainty is kept under control by performing a large enough number of simulations and iteratively choosing for the fit the values of c_{3W} maximizing the interference term.

The analysis has been performed for three different values of the invariant mass Monte Carlo cut-off: $\Lambda_{\rm MC} = 1, 1.5, 2$ TeV. These are reasonable choices in view of the current direct exclusion bounds and correspond to m^T_{WZ} cuts at 700, 1000, 1500 GeV respectively.

For the backgrounds we have followed closely the results in [37], obtained for 8 TeV center of mass energy, where it was shown that the dominant background for the anomalous TGCs is the SM W and Z boson production. The second most important background comes from the misidentified leptons $\sim 12\%$ and ZZ final state $\sim 7\%$ and the contribution of the $t\bar{t}$ is at percent level. Since most of these backgrounds come from the $q\bar{q}$ initial state (except for $t\bar{t}$ which is small) at 14 TeV we expect a very similar situation. In the study described here, only the SM weak boson production is considered, as a background; the other contributions will provide an additional increase of the background by $\sim 20\%$ and the relaxations of the bounds by $\sim 10\%$, which is within the precision level desired here. For systematic uncertainties the results in [37] are used, where it was reported that the dominant errors come from the muon and electron identification efficiencies and it was estimated to be at the level of 2.4%.

	Lumi. 300 fb^{-1}		Lumi. 3000 fb^{-1}		Q [TeV]
	95% CL	68% CL	95% CL	68% CL	
Excl.	[-1.06,1.11]	[-0.59,0.61]	[-0.44,0.45]	[-0.23,0.23]	1
Excl., linear	[-1.50,1.49]	[-0.76,0.76]	[-0.48,0.48]	[-0.24,0.24]	
Incl.	[-1.29,1.27]	[-0.77,0.76]	[-0.69,0.67]	[-0.40,0.39]	
Incl., linear	[-4.27,4.27]	[-2.17,2.17]	[-1.37,1.37]	[-0.70,0.70]	
Excl.	[-0.69,0.78]	[-0.39,0.45]	[-0.31,0.35]	[-0.17,0.18]	1.5
Excl., linear	[-1.22,1.19]	[-0.61,0.61]	[-0.39,0.39]	[-0.20,0.20]	
Incl.	[-0.79,0.85]	[-0.46,0.52]	[-0.41,0.47]	[-0.24,0.29]	
Incl., linear	[-3.97,3.92]	[-2.01,2.00]	[-1.27,1.26]	[-0.64,0.64]	
Excl.	[-0.47,0.54]	[-0.27,0.31]	[-0.22,0.26]	[-0.12,0.14]	2
Excl., linear	[-1.03,0.99]	[-0.52,0.51]	[-0.33,0.32]	[-0.17,0.17]	
Incl.	[-0.52,0.57]	[-0.30,0.34]	[-0.27,0.31]	[-0.15,0.19]	
Incl., linear	[-3.55,3.41]	[-1.79,1.75]	[-1.12,1.11]	[-0.57,0.57]	

Table 3.2: Exclusive (*Excl.*) bounds on $c_{3W}/\Lambda^2 \times \text{TeV}^2$ are obtain according to the method described in the main text, binning in ϕ_Z and p_j^T. Inclusive (*Incl.*) bounds are obtained with no binning and jet veto at $p_j^T \leqslant 100$ GeV. The bounds of the rows *Excl./Incl., linear* are obtained by including only the linear terms in c_{3W} in the BSM cross section. The total leakage in the various bins of m_{WZ}^T is $\lesssim 5\%$ for each value of Q.

The statistical analysis is performed with the Bayesian approach, where systematic errors are described with a single gaussian nuisance parameter ξ, as will be shown in Eq. (3.6.9).

The bounds on c_{3W}/Λ^2 obtained with this method are presented in Table 3.2, where the LHC prospects for 300 fb^{-1} as well as for 3 ab^{-1} luminosity (Lumi.) values are reported. Exclusive (*Excl.*) bounds are obtained according to the method described above, binning in ϕ_Z and p_j^T, while inclusive (*Incl.*) ones correspond to no binning in ϕ_Z and to $p_j^T \leqslant 100$ GeV cut. The total leakage in the various bins of m_{WZ}^T is imposed to be $\lesssim 5\%$ for each value of Q, that is roughly equal to the Monte Carlo cut-off Λ_{MC}; such bins are selected using Fig. 3.8.

The bounds of the rows *Excl./Incl., linear* are obtained by including only the linear terms in c_{3W} in BSM piece of the cross section. In the linear analysis, values of the Wilson Coefficient $|c_{3W}| \gtrsim 3$ lead to negative number of events. Nevertheless, such values lie outside the credibility intervals of the fit. In order to avoid this issue for arbitray values of c_{3W} during the scan, the following modification of (3.5.7) has been used

$$M_{th} = (n_{\text{SM}} + c_{3W}\, n_{int}^e) \times \theta(n_{\text{SM}} + c_{3W}\, n_{int}^e), \tag{3.6.8}$$

where the θ is the usual step function. Generically, this later procedure is of course inconsistent. However, comparing linear v.s. non-linear results gives a sense of how much sensitive are the bounds to the quadratic piece term BSM_6^2 in the cross section. In this respect, note that

the exclusive analysis sensitivity to the linear terms has drastically increased compared to the inclusive one. For instance, the gain from the second to the first row in Table 3.2 is very mild, implying that the bound is mostly proving the interference term. Instead, the bounds from the third to the fourth row drastically decrease implying that the consistent bound of the third row is giving a lot of power to the quadratic pieces in c_{3W}^2. This comparison illustrates the improvement from the differential distributions versus the inclusive analyses. Of course such a gain is always expected. However, in this case the improvement is dramatic because, as explained in Section 3.3, the interference terms of the differential cross section have a qualitatively different behavior, namely they grow with the center of mass diboson energy.

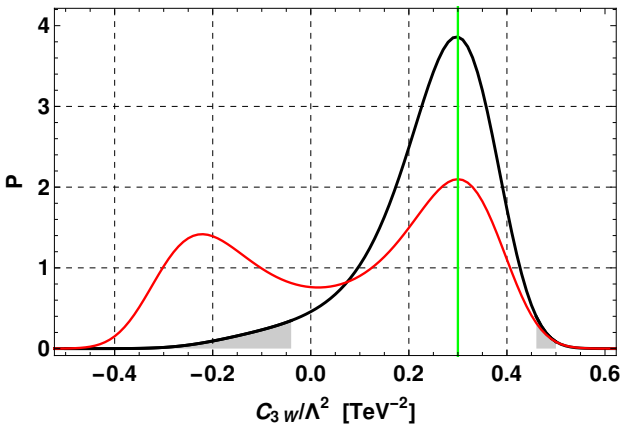

Figure 3.11: Posterior probability for the inclusive and exclusive analysis at LO after 3 ab^{-1} at LHC, see details in the main text.

This radical increase towards the sensitivity of the interference term is illustrated in Fig. 3.11. There, a signal corresponding to $c_{3W}/\Lambda^2 = 0.3$ TeV^{-2} has been injected. The red and black curves are posterior probabilities with m_{WZ}^T cut at 1500 GeV and correspond to inclusive and exclusive analysis respectively, the shaded grey area indicates the 95% credibility intervals for the exclusive analysis. One can clearly see that the considered differential distributions would be able to access the sign of the c_{3W} Wilson Coefficient otherwise hidden from the inclusive searches.

Further details of this preliminary analysis of $\mathcal{O}_{3W}$ at LO are provided in Appendix A. In particular, in Table A.2, there is a comparison of results obtained with one single differential distribution each time: both the distributions in p_j^T and in ϕ_Z bring an increase of sensitivity to the interference term, but the latter has a stronger effect. Indeed, the azimuthal binning reduces the confidence intervals by $\sim 20\%$ while the distribution in the transverse momentum of an extra hard jet only by $\sim 10\%$; furthermore the former provides the major contribution to bounds in the case in which only the c_{3W} linear term in the EFT expansion is considered.

Thus, in the more accurate analysis that will be presented in the following Sections, one has to remember that the azimuthal angular distribution allows us to gain stronger improvement, with respect to NLO effects, in the sensitivity to λ_Z anomalous TGC and in particular to the interference between the associated BSM amplitude and the SM. As a consequence, even

performing simulations and analysis beyond leading order in the perturbation theory, the possibility to exploit angular modulation can be useful for a better study of O_{3W} and $O_{3\tilde{W}}$ deformations.

3.6.5 Sensitivity to the BSM operators

In [2], we proceed in setting the bounds on the c_{3W} and $c_{3\tilde{W}}$ Wilson Coefficients as follows. The events, that are simulated as explained in 3.6.1 and reproducing the detector effects on the angular variables by applying Eq. (3.6.2), are categorized with respect to the WZ system transverse mass, with m^T_{WZ} bins between [0,1000] GeV in steps of 100 GeV, then [1000,1200] GeV and [1200,1500] GeV bins, as done in the analysis described in Section 3.6.4. Furthermore, angular binning is applied, since, as shown with the preliminary analysis of the previous Section, it can be useful even at the next to leading order, at which the interference term of the cross section is intrinsically different from zero and growing with energy. An azimuthal distribution is constructed with four ϕ_Z and two ϕ_W bins, equally spaced in the range 0 to π. They correspond to different combinations of signs for the $\cos(2\phi_Z)$, $\sin(2\phi_Z)$ and $\cos(2\phi_W)$ factors that enter in the modulation, shown in Eq. (3.3.12), which characterizes the angular differential distribution of the BSM$_6$×SM interference in presence of O_{3W} and $O_{3\tilde{W}}$ aTGC operators. These factors are invariant under the azimuthal ambiguities $\phi_Z \leftrightarrow \phi_Z - \pi$ and $\phi_W \leftrightarrow \pi - \phi_W$, while the $\sin(2\phi_W)$ term cancels upon the uncertainty on ϕ_W, as explained in Section 3.3.4. On the other hand, for simplicity a binning in the p^T of extra jets is not applied, since its effects are milder with respect to the ones from angular distributions, as seen in the previous Section.

Only the SM irreducible WZ background is considered, which is the main source of background for this process [33], and a global efficiency of 0.6 is imposed, for the final state reconstruction for all lepton flavor combinations. Then, by assuming a Poissonian distributed statistics, the statistical analysis is done using the Bayesian approach, where systematical errors are estimated using one nuisance parameter ξ, normally distributed

$$p(N_{\rm th}|n_{\rm obs}) \propto \int d\xi e^{-\xi N_{\rm th}} (\xi N_{\rm th})^{n_{\rm obs}} \exp\left[\frac{(\xi-1)^2}{2\sigma^2_{syst}}\right] . \tag{3.6.9}$$

The binning in ϕ_W turns out to have a marginal impact on the limits determination, which is due to the large smearing on the ϕ_W variable with respect to Z decay products azimuthal angles. Binning events with respect to ϕ_Z, ϕ_W and m^T_{WZ}, the 95% posterior probability limits on c_{3W} and $c_{3\tilde{W}}$ shown in Fig. 3.12 are obtained. The limits are shown as a function of the maximum m^T_{WZ} bin value used for the computation of the bounds, that for a fixed desired precision can be made correspond to a certain EFT cut-off, as in Fig. 3.8. An integrated luminosity of 3000 fb^{-1} is taken into account, i.e. corresponding to the end of the high luminosity phase of the LHC, and a systematic error of 5% is assumed.

Then, in Fig. 3.13, a maximum value of 1500 GeV, for the considered m^T_{WZ} bins, is fixed and we show the 68% and 95% limits in the $c_{3W} - c_{3\tilde{W}}$ plane assuming the null hypothesis of SM (left panel) or of a signal injection with $c_{3W} = c_{3\tilde{W}} = 0.4$ TeV^{-2} (right panel), again with a systematic uncertainty of 5% and an integrated luminosity of 3000 fb^{-1}. There the black and red curves correspond to the probability contours with and without the binning in the ϕ_Z and

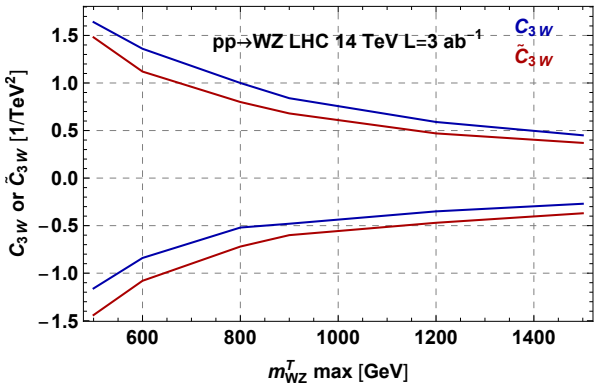

Figure 3.12: 95% bound on the c_{3W} and $c_{3\tilde{W}}$ Wilson Coefficients computed with four and two equally spaced angular bins for ϕ_Z and ϕ_W respectively, as a function of the largest WZ system transverse mass bin used for the 14 TeV LHC with 3000 fb^{-1} of integrated luminosity. A systematic error of 5% has been assumed.

ϕ_W angles and the shaded areas in the left panel correspond to the bounds derived from the non observation of a neutron and electron EDM, discussed in Section 3.8.

We observe that the use of the azimuthal variables only marginally improves the limits when the SM is assumed: adding angular distribution, we restrict the bounds only by $\sim 5\%$. The situation is a bit different in the LO analysis of λ_Z, performed in Section 3.6.4, where one can see that a difference of $\sim 10 - 20\%$ arises when we add angular binning. This comes out from the combination of three different effects. Firstly, we are considering both the linear and the quadratic term in the EFT expansion, where the latter is not affected from the helicity selection rule cancellation and is not enhanced by the kind of angular binning used here to resurrect the interference term. It turns out, as we will show in the next paragraph, that the quadratic contribution to bounds is more important with respect to what happened in Table 3.2, in which only the CP-even operator was considered, without virtual gluons and detector effects. Secondly the helicity selection rules are violated by QCD NLO effects, as explained in Section 3.4, and thus the resurrection of a non vanishing interference is present even without angular differential distribution. Lastly, the imposition of kinematic cuts to select the analysis signal region have also the effect of restoring the interference between the SM and the BSM amplitude: in Section 3.3.5 it has been shown that some of the cuts lead to a partial selection of the azimuthal angles, even if for the $W\gamma$ process the effect is much stronger and the smaller number of final state particles makes it easier to understand the kinematic origin of this behavior. However, one can notice that the use of the azimuthal angles is crucial in the case of a signal discovery at the LHC. As illustrated in the right panel of Fig. 3.13 these variables can in fact be used to disentangle the contribution of the O_{3W} and $O_{3\tilde{W}}$ operators as well as to measure the sign of the Wilson Coefficients.

In order to analyze further the importance of the linear terms in the expansion of the cross section in Eq. (3.6.3), it is useful to extract bounds for the Wilson Coefficients without considering the quadratic terms in the EFT expansion. In doing that, one has to avoid the appearance of negative estimations for the expected number of events, using the modification shown in Eq. (3.6.8). The binning in the azimuthal angles increases the sensitivity on the

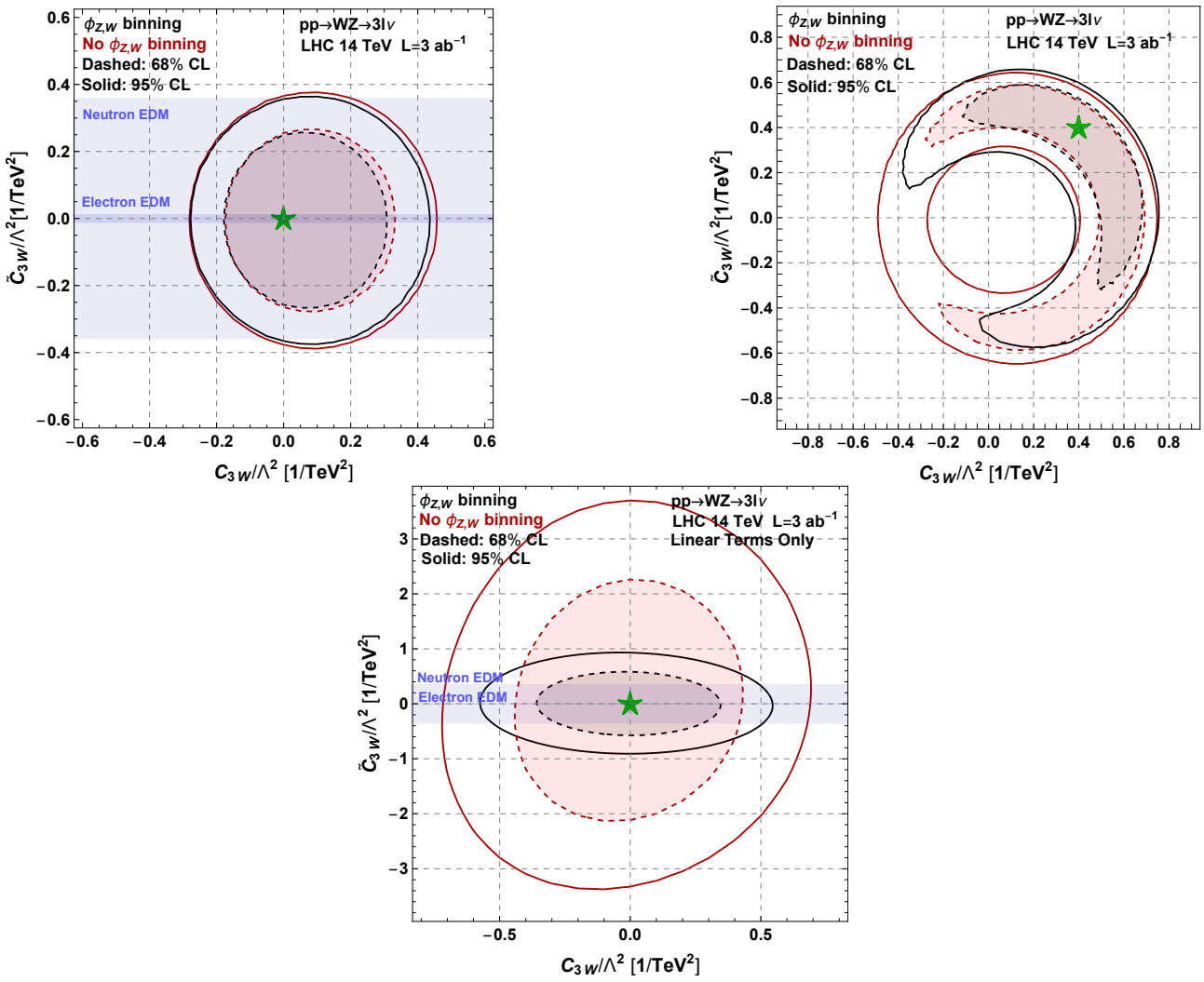

Figure 3.13: 68% (dashed) and 95% (solid) posterior probability contours for the analysis with (black) and without (red) the binning in the ϕ_Z and ϕ_W angles (see main text for more details). The left and right hand upper plots are obtained assuming the SM and a BSM signal with $c_{3W} = c_{3\tilde{W}} = 0.4$, both represented by a green star. The light and dark shaded blue correspond to the limits obtained by the non observation of a neutron and electron EDM discussed in Section 3.8. On the lower plot there are the exclusion contours obtained assuming only the linear terms in the EFT expansion. Only events with $m^T_{WZ} < 1.5$ TeV are used.

$O_{3\tilde{W}}$ by a factor ~ 4, while it has a marginal improvement on O_{3W}, due the modulation from cuts effect discussed in the Section 3.3.5: only for the CP-even interference term a non trivial ϕ_W distribution can be built, due to the fact that a $\sin(2\phi_W)$ factor is washed out by angular ambiguities. Comparing the *linear* and *quadratic* bounds, one can see that the former are roughly factor of two worse for both the O_{3W} and the $O_{3\tilde{W}}$ operators. This means that our analysis can be applied only to the UV completions for which the contribution of the dimension 8 operators is smaller than both the quadratic and linear dimension 6 terms, that have almost the same weights on the computation of confidence intervals. Anticipating the results of the Section 3.7.1 and Section 3.9, we find that for $W\gamma$ analysis at 14 and 27 TeV and for WZ

analysis at 27 TeV the bounds are instead dominated by the linear terms, similarly to what happened in the preliminary analysis of Section 3.6.4.

Comparing Fig. 3.12 with the results of Table 3.2, one can see that adding NLO and detector effects the bounds on c_{3W} are enlarged by a factor ~ 1.5 and the obtained interval becomes more asymmetric, since, as explained, there are effects leading to a non zero interference even upon integration over angular phase space.

One can wonder for which kind of theories the obtained bounds are relevant. We can see that at most we are getting towards the constraints $c_{3W,3\tilde{W}}/\Lambda^2 \lesssim 0.4/\text{TeV}^2$. Weakly coupled renormalizable theories lead to the Wilson Coefficients which are at least one order of magnitude smaller, as can be seen in (3.2.28), unless we are dealing with abnormally large multiplicities of new electroweak states just above the LHC reach. At the same time more strongly coupled theories can lead to larger values of Wilson Coefficients, to which we can be sensitive with the current LHC precision.

3.7 Analysis and results: $pp \to W\gamma$ process

Another process that can be used to test the CP-Even and CP-Odd operators of Eq. (3.1.11) and (3.1.13) is $pp \to W^{\pm}\gamma$. As for the WZ case, also here a fully leptonic final state is considered, since, despite having a smaller branching ratio and the presence of an invisible neutrino, it is generally a cleaner channel with respect to the hadronic counterpart. The comparison of the LO and higher orders samples is not performed here for the $W\gamma$ process, since the validation of the simulation framework is already done for the WZ case, and from the beginning of the discussion the event samples are generated at NLO accuracy.

3.7.1 Sensitivity to the BSM operators

We now proceed to the analysis of the $W\gamma$ final state as done in [2], closely following the 7 TeV CMS results reported in [34], where a measurement of the $W\gamma$ inclusive cross section has been performed. As a first step, fully leptonic $W\gamma$ events have been generated for a center of mass energy of 7 TeV and the same cuts enforced in the considered CMS search have been applied. In particular CMS required the presence of a lepton with $p_T > 35$ GeV and $|\eta| < 2.5$ and of a photon with $p_T > 15$ GeV and $|\eta| < 2.1$ and asked for a separation $\Delta R(\ell, \gamma) > 0.7$. A cut on $M_T^W > 70$ GeV is also applied that, as mentioned, strongly suppresses the backgrounds from processes without genuine missing transverse energy. Then by comparing the obtained NLO predictions with the results of [34] one can extract the efficiencies for reconstructing the $\ell\gamma$ final state, which have been quantified to be 0.45 for the electron and 0.7 for the muon. Then, the same efficiency values are used for the case of the 14 TeV LHC, in which a 20 GeV cut on p_T^{γ} has been imposed at generator level. In order to estimate the detector effects on the determination of the azimuthal angle, one can follow exactly the same procedure as for the

WZ process (see Eq. 3.6.2) and the following smearing function are found

$$\phi_W^{\rm smear} = \phi_W \pm \Delta\phi_W^{\rm smear}, \quad \Delta\phi_W^{\rm smear} = \begin{cases} [0, 0.4] \text{ with probability } 0.63 \\ [0.4, \pi/2] \text{ with probability } 0.37. \end{cases} \tag{3.7.1}$$

One can notice that in the case of the $W\gamma$ process the irreducible SM background makes only $\sim 50\%$ of the total event rate [34]. For this reason, in the analysis of [2] we have considered an equal yield for the irreducible and reducible background. This has been practically done by multiplying by a factor of two the σ_0 coefficients of the Eq. (3.6.3) without touching the interference terms, since, clearly, the reducible background does not interfere with the BSM operators under study. The irreducible background is again computed at NLO QCD accuracy as done for the WZ case. The events are binned with respect to two angular ϕ_W intervals, defined as $\phi \in [\pi/4, 3\pi/4]$ and $\phi \in [0, \pi/4] \cup [3\pi/4, \pi]$, and with respect to the $W\gamma$ system transverse mass defined as

$$\left(m_{W\gamma}^T\right)^2 = \left(\sqrt{m_W^2 + \sum_{i=x,y} (p_i^e + \not{p}_i)^2} + p_T^\gamma\right)^2 - \sum_{i=x,y} \left(p_i^e + \not{p}_i + p_i^\gamma\right)^2, \tag{3.7.2}$$

with $m_{W\gamma}^T$ bins between [0,1000] GeV in steps of 100 GeV, [1000,1200] GeV and [1200,1500] GeV. This binning variable allows to make the comparison with the WZ analysis as clear as possible. By adopting this procedure, the results illustrated in Fig. 3.14 and Fig. 3.15 are obtained. In Fig. 3.14 the bounds are shown as a function of the maximum $m_{W\gamma}^T$ bin value used for the computation and for an integrated luminosity of 3000 fb^{-1}, assuming a systematic error of 5% in Eq. (3.6.9). It turns out that the dependence on the maximum $m_{W\gamma}^T$ is different for the CP-even and CP-odd operators. This is due to the fact that we can only restore the interference for the CP-even operator, due to the ambiguity in the W boson decay azimuthal angle described in Eq. (3.3.21). We have also checked that for the obtained bounds with $m_{W\gamma}^T \lesssim 1$ TeV the yields for the CP-even operator are dominated by the interference terms. On the other side at higher energies the quadratic terms start to dominate and the constraints on both the CP-even and CP-odd operators become similar. Then, in Fig. 3.15 a maximum value of 1500 GeV for $m_{W\gamma}^T$ has been fixed and the 68% and 95% confidence level limits are shown. There, the black and red curve are computed by binning in the ϕ_W angle or with a ϕ_W inclusive analysis respectively; the left and right hand plots correspond respectively to the assumptions of SM only or a BSM signal with $c_{3W} = -c_{3\tilde{W}} = 0.3$. Again, also the bounds from the neutron and electron EDM non observation are shown; they will be discussed further in the following Section. As for the WZ case, it is evident that for the SM like signal the binning in the ϕ_W angle practically does not change the results. This is a consequence, together with NLO contributions, of *modulation from cuts* effect described in the Section (3.3.5), since the hard cut on the M_T^W in combination with a high-p_T of the photon automatically select the value of the W decay azimuthal angle to be close to $\pi/2$. This effect is stronger in $W\gamma$ analysis, due to a more strict M_T^W cut; indeed, differently from the WZ case, one can see on the right panel of Fig. 3.15 that even assuming an injected signal, the results remain the same with and without the azimuthal angle binning. As expected from Eq. (3.3.13) and Eq. (3.3.21) the analysis can differentiate the sign of the CP-even interaction c_{3W} but it is insensitive to the sign of the CP-odd $c_{3\tilde{W}}$ coupling. In the lower panel of the Fig. 3.15 one can see the bounds obtained by

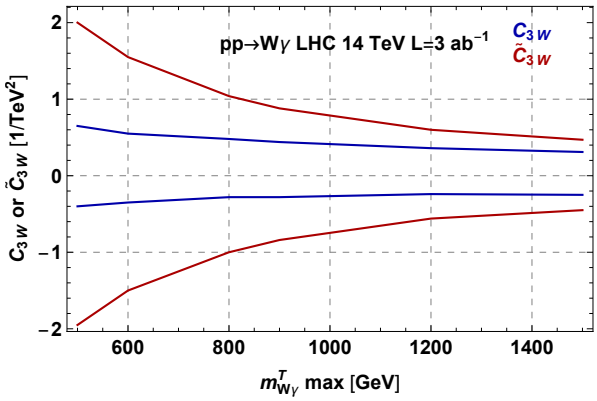

Figure 3.14: 95% bound on the c_{3W} and $c_{3\tilde{W}}$ Wilson Coefficients computed with angular ϕ_W bins (defined in the text) as a function of the largest $W\gamma$ system transverse mass bin used for the 14 TeV LHC with 3000 fb^{-1} of integrated luminosity. A systematic error of 5% has been assumed.

including only the linear terms in the production cross section Eq. (3.6.3). As expected the bounds are blind to $c_{3\tilde{W}}$ but for c_{3W} they are similar to the ones obtained by the analysis with the complete $\mathcal{O}_{3W}$ and $\mathcal{O}_{3\tilde{W}}$ EFT.

3.8 Bounds from EDMs

The CP-odd operator $O_{3\tilde{W}}$ of Eq. (3.1.13) gives also a one-loop contribution to the neutron and electron Electric Dipole Moments (EDMs). Since there are strong constraints from the non observation of EDMs of elementary particles, these null measurements can potentially lead to tight bounds on $c_{3\tilde{W}}$. In particular the effective operator

$$O_\gamma = ie\frac{\tilde{\lambda}_\gamma}{M_W^2} W^+_{\lambda\mu} W^{-,\mu}_{\nu} \tilde{F}^{\nu\lambda} \tag{3.8.1}$$

generates the EDM operator for a fermion ψ

$$O_{\rm EDM} = \frac{d_f}{2}\bar{\psi}\sigma_{\mu\nu}\tilde{F}^{\mu\nu}\psi, \tag{3.8.2}$$

where $\tilde{F}^{\mu\nu}$ is the dual of the electromagnetic field strength tensor and

$$d_f = \frac{g^2 e\tilde{\lambda}_\gamma}{64\pi^2 M_W^2} m_\psi \tag{3.8.3}$$

as it has been derived in [51, 52].

For the case of the neutron, using the form factors of [53], one obtains

$$d_n \simeq (1.77 d_d - 0.48 d_u - 0.01 d_s) \simeq 1.3\tilde{\lambda}_\gamma \times 10^{-23} e \text{ cm}. \tag{3.8.4}$$

By using the latest result reported in the Particle Data Group [54], namely $|d_n| < 0.3 \times 10^{-25}$ e cm at 90% CL, the following limit on the anomalous coupling $\tilde{\lambda}_\gamma$ can be derived

$$|\tilde{\lambda}_\gamma| \lesssim 0.0023 \tag{3.8.5}$$

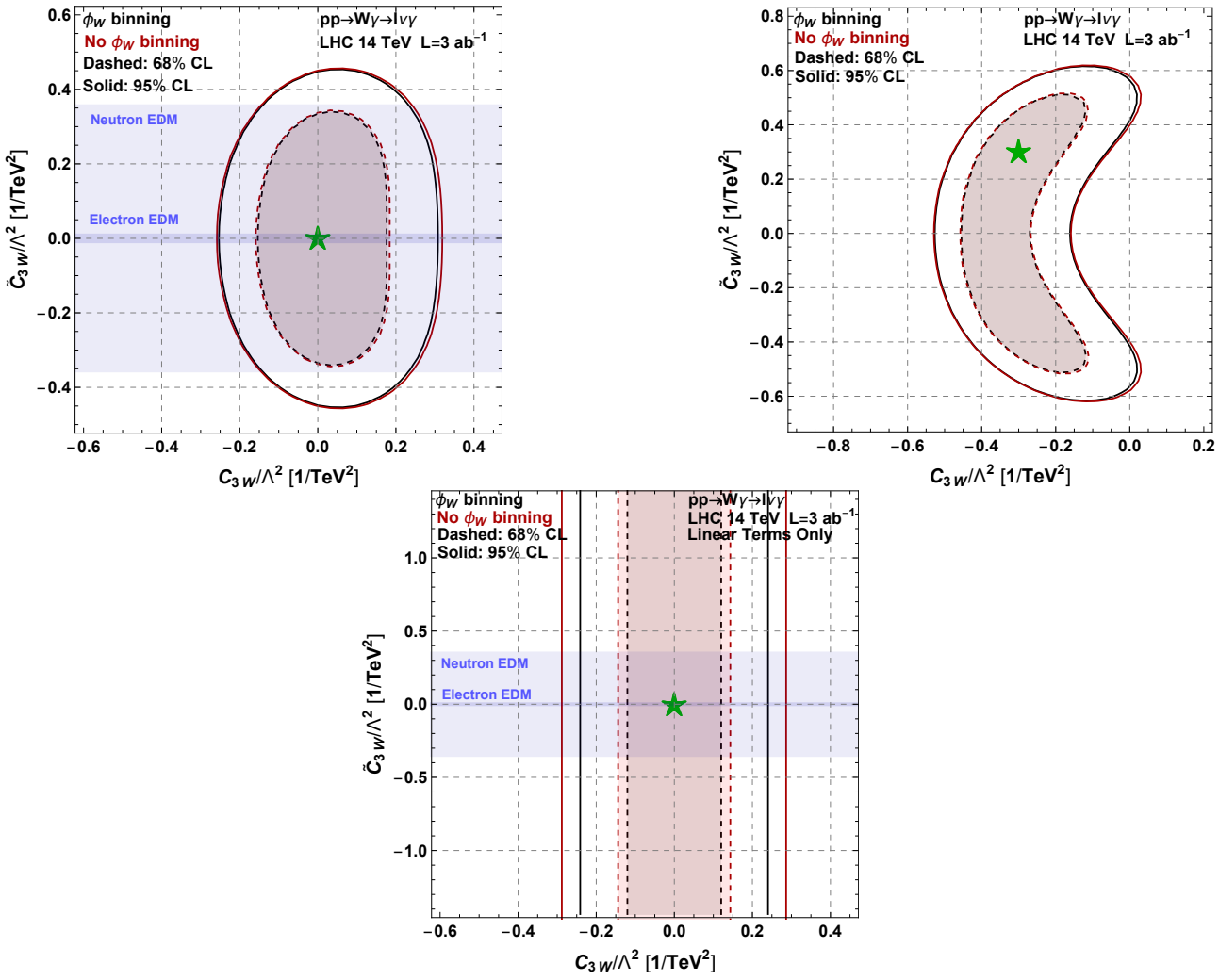

Figure 3.15: 68% (dashed) and 95% (solid) posterior probability contours for the analysis with (black) and without (red) the binning in the ϕ_W angle (see main text for more details). The left and right hand upper plots are obtained assuming the SM and a BSM signal with $-c_{3W} = c_{3\tilde{W}} = 0.3$, both represented by a green star. The light and dark shaded blue correspond to the limits obtained by the non observation of a neutron and electron EDM discussed in Section 3.8. On the lower plot there are the exclusion contours obtained assuming only the linear terms in the EFT expansion. Only events with $m^T_{W\gamma} < 1.5$ TeV are used.

which translates in an upper bound on the WC of the CP-odd $d = 6$ operator $\mathcal{O}_{3\tilde{W}}$

$$\left|\frac{c_{3\tilde{W}}}{\text{TeV}^2}\right| \lesssim \frac{0.36}{\text{TeV}^2}\,. \tag{3.8.6}$$

This constraint is of the same order as the bounds attainable at the end of the HL-LHC phase from the precision measurements of the $W\gamma$ and WZ processes.

On the other side the experimental limit on the electron EDM is much stronger than the one of the neutron: $|d_e| < 0.87 \times 10^{-28} e$ cm at 90% CL [54]. This leads to a much stronger constraint on the Wilson Coefficient of the CP violating triple gauge coupling operator. Namely

we obtain

$$|\tilde{\lambda}_\gamma| \lesssim 8.3 \times 10^{-5}, \tag{3.8.7}$$

which implies

$$\left|\frac{c_{3\tilde{W}}}{\text{TeV}^2}\right| \lesssim \frac{0.013}{\text{TeV}^2}\,. \tag{3.8.8}$$

It is a bound far beyond the reach of current and future collider experiments.

However, these bounds can potentially be relaxed in presence of additional new physics contribution affecting the O_{EDM} operator of Eq. (3.8.2) and cancelling against the one-loop contribution arising from $O_{3\tilde{W}}$. This possibility will not be discussed here any further, stressing again that the limits arising from the non observation of an electron EDM are potentially more constraining that the ones arising from direct LHC measurements.

3.9 High Energy LHC

By the end of 2035 the LHC experiments ATLAS and CMS will have collected $\sim$ 3 ab^{-1} of integrated luminosity each, ending the HL phase of the CERN machine. Various collider prototypes have been proposed in the recent years for the post LHC era. These include leptonic machines such as ILC and CLIC ideal for performing precision measurements of the Higgs couplings, and hadronic machines, as the FCC-hh, a 100 TeV proton-proton collider, with huge potentiality for the discovery of resonant new physics above the TeV scale, that however requires enormous efforts, among which a new $\sim$ 100 Km tunnel. Hence in the last years a lot of attention has been given to the possibility of building a higher energy proton collider within the LHC tunnel. Thanks to new techniques with which it would be possible to build 16 T magnets, a centre of mass energy of 27 TeV can be envisaged. This doubling of energy with respect to the LHC can offer great physics opportunities [55] both for on-shell particle productions, but also for indirect measurements as the ones discussed here.

In this Section there is an analysis of the High Energy (HE) prospects for the measurements of c_{3W} and $c_{3\tilde{W}}$ Wilson Coefficients; procedures similar to the ones discussed in Section 3.6 and Section 3.7 are applied. We focus on two benchmark of integrated luminosities: 3 ab^{-1} and 15 ab^{-1}. The results are shown in Fig. 3.16 - Fig. 3.19, in complete analogies with the figures of the previous Sections.

For what concerns the WZ analysis, one can see that the relative improvement from the binning in the azimuthal ϕ_Z and ϕ_W angles increases compared to the 14 TeV analysis, since the derived bounds are getting closer to the values of the Wilson Coefficients when the interference term dominates the cross section. Similar effects hold for the $W\gamma$ process. Indeed, the effect of the modulation from cuts becomes less important since, for the same values of the $m^T_{W\gamma}$ variable, larger values of the longitudinal momentum are expected at higher collision energies, so that the selection of $\phi_W \sim \pi/2$ bin becomes less strong, as discussed in Section 3.3.5.

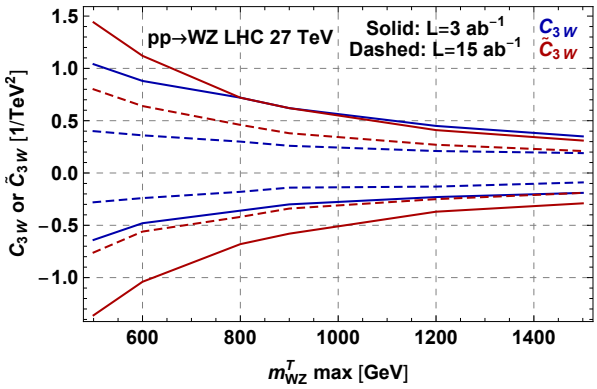

Figure 3.16: 95% bound on the c_{3W} and $c_{3\tilde{W}}$ Wilson Coefficients computed with four and two equally spaced angular bins for ϕ_Z and ϕ_W respectively, as a function of the largest WZ system transverse mass bin used for the 27 TeV LHC with 3 ab^{-1} (solid) and 15 ab^{-1} (dashed) of integrated luminosity. A systematic error of 5% has been assumed.

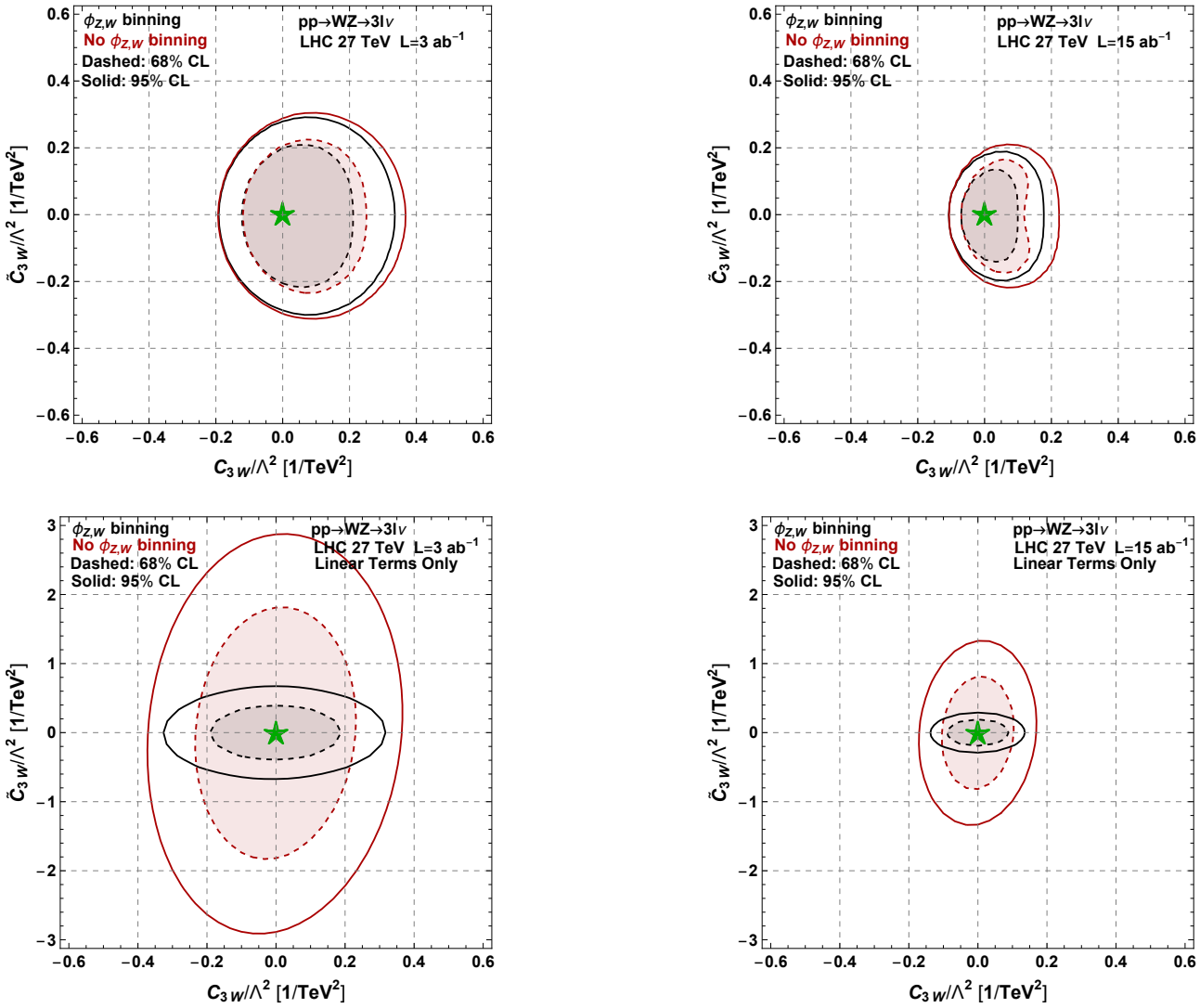

Figure 3.17: 68% (dashed) and 95% (solid) posterior probability contours for the WZ at 27 TeV analysis with (black) and without (red) the binning in the ϕ_Z and ϕ_W angles (see main text for more details). Only events with $m^T_{WZ} < 1.5$ TeV are used. The upper and lower panels correspond to the limits obtained with and without the inclusion of the quadratic term in the EFT expansion respectively.

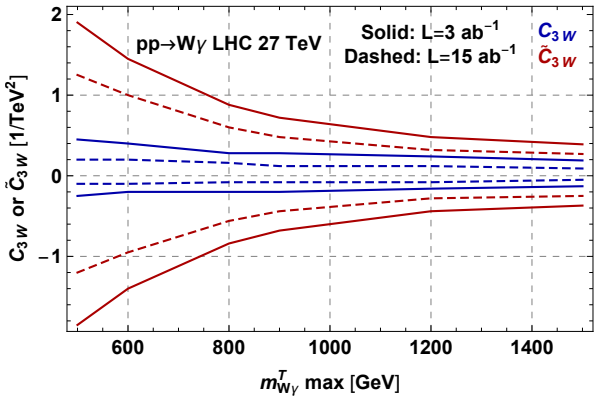

Figure 3.18: 95% bound on the c_{3W} and $c_{3\tilde{W}}$ Wilson Coefficients computed with two equally spaced angular ϕ_W bins as a function of the largest $W\gamma$ system transverse mass bin used for the 27 TeV LHC with 3 ab^{-1} (solid) and 15 ab^{-1} (dashed) of integrated luminosity. A systematic error of 5% has been assumed.

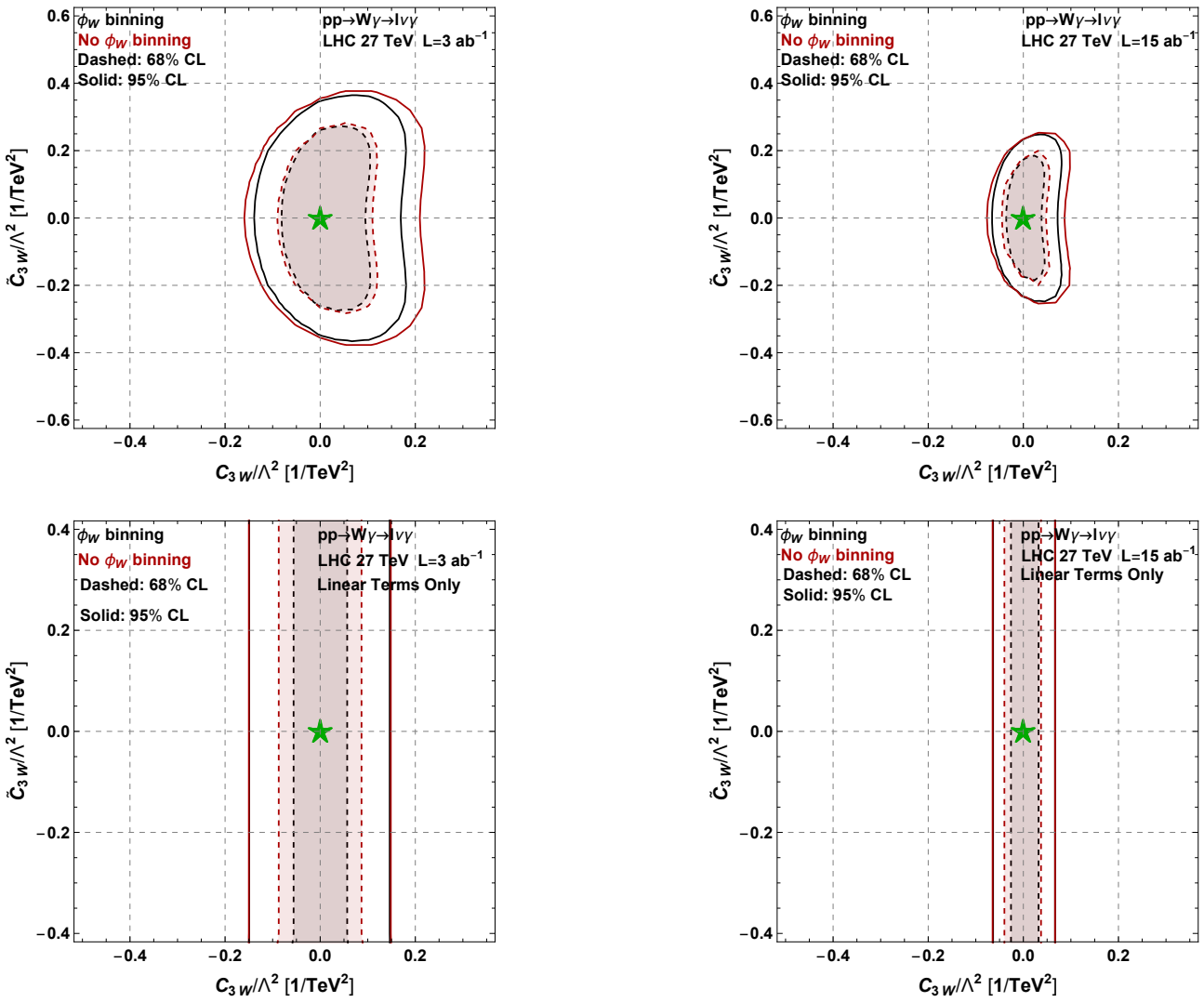

Figure 3.19: 68% (dashed) and 95% (solid) posterior probability contours for the $W\gamma$ at 27 TeV analysis with (black) and without (red) the binning in the ϕ_W angle (see main text for more details). Only events with $m^T_{W\gamma} < 1.5$ TeV are used. The upper and lower panels correspond to the limits obtained with and without the inclusion of the quadratic term in the EFT expansion respectively.

Chapter 4

Flavor Anomalies

Another very interesting and promising sector to search for new physics evidence is provided by semileptonic B decays. Indeed, in the last few years, experimental observations have pointed out some hints of Lepton Flavor Universality (LFU) violation in charged and neutral current semileptonic b decays $b \to cl\nu$ and $b \to sll$, showing a discrepancy with respect to the Standard Model expectations. These are the so-called *flavor anomalies*, since the statistical significance of these experimental results is not large enough to claim a discovery. In the most recent data [56], not a single measurement is enough significant to claim new physics discovery and there has been a slight decrease in the overall statistical significance, with respect to the previous analysis. However, different measurements show an internal consistency and the combined significances are 3.7σ for neutral current interactions and 3.1σ in charged current ones. There are deviations also in other measurements: the $B_c \to J/\Psi$ ratio [57]; polarization observables in charged current interactions such as $F_L^{D^*}$, i.e. the D^{*-} polarization in the decay $B^0 \to D^{*-}\tau^+\nu_\tau$ [58], and $\mathcal{P}_\tau^{D^*}$, i.e. the τ polarization in the decay $\bar{B} \to D^*\tau^-\bar{\nu}_\tau$ [59]; angular distributions in the neutral current processes $B \to K^*\mu^+\mu^-$ [60] and $B_s^0 \to \mu^+\mu^-$ [61], [62]. These discrepancies cannot be explained within SM and, at the same time, similar LFU violating effects have not been observed in the K and π decays: this suggests that the new physics that might account for the experimental anomalies observed in the B sector should be coupled mainly to the third fermion generation.

A unique explanation for both anomalies would imply a non-trivial Beyond Standard Model dynamics at TeV scale, possibly related to the solution of SM flavor puzzle. Classes of SM UV completions, that are interesting *di per se*, have been studied in order to account for the measured discrepancies without violating constraints from other correlated observables.

The EFT approach, discussed in Chapter 2, can be used to describe low energy effects that might explain these flavor anomalies, through $d = 6$ effective operators, in a way as model independent as possible. However, charged current anomalies arise in processes that are tree-level interactions in SM; thus, a certain fraction of BSM contribution to the branching ratios is a quite large effect and the explanation requests a quite light new physics scale, of the order of 1 TeV. Therefore, the description of the discrepancies compatible with other low energy observables is not feasible in a completely model independent way.

One has to assume the presence of some specific heavy mediator generating the effective vertices, which might provide some cancellation in correlated observables that are strongly constrained. Thus, simplified models are largely used, in order to grant the consistency with low energy observables and high-p_T data. As will be discussed, one could consider mediators having the same quantum numbers of electroweak SM gauge bosons, but also leptoquarks, which is to say bosons that couple to a quark and a lepton. One of the best combined explanations of data is provided by models with a single vector leptoquark $U_1 \sim (\mathbf{3}, \mathbf{1})_{2/3}$, as shown in [63]. This mediator will be indeed taken into account also in the present analysis. After the most recent data, possibility of combined explanation is even higher, due to the decrease in the tension of the processes involved in the anomalies with high-p_T and low energy data, since the deviation from SM has become lower. Once successful effective descriptions of flavor anomalies with simplified models are found, one may wonder if they could be embedded within a consistent UV completion, which might be of large interest *di per se* as the study of a possible extension of SM useful to address some of the experimental or theoretical puzzles. This is also motivated by the fact that in simplified models the presence of non renormalizable Lagrangians implies that only a limited set of low energy observables can be reliably estimated: the ones that arise at tree-level from effective four fermion vertices and some of the ones that emerge at one-loop level. In the literature one can find some good examples of these efforts, such as the ones in [64, 65, 66, 67, 68, 69, 70, 71].

This Chapter will be mainly focused on the analysis of the charged current anomalies, namely on the ratios R_D and R_{D^*} defined in the following way

$$R_{D^{(*)}} = \frac{\mathcal{B}\left(B \to D^{(*)}\,\tau\,\nu\right)}{\mathcal{B}\left(B \to D^{(*)}\,\ell_0\,\nu\right)}\,, \tag{4.0.1}$$

where the ℓ_0 stands for either e or μ. Indeed, a consistent explanation of this kind of anomalies is more challenging with respect to the description of neutral current flavor anomalies and requires a stronger NP effect. It suggests the presence of some (heavy) scalar or vector mediator integrated out at tree-level, whose study might be useful in many contexts.
The ratios of branching ratios are taken into account in such a way that in the considered R_D and R_{D^*} many theoretical uncertainties cancel out between numerator and denominator, ending up with quite clean observables.

The experimental results obtained by the Heavy Flavour Averaging Group (HFLAV) in 2016 [72] and in 2019 [73], with the latest Belle measurements [56], as well as the SM predictions, are summarized in Table 4.1 and Fig. 4.1, for R_D and R_{D^*}.

It can be seen how in the latest measurements the deviation from the SM expected values is slightly decreased. In Table 4.1 also three other relevant recent measurements are shown, namely $P_\tau(D^*)$ and $F_L^{D^*}$, described above, and $R_{J/\psi}$, a ratio similar to Eq. (4.0.1) for the decay $B_c \to J/\psi\,\tau\,\nu$. The determination of these observables is however rather imprecise at the moment. It can be seen that a successful explanation of the $R_{D^{(*)}}$ anomalies requires a new physics (NP) contribution of the order of at least 10 - 20% of the SM contribution to the branching ratio. As anticipated, since the SM contribution is generated at the tree-level by $W^\pm$ boson exchange, this is a rather large effect, which puts any NP explanation under strong pressure arising from experimental measurements of other $\Delta F = 1$ and $\Delta F = 2$ processes, electroweak precision observables and direct searches at the LHC.

Observable	SM prediction		Measurement	
R_D	0.300 ± 0.008	[74]	0.407 ± 0.046	[72]
	0.299 ± 0.011	[75]	$0.307 \pm 0.037(\text{stat.}) \pm 0.016(\text{syst.})$ (2019)	[56]
	0.299 ± 0.003	[76]	$0.34 \pm 0.027(\text{stat.}) \pm 0.013(\text{syst.})$ (2019)	[73]
R_{D^*}	0.252 ± 0.003	[77]	0.304 ± 0.015	[72]
	0.260 ± 0.008	[78]	$0.283 \pm 0.018(\text{stat.}) \pm 0.014(\text{syst.})$ (2019)	[56]
			$0.295 \pm 0.011(\text{stat.}) \pm 0.008(\text{syst.})$ (2019)	[73]
$P_\tau(D^*)$	-0.47 ± 0.04	[78]	$-0.38 \pm 0.51(\text{stat.})\, ^{+0.21}_{-0.16}(\text{syst.})$	[79, 80]
$F_L^{D^*}$	0.441 ± 0.006	[81]		
	0.457 ± 0.010	[82]	$0.60 \pm 0.08(\text{stat.}) \pm 0.04(\text{syst.})$	[58]
$R_{J/\psi}$	0.290		0.71 ± 0.25	[83]

Table 4.1: Observables, their SM predictions and the experimentally measured values. The experimental averages for R_D and R_{D^*} shown in the third column are based on [84, 85, 86, 87, 88, 79, 89]. The SM prediction of $R_{J/\psi}$ is based on the form factors given in [90]. As the $B_c \to J/\psi$ form factors are not very reliably known, the uncertainty for $R_{J/\psi}$ is not shown. However, it is expected to be similar to that of R_{D^*}.

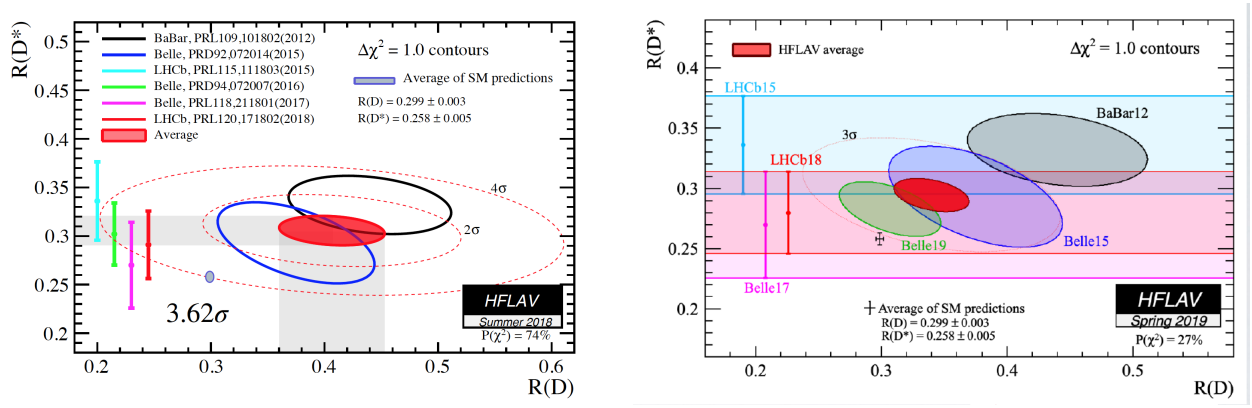

Figure 4.1: Measurements of R_D and R_{D^*}, averaged for each experiment, performed by HFLAV collaboration in 2018 [91] on the left and 2019 [73] on the right, together with the global average and the SM prediction.

The present analysis is based on [3]. In the first part (Sections 4.1 - 4.5), there is a comprehensive analysis of the possible explanations of charged current anomalies in a as model independent way as possible. A bottom-up approach, making use of EFT, is applied and the various implications of (linearly realized) $SU(2)_L \times U(1)_Y$ symmetry in SMEFT are discussed. In particular, the focus is on the correlations among the observables which could be used in the future to decipher the physics behind these anomalies. The analysis is performed taking into account the experimental data provided in [72].

In the second part of the Chapter (Section 4.6 and 4.7), these results are applied to simplified models with vector heavy mediators, that can be embedded within Composite Higgs models

with Partial Compositeness. Scenarios with the vector leptoquark $U_1 \sim (\mathbf{3},\mathbf{1})_{2/3}$ are also analyzed. An explanation of the flavor anomalies within this framework has received a lot of attention in the recent past [92, 93, 94, 95, 96, 97, 98, 65, 99, 100, 101, 67]. However, this scenario, motivated by the Higgs mass naturalness problem, generically predicts flavor violating and flavor non universal effects which are often too large to be compatible with experimental measurements. This can be partially cured by introducing additional flavor symmetries suppressing the undesirable effects [92, 95, 65]. In this work, instead of explicitly relying on flavor symmetries, an agnostic approach is used and we rely only on the correlations, coming from the partial compositness framework, among the various observables . Interestingly, even without making any assumption on the flavor structure of the composite sector, it is possible to find strong correlations between $\Delta F = 1$ and $\Delta F = 2$ observables leading to an upper bound on the scale of compositeness.

4.1 Operators for $b \to c\,\ell\,\nu$ decay

The leading contribution, in an EFT valid at the b mass scale, to the Lagrangian relevant for the parton level process $b \to c\,\ell\,\nu$, is sum of the SM term and of higher dimension operators as follows

$$\mathcal{L}_{\rm eff}^{b\to c\,\ell\,\nu} = \mathcal{L}_{\rm eff}^{b\to c\,\ell\,\nu}|_{\rm SM} - \sum \frac{g_i^{cb\ell\nu}}{\Lambda^2}\mathcal{O}_i^{cb\ell\nu} + \text{h.c.} + ... \quad (\ell = \tau,\mu,\text{e}) \tag{4.1.1}$$

where the ellipses refer to terms which are suppressed by additional factors of $(\frac{\partial}{\Lambda})^2$. As $(\frac{\partial}{\Lambda})^2 \sim (\frac{M_B}{\Lambda})^2$ for the processes of interest, these ellipses are completely negligible for new physics scales heavier than the electroweak scale. As a consequences, the dominant BSM effects in these interactions are described by $d = 6$ four fermion operators; the problems around the validity of the EFT truncation (see Section 2.1) can be safely neglected. One can notice that we are dealing with an EFT defined in the electroweak broken phase, usually called Weak Effective Theory (WET), composed by the three generations of leptons and neutrinos and by the five lightest quarks and obeying to $SU(3)_c \times U(1)_{em}$ gauge symmetry, as anticipated in Chapter 2. This approach is valid if no new physics is present with mass scale below the b quark mass. The Standard Model Lagrangian, expressed in WET, for this semileptonic b decays is

$$\mathcal{L}_{\rm eff}^{b\to c\,\ell\,\nu}|_{\rm SM} = -\frac{2G_F V_{cb}}{\sqrt{2}}\left(\mathcal{O}_{\rm VL}^{cb\ell\nu} - \mathcal{O}_{\rm AL}^{cb\ell\nu}\right) . \tag{4.1.2}$$

The four fermion operators involve a lepton bilinear and a fermion bilinear with b and c quarks, with different Lorentz structure; they are defined in the following basis

$$\begin{aligned}
\mathcal{O}_{\rm VL}^{cb\ell\nu} &= [\bar{c}\,\gamma^\mu\,b][\bar{\ell}\,\gamma_\mu\,P_L\,\nu] & \mathcal{O}_{\rm VR}^{cb\ell\nu} &= [\bar{c}\,\gamma^\mu\,b][\bar{\ell}\,\gamma_\mu\,P_R\,\nu] \\
\mathcal{O}_{\rm AL}^{cb\ell\nu} &= [\bar{c}\,\gamma^\mu\,\gamma_5\,b][\bar{\ell}\,\gamma_\mu\,P_L\,\nu] & \mathcal{O}_{\rm AR}^{cb\ell\nu} &= [\bar{c}\,\gamma^\mu\,\gamma_5\,b][\bar{\ell}\,\gamma_\mu\,P_R\,\nu] \\
\mathcal{O}_{\rm SL}^{cb\ell\nu} &= [\bar{c}\,b][\bar{\ell}\,P_L\,\nu] & \mathcal{O}_{\rm SR}^{cb\ell\nu} &= [\bar{c}\,b][\bar{\ell}\,P_R\,\nu] \\
\mathcal{O}_{\rm PL}^{cb\ell\nu} &= [\bar{c}\,\gamma_5\,b][[\bar{\ell}\,P_L\,\nu] & \mathcal{O}_{\rm PR}^{cb\ell\nu} &= [\bar{c}\,\gamma_5\,b][[\bar{\ell}\,P_R\,\nu] \\
\mathcal{O}_{\rm TL}^{cb\ell\nu} &= [\bar{c}\,\sigma^{\mu\nu}\,b][\bar{\ell}\,\sigma_{\mu\nu}\,P_L\,\nu] & \mathcal{O}_{\rm TR}^{cb\ell\nu} &= [\bar{c}\,\sigma^{\mu\nu}\,b][\bar{\ell}\,\sigma_{\mu\nu}\,P_R\,\nu] .
\end{aligned} \tag{4.1.3}$$

The operators on the left hand side involve lepton currents with left handed chirality, while the operators in the right column right chiral lepton currents and therefore right handed neutrinos. In this work, the latter are not taken into account. This choice can be motivated by the fact that amplitudes with four fermion operators involving right handed lepton currents do not interfere with the SM process. This means, by naive dimensional analysis, that in order to explain the experimental data by the operators with right chirality neutrinos, the required new physics scale has to be lower than that for the operators with the standard left handed leptons, since in the former case the leading BSM term of the cross section can appear only at the $\sim 1/\Lambda^4$ order. However, in the literature the possibility of addressing flavor anomalies introducing right handed neutrinos has been recently explored, as in [102, 103, 104, 71].

In the following, the Wilson Coefficients of the four fermion operators are normalized at the scale $\Lambda_{\rm SM}$ that characterizes the SM four fermion interaction, namely:

$$\frac{2G_F V_{cb}}{\sqrt{2}} = \frac{1}{\Lambda_{\rm SM}^2} \approx \frac{1}{(1.2\,\text{TeV})^2}\,. \tag{4.1.4}$$

Thus, we have

$$\mathcal{L}_{\rm eff}^{b\to c\,\ell\,\nu} \;=\; \mathcal{L}_{\rm eff}^{b\to c\,\ell\,\nu}|_{\rm SM} - \sum \frac{g_i^{cb\ell\nu}}{\Lambda^2}\mathcal{O}_i^{cb\ell\nu} + \text{h.c.} = -\frac{2\mathrm{G_F V_{cb}}}{\sqrt{2}}\sum \mathrm{C_i^{cb\ell\nu}}\mathcal{O}_{\rm i}^{\rm cb\ell\nu} + \text{h.c.} \tag{4.1.5}$$

where, $\dfrac{g_{\rm VL}^{cb\ell\nu}}{\Lambda^2} = \dfrac{2G_F V_{cb}}{\sqrt{2}}(C_{\rm VL}^{cb\ell\nu} - 1)$, $\dfrac{g_{\rm AL}^{cb\ell\nu}}{\Lambda^2} = \dfrac{2G_F V_{cb}}{\sqrt{2}}(C_{\rm AL}^{cb\ell\nu} + 1)$, $\dfrac{g_{\rm SL,PL,TL}^{cb\ell\nu}}{\Lambda^2} = \dfrac{2G_F V_{cb}}{\sqrt{2}}C_{\rm SL,PL,TL}^{cb\ell\nu}$.

The Wilson Coefficients $C_i^{cb\ell\nu}$ accounts also for the SM interaction, that corresponds to

$$C_{\rm VL}^{cb\ell\nu} = 1\,,\; C_{\rm AL}^{cb\ell\nu} = -1,\; C_{\rm SL,PL,TL}^{cb\ell\nu} = 0. \tag{4.1.6}$$

Although there are five operators with left chiral neutrinos, not all of them contribute to both R_D and R_{D^*}: there are only 3 independent operators relevant for R_D and 4 for R_{D^*}. This is because the following matrix elements vanish identically, due to chirality properties of the mesons:

$$\langle D(p_D, M_D)|\bar{c}\gamma^\mu\gamma_5 b|B(p_B, M_B)\rangle \;=\; 0\,, \tag{4.1.7}$$

$$\langle D(p_D, M_D)|\bar{c}\gamma_5 b|B(p_B, M_B)\rangle \;=\; 0\,, \tag{4.1.8}$$

$$\langle D^*(p_{D^*}, M_{D^*}, \epsilon_{D^*})|\bar{c}b|B(p_B, M_B)\rangle \;=\; 0\,. \tag{4.1.9}$$

Thus, the operators $\mathcal{O}_{\rm AL}^{cb\ell\nu}$ and $\mathcal{O}_{\rm PL}^{cb\ell\nu}$ do not contribute to R_D, and similarly, the operator $\mathcal{O}_{\rm SL}^{cb\ell\nu}$ does not contribute to R_{D^*}.

4.1.1 Correlation with the Decay Width of the B_c meson

The effective operators in Eq. (4.1.3), that describe at m_b scale the semileptonic b decays $b \to cl\nu$, contribute also to the lepton decays of B_c meson, in which the same four fermion interaction among b, c, l, ν is involved. Therefore, R_D and R_{D^*} observables are strongly correlated to the $B_c \to \tau\nu$ decay width.

The differential decay rate for the process $B_c^-(p) \to \tau^-(k_1) + \bar{\nu}_\tau(k_2)$ is given by

$$\frac{d\Gamma}{d\Omega} = \frac{1}{32\pi^2}\frac{|\mathbf{k_1}|}{m_{B_c}^2}\overline{|\mathcal{M}|^2}$$

where, $\mathbf{k_1}$ is the 3-momentum of the τ in the rest frame of the B_c meson, namely $|\mathbf{k_1}| = \frac{m_{B_c}^2 - m_\tau^2}{2m_{B_c}}$.

The matrix element $\mathcal{M}$ is given by

$$\begin{aligned} i\mathcal{M} &= \frac{2G_F V_{cb}}{\sqrt{2}}\Big[C_{\rm AL}^{cb\tau}\,\langle 0|\bar{c}\gamma^\mu\gamma_5 b|B_c(p)\rangle\,\bar{u}(k_1)(i\gamma_\mu P_L)v(k_2) + C_{\rm PL}^{cb\tau}\,\langle 0|\bar{c}\gamma_5 b|B_c(p)\rangle\,\bar{u}(k_1)(iP_L)v(k_2) \\ &\quad + C_{AR}^{cb\tau}\,\langle 0|\bar{c}\gamma^\mu\gamma_5 b|B_c(p)\rangle\,\bar{u}(k_1)(i\gamma_\mu P_R)v(k_2) + C_{PR}^{cb\tau}\,\langle 0|\bar{c}\gamma_5 b|B_c(p)\rangle\,\bar{u}(k_1)(iP_R)v(k_2)\Big]. \end{aligned} \tag{4.1.10}$$

One can notice that the operators $\mathcal{O}_{\rm VL,VR}^{cb\ell\nu}$, $\mathcal{O}_{\rm SL,SR}^{cb\ell\nu}$ and $\mathcal{O}_{\rm TL,TR}^{cb\ell\nu}$ do not contribute because the corresponding matrix elements vanish identically:

$$\langle 0|\bar{c}\gamma^\mu b|B_c(p_{B_c}, M_{B_c})\rangle = 0\,, \tag{4.1.11}$$

$$\langle 0|\bar{c}b|B_c(p_{B_c}, M_{B_c})\rangle = 0\,, \tag{4.1.12}$$

$$\langle 0|\bar{c}\sigma^{\mu\nu}b|B_c(p_{B_c}, M_{B_c})\rangle = 0\,. \tag{4.1.13}$$

Thus, vector, scalar and tensor contributions to R_D or R_{D^*} are not constrained by the bounds coming from B_c decay: only the axial vector and pseudo scalar four fermion operators that may enter in R_{D^*} are correlated to the B_c decay width.

As shown in the Appendix A of [3], the branching ratio of $B_c^- \to \tau^- + \bar{\nu}_\tau$ decay is

$$\begin{aligned} \mathcal{B}(B_c^- \to \tau^-\bar{\nu}_\tau) &= \frac{1}{8\pi}G_F^2|V_{cb}|^2 f_{B_c}^2 m_\tau^2 m_{B_c}\tau_{B_c}\left(1 - \frac{m_\tau^2}{m_{B_c}^2}\right)^2 \times \\ &\left(\left|C_{\rm AL}^{cb\tau} - \frac{m_{B_c}^2}{m_\tau(m_b+m_c)}C_{\rm PL}^{cb\tau}\right|^2 + \left|C_{AR}^{cb\tau} - \frac{m_{B_c}^2}{m_\tau(m_b+m_c)}C_{PR}^{cb\tau}\right|^2\right) \end{aligned} \tag{4.1.14}$$

where f_{B_c} is such that $\langle 0|\bar{c}\gamma^\mu\gamma_5 b|B_c(p)\rangle = i f_{B_c} p^\mu$ and $\langle 0|\bar{c}\gamma_5 b|B_c(p)\rangle = -i f_{B_c}\frac{m_{B_c}^2}{m_b+m_c}$.

The variation of $\mathcal{B}(B_c \to \tau\,\nu_\tau)$ as a function of the WCs $C_{\rm AL}^\tau$ or $C_{\rm PL}^\tau$ of the axial vector and pseudo scalar operators is shown in Fig. 4.2, with all the other contributions fixed to be given by the SM. One can notice that, even scanning over all the $C_{\rm AL}^\tau$ values in [-2,0], it is almost not possible to evade the experimental bounds on $\mathcal{B}(B_c \to \tau\,\nu_\tau)$: the constraints from B_c decay on the axial vector contribution to R_{D^*} might be safely neglected, while they are relevant only for the pseudo scalar operator.

4.1.2 Correlation with $R_{J/\psi}$, $\mathcal{P}_\tau(D^*)$, $F_L^{D^*}$

Together with the $B_c \to \tau\nu$ branching ratio, there are also other observables correlated to R_D and R_{D^*} even within a Weak Effective Theory, without introducing $SU(2)_L \times U(1)_Y$ gauge

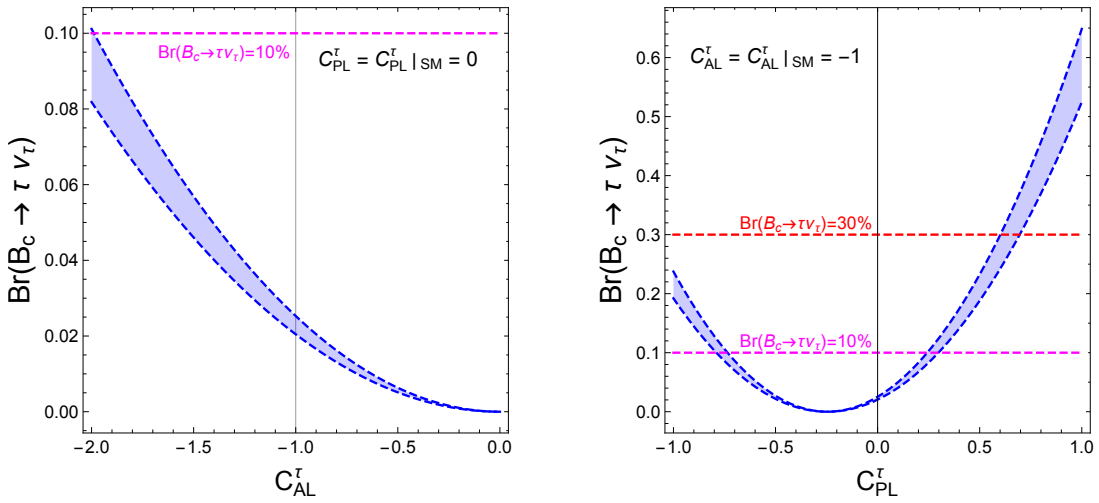

Figure 4.2: The $\mathcal{B}(B_c \to \tau\,\nu_\tau)$ as a function of $C^\tau_{\rm AL}$ and $C^\tau_{\rm PL}$. The upper bounds of 30% and 10% on this branching ratio from [105] and [106] respectively are also shown. The SM branching ratio is $\approx 2\%$. $f_{B_c} = 0.434 \pm 0.015$ GeV [107] has been used.

invariance. They all involve $b\,c\,\tau\,\nu$ effective four fermion interaction and they are $R_{J/\psi}$, $\mathcal{P}_\tau(D^*)$ and $F_L^{D^*}$, that were presented in Section 4 and are summarized in the following.

$R_{J/\psi}$, as anticipated, is defined as

$$R_{J/\psi} = \frac{\mathcal{B}\,(B_c \to J/\psi\,\tau\,\nu)}{\mathcal{B}\,(B_c \to J/\psi\,\ell_0\,\nu)}\,, \tag{4.1.15}$$

where the ratio, as in the case of $R_{D^{(*)}}$, allows a cancellation of uncertainties.
The quark content of J/ψ is $J/\psi \sim c\bar{c}$ and, thus, the process $B_c \to J/\psi\,\tau\,\nu$ arises from the same $b \to c\,\tau\,\nu$ transition involved in charged current flavor anomalies. The only effective $\mathcal{O}_{\rm iL}$ operator matrix element that vanishes between J/ψ and B_c states is the scalar one, $\mathcal{O}_{\rm SL}$. However, also the ones of the pseudo scalar and the vector interaction are small: $R_{J/\psi}$ is mostly constraining the WCs of $\mathcal{O}_{\rm AL}$ and $\mathcal{O}_{\rm TL}$, as will be shown in Section 4.4.

The most recent measurement of $R_{J/\psi}$ is [83]

$$R_{J/\psi} = 0.71 \pm 0.25 \tag{4.1.16}$$

which shows a discrepancy with respect to the SM prediction, that is around ~ 0.29. This can provide a hint of new physics, together with flavor anomalies; however, the deviation is so large that creates some tension and can be hardly accommodated within a scenario with a BSM contribution explaining, for example, R_{D^*}.

Then, there are polarization observables associated to $B \to D^*\,\tau\,\nu$ decay: $\mathcal{P}_\tau^{D^*}$, i.e. the τ polarization asymmetry in the longitudinal direction, and $F_L^{D^*}$, which refers to the D^*

longitudinal polarization. Their most recent measurements, as anticipated, are [79, 80] and [58]

$$\begin{aligned} P_\tau(D^*) &= -0.38 \pm 0.51(\text{stat.})\, ^{+0.21}_{-0.16}(\text{syst.}) \\ F_L^{D^*} &= 0.60 \pm 0.08(\text{stat.}) \pm 0.04(\text{syst.})\,. \end{aligned} \tag{4.1.17}$$

The central value of the first observable, $P_\tau(D^*)$, has smaller absolute value with respect to the SM prediction, that is around -0.47. However, the statistical and systematic errors are very large at the moment and thus the agreement with the standard expectation is good. In the future, Belle II will provide a more precise measurement for these observables.

On the other hand, $F_L^{D^*}$ is at distance of 1.6σ from its SM prediction, that is ~ 0.45.

All these observables can be used to set bounds on Wilson Coefficients that could contribute to charged current flavor anomalies. They can help, together with $\mathcal{B}(B_c \to \tau\nu)$, ruling out some scenarios or discriminating among different WET descriptions. However, the current precision on these measurements is quite poor.

4.2 Neutral current flavor anomalies and panoramic on other low energy observables

So far, the discussion has been focused on observables in which $b\,c\,\tau\nu$ effective interaction is directly involved. However, once gauge invariance is introduced and a SMEFT description is considered (see Section 4.5), charged current flavor anomalies turn out to be correlated to neutral current interactions and also to other low energy observables, that are summarized in the following.

- **$\mathbf{b \to sll}$.**

  These neutral current interactions are induced by the same gauge invariant effective $d = 6$ operators involved in $b \to c\tau\nu$. LFU violation in these semileptonic b decays affects the $R_{K^{(*)}}$ ratios, defined as:

  $$R_{K^{(*)}} = \frac{\mathcal{B}\left(B \to K^{(*)}\,\mu\,\mu\right)}{\mathcal{B}\left(B \to K^{(*)}\,e\,e\right)}\,. \tag{4.2.1}$$

  In SM, the above ratios are in very good approximation equal to the unity. However, as anticipated, recent data show a discrepancy to this lepton universality hypothesis, around $\sim 2 \div 2.5\sigma$ level (see Table 4.2).

  Within Standard Model, the $b \to sll$ transition arises at loop level. Therefore, the new physics scale necessary to explain this $10 - 20\%$ deviation is ~ 30TeV, larger than the one needed to account for charged current flavor anomalies. In Section 4.7.4, there will be an analysis of the possibility to explain also neutral current flavor anomalies in the models that will be studied to fit $R_{D^{(*)}}$ experimental values.

R_k $[1.1, 6]\text{GeV}^2$	0.846 ± 0.062	LHCb [108, 109]
R_{K^*} $[0.045, 1.1]\text{GeV}^2$	0.66 ± 0.11	LHCb [110]
	$0.52^{+0.36}_{-0.26}$	Belle [111]
R_{K^*} $[1.1, 6]\text{GeV}^2$	0.69 ± 0.12	LHCb [110]
	$0.96^{+0.45}_{-0.29}$	Belle [111]
R_{K^*} $[15, 19]\text{GeV}^2$	$1.18^{+0.52}_{-0.32}$	Belle [111]

Table 4.2: R_K and R_{K^*} measured values, by the experimental collaborations shown in the third column, within a given range of the dilepton squared mass indicated in the first column.

Together with $R_{K^{(*)}}$ ratios, other observables associated to these neutral current semileptonic interactions are $\mathcal{B}(B_s \to \tau\tau)$ and $\mathcal{B}(B \to K\tau\tau)$.

- **$b \to s\nu\nu$.**

  The $b \to s\nu\nu$ is another semileptonic neutral current decay that might be correlated to $b \to c\tau\nu$. As will be shown in Section 4.5.4, in a completely model independent SMEFT description, the Wilson Coefficients involved in the $R_{D^{(*)}}$ explanation are strongly constrained by the bounds on $\mathcal{B}(B \to K^{(*)}\nu\nu)$, in which there is not observed deviation with respect to SM. However, in the models that will be considered in the following, the $b \to s\nu\nu$ transition is absent at tree-level and this guarantees safety from this kind of constraints (see Sections 4.7.2 and 4.7.3).

- **LFV observables**

  The same SMEFT operators inducing the semileptonic interactions $b\,s\,l\,l$ and $b\,c\,\tau\,\nu$, that are off-diagonal in the quark flavor but preserve lepton one, can also generate lepton flavor violating processes, such as $b \to s\tau\mu$, involved in $B^+ \to K^+\tau\mu$ and $B_s \to \tau\mu$ observables. Only the first one has been measured so far.

- **LFU in τ decay**

  The $d = 6$ operators used to describe $b \to c\tau\nu$ also modify the W and Z couplings to fermions. This can occur at tree-level if flavor anomalies are explained with an effective scalar fermion operator such as the one analyzed in Section 4.5.3. Taking into account instead SMEFT four fermion operators, the modification of EW gauge boson vertices arises at one-loop level, as shown in Section 4.5.4, but it is still present and might be sizable. The strongest constraints on this kind of effects for W vertices are indirect and come from the measurements of LFU in τ lepton decays, in which the $W\tau\nu$ coupling enters (see discussion around Eq. (4.5.23)).

- **$\Delta F = 2$.**

  Semileptonic four fermion interactions can be also correlated to four quark effective operators, such as the ones inducing $\Delta F = 2$ transitions, e.g. $\bar{B}_s - B_s$ mixing, in which we have indeed a second-third generation transition in the quark sector. This correlation

depends on the considered simplified model. For example, in presence of colorless heavy mediators, such as the ones analyzed in Section 4.7.2, these $b\,b\,s\,s$ interactions arise at tree-level, while in models with leptoquarks (see Section 4.7.3) they emerge at one-loop. These $\Delta F = 2$ processes are strongly constrained, which is one of the major reasons why simplified models with leptoquarks, in which they are absent at tree-level, are more viable than other scenarios, as will be discussed in the following.

- **Dipoles**

  Dipole operators might be generated at one-loop by the same heavy mediators that induce the deviations in $b \to c\tau\nu$ and $b \to sll$. This occurs if couplings of new physics with right handed fermions are assumed, which is not in general necessary to describe flavor anomalies. Processes as the radiative LFV τ decay $\tau \to \mu\gamma$ and the radiative b decay $b \to s\gamma(g)$ can emerge and the bounds on them would constrain the WC of the effective $b\,c\,\tau\,\nu$ interaction.

- $\mathbf{b \to u\tau\nu}$

  The effective operators that generate $b \to c\tau\nu$ induce also the other flavor off-diagonal charged current b decay into τ, i.e. $b \to u\tau\nu$, that enters in the $\mathcal{B}(B \to \tau\nu)$ observable. In this case, however, the correlation between the WCs of the two four fermion interactions might be milder, since the coefficients associated to two different quark generation transitions are involved, in one case between third and second families, in the other between third and first ones.

4.3 High-p_T constraints and collider searches

The new physics that is at the origin of flavor anomalies can also generate effects in the high energy processes studied at colliders. If the mass scale of the mediators, responsible for this LFU violation, is outside the kinematical reach of LHC, the entire spectrum at colliders is below the NP scale and EFT approach can be applied even at large energies, e.g. in the analysis of high-p_T tails. These measurements are less precise than precision tests on the low energy observables described in the previous Section; however, even in this case one can reach same or better sensitivity to LFU violation, taking advantage from the energy growth of the non SM contributions to the cross section, that at leading order is naively expected to be $\sim E^2/\Lambda^2$.

The same $d = 6$ SMEFT operators which induce $b\,c\,\tau\,\nu$ and $b\,s\,l\,l$ (see Section 4.5) also generate the contact semileptonic interactions involved in $\tau^+\tau^-$, l^+l^-, $\tau\mu$ and $\tau\nu$ production from proton-proton collision. In the analysis of high-p_T tails, only the contribution of four fermion operators is considered: the effect from the scalar fermion operators (discussed in Section 4.5.3), that modify the W and Z vertices, does not grow with energy, being quadratically suppressed by the Higgs VEV, and, furthermore, it is strongly constrained by Z pole measurements. The bounds from non flavor violating processes are stronger and more competitive, since the corresponding NP contribution is less constrained by low energy observables. However, the correlation between the Wilson Coefficients of these flavor conserving four fermion interactions

with the WCs relevant for $R_{D^{(*)}}$ (or also $R_{K^{(*)}}$) depends on some assumptions about the flavor structure of the EFT, for example Minimal Flavor Violation (MFV) or $U(2)$ flavor symmetry, or on the specific construction of a considered simplified model. On the contrary, the analysis presented in the following Sections will be as general as possible and will be performed avoiding any non necessary hypothesis about flavor symmetries and hierarchies.

Therefore, with high-p_T measurements, one can constraints EFTs and simplified models with particular flavor structures, addressing flavor anomalies. In particular, the analysis of $\tau\tau$ production at LHC is relevant in setting bounds to models explaining $R_{D^{(*)}}$, while the study of ll tails, with l standing for electron or muon, can put constraints on scenarios that describe $R_{K^{(*)}}$ value. In this way, one can obtain lower bounds on the NP mediators mass scale and upper bounds on their coupling to fermions.

In [112], there is the study of bounds from $bb \to \tau\tau$ to EFTs displaying a $U(2)$ flavor symmetry in the first two generations and on simplified models with both colorless and colored mediators, showing a tension between these $R_{D^{(*)}}$ explanations and the high-p_T ATLAS data at 13 TeV. In [113], an analysis of dilepton Drell-Yann is performed, i.e. $pp \to l^+l^-$, $l = e, \mu$, in order to set bounds on models addressing neutral current flavor anomalies. Constraints are set on the Wilson Coefficients of all the four fermion operators in the SMEFT, under assumption of MFV or $U(2)$ symmetry, also within simplified models. It turns out that high-p_T dimuon tails probe regions of the parameter space that are relevant for $R_{K^{(*)}}$ and, in particular, the MFV hypothesis creates significant tension between low energy observables and large energy data.

If the mass scale of the new physics, that is responsible for this LFU violation, is within the kinematical reach of LHC, one cannot study the full spectrum integrating out the heavy mediators and applying EFT approach. It is possible to set constraints on simplified models exploiting direct searches of mediators, such as studying their single [114] and pair [115] production. Even in this case, the analysis of $\tau\tau$, $\tau\mu$, $\tau\nu$, $\mu\mu$ final states is useful to provide the most stringent bounds, as shown in [112] and more recently in [115] for specific simplified models. Colorless mediators contribute to these processes via s channel resonances, while the colored ones through t channel interactions; as a consequence, in the first case there is strong dependence on the decay width of the NP particles, which does not occur in the second case.

4.4 Explaining R_D and R_{D^*} in Weak Effective Theory

In this Section, the possible role of various WET dimension 6 operators in explaining the R_D and R_{D^*} anomalies is studied and reviewed, following the analysis of [3], which summarizes also some results shown in literature, *e.g.* in [116, 117, 118, 119, 120, 121, 122, 123, 124, 125, 126, 127, 128].

In the following, using [72] as in [3], the fit of charged current flavor anomalies together with some low energy observables is performed in presence of specific different sets of effective four fermion operators among the ones in Eq. (4.1.3). The notation $\mathcal{O}_{\rm i}^{cb\ell\nu} = \mathcal{O}_{\rm i}^{\ell}$ will be used.

4.4.1 Vector and Axial Vector operators

Here only the vector and axial vector operators $\mathcal{O}^{\tau}_{\mathrm{VL}}$ and $\mathcal{O}^{\tau}_{\mathrm{AL}}$ of Eq. (4.1.3) are considered: we investigate whether they are capable of explaining R_D and R_{D^*} anomalies simultaneously, without being incompatible with the recent measurement of $R_{J/\psi}$.

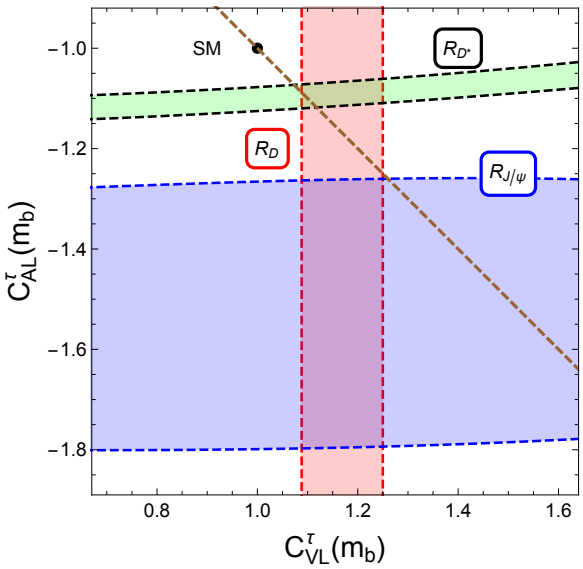

Figure 4.3: The vertical red band corresponds to the values of C^{τ}_{VL} that satisfy the experimental measurement of R_D within 1σ uncertainty. Similarly, the green (blue) region corresponds to the values of C^{τ}_{VL} and C^{τ}_{AL} that satisfy the experimental measurement of R_{D^*} ($R_{J/\psi}$) within 1σ. All the WCs are defines at the m_b scale. The oblique dashed line is the locus of the equation $C^{\tau}_{\mathrm{VL}} = -C^{\tau}_{\mathrm{AL}}$.

In Fig. 4.3, there are the regions in the C^{τ}_{VL} - C^{τ}_{AL} plane (see Eq. (4.1.5)) that satisfy the experimental data on R_D, R_{D^*} and $R_{J/\psi}$ within 1σ uncertainty. The uncertainties in the form factors have been carefully taken into account in obtaining the various allowed regions. The plotted WCs are evaluated at the b mass scale, at which the Weak Effective Theory of Eq. (4.1.2) and (4.1.5) is valid. Constraints coming from the upper bounds on the $B_c \to \tau\nu$ branching ratio are not taken into account, since, as discussed in Section 4.1.1, they are absent in the case of C^{τ}_{VL} and negligible for C^{τ}_{AL}. It can be seen that there is an overlap region, between the red and green bands, that successfully accounts for both R_D and R_{D^*} observed values. This region is outside the 1σ experimental measurement of $R_{J/\psi}$, but there is consistency at $\approx 1.5\,\sigma$.

Therefore, the combination of effective vector and axial vector four fermion interactions provides a quite good explanation of charged current flavor anomalies, without being strictly ruled out by the bounds on correlated observables. Furthermore, a scenario with only these effective four fermion operators can be obtained in the low energy limit of many simplified models, as will be pointed out in the following Sections.

It is interesting that $C^{\tau}_{\mathrm{VL}} = -C^{\tau}_{\mathrm{AL}} \approx 1.1$ falls in the overlap region mentioned above. As we will see in the next Section, the relation $C^{\tau}_{\mathrm{VL}} = -C^{\tau}_{\mathrm{AL}}$ is expected if $SU(2)_L \times U(1)_Y$ gauge

invariance is linearly realized at the dimension 6 level, namely if we are within SMEFT, that is needed for the descriptions at scales above the one of electroweak symmetry breaking. One should also notice that these $V-A$ processes are the ones that can interfere with the Standard Model tree-level $b \to cl\nu$ interaction and thus can contribute to the leading non SM term of the EFT expanded cross section.

The success of a WET with only $C^\tau_{\rm VL} = -C^\tau_{\rm AL}$ has been also shown in [128]. There, a χ^2 fit in presence of four the NP parameters $C^\tau_{\rm VL} - C^\tau_{\rm AL}$, $C_{\rm SL}$, $C_{\rm PL}$ and $C_{\rm TL}$ is performed, with a bottom-up approach, taking into account also information from the q^2 distribution of $\Gamma(B \to D^{(*)}\tau\nu_\tau)$ and $F_L^{D^*}$, i.e. the longitudinal polarization fraction of D^* in $B \to D^*\tau\nu_\tau$. The fit tells us that there is a preference of NP presence with respect to the hypothesis of SM only; furthermore, even if there is not a strong preference to a particular Wilson Coefficient in the global fit, performing the analysis with each single WC at a time a scenario with $C^\tau_{\rm VL} - C^\tau_{\rm AL}$ only is preferred and well compatible with data.

Note that the vector and axial vector operators do not have anomalous dimensions if only QCD interactions are considered (see, for example, appendix-E of [129] and also [130]). Hence, their values at NP scale do coincide with the ones at b mass scale considered here, i.e. $C^\tau_{\rm VL,AL}(\Lambda) = C^\tau_{\rm VL,AL}(m_b)$, up to loop level electroweak corrections, and a EFT with only $\mathcal{O}_{\rm VL}$ and $\mathcal{O}_{\rm AL}$ at energies of order m_b does not present other effective four fermion operators at the matching scale.

4.4.2 Scalar and Pseudo-scalar operators

Here, the scalar and pseudo-scalar operators, $\mathcal{O}^\tau_{\rm SL}$ and $\mathcal{O}^\tau_{\rm PL}$ respectively, are analyzed, assuming that all the Wilson Coefficients of the other operators are fixed to their SM values. In the left panel of Fig. 4.4, there is the parameter space that satisfies the individual experimental data on R_D, R_{D^*} and $R_{J/\psi}$ within 1σ uncertainty. As discussed before, while the operator $\mathcal{O}^\tau_{\rm SL}$ contributes to R_D only, the operator $\mathcal{O}^\tau_{\rm PL}$ contributes only to R_{D^*}. This explains the vertical and horizontal nature of the allowed regions for R_D and R_{D^*} respectively.

The operator $\mathcal{O}^\tau_{\rm PL}$ directly contributes also to the decay $B_c \to \tau\nu$, while this does not occur for $\mathcal{O}^\tau_{\rm SL}$, as discussed in Section 4.1.1. The regions below the two horizontal dashed lines correspond to $\mathcal{B}(B_c \to \tau\nu) < 30\%$ and $< 10\%$, which were claimed to be the indirect experimental upper bounds by the authors of [105] and [106] respectively. Thus, an explanation of R_{D^*} by the operator $\mathcal{O}^\tau_{\rm PL}$ is in serious tension with the upper bound on $\mathcal{B}(B_c \to \tau\nu)$, within a EFT with only the scalar and pseudo scalar operators.

The right panel of Fig. 4.4 shows the renormalization group (RG) running (considering only QCD interactions) of the Wilson Coefficients $C^\tau_{\rm SL}$ and $C^\tau_{\rm PL}$ from the m_b scale up to 5 TeV using the following equation [129]:

$$C(m_b) = \left[\frac{\alpha_s(m_t)}{\alpha_s(m_b)}\right]^{\frac{\gamma}{2\beta_0^{(5)}}} \left[\frac{\alpha_s(\Lambda)}{\alpha_s(m_t)}\right]^{\frac{\gamma}{2\beta_0^{(6)}}} C(\Lambda)\,, \tag{4.4.1}$$

where, $\gamma = -8$ and $\beta_0^{(nf)} = 11 - \frac{2nf}{3}$ is the β-function of the QCD coupling in presence of n_f quark flavors. The values at the m_b scale are taken from the allowed bands in the left panel.

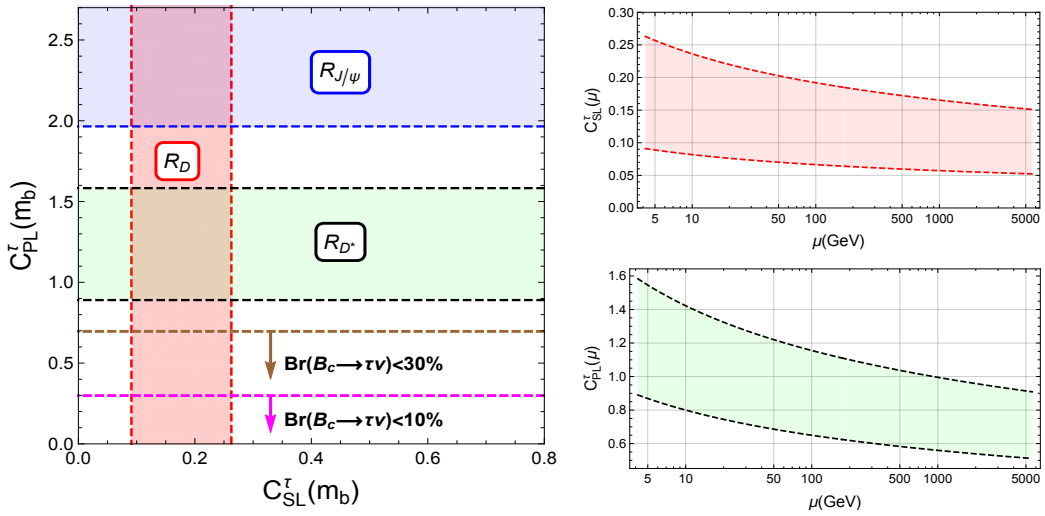

Figure 4.4: Left panel : the red and green (blue) bands correspond to the values of $C^\tau_{\rm SL}$ and $C^\tau_{\rm PL}$ that satisfy the experimental measurement of R_D and R_{D^*} ($R_{J/\psi}$) within 1σ respectively. The values of $C^\tau_{\rm PL}$ that correspond to $\mathcal{B}(B_c \to \tau\nu) < 30\%$ and $< 10\%$ are also shown. **Right panel** : renormalization group running of the WCs $C^\tau_{\rm SL}$ and $C^\tau_{\rm PL}$.

4.4.3 Tensor operator

In this Section, a scenario with the tensor operator only is taken into account. In Fig. 4.5, we show the allowed values of $C^\tau_{\rm TL}$ that are consistent with the 1σ experimental measurements of R_D, R_{D^*} and $R_{J/\psi}$. The values enclosed by the green vertical dashed lines correspond to simultaneous explanation of R_D and R_{D^*} anomalies. Note however that the prediction for $R_{J/\psi}$ in this $C^\tau_{\rm TL}$ region is $\approx 0.17 - 0.23$, which is below the SM prediction and quite far from the current experimental central value. The RG running of $C^\tau_{\rm TL}$ is shown in the right panel of Fig. 4.5 (using Eq. (4.4.1) with $\gamma = 8/3$ [129]) where the initial values of $C^\tau_{\rm TL}$ at the m_b scale correspond to the range enclosed by the two vertical dashed lines in the left panel.

Note that the tensor operator does not contribute to the decay $B_c \to \tau\nu$ because the matrix element $\langle 0|\bar{c}\,\sigma^{\mu\nu}\,b|\bar{B}_c\rangle$ identically vanishes (see Eq. (4.1.13)). Hence, there is no constraint on $C^\tau_{\rm TL}$ from the process $B_c \to \tau\nu$.

4.4.4 Combination of Tensor, Scalar and Pseudo-scalar operators

In this Section, we consider a Weak Effective Theory in which the scalar, pseudo-scalar and tensor operators are present simultaneously. In the left panel of Fig. 4.6, the various allowed regions in the $C^\tau_{\rm TL}$ - $C^\tau_{\rm SL}$ plane are shown, assuming the relation $C^\tau_{\rm SL} = -C^\tau_{\rm PL}$, that is motivated by the presence of simplified models in which left handed quark scalar bilinears are generated. It can be seen that a simultaneous explanation of the R_D and R_{D^*} anomalies requires $C^\tau_{\rm SL}(m_b) = -C^\tau_{\rm PL}(m_b) \in [0.08, 0.23]$ and $C^\tau_{\rm TL}(m_b) \in [-0.11, -0.06]$, corresponding to the small overlap of the red and green regions for positive values of $C^\tau_{\rm SL}$ and negative values of $C^\tau_{\rm TL}$. In fact, one

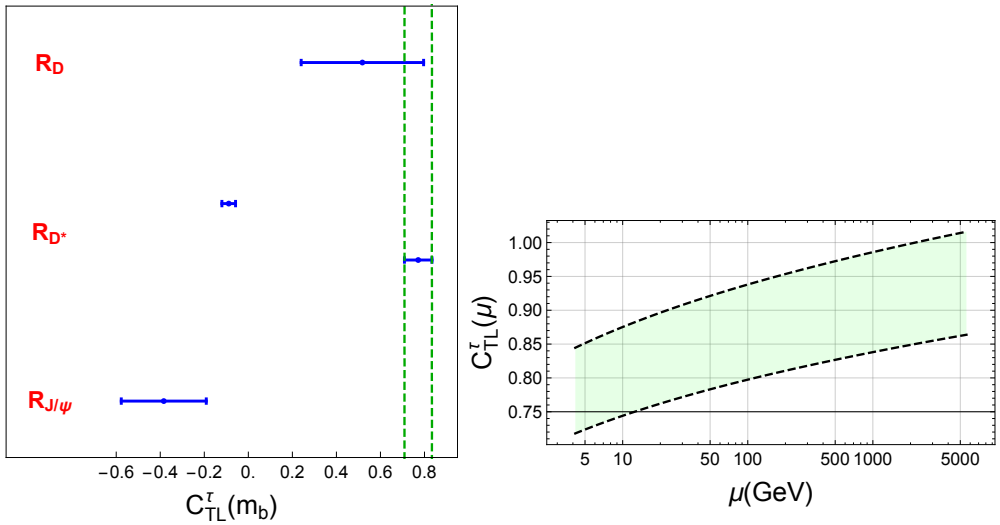

Figure 4.5: Left panel : the horizontal lines correspond to the values of $C^{\tau}_{\rm TL}$ that satisfy the experimental measurement of R_D, R_{D^*} and $R_{J/\psi}$ within 1σ. The green band corresponds to values of $C^{\tau}_{\rm TL}$ that explains R_D and R_{D^*} simultaneously. **Right panel** : renormalization group running of $C^{\tau}_{\rm TL}$.

should consider values of $C^{\tau}_{\rm AL}$ smaller than one, and thus $C^{\tau}_{\rm SL} > -1$, in order to avoid the tension with the upper bounds on $\mathcal{B}(B_c \to \tau\nu)$ observable, as can be seen from Fig. 4.4. There is also an overlap region enclosing $C^{\tau}_{\rm SL} = -C^{\tau}_{\rm PL} = 0$ and for non zero $C^{\tau}_{\rm TL}$, which corresponds to the tensor solution discussed in the previous Section. The individuated region of WC values that account for charged current flavor anomalies, however, does not lead to a $R_{J/\psi}$ prediction compatible with experimental data: there is a certain tension with this observable that, though, might be ameliorated by future more precise measurements of $R_{J/\psi}$.

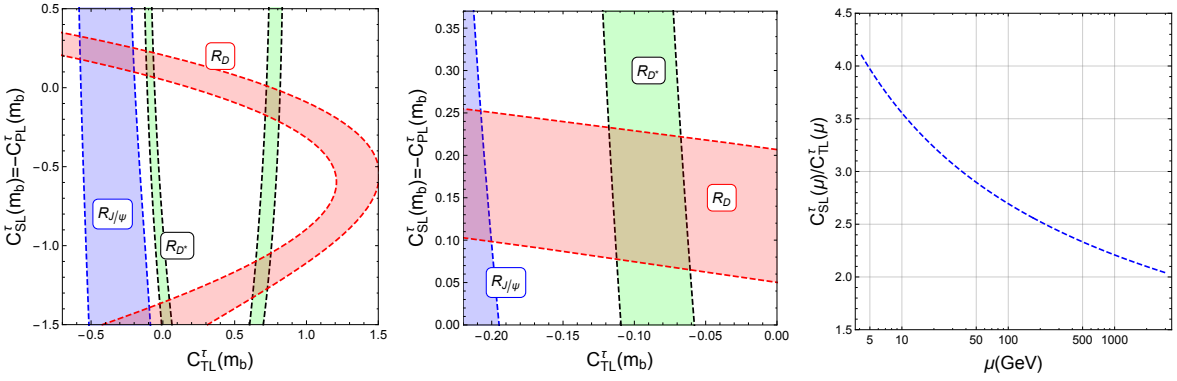

Figure 4.6: Left panel: the red and green (blue) shaded regions correspond to the values of $C^{\tau}_{\rm SL} = -C^{\tau}_{\rm PL}$ and $C^{\tau}_{\rm TL}$ that satisfy the experimental measurement of R_D and R_{D^*} ($R_{J/\psi}$) within 1σ respectively. **Middle panel**: the small overlap of the red and green regions for positive (negative) values of $C^{\tau}_{\rm SL}$ ($C^{\tau}_{\rm TL}$) is magnified separately. **Right panel**: the RG evolution of the coupling ratio $C^{\tau}_{\rm SL}/C^{\tau}_{\rm TL}$ is shown, assuming $C^{\tau}_{\rm SL}/C^{\tau}_{\rm TL} = 2$ at 3 TeV.

It is interesting to notice that there exist scalar leptoquark models, e.g. a model with $R_2 \sim (\mathbf{3},\mathbf{2})_{7/6}$ (see Section 4.6), that generate the operator $(\bar{c}P_L\nu)(\bar{\tau}P_L b)$ at the matching scale Λ, see for example [131]. This operator arises from a $SU(2)_L \times U(1)_Y$ gauge invariant operator $\left(\bar{l}'^k u'\right)\epsilon_{jk}\left(\bar{q}'^j e'\right)$ which, by using Fierz transformation, gives

$$\left(\bar{l}'^k u'\right)\epsilon_{jk}\left(\bar{q}'^j e'\right) = -\frac{1}{8}\left[4\left(\bar{l}'^j e'\right)\epsilon_{jk}\left(\bar{q}'^k u'\right) + \left(\bar{l}'^j \sigma_{\mu\nu} e'\right)\epsilon_{jk}\left(\bar{q}'^k \sigma^{\mu\nu} u'\right)\right],$$

where the same notation of Section 4.5 has been used. Then, the WET operator obtained integrating out R_2 can be written in terms of the operators in Eq. (4.1.3) after performing the Fierz transformation

$$(\bar{c}P_L\nu)(\bar{\tau}P_L b) = -\frac{1}{8}\left[2(\mathcal{O}^\tau_{\rm SL} - \mathcal{O}^\tau_{\rm PL}) + \mathcal{O}^\tau_{\rm TL}\right]. \tag{4.4.2}$$

Thus, at the matching scale of the EFT one gets

$$C^\tau_{\rm SL}(\Lambda) = -C^\tau_{\rm PL}(\Lambda) = 2C^\tau_{\rm TL}(\Lambda)\,. \tag{4.4.3}$$

This was the motivation to consider $C^\tau_{\rm SL} = -C^\tau_{\rm PL}$ in Fig. 4.6. The ratio $C^\tau_{\rm SL}/C^\tau_{\rm TL}$, however, increases with the decreasing RG scale as shown in the right panel of Fig. 4.6. Assuming $C^\tau_{\rm SL}(\Lambda)/C^\tau_{\rm TL}(\Lambda) = 2$ for $\Lambda = 3$ TeV, we get $C^\tau_{\rm SL}(m_b)/C^\tau_{\rm TL}(m_b) \approx 4$, which is quite large with respect to the experimentally consistent ratio that emerges from the allowed region of Fig. 4.6.

Note that, in the above discussion, only real values of the Wilson Coefficients are considered. Allowing for complex WCs may lead to the possibility to consistently explain charged current flavor anomalies in a simplified model with R_2 scalar leptoquark, generating a combination of left handed scalar and tensor effective operators (see for example [69]).

4.4.5 Combination of vector and scalar operators

Here, a scenario where both vector and scalar operators are present (see, for example [64] for a model) is briefly commented. In Fig. 4.7, the allowed regions in the $C^\tau_{\rm VL}$ - $C^\tau_{\rm SL}$ plane are shown, assuming $C^\tau_{\rm VL} = -C^\tau_{\rm AL}$ and $C^\tau_{\rm SL} = \pm C^\tau_{\rm PL}$.

It can be seen that the overlap of the red and green regions (that corresponds to the simultaneous solution of R_D and R_{D^*}) touches the $C^\tau_{\rm SL} = \pm C^\tau_{\rm PL} = 0$ point. Furthermore, there is not mixing among vector and scalar operators under RG evolution, as far as only QCD effects are taken into account. Thus, a combination of the vector and scalar operators extends the solution with only the vector operator discussed in Section 4.4.1. Interestingly, if the red shaded region shrinks in the future due to more precise measurement of $R_{D^{(*)}}$ (without affecting the current central value much), the combination of scalar and vector operators may lead to a better fit than with only vector operators.

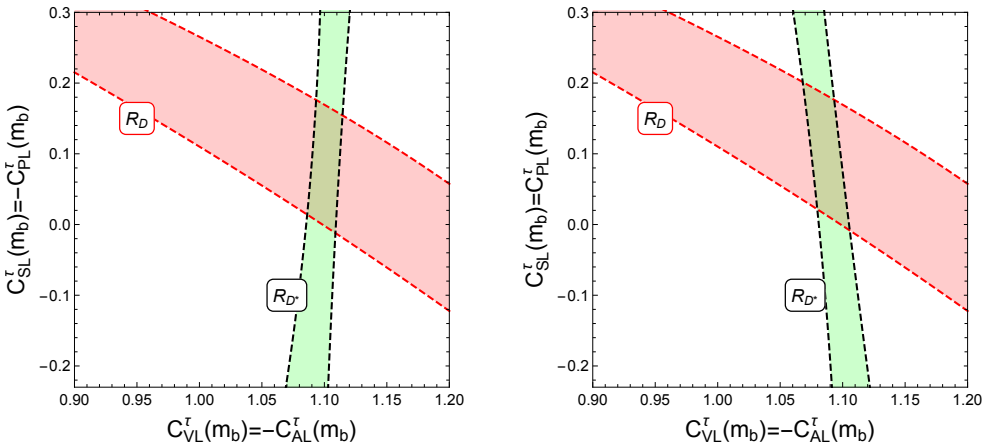

Figure 4.7: The red and green shaded regions correspond to the values of $C^\tau_{\rm VL}$ $(= -C^\tau_{\rm AL})$ and $C^\tau_{\rm SL}$ $(= -C^\tau_{\rm PL}$ for the left panel and $= C^\tau_{\rm PL}$ for the right panel) that satisfy the experimental measurement of R_D and R_{D^*} within 1σ respectively.

4.4.6 Summary of various explanations and their discrimination

In the previous Subsections we saw that simultaneous explanations of the R_D and R_{D^*} charged current flavor anomalies are possible by

1. a combination of vector and axial vector operators (red-green overlap region in Fig. 4.3)
2. a combination of scalar and pseudo scalar operators (red-green overlap region in Fig. 4.4)
3. tensor operator only (the region between the two dashed vertical lines in Fig. 4.5)
4. a combination of scalar, pseudo scalar and tensor operators (red-green overlap region in Fig. 4.6, in particular the one with positive values of $C^\tau_{\rm SL}$ and negative values of $C^\tau_{\rm TL}$).

The second solution is almost ruled out by the tension with indirect upper bound on the branching ratio of $B_c \to \tau\nu$. On the other hand, a scenario with a combination of vector and scalar operators is not considered here, because, as seen, it turns out that it is only an extension of the solution with vector and axial vector operators only: the experimentally allowed region is around $C^\tau_{\rm SL} = C^\tau_{\rm PL} = 0$.

The three possible solutions, namely the first, the third and the fourth, might be distinguished exploiting other low energy observables, i.e. by measuring the τ-polarisation $(P_\tau(D^*))$ in $\bar{B} \to D^*\tau^-\bar{\nu}_\tau$, forward-backward asymmetry $(\mathcal{A}_{\rm FB}(D^*))$ and $R_{J/\psi}$ ratio. In Fig. 4.8, there is the plot the predictions for $P_\tau(D^*)$, $\mathcal{A}_{\rm FB}(D^*)$ and $R_{J/\psi}$ for values of the WCs that correspond to various simultaneous solutions of R_D and R_{D^*} anomalies. It can be seen that it is indeed possible to discriminate the three solutions by measuring $P_\tau(D^*)$, $\mathcal{A}_{\rm FB}(D^*)$ and $R_{J/\psi}$. In fact, as shown in the right panel of Fig. 4.8, $R_{J/\psi}$ can be a very good discriminating observable between the first and third solutions. Of course, with more data, various kinematical distributions can also be used to discriminate the different Lorentz structures [132, 116, 133, 134, 135, 136, 124, 127, 128].

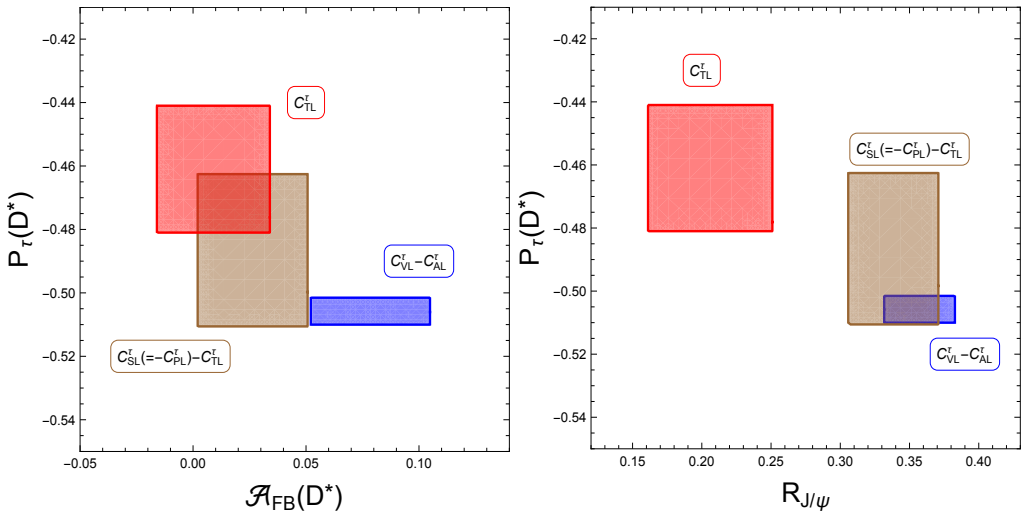

Figure 4.8: Predictions for $P_\tau(D^*)$, $\mathcal{A}_{\rm FB}(D^*)$ and $R_{J/\psi}$ for values of the WCs that correspond to various simultaneous solutions of R_D and R_{D^*} anomalies. See main text for more details.

In the analysis that follows, the focus will be on the first case, with effective operators having vectorial Lorentz structure. Indeed, it is the scenario in which charged current flavor anomalies can be addressed suffering less tension with other low energy observables, such as the branching ratio of $B_c \to \tau\nu$ decay and $R_{J/\psi}$, even in absence of right handed neutrinos and taking real Wilson Coefficients. Furthermore, it is not difficult to obtain such Weak Effective Theory in simplified models.

4.5 Explaining R_D and R_{D^*} in SMEFT, with linearly realized $SU(2)_L \times U(1)_Y$ gauge invariance

In the previous Sections, the analysis of charged current flavor anomalies was performed within Weak Effective Theory, namely with operators which were manifestly $SU(3)_c \times U(1)_{em}$ invariant, but invariance under the full electroweak group was not demanded. However, in order to study the high energy structure of the theory explaining R_D and R_{D^*} and in order to relate the Wilson Coefficient values observed at m_b scale to the ones evaluated at the matching scale of the EFT, one should consider the SMEFT with full $SU(3)_c \times SU(2)_L \times U(1)_Y$ invariance, valid between the EW SSB scale and the cutoff Λ at which new states are integrated out (see Chapter 2). In this Section the consequences of electroweak gauge invariance are investigated.

4.5.1 List of operators

The $SU(3)_c \times SU(2)_L \times U(1)_Y$ invariant dimension 6 operators that lead to the semileptonic $b \to c\,\tau\,\nu$ decay, in absence of right handed neutrinos, are given by

$$\mathcal{L}^{\rm dim6} = -\frac{1}{\Lambda^2}\sum_{p'r's't'}\Big\{[C^{(3)}_{lq}]'_{p'r's't'}\left(\bar{l}'_{p'}\gamma_\mu\sigma^I l'_{r'}\right)\left(\bar{q}'_{s'}\gamma^\mu\sigma^I q'_{t'}\right) + \text{h.c.} \tag{4.5.1}$$

$$+[C_{ledq}]'_{p'r's't'}\left(\bar{l}'^{j}_{p'}e'_{r'}\right)\left(\bar{d}'_{s'}q'^{j}_{t'}\right) + \text{h.c.} \tag{4.5.2}$$

$$+[C^{(1)}_{lequ}]'_{p'r's't'}\left(\bar{l}'^{j}_{p'}e'_{r'}\right)\epsilon_{jk}\left(\bar{q}'^{k}_{s'}u'_{t'}\right) + \text{h.c.} \tag{4.5.3}$$

$$+[C^{(3)}_{lequ}]'_{p'r's't'}\left(\bar{l}'^{j}_{p'}\sigma_{\mu\nu}e'_{r'}\right)\epsilon_{jk}\left(\bar{q}'^{k}_{s'}\sigma^{\mu\nu}u'_{t'}\right) + \text{h.c.} \tag{4.5.4}$$

$$--$$

$$+[C^{(3)}_{\phi l}]'_{p'r'}\left(\phi^\dagger i\overleftrightarrow{D}^I_\mu\phi\right)\left(\bar{l}'_{p'}\,\sigma^I\gamma^\mu\,l'_{r'}\right) + \text{h.c.} \tag{4.5.5}$$

$$--$$

$$+[C^{(3)}_{\phi q}]'_{p'r'}\left(\phi^\dagger i\overleftrightarrow{D}^I_\mu\phi\right)\left(\bar{q}'_{p'}\,\sigma^I\gamma^\mu\,q'_{r'}\right) + \text{h.c.} \tag{4.5.6}$$

$$+[C_{\phi ud}]'_{p'r'}\left(\phi^j\epsilon_{jk}\,i(D_\mu\phi)^k\right)\left(\bar{u}'_{p'}\gamma^\mu d'_{r'}\right) + \text{h.c.}\Big\} \tag{4.5.7}$$

where ϵ_{ij} is antisymmetric with $\epsilon_{12} = +1$ and

$$\phi^\dagger i\overleftrightarrow{D}^I_\mu\phi = i\left(\phi^\dagger\sigma^I D_\mu\phi - (D_\mu\phi)^\dagger\sigma^I\phi\right) \tag{4.5.8}$$
$$D_\mu\phi = (\partial_\mu + ig_2\frac{\sigma^I}{2}W^I_\mu + ig_1 Y_\phi B_\mu)\phi\ , Y_\phi = \frac{1}{2}\,.$$

The operator structure $\left(\bar{l}'^{j}_{p'}\sigma_{\mu\nu}e'_{r'}\right)\left(\bar{d}'_{s'}\sigma^{\mu\nu}q'^{j}_{t'}\right)$ is absent since it vanishes algebraically.

The Wilson Coefficients are matrices in the flavor space. The notation as in [6] has been used: the primes represent the fact that the operators and couplings are written in the gauge basis.

As anticipated, we focus on effective operators with vector structure in the fermion bilinears.

The operators $[\mathcal{O}^{(3)}_{\phi q}]_{p'r'}$ and $[\mathcal{O}_{\phi ud}]_{p'r'}$ modify the charged current vertex of the quarks with a gauge boson, also the one of our interest $\bar{c}bW$. However, this affects both the $b \to c\,\tau\,\nu$ and $b \to c\,\ell_0\,\nu$ decays in the same way, with $\ell_0 = e, \mu$. Consequently, the operators $[\mathcal{O}^{(3)}_{\phi q}]_{p'r'}$ and $[\mathcal{O}_{\phi ud}]_{p'r'}$ do not induce LFU violation effects and are not relevant for the explanation of the R_D and R_{D^*} anomalies and can be ignored.

Thus, we are left with the four fermion operator of Eq. (4.5.1) and the scalar fermion operator of Eq. (4.5.5), that involve only currents of left chiral fields. Consequently, these operators only lead to V-A interactions, corresponding to the case with $C^\tau_{\rm VL} = -C^\tau_{\rm AL}$ in the electroweak broken phase described in the previous Sections; thus, the corresponding amplitudes interfere with the SM one. It is not true in general that linearly realized $SU(2)_L \times U(1)_Y$ gauge invariance forbids V+A operators at the dimension 6 level. Indeed, the operator in

Eq. (4.5.7) generates V+A interactions, but, as mentioned before, it does not lead to lepton non-universality at the dimension 6 level. This is an important consequence of linearly realized $SU(2)_L \times U(1)_Y$ gauge invariance.

Note, however, that at the dimension 8 level, it is possible to have $(\mathcal{O}^{\tau}_{\rm VL} + \mathcal{O}^{\tau}_{\rm AL})$ operators violating LFU. For example, consider the operator

$$\mathcal{O}^{8}_{\rm RL} = \frac{1}{\Lambda^4}\left(\bar{l}'_{p'}\phi\right)\gamma_\mu\left(l'_{r'}\phi\right)\left(\bar{u}'_{s'}\gamma^\mu d'_{t'}\right) \tag{4.5.9}$$

where the objects inside each of the parenthesis are constructed as SU(2)L singlets. After electroweak symmetry breaking, this operator generates the following interaction term

$$\frac{v^2}{\Lambda^2}\frac{1}{\Lambda^2}\left[\bar{\ell}\,\gamma_\mu\,P_L\,\nu\right]\left[\bar{c}\,\gamma^\mu\,P_R\,b\right] \tag{4.5.10}$$

with right handed current in the quark sector. However, in the following analysis dimension 8 operators will be ignored.

4.5.2 Correspondence with Wilson Coefficients of WET

Now, an expansion in components of the various $SU(2)$ multiplets is performed, together with electroweak symmetry breaking, in order to relate the Wilson Coefficients of the $SU(2)_L \times U(1)_Y$ invariant operators to those in Section 4.1. Focusing on the operators of Eq. (4.5.1) and Eq. (4.5.5):

$$\begin{aligned}\left(\bar{l}'_{p'}\gamma_\mu\sigma^I l'_{r'}\right)\left(\bar{q}'_{s'}\gamma^\mu\sigma^I q'_{t'}\right) &= \left(\bar{\nu}'_{p'}\gamma^\mu P_L\nu'_{r'}\right)\left(\bar{u}'_{s'}\gamma_\mu P_L u'_{t'}\right) + \left(\bar{e}'_{p'}\gamma^\mu P_L e'_{r'}\right)\left(\bar{d}'_{s'}\gamma_\mu P_L d'_{t'}\right)\\ &\quad - \left(\bar{e}'_{p'}\gamma^\mu P_L e'_{r'}\right)\left(\bar{u}'_{s'}\gamma_\mu P_L u'_{t'}\right) - \left(\bar{\nu}'_{p'}\gamma^\mu P_L\nu'_{r'}\right)\left(\bar{d}'_{s'}\gamma_\mu P_L d'_{t'}\right)\\ &\quad + 2\left(\bar{\nu}'_{p'}\gamma^\mu P_L e'_{r'}\right)\left(\bar{d}'_{s'}\gamma_\mu P_L u'_{t'}\right) + 2\left(\bar{e}'_{p'}\gamma^\mu P_L\nu'_{r'}\right)\left(\bar{u}'_{s'}\gamma_\mu P_L d'_{t'}\right) \end{aligned}\tag{4.5.11}$$

$$\begin{aligned}\left(\phi^\dagger i\overleftrightarrow{D}^I_\mu\phi\right)\left(\bar{l}'_{p'}\,\sigma^I\gamma^\mu\,l'_{r'}\right) &= \Bigg[-\frac{1}{2}\frac{g_2}{\cos\theta_W}Z_\mu\left(\overline{\nu}'_{p'}\gamma^\mu P_L\nu'_{r'}\right) + \frac{1}{2}\frac{g_2}{\cos\theta_W}Z_\mu\left(\overline{e}'_{p'}\gamma^\mu P_L e'_{r'}\right)\\ &\quad - \frac{g_2}{\sqrt{2}}W^+_\mu\left(\overline{\nu}'_{p'}\gamma^\mu P_L e'_{r'}\right) - \frac{g_2}{\sqrt{2}}W^-_\mu\left(\overline{e}'_{p'}\gamma^\mu P_L\nu'_{r'}\right)\Bigg]\left(v^2+2vh+h^2\right)\,.\end{aligned}\tag{4.5.12}$$

The scalar and tensor operators can be decomposed similarly. It is clear that, as a consequence of the manifest $SU(2)_L \times U(1)_Y$ gauge invariance, the operators relevant for the explanation of the R_D and R_{D^*} anomalies are no more independent from other operators, in particular to the ones that give rise to neutral current interactions, both through four fermion effective vertices (Eq. (4.5.11)) and via a modification of the Z coupling to fermions (Eq. (4.5.12)).

Rotation from the gauge to the mass eigenstates.

Since the observable lepton flavor universality violating effects should be studied in the fermion mass basis, a rotation is performed, using the following mixing matrices, that relate gauge and

mass eigenstates

$$(e_{L,R})_{r'} = (V^e_{L,R})_{r'r}(e_{L,R})_r, \quad (\nu_{L,R})_{r'} = (V^\nu_{L,R})_{r'r}(\nu_{L,R})_r\,,$$
$$(u_{L,R})_{r'} = (V^u_{L,R})_{r'r}(u_{L,R})_r, \quad (d_{L,R})_{r'} = (V^d_{L,R})_{r'r}(d_{L,R})_r \tag{4.5.13}$$

The CKM and PMNS matrices are defined as

$$V_{\rm CKM} = (V^u_L)^\dagger V^d_L, \quad V_{\rm PMNS} = (V^\nu_L)^\dagger V^e_L\,. \tag{4.5.14}$$

Using the above definition of the mixing matrices, one obtains that the deviations from the SM values for the Wilson Coefficients of the vector and axial vector effective four fermion operators $\mathcal{O}^\tau_{\rm VL}$ and $\mathcal{O}^\tau_{\rm AL}$ can be expressed as a function of some elements of the WCs related to the gauge invariant operators of Eq. (4.5.1) and (4.5.5), that are matrices in flavor space, in the following way

$$\Delta C^{cb\tau\nu_3}_{\rm VL} = \frac{\Lambda^2_{\rm SM}}{\Lambda^2}\left[[\tilde{C}^{(3)e\nu ud}_{lq}]_{3323} + \left([\tilde{C}^{(3)\nu edu}_{lq}]_{3332}\right)^*\right]$$
$$-\frac{\Lambda^2_{\rm SM}}{\Lambda^2}\left[[\tilde{C}^{(3)e\nu}_{\phi l}]_{33} + \left([\tilde{C}^{(3)\nu e}_{\phi l}]_{33}\right)^*\right]V_{cb} \tag{4.5.15}$$
$$\Delta C^{cb\tau\nu_3}_{\rm AL} = -\Delta C^{cb\tau\nu_3}_{\rm VL} \tag{4.5.16}$$

where ν_3 is the third neutrino mass eigenstate and the $[\tilde{C}]$ couplings are related to the $[C]'$ couplings of Section 4.5.1 by appropriate mixing matrices, for example (see Appendix B for the complete basis rotation of the operators in Eq. (4.5.1) -(4.5.7))

$$\sum_{p',r',s',t'} [C^{(3)}_{lq}]'_{p'r's't'}(V^\nu_L)^\dagger_{pp'}(V^\nu_L)_{r'r}(V^u_L)^\dagger_{ss'}(V^u_L)_{t't} \equiv [\tilde{C}^{(3)\nu\nu uu}_{lq}]_{prst}\,. \tag{4.5.17}$$

One can notice that the contribution from the scalar fermion operator $\left(\phi^\dagger i\overleftrightarrow{D}^I_\mu\phi\right)\left(\bar{l}'_{p'}\,\sigma^I\gamma^\mu\,l'_{r'}\right)$ has a further V_{cb} suppression with respect to the one from the four fermion operator $\left(\bar{l}'_{p'}\gamma_\mu\sigma^I l'_{r'}\right)$.

Obviously, the condition $C^\tau_{\rm VL} = -C^\tau_{\rm AL}$ is fulfilled, since the contributions to these WCs come from operators involving left handed fermion currents. Similar relations can also be found for the scalar and tensor operators.

From the above expression of $\Delta C^{cb\tau\nu_3}_{\rm VL} = -\Delta C^{cb\tau\nu_3}_{\rm AL}$ it is evident that these WCs depends on $\tilde{C}^{(3)}_{lq}$ and $\tilde{C}^{(3)}_{\phi l}$ parameters entering also in other observables: electroweak gauge invariance implies a strong correlation between flavor violating neutral and charged current observables, i.e. between $b \to c\tau\nu$ amplitude and other (strictly) constrained low energy processes, which will be analyzed in the following Sections.

4.5.3 Constraints on $C^{(3)}_{\phi l}$ from correlated observables

The operator $\mathcal{O}^{(3)}_{\phi l} = \left(\phi^\dagger i\overleftrightarrow{D}^I_\mu\phi\right)\left(\bar{l}'_{p'}\,\sigma^I\gamma^\mu\,l'_{r'}\right)$ modifies the leptonic charged and neutral current vertices of W and Z bosons respectively (see Eq. (4.5.12)). In particular, in order to explain the

$R_{D^{(*)}}$ data by this operator, lepton non-universality has to be introduced in the W vertex; as a consequence of gauge invariance, the violation of LFU is then induced also in the Z coupling. Assuming that NP contribution enters in the boson coupling with the third fermion generation, we study the modification of the $W\tau\nu$ effective vertex, which in presence of this scalar fermion operator is

$$\mathcal{L}_{W\tau\nu} = -\frac{g_2}{\sqrt{2}}(1+\Delta g_W)\left(W^-_\mu \bar{\tau}\gamma^\mu P_L \nu_\tau + h.c.\right), \tag{4.5.18}$$

$$\Delta g_W = \left[\left([\tilde{C}^{(3)e\nu}_{\phi l}] + [\tilde{C}^{(3)\nu e}_{\phi l}]^\dagger\right)_{33}\right]\frac{v^2}{\Lambda^2}. \tag{4.5.19}$$

However, a strong bound on such LFU violating effects exists from LEP [137]:

$$\frac{\mathcal{B}(W^+\to\tau^+\nu)}{[\mathcal{B}(W^+\to\mu^+\nu)+\mathcal{B}(W^+\to e^+\nu)]/2} = 1.077\pm 0.026\,. \tag{4.5.20}$$

This means that the branching ratio of $W^+\to\tau^+\nu$ can exceed that of $W^+\to\mu^+\nu$ or $W^+\to e^+\nu$ at most by 10.3% at 1σ. Thus the correction to the $W\tau\nu$ vertex can at most be 5% of the SM, assuming that the $W\bar{\mu}\nu$ and $W\bar{e}\nu$ vertices have no NP contribution. This translates into an upper bound on the elements of $\tilde{C}^{(3)e\nu}_{\phi l}$ WC associated to the third generation

$$-\left[\left([\tilde{C}^{(3)e\nu}_{\phi l}] + [\tilde{C}^{(3)\nu e}_{\phi l}]^\dagger\right)_{33}\right]\frac{v^2}{\Lambda^2} \lesssim 0.05\,, \tag{4.5.21}$$

which, from the second line of Eq. (4.5.15), implies

$$\Delta C^\tau_{\rm VL} = -\Delta C^\tau_{\rm AL} < 0.05\,, \tag{4.5.22}$$

where $v^2 = 1/(\sqrt{2}G_F) = \Lambda^2_{\rm SM}V_{cb} \approx (246\text{ GeV})^2$ has been used.

As shown in Section 4.4.1, $\Delta C^\tau_{\rm VL} = -\Delta C^\tau_{\rm AL} < 0.05$ is not enough to explain the $R_{D^{(*)}}$ data within their $1\,\sigma$ experimental ranges. It is also related to the fact that, as can be seen from Eq. (4.5.15), contribution of this operator to the WCs $C^\tau_{\rm VL} = -C^\tau_{\rm AL}$ is suppressed by V_{cb} compared to the other contribution, from the four fermion operator.

A much stronger indirect constraint on the $W\tau\nu$ coupling can be obtained from measurements of leptonic τ decays assuming that no other four fermion operator that can either contribute to $\tau\to e\,\nu\,\bar{\nu}$ or $\mu\to e\,\nu\,\bar{\nu}$ exists [138]. Assuming no NP in the $W\mu\,\nu$ vertex, this gives

$$-0.4\times 10^{-3} \lesssim -\left[\left([\tilde{C}^{(3)e\nu}_{\phi l}] + [\tilde{C}^{(3)\nu e}_{\phi l}]^\dagger\right)_{33}\right]\frac{v^2}{\Lambda^2} \lesssim 2.6\times 10^{-3}\,. \tag{4.5.23}$$

which would imply a constraint on the vector and axial vector WCs by far too strict to account for charged current flavor anomalies

$$\Delta C^\tau_{\rm VL} = -\Delta C^\tau_{\rm AL} \lesssim 10^{-3}\,. \tag{4.5.24}$$

The scalar fermion $d = 6$ operator also modifies the Z coupling to left handed fermion currents; in particular the modification of $Z_\mu \bar{\tau}\gamma^\mu P_L \tau$ is given by

$$\mathcal{L}_{Z\tau\tau} = -\frac{g_2}{\cos\theta_W} Z_\mu \left((g_L^\tau + \Delta g_L^\tau) \bar{\tau}\gamma^\mu P_L \tau + (g_R^\tau + \Delta g_R^\tau) \bar{\tau}\gamma^\mu P_R \tau \right) , \tag{4.5.25}$$

$$\begin{aligned} g_L^\tau = \; -1/2 + \sin^2\theta_W \approx -0.27 \quad \text{and} \quad g_R^\tau = \sin^2\theta_W \approx 0.23 \quad (g_{V,A}^\tau = g_L^\tau \pm g_R^\tau) \\ \Delta g_L^\tau = \tfrac{1}{2} \left[\left([\tilde{C}_{\phi l}^{(3)e\nu}] + [\tilde{C}_{\phi l}^{(3)\nu e}]^\dagger \right) V_{\text{PMNS}} \right]_{33} \tfrac{v^2}{\Lambda^2} , \quad \Delta g_R^\tau = 0 . \end{aligned} \tag{4.5.26}$$

Using the experimental constraint on the Z coupling from LEP [139], which provides an upper bound on the modification $|\Delta g_L^\tau|$, and assuming that there is no NP in the decays to light leptons, one gets again an upper bound on the 33 elements of the WC matrix $\tilde{C}_{\phi l}^{(3)e\nu}$

$$|\Delta g_L^\tau| \lesssim 6 \times 10^{-4} \quad \Rightarrow \quad \left| \left([\tilde{C}_{\phi l}^{(3)e\nu}] + [\tilde{C}_{\phi l}^{(3)\nu e}]^\dagger \right)_{33} \right| \lesssim 0.02 \left(\frac{\Lambda^2}{\text{TeV}^2} \right) \tag{4.5.27}$$

$$\Rightarrow \quad \Delta C_{\text{VL}}^\tau \lesssim 0.001 . \tag{4.5.28}$$

where $(V_{\text{PMNS}})_{33} = 1$ has been assumed. In any case, given the strong experimental constraints, the results would not be changed if correct values of V_{PMNS} matrix were used. It is an upper bound much more strict than the one in Eq. (4.5.22), comparable to the indirect constraint from leptonic τ decay.

Similarly, the scalar fermion operator induces a modification of the Z coupling with third generation (LH) neutrinos

$$\Delta g_L^\nu = -\frac{1}{2} \left[V_{\text{PMNS}} \left([\tilde{C}_{\phi l}^{(3)e\nu}] + [\tilde{C}_{\phi l}^{(3)\nu e}]^\dagger \right) \right]_{33} \frac{v^2}{\Lambda^2} . \tag{4.5.29}$$

Compared with the experimental constraint [139], one obtains the upper bound

$$|\Delta g_L^\nu| \lesssim 1.2 \times 10^{-3} . \tag{4.5.30}$$

which is quite strong, but in any case milder than the one of Eq. (4.5.27) coming from $Z\tau\tau$ coupling.

Given these constraints, coming from measurements of correlated low energy observables in which no hint of LFU violation is seen, it is clear that the operator $\mathcal{O}_{\phi l}^{(3)}$ alone is unable to explain the $R_{D^{(*)}}$ data; thus, this operator will be ignored in the following.

4.5.4 Constraints on $C_{lq}^{(3)}$ from correlated observables.

Here, a EFT with only the operator $\mathcal{O}_{lq}^{(3)}$ of Eq. (4.5.1) is considered and the correlations arising from it are investigated. Indeed, as previously seen, in the present work the analysis is centered on vector effective operators, which constitute a EFT that is not disfavored by the upper bound on $\mathcal{B}(B_c \to \tau\,\nu)$, that has less tension with $R_{J/\psi}$ measurements and that can be

easily obtained in simplified models with vector heavy mediators. Since in Section 4.5.3 it has been shown that a consistent explanation of charged current flavor anomalies, together with some precision measurements (such as weak boson couplings and τ decay in which no LFU violation is observed), is not feasible with the scalar fermion operator $\mathcal{O}_{\phi l}^{(3)}$ alone, we are left with the hypothesis of a EFT with the four fermion $d = 6$ gauge invariant operator.

Without loss of generality, we now go to a basis where the left chiral down quarks and left chiral charged leptons are in the mass basis, which just means that primed WCs of Section 4.5.1 are defined in this basis. This amounts to setting

$$V_L^e = \mathbb{1}_{3\times 3} \quad , \qquad V_L^d = \mathbb{1}_{3\times 3} \, . \tag{4.5.31}$$

In this basis, we have

$$V_{\rm CKM} = V_L^{u\dagger} \quad , \qquad V_{\rm PMNS} = V_L^{\nu\dagger} \, . \tag{4.5.32}$$

Let us consider the contribution to the operator $(\bar{\tau}\gamma^\mu P_L \nu)\,(\bar{c}\gamma_\mu P_L b)$, namely to $\mathcal{O}^\tau_{\rm VL} - \mathcal{O}^\tau_{\rm AL}$ of Section 4.1. As a function of the WCs $[C_{lq}^{(3)}]'_{p'r's't'}$, associated to operators before the rotation into the mass basis, assuming that they are diagonal in the lepton flavors, one gets

$$C_{lq}^{(3)\prime}\mathcal{O}_{lq}^{(3)} \supset -2\left([\tilde{C}_{lq}^{(3)e\nu ud}]_{3r23} + ([\tilde{C}_{lq}^{(3)\nu edu}]_{r332})^*\right)(\bar{\tau}\gamma^\mu P_L \nu_r)\,(\bar{c}\gamma_\mu P_L b) \tag{4.5.33}$$

$$\begin{aligned} &= -2\Big(([C_{lq}^{(3)}]'_{3313} + ([C_{lq}^{(3)}]'_{3331})^*)V_{cd} + ([C_{lq}^{(3)}]'_{3323} + ([C_{lq}^{(3)}]'_{3332})^*)V_{cs} \\ &+([C_{lq}^{(3)}]'_{3333} + ([C_{lq}^{(3)}]'_{3333})^*)V_{cb}\Big) \times [V^\dagger_{\rm PMNS}]_{3r}\,(\bar{\tau}\gamma^\mu P_L \nu_r)\,(\bar{c}\gamma_\mu P_L b) \end{aligned} \tag{4.5.34}$$

Note that $\nu_{L\tau} = [V^\dagger_{\rm PMNS}]_{3r}\,\nu_{L\,r}$, $\nu_{L\tau}$ is the τ-flavor neutrino, while r stands for anyone of the three neutrino mass eigenstates. We end up with the sum of three different contributions, each one proportional to a $V_{\rm CKM}$ matrix element. As discussed in the previous Sections, in order to explain the anomalies at the $1\,\sigma$ level, the coefficient of the operator $(\bar{\tau}\gamma^\mu P_L \nu_\tau)\,(\bar{c}\gamma_\mu P_L b)$ in Eq. (4.5.34) should at least be ~ 0.16 at $\Lambda = \Lambda_{\rm SM}$. This gives

$$\begin{aligned} &([C_{lq}^{(3)}]'_{3313} + ([C_{lq}^{(3)}]'_{3331})^*)V_{cd} + ([C_{lq}^{(3)}]'_{3323} + ([C_{lq}^{(3)}]'_{3332})^*)V_{cs} + \\ &+([C_{lq}^{(3)}]'_{3333} + ([C_{lq}^{(3)}]'_{3333})^*)V_{cb} \gtrsim 0.06\left(\frac{\Lambda^2}{\rm TeV^2}\right) . \end{aligned} \tag{4.5.35}$$

One should understand whether this condition is consistent with the low energy data, such as other measurements of $\Delta F = 1$ B-meson decays or precision tests on Z and W couplings. In the following, there is an analysis of the constraints that separately apply on the coefficients of the three different terms in Eq. (4.5.34).

- Constraints on $[\mathbf{C_{lq}^{(3)}}]'_{\mathbf{3313}}$

  The first term on the left hand side of Eq. (4.5.35) contributes to $b \to d\,\bar{\nu}\,\nu$ parton interaction, leading to the $B^0 \to \pi^0 \bar{\nu}\,\nu$ process. Using the experimental bound on $\mathcal{B}(B^0 \to \pi^0 \bar{\nu}\,\nu)$ [140] and the corresponding SM prediction from [141], one obtains

$$-0.018\left(\frac{\Lambda^2}{\rm TeV^2}\right) \lesssim [C_{lq}^{(3)}]'_{3313} + [C_{lq}^{(3)\prime *}]_{3331} \lesssim 0.023\left(\frac{\Lambda^2}{\rm TeV^2}\right) . \tag{4.5.36}$$

The same coupling enters in the charged current four fermion interaction $b\,u\,\tau\,\nu_\tau$ and thus it can also be constrained by measurement of $\mathcal{B}(B_u \to \tau\,\nu_\tau)$. Assuming that the maximum allowed value of this branching ratio is twice the one of the SM [142], if only $\mathcal{O}_{lq}^{(3)}$ is present we get a bound comparable with the previous one

$$-0.15\left(\frac{\Lambda^2}{\text{TeV}^2}\right) \lesssim [C_{lq}^{(3)}]'_{3313} + [C_{lq}^{(3)}]'^*_{3331} \lesssim 0.025\left(\frac{\Lambda^2}{\text{TeV}^2}\right) . \tag{4.5.37}$$

- Constraints on $[\mathbf{C_{lq}^{(3)}}]'_{\mathbf{3323}}$

  This matrix element of the WC $[C_{lq}^{(3)}]'$ enters also in the contribution to the $(\bar\nu\gamma^\mu P_L\nu)\,(\bar s\gamma_\mu P_L b)$ effective interaction, that describes at parton level the decay $B \to K^*\bar\nu\nu$, as follows

$$\left([C_{lq}^{(3)}]'_{p'r'23} + [C_{lq}^{(3)}]'^*_{r'p'32}\right)(\bar\nu_{p'}\gamma^\mu P_L\nu_{r'})\,(\bar s\gamma_\mu P_L b) . \tag{4.5.38}$$

  Experimental bound on $\mathcal{B}(B^0 \to K^{*0}\bar\nu\nu)$ [140] then requires the Wilson Coefficients to satisfy (the SM prediction is taken from [143]),

$$-0.005\left(\frac{\Lambda^2}{\text{TeV}^2}\right) \lesssim [C_{lq}^{(3)}]'_{3323} + [C_{lq}^{(3)}]'^*_{3332} \leqslant 0.025\left(\frac{\Lambda^2}{\text{TeV}^2}\right) . \tag{4.5.39}$$

Thus, the maximum contribution from the V_{cu} and V_{cs} terms of Eq. (4.5.35), subject to the constraints in Eq. 4.5.39 and 4.5.37, is $\approx 0.03\,(\Lambda^2/\text{TeV}^2)$. This translates into a lower bound on the contribution to $b \to c\tau\nu$ proportional to V_{cb} (see also [144] for a related discussion)

$$([C_{lq}^{(3)}]'_{3333} + [C_{lq}^{(3)}]'^*_{3333})V_{cb} \gtrsim 0.03\left(\frac{\Lambda^2}{\text{TeV}^2}\right) . \tag{4.5.40}$$

It is important to investigate whether also the WC element $([C_{lq}^{(3)}]'_{3333} + [C_{lq}^{(3)}]'^*_{3333})$ is constrained by other measurements.

- Constraints on $[\mathbf{C_{lq}^{(3)}}]'_{\mathbf{3333}}$

  This parameter enters in the $\mathcal{O}_{lq}^{(3)}$ contribution to the neutral current, pure third generation and down-type fermion operator $(\bar\tau\gamma^\mu P_L\tau)\left(\bar b\gamma_\mu P_L b\right)$ through the coefficient

$$[\tilde C_{lq}^{(3)eedd}]_{3333} + ([\tilde C_{lq}^{(3)eedd}]_{3333})^* = [C_{lq}^{(3)}]'_{3333} + ([C_{lq}^{(3)}]'_{3333})^* . \tag{4.5.41}$$

  Direct searches of processes involving two final τ leptons constrain this coupling weakly[112]:

$$\left|[C_{lq}^{(3)}]'_{3333} + ([C_{lq}^{(3)}]'_{3333})^*\right| < 2.6\left(\frac{\Lambda^2}{\text{TeV}^2}\right) . \tag{4.5.42}$$

  Moreover, the same coupling also appears in the coefficient of the operator $(\bar\tau\gamma^\mu P_L\tau)\,(\bar t\gamma_\mu P_L t)$, which is

$$\left[\tilde C_{lq}^{(3)eeuu}\right]_{3333} + \left[\tilde C_{lq}^{(3)eeuu}\right]^*_{3333} \tag{4.5.43}$$

$$\text{where} \qquad \left[\tilde{C}^{(3)eeuu}_{lq}\right]_{3333} = \left[C^{(3)}_{lq}\right]'_{p'r's't'} \left(V^e_L\right)^\dagger_{3p'} \left(V^e_L\right)_{r'3} \left(V^u_L\right)^\dagger_{3s'} \left(V^u_L\right)_{t'3} =$$

$$\begin{aligned} = \; & \left[C^{(3)}_{lq}\right]'_{3333} |V_{tb}|^2 + \left[C^{(3)}_{lq}\right]'_{3323} V_{ts} V^*_{tb} + \left[C^{(3)}_{lq}\right]'_{3332} V_{tb} V^*_{ts} + \\ & \left[C^{(3)}_{lq}\right]'_{3311} |V_{td}|^2 + \left[C^{(3)}_{lq}\right]'_{3313} V_{td} V^*_{tb} + \left[C^{(3)}_{lq}\right]'_{3331} V_{tb} V^*_{td} + \\ & \left[C^{(3)}_{lq}\right]'_{3322} |V_{ts}|^2 + \left[C^{(3)}_{lq}\right]'_{3312} V_{td} V^*_{cb} + \left[C^{(3)}_{lq}\right]'_{3321} V_{cb} V^*_{td} \,. \end{aligned} \tag{4.5.44}$$

The 2nd, 3rd, 5th and 6th terms in Eq. (4.5.44) are small because of bounds in Eq. (4.5.37) and (4.5.39). All the terms which are of the form $[C^{(3)}_{lq}]'_{33ij}$, $i,j = 1,2$ are constrained by direct searches of $\tau\,\tau$ final state, discussed in Section 4.3. Since the di-jet $\to \tau\tau$ cross section is enhanced compared to that of $\bar{b}\,b \to \tau^+\tau^-$ due to larger parton distribution functions, these bounds are stronger than Eq. (4.5.42) by a factor of ~ 2 for $([C^{(3)}_{lq}]'_{3322} + \text{c.c})$ to a factor of ~ 8 for $([C^{(3)}_{lq}]'_{3311} + \text{c.c})$.
Thus, the only term which remains is of the form

$$\left(\left[C^{(3)}_{lq}\right]'_{3333} + \left[C^{(3)}_{lq}\right]'^*_{3333}\right) |V_{tb}|^2 \,. \tag{4.5.45}$$

This $(\bar{\tau}\gamma^\mu P_L \tau)\,(\bar{t}\gamma_\mu P_L t)$ operator contributes at one-loop level to the modification of the Z coupling to τ, namely to Δg^τ_L [145], analyzed also in the case of $\mathcal{O}^{(3)}_{\phi l}$. Indeed, $[C^{(3)}_{lq}]'$ enters in the one-loop renormalization of the WC $[C^{(3)}_{\phi l}]'$. As Δg^τ_L is very strongly constrained, see Eq. (4.5.27), this provides a stringent constraint on the coupling of Eq. (4.5.45). As will be shown in Eq. (4.5.64) of Section 4.5.4, one can find

$$\left|[C^{(3)}_{lq}]'_{3333} + [C^{(3)}_{lq}]'^*_{3333}\right| \lesssim \frac{0.017}{V_{cb}} \left(\frac{\Lambda}{\text{TeV}}\right)^2 \frac{1}{1 + 0.6 \log \frac{\Lambda}{\text{TeV}}} \,, \tag{4.5.46}$$

which is clearly incompatible with the lower bound of Eq. (4.5.40).

This rules out the possibility of explaining $R_{D^{(*)}}$ anomalies by this V_{cb} term, unless there are other contributions to the modifications of the Z couplings making it compatible with the experimental observations.

So far, it has been assumed that only one gauge invariant operator at a time was present and provided the NP contribution at the origin of charged current flavor anomalies. However, as discussed, it is impossible in this way to explain R_D and R_{D^*} without inducing LFU violating effects in other correlated processes, in which they are not observed. The presence of other operators can however help evade some of these constraints [63]. For example, one possibility is to assume the presence also of the operator $\mathcal{O}^{(1)}_{lq}$ analogous to $\mathcal{O}^{(3)}_{lq}$ but in which the fermion currents are $SU(2)_L$ singlets

$$\mathcal{L}^{\text{dim6}} \supset -\frac{1}{\Lambda^2} \sum_{p'r's't'} [C^{(1)}_{lq}]'_{p'r's't'} \left(\bar{l}'_{p'} \gamma_\mu l'_{r'}\right) \left(\bar{q}'_{s'} \gamma^\mu q'_{t'}\right) + \text{h.c.} \,. \tag{4.5.47}$$

For appropriate values of the WCs, it can cancel the large contribution from the triplet operator both in $b \to s\,\bar{\nu}\,\nu$ [63] and Δg^τ_L [145, 146]. However, new physics contributions to Δg^τ_L, Δg^ν_L

and Δg_W^τ cannot be cancelled simultaneously. In fact, while the operator $\mathcal{O}_{lq}^{(3)}$ generates the operator $\mathcal{O}_{\phi l}^{(3)}$ and not $\mathcal{O}_{\phi l}^{(1)}$ through RG running, the operator $\mathcal{O}_{lq}^{(1)}$ generates the operator $\mathcal{O}_{\phi l}^{(1)}$ and not $\mathcal{O}_{\phi l}^{(3)}$. Another way to see this is that the operator $\mathcal{O}_{\phi l}^{(3)}$ contributes to Δg_L^τ and Δg_L^ν with opposite signs, due to the fact that charged leptons and neutrinos have opposite T_3 charges (see Eq. (4.5.12)), while $\mathcal{O}_{\phi l}^{(1)}$ contributes to them with the same sign. Thus, taking into account constraints from Δg_L^ν , Δg_L^τ and Δg_W^τ, in presence of both four fermion operators, one gets (see Section 4.5.4)

$$\left|[C_{lq}^{(3,1)}]'_{3333} + [C_{lq}^{(3,1)}]'^*_{3333}\right| \lesssim \frac{0.025}{V_{cb}} \left(\frac{\Lambda}{\text{TeV}}\right)^2 \frac{1}{1 + 0.6 \log \frac{\Lambda}{\text{TeV}}} \,. \tag{4.5.48}$$

Again, it is a too strict bound if we want to explain $R_{D^{(*)}}$ using $\mathcal{O}_{lq}^{(3)}$ operator. This makes the explanation of the charged current anomalies by the third term of Eq. (4.5.35) impossible even in the presence of the operator of Eq. (4.5.47). This leaves us with two possibilities :

I. The anomaly is explained by the second term, proportional to V_{cs}, in Eq. (4.5.35). The tension with the $\mathcal{B}(B^0 \to K^{*0}\bar{\nu}\nu)$ in Eq. (4.5.39) is assumed to be cured by cancellation between the $\mathcal{O}_{lq}^{(3)}$ and $\mathcal{O}_{lq}^{(1)}$ contribution. However, in this case, the flavor structure of the SM UV completion must be such that the last term of Eq. (4.5.35) is significantly smaller than the second one: this cannot be achieved on the base of a completely model independent and agnostic approach.

II. The other possibility is to assume the presence of appropriate UV contribution at the matching scale that takes care of the $\Delta g_L^{\tau,\nu}$ constraints. In this case, one can explain charged current flavor anomalies by the third (V_{cb}) term of Eq. (4.5.35) alone.

In Partial Compositeness framework, as the one studied in Sections 4.7.2 and 4.7.3, elements of both the above mechanisms can in principle be present.

Now, we discuss a couple of $\Delta F = 1$ observables, associated to b decays and correlated to the $b \to c\tau\nu$ amplitude relevant for $R_{D^{(*)}}$, whose relevance may change if the four fermion operator $\mathcal{O}_{lq}^{(1)}$ is added to an EFT with $\mathcal{O}_{lq}^{(3)}$, even if they do not provide strong constraints at the moment.

- **$b \to s\tau\tau$**

  The coefficient of the operator $(\bar{\tau}\gamma^\mu P_L \tau)\,(\bar{s}\gamma_\mu P_L b)$ is given by

  $$-\left([C_{lq}^{(3)}]'_{3323} + ([C_{lq}^{(3)}]'^*_{3332}\right). \tag{4.5.49}$$

  Considering a scenario (I), where $B \to K^*\bar{\nu}\nu$ transition, that otherwise is at the origin of stronger constraints with respect to $B_s \to \tau^+\tau^-$, is cancelled by the $\mathcal{O}_{lq}^{(1)}$ operator and the $\mathcal{O}_{lq}^{(3)}$ contribution to $R_{D^{(*)}}$ is dominated by the V_{cs} term, the WC of this neutral current four fermion operator is $\Delta C_9^\tau = -\Delta C_{10}^\tau = -35$ and the corresponding Lagrangian is

  $$\mathcal{L}_{b\to s\tau\tau} = -35\,\frac{4G_F}{\sqrt{2}}\,V_{tb}V_{ts}^*\,\frac{\alpha_{em}}{4\pi}\,[\bar{\tau}\gamma^\mu(1-\gamma_5)\tau][\bar{s}\gamma_\mu P_L b]\,. \tag{4.5.50}$$

giving rise to large enhancement in $B_s \to \tau^+\tau^-$ (by a factor of ~ 50 compared to the SM in the branching ratio) and $B \to K/K^*\,\tau^+\tau^-$ decays (by a factor of ~ 60 (for K), 75 (for K^*) compared to the SM in the branching ratio). It is interesting to notice that large enhancement in $\mathcal{B}(B_s \to \tau^+\tau^-)$ was also proposed as a possible solution to the like-sign di-muon charge asymmetry observed in one of the experiments in Tevatron [147, 148].

- $\mathbf{b \to u\tau\nu}$

  The $\mathcal{O}_{lq}^{(3)}$ operator generates a contribution to $(\bar{\tau}\gamma^\mu P_L \nu)\,(\bar{u}\gamma_\mu P_L b)$, through the WC

$$
\begin{aligned}
&-\left(2[\tilde{C}_{lq}^{(3)e\nu ud}]_{3r13} + 2([\tilde{C}_{lq}^{(3)\nu edu}]_{r331})^*\right)(\bar{\tau}\gamma^\mu P_L \nu_r)\,(\bar{u}\gamma_\mu P_L b) && (4.5.51)\\
&= -2\Big(([C_{lq}^{(3)}]'_{3313} + ([C_{lq}^{(3)}]'_{3331})^*)V_{ud} + ([C_{lq}^{(3)}]'_{3323} + ([C_{lq}^{(3)}]'_{3332})^*)V_{us}\\
&\qquad +([C_{lq}^{(3)}]'_{3333} + ([C_{lq}^{(3)}]'_{3333})^*)V_{ub}\Big) \times (\bar{\tau}\gamma^\mu P_L \nu_\tau)\,(\bar{u}\gamma_\mu P_L b) && (4.5.52)
\end{aligned}
$$

  where $\nu_{L\tau} = [V_L^\nu]_{3r}\nu_r$ and under the assumption that the NP Wilson Coefficients, $[C_{lq}^{(3)}]'_{p'r's't'}$, are diagonal in the lepton flavor. This four fermion interaction, correlated to charged current flavor anomalies, was already considered in the derivation of the bound in Eq. (4.5.37). Now, however, we assume the presence of both singlet and triplet operators and thus the $b \to s(d)\nu\nu$ transitions do not lead to any constraints. Then, if the second (third) term in Eq. (4.5.35) is responsible for $R_{D^{(*)}}$ anomalies, i.e. saturates the inequality, then it also provides the dominant contribution in Eq. (4.5.52) and the coupling of this charged current semileptonic b decay, expressed in terms of V_{ub} is

$$
\mathcal{L}_{b\to u\tau\nu} \;\approx\; -0.2(0.1)\,\frac{4G_F}{\sqrt{2}}\,V_{ub}\,(\bar{\tau}\gamma^\mu P_L \nu_\tau)\,(\bar{u}\gamma_\mu P_L b)\;, \qquad (4.5.53)
$$

  which leads to approximately 45% (20%) increase in $\mathcal{B}(B_u \to \tau\,\nu_\tau)$ with respect to SM.

  Instead, if one assumes that the first term in Eq. (4.5.35) is responsible for charged current flavor anomalies and saturates the inequality, the corresponding NP coupling for $b \to u\tau\nu$ becomes

$$
\mathcal{L}_{b\to u\tau\nu} \;\approx\; -4\,\frac{4G_F}{\sqrt{2}}\,V_{ub}\,(\bar{\tau}\gamma^\mu P_L \nu_\tau)\,(\bar{u}\gamma_\mu P_L b)\;, \qquad (4.5.54)
$$

  which is obviously ruled out by experimental data. Thus, even in the presence of cancellation in $b \to d\,\bar{\nu}\,\nu$, an explanation of $R_{D^{(*)}}$ by the first term in Eq. (4.5.35) seems very unlikely.

Similar analysis can also be done for the scalar, pseudo scalar and tensor operators. However, as seen in Section 4.4.2, the scalar and pseudo scalar operators alone cannot explain the anomalies because of the strong constraint from $B_c \to \tau\nu$.
The tensor operator, $[C_{lequ}^{(3)}]'_{p'r's't'}\left(\bar{l'}^j_{p'}\sigma^{\mu\nu}e'_{r'}\right)\epsilon_{jk}\left(\bar{q'}^k_{s'}\sigma_{\mu\nu}u'_{t'}\right)$, on the other hand, cannot contributes to the process $B_c \to \tau\nu$ (see Eq. (4.1.13)), and generates, along with the charged current operator which is relevant for charged current flavor anomalies, also neutral current operators involving up-type quarks, from which the corresponding WC can receive constraints.

Mixing of $[C_{lq}^{(3,1)}]'$ and $[C_{\phi l}^{(3,1)}]'$ at one-loop level

In this Section, the one-loop renormalization of the Wilson Coefficients $[C_{\phi l}^{(3,1)}]'$, of the operators $\mathcal{O}_{\phi l}^{(3,1)}$, is described, stressing how the WCs $[C_{lq}^{(3,1)}]'$ enter in this RG flow, providing a mixing between the two categories of $d = 6$ gauge invariant operators. This has been used in the derivations of the bounds in Eq. (4.5.46) and (4.5.48). In particular, we will consider an EFT which at the cutoff scale Λ has only the four fermion operators $\mathcal{O}_{lq}^{(3,1)}$, that generate at one-loop level effective scalar lepton operators at lower energy scales, modifying also the boson couplings to leptons.

The β-functions of third generation matrix elements $[C_{\phi l}^{(3)}]'_{33}$ and $[C_{\phi l}^{(1)}]'_{33}$, in presence of only $\mathcal{O}_{\phi l}^{(3,1)}$ and $\mathcal{O}_{lq}^{(3,1)}$, can be approximately written as [130, 149]:

$$\begin{aligned} 16\pi^2 \frac{d}{d\log\mu}[C_{\phi l}^{(3)}]'_{33} &= \left(-5g_2^2 + 6y_t^2 + 6y_b^2 + 4y_\tau^2\right)[C_{\phi l}^{(3)}]'_{33} + 3y_\tau^2\,[C_{\phi l}^{(1)}]'_{33} \\ &\quad + \left(2g_2^2 - 6y_b^2 - 6y_t^2\right)[C_{lq}^{(3)}]'_{3333}\,, \qquad (4.5.55) \\ 16\pi^2 \frac{d}{d\log\mu}[C_{\phi l}^{(1)}]'_{33} &= \left(\frac{1}{3}g_1^2 + 6y_t^2 + 6y_b^2 + 6y_\tau^2\right)[C_{\phi l}^{(1)}]'_{33} + 9y_\tau^2\,[C_{\phi l}^{(3)}]'_{33} \\ &\quad + \left(\frac{2}{3}g_1^2 - 6y_b^2 + 6y_t^2\right)[C_{lq}^{(1)}]'_{3333}\,. \qquad (4.5.56) \end{aligned}$$

If the RG evolution is dominated by the $\mathcal{O}_{lq}^{(3,1)}$ contribution, present at Λ scale, one gets at top mass scale

$$[C_{\phi l}^{(3)}]'_{33}(m_t) \simeq 0.027\,[C_{lq}^{(3)}]'_{3333}(\Lambda)\,\log(\Lambda/m_t)\,, \qquad (4.5.57)$$

$$[C_{\phi l}^{(1)}]'_{33}(m_t) \simeq -0.034\,[C_{lq}^{(1)}]'_{3333}(\Lambda)\,\log(\Lambda/m_t)\,. \qquad (4.5.58)$$

After electroweak symmetry breaking, the scalar fermion operators $\mathcal{O}_{\phi l}^{(3,1)}$ leads to a modification of the Z and W vertices with leptons. Concerning the third flavor generation, at m_t scale one obtains

$$\begin{aligned} \Delta g_L^\tau &\simeq \frac{1}{2}\left([C_{\phi l}^{(3)}]'_{33}(m_t) + [C_{\phi l}^{(3)}]'^{*}_{33}(m_t) + [C_{\phi l}^{(1)}]'_{33}(m_t) + [C_{\phi l}^{(1)}]'^{*}_{33}(m_t)\right)\frac{v^2}{\Lambda^2} \\ &\simeq \left(0.0014\,([C_{lq}^{(3)}]'_{3333} + [C_{lq}^{(3)}]'^{*}_{3333}) - 0.0018\,([C_{lq}^{(1)}]'_{3333} + [C_{lq}^{(1)}]'^{*}_{3333})\right) \\ &\qquad \times \left(\frac{\text{TeV}}{\Lambda}\right)^2 (1 + 0.6\log(\Lambda/\text{TeV})) \qquad (4.5.59) \end{aligned}$$

$$\begin{aligned} \Delta g_L^\nu &\simeq \frac{1}{2}\left(-[C_{\phi l}^{(3)}]'_{33}(m_t) - [C_{\phi l}^{(3)}]'^{*}_{33}(m_t) + [C_{\phi l}^{(1)}]'_{33}(m_t) + [C_{\phi l}^{(1)}]'^{*}_{33}(m_t)\right)\frac{v^2}{\Lambda^2} \\ &\simeq -\left(0.0014\,([C_{lq}^{(3)}]'_{3333} + [C_{lq}^{(3)}]'^{*}_{3333}) + 0.0018\,([C_{lq}^{(1)}]'_{3333} + [C_{lq}^{(1)}]'^{*}_{3333})\right) \\ &\qquad \times \left(\frac{\text{TeV}}{\Lambda}\right)^2 (1 + 0.6\log(\Lambda/\text{TeV})) \qquad (4.5.60) \end{aligned}$$

$$\begin{aligned}\Delta g_W^\tau &\simeq -\left([C_{\phi l}^{(3)}]'_{33}(m_t) + [C_{\phi l}^{(3)}]'^{*}_{33}(m_t)\right)\frac{v^2}{\Lambda^2} \\ &\simeq -0.0028\left([C_{lq}^{(3)}]'_{3333} + [C_{lq}^{(3)}]'^{*}_{3333}\right)\left(\frac{\text{TeV}}{\Lambda}\right)^2(1+0.6\log(\Lambda/\text{TeV})) \qquad (4.5.61)\end{aligned}$$

Therefore, the four fermion operators generated at the integration out Λ scale give rise at one-loop level to non standard $Z\tau\tau$, $Z\nu\nu$ and $W\tau\nu$ effective couplings, that are constrained by precision measurements. One can indeed notice that the relative sign between the contributions from $\mathcal{O}_{\phi l}^{(3)}$ and $\mathcal{O}_{\phi l}^{(1)}$ (or equivalently from $\mathcal{O}_{lq}^{(3)}$ and $\mathcal{O}_{lq}^{(1)}$) to Δg_L^τ and Δg_L^ν is different: a cancellation only in one of these couplings can be ensured by an appropriate choice of the two Wilson Coefficients.

Using $|\Delta g_L^\tau| \lesssim 6\times 10^{-4}$, and in the absence of $[C_{lq}^{(1)}]'_{3333}$, the bounds that can be derived on the third generation element of the $\mathcal{O}_{lq}^{(3)}$ WC is

$$\left|[C_{lq}^{(3)}]'_{3333} + [C_{lq}^{(3)}]'^{*}_{3333}\right| \lesssim \frac{0.43}{(1+0.6\log(\Lambda/\text{TeV}))}\left(\frac{\Lambda}{\text{TeV}}\right)^2 \qquad (4.5.62)$$

$$(4.5.63)$$

In the presence of both $[C_{lq}^{(1)}]'_{3333}$ and $[C_{lq}^{(3)}]'_{3333}$, combining all the constraints on Δg_W^τ, Δg_L^τ and $|\Delta g_L^\nu| < 1.2\times 10^{-3}$, one instead gets

$$\begin{gathered}\left|[C_{lq}^{(1)}]'_{3333} + [C_{lq}^{(1)}]'^{*}_{3333}\right| \lesssim \tfrac{0.5}{(1+0.6\log(\Lambda/\text{TeV}))}\left(\tfrac{\Lambda}{\text{TeV}}\right)^2 \\ \tfrac{-0.63}{(1+0.6\log(\Lambda/\text{TeV}))}\left(\tfrac{\Lambda}{\text{TeV}}\right)^2 \lesssim [C_{lq}^{(3)}]'_{3333} + [C_{lq}^{(3)}]'^{*}_{3333} \lesssim \tfrac{0.14}{(1+0.6\log(\Lambda/\text{TeV}))}\left(\tfrac{\Lambda}{\text{TeV}}\right)^2 . \qquad (4.5.64)\end{gathered}$$

Going beyond the Effective Field Theory analysis

In the previous Sections, it has been illustrated that some other processes e.g., $B \to K^* \nu\,\nu$, $Z\,\tau\,\tau$ and $Z\,\nu\,\nu$ couplings can provide stringent restrictions on the possible explanations of R_D and R_{D^*} anomalies. It emerged that a completely model independent analysis is not entirely successful: some specific assumption on the UV completion should be present in all possible explanations of charged current flavor anomalies, if one wants to be consistent with low energy data.

Furthermore, it would be interesting also to study the correlations with the various $\Delta F = 2$ observables, where the constraints on new physics contributions are particularly strong. Such an analysis requires assumptions on the underlying UV theory, such as power counting rules or specific flavor structure.

Therefore, simplified models with specific heavy mediators are taken into account. In Section 4.6 there is a summary of the different scenarios that could account for flavor anomalies, both charged and neutral current ones, without being ruled out by measurements of correlated observables. Indeed, one is interested in a combined explanation of all flavor anomalies and low energy data, connecting also these deviations from SM to the search of new physics at high-p_T.

In Section 4.7 the focus will be on two chosen simplified models, the ones leading to an EFT with vector four fermion operators, as previously discussed, embedded in a UV completion with Composite Higgs and Partial Compositeness of fermions and vectors.

4.6 Panoramic of Simplified Models

In the literature, many scalar and vector heavy mediators have been considered and are here summarized. They generate the parton level transition $b \to c l \nu$ relevant for $R_{D^{(*)}}$, but also the $b \to s l l$ decay involved in neutral current flavor observable $R_{K^{(*)}}$ (see Section 4.7.4): the interest is the combined explanation of all flavor anomalies. The majority of the resulting EFTs has been already ruled out by the compatibility with the data on low energy observables, high-p_T and direct searches at colliders.

One can consider colorless intermediate states, that generates $b \to c l \nu$ and $b \to s l l$ semileptonic decays through s channel four fermion interactions between a quark and a lepton bilinear. In order to have NP contribution to the processes associated to both charged and neutral current anomalies, non trivial $SU(2)_L$ multiplets should be considered for this mediators. There are the following possibilities, of scalar and vector heavy new particles.

- **Spin 0 colorless bosons**

  One of the simplest possibilities could be to generate the four fermion interactions relevant for flavor anomalies integrating out a heavy scalar $SU(2)_L$ doublet analogous to the Higgs boson and extending the Higgs sector [150], [151], [152]. This simplified model leads to an effective theory describing the $b\,c\,\tau\,\nu$ four fermion interaction via scalar operators.

However, as seen in Section 4.4.2, this particular WET is almost already ruled out by the upper bounds on the $B_c \to \tau\nu$ branching ratio [135], [106], which has strong tension with R_{D^*} if both are generated by a $\mathcal{O}_{\rm PL}$ operator. Then, this simplified model will not be discussed further.

- **Spin 1 colorless bosons**

  Another possibility, widely analyzed in the literature [153], [154], [155], [112], [126], is a $SU(2)_L$ vector triplet $\mathbf{W'} \sim (\mathbf{1}, \mathbf{3})_0$, where $\mathbf{1}$ and $\mathbf{3}$ are the $SU(3)_c$ and $SU(2)_L$ representations respectively and 0 is the $U(1)_Y$ charge. Thus, there are charged $W'^{\pm}$ bosons and a neutral Z' boson, analogously to what happens in the Standard Model. In this way, both the charged and neutral current b decays arise at tree-level.

  Through the integration out of the vectors the effective four fermion operators with vector currents are generated, which is to say that in the Weak Effective Theory $R_{D^{(*)}}$ is described via $\mathcal{O}_{\rm VL}$ and $\mathcal{O}_{\rm AL}$; in particular, if $\mathbf{W'}$ couples with only left handed currents, we end up with $b \to cl\nu$ arising from only the left chiral operator $\mathcal{O}_{\rm VL} - \mathcal{O}_{\rm AL}$.

  However, the same occurs also for other Flavor Changing Neutral Current (FCNC) processes and $\Delta F = 2$ transitions that are strongly constrained. Furthermore, there are also deviations in Z couplings induced at one-loop level, as explained in Section 4.5.4 and 4.5.4, that might be avoided only with specific assumptions in the UV completion. Therefore, these models receive severe bounds from low energy observables. Furthermore, also high-p_T searches of tt and $\tau\tau$ resonances set significant lower bounds on the mass of the vector mediator, that on the other hand is required to be quite light in order to explain charged current flavor anomalies.

  Thus, these simplified models suffer strong tensions among different measurements, even if they may succeed in producing the observed deviations both in $R_{D^{(*)}}$ and $R_{K^{(*)}}$. An embedding of these models will be taken into account in the following Sections.

Then, also colored mediators [156] can be considered, they are the so-called leptoquarks (LQs). They have the peculiar property to turn leptons into quarks and vice versa; thus, they could provide a kind of unification of matter. They can generate a $qq \to ll$ transition via t or u channel processes. In order to build a gauge invariant leptoquark-quark-lepton coupling, the LQ should necessarily be a $SU(3)_c$ triplet (or antitriplet), while both the singlet, doublet and triplet transformations under $SU(2)_L$ are allowed. Furthermore, leptoquarks might be both scalars and vectors. In the following, the LQs that can originate a $b \to cl\nu$ transition, even in absence of right handed neutrinos, are listed and classified with respect to the $SU(2)_L$ structure and to the spin.

- **Spin 0 leptoquarks**

  1. $S_3 \sim (\bar{\mathbf{3}}, \mathbf{3})_{1/3}$. This scalar is a $SU(2)_L$ triplet. Thus, in order to grant gauge invariance, S_3 renormalizable couplings with fermions should involve two $SU(2)_L$ doublets, and thus only left handed quarks and leptons. The interactions between

this LQ and matter are described, using the notation of Eq. (4.5.1)-(4.5.7) for fermions, by two operators: $\overline{q^c}'\,\epsilon\,\sigma^A\,l'\,S_3^A$, involving both quarks and leptons, and $\overline{q^c}'\,\epsilon\,\sigma^A\,q'\,S_3^{A\dagger}$, in which only quarks enter.

The former generates at tree-level the $b \to c l \nu$ transition, relevant for charged current flavor anomalies: integrating it out one obtains the four fermion gauge invariant operators $\mathcal{O}_{lq}^{(3,1)}$, leading to the $V-A$ effective operator $\mathcal{O}_{\rm VL} - \mathcal{O}_{\rm AL}$ in the WET limit. In Section 4.4.1, it was shown that an effective theory with only $\mathcal{C}_{\rm VL} = -\mathcal{C}_{\rm AL}$ can account for the measured values of R_D and R_{D^*}. In the same way, also other low energy observables can receive a NP contribution; neutral current flavor anomalies might be generated too, together with other FCNCs and with Z coupling modifications, that are strongly constrained. On the other hand the renormalizable qqS_3 interaction leads to dangerous proton decay: its presence should be avoided, introducing some symmetry.

A simplified model with S_3 alone, however, is not viable, since it cannot accommodate flavor anomalies without generating too large LFU violating effects in correlated processes, such as $b \to s\nu\nu$ and $Z\nu\nu$ coupling.

2. $S_1 \sim (\bar{\mathbf{3}}, \mathbf{1})_{1/3}$. It is a $SU(2)_L$ singlet and couples both to left and right handed fermions. In absence of right handed neutrinos, the interactions with matter are given by: $\overline{q^c}'\,\epsilon\,l'\,S_1$, $\overline{u^c}'\,e'\,S_1$, $\overline{q^c}'\,\epsilon\,q'\,S_1^*$ and $\overline{u^c}'\,d'\,S_1^*$.

   The last two operators should be forbidden in order to avoid proton decay. The first one generates $\mathcal{O}_{lq}^{(3,1)}$ terms in the SMEFT and $V-A$ $bc\tau\nu$ interactions in the low energy limit, that as discussed allow us to fit $R_{D^{(*)}}$. Then, the LQ coupling with a quark and a lepton $SU(2)_L$ singlets gives rise to the $\mathcal{O}_{lequ}^{(1)}$ and $\mathcal{O}_{lequ}^{(3)}$ gauge invariant operators (see Eq. (4.5.3) and (4.5.4)), with the relation $\mathcal{C}'^{(1)}_{lequ} = -4\,\mathcal{C}'^{(3)}_{lequ}$.

   This leads in the WET to $\mathcal{O}_{\rm SL} - \mathcal{O}_{\rm PL}$ and $\mathcal{O}_{\rm TL}$ scalar and tensor operators, with $\mathcal{C}_{\rm SL} = -\mathcal{C}_{\rm PL} \approx -4\,\mathcal{C}_{\rm TL}$ at m_b scale: this ratio is allowed by a combined fit of R_D and R_{D^*}, as can be seen in Fig. 4.6. As in the case of S_3, anomaly explanation with only this scalar $SU(2)_L$ singlet LQ is in tension with other low energy observables, even if we allow for the presence of right handed neutrinos [104].

3. $R_2 \sim (\mathbf{3}, \mathbf{2})_{7/6}$. It is a $SU(2)_L$ doublet and, thus, can only couple with one fermion doublet and one fermion singlet. The gauge invariant renormalizable interactions between R_2 and matter are: $\overline{u}'\,R_2\,\epsilon\,l'$ and $\overline{e}'\,R_2\,\epsilon\,q'$.

   One can notice that in this case a pure quark-leptoquark interaction is not allowed. As discussed in Section 4.4.4, integrating out this scalar LQ one gets the SMEFT operators of Eq. (4.5.3) and (4.5.4) and the scalar and tensor WET operators $\mathcal{O}_{\rm SL} - \mathcal{O}_{\rm PL}$ and $\mathcal{O}_{\rm TL}$, with $\mathcal{C}_{\rm SL} = -\mathcal{C}_{\rm PL} \approx +4\,\mathcal{C}_{\rm TL}$ at m_b scale.

   As we have seen, it is not possible to fit charged current flavor anomalies without evading other constraints, such as the ones associated to $\mathcal{B}(B_c \to \tau\nu)$ decay, if we assume to have real Wilson Coefficients. On the other hand, with complex couplings a consistent $R_{D^{(*)}}$ explanation is possible in a simplified model with R_2 leptoquark [69].

- **Spin 1 leptoquarks**

  1. $V_2 \sim (\mathbf{3},\mathbf{2})_{5/6}$. It is a vector leptoquark that presents the same $SU(3)_c$ and $SU(2)_L$ properties as R_2. Thus, it is coupled to a quark and a lepton, one of which should be a $SU(2)_L$ doublet and the other a singlet: $\overline{d^c}'\,\gamma^\mu\,V_{2\mu}\,\epsilon\,l'$ and $\overline{q^c}'\,\gamma^\mu\,\epsilon\,V_{2\mu}\,e'$. Therefore, integrating out V_2, one obtains the gauge invariant operator $\mathcal{O}_{ledq}$ of Eq. (4.5.2) and in the broken phase only the $\mathcal{O}_{\rm SL}+\mathcal{O}_{\rm PL}$ scalar four fermion interaction. As shown in Section 4.4.2, this term alone is not sufficient to fit charged current flavor anomalies respecting the bounds related to B_c decay.

  2. $U_1 \sim (\mathbf{3},\mathbf{1})_{2/3}$. This vector LQ is a $SU(2)_L$ singlet and can have pure left handed and pure right handed interactions: $\overline{d}'\,\gamma^\mu\,U_{1\mu}\,e'$ and $\overline{q}'\,\gamma^\mu\,U_{1\mu}\,l'$. Integrating it out, we end up with a SMEFT made of $\mathcal{O}_{ledq}$ and $\mathcal{O}_{lq}^{(3,1)}$, with $\mathcal{C}_{\rm SL}=\mathcal{C}_{\rm PL}$ and $\mathcal{C}_{\rm VL}=-\mathcal{C}_{\rm AL}$ non zero WCs in the WET describing $b\to cl\nu$.
     As discussed, this scenario with scalar and vector operators may provide a combined explanation of R_D and $R_{D^{(*)}}$ when scalar interactions are negligible and we are left with $V-A$ effective couplings. Therefore, for what concerns this analysis, one might take into account the $\overline{q}'\,\gamma^\mu\,U_{1\mu}\,l'$ term only, as will be done in the following. The success of U_1 in addressing flavor anomalies, both charged and neutral current ones, has been widely treated in the literature, see for example [63]. Furthermore, this mediator arises automatically in Pati Salam model [157], making it simple to embed it in a UV completion [92, 95, 65, 70, 71].

  3. $U_3 \sim (\mathbf{3},\mathbf{3})_{2/3}$. In order to guarantee gauge invariance, it can couples only with $SU(2)_L$ doublets of left handed fermions: $\overline{q}'\,\gamma^\mu\,\sigma^A U^A_{3\mu}\,l'$. Thus, one gets only $\mathcal{O}_{lq}^{(3,1)}$ in the SMEFT and $V-A$ interactions at b mass scale. However, it is not possible to fit flavor anomalies while avoiding constraints from correlated low energy observables, in presence of this mediator only.

Therefore, the viable simplified models for flavor observables explanation are the following:

- The simultaneous presence of S_1 and S_3 scalar leptoquarks (see [67] for a UV embedding). In this way, it is possible to have a cancellation between the contributions to $b\to s\nu\nu$ transition and to $Z\nu\nu$ coupling; the origin of anomalies does not lead anymore to the violations of other low energy observable constraints.

- R_2 scalar leptoquark in presence of complex valued Wilson Coefficients.

- U_1 vector leptoquark.

- W' and Z' colorless vectors, for charged and neutral current interactions.

In the following Sections, the last two possibilities will be further analyzed. In this way, only four fermion operators with left handed charged and neutral vector currents are evoked in order to address flavor anomalies. In fact, couplings of new physics with right handed fermions are not necessary to fit data and one of the simplest choices can be not to introduce them.

4.7 Partial Compositeness and Composite Higgs

As we discussed before, explanations for the R_D and R_{D^*} anomalies call for new physics close to the TeV scale, which is also expected for the naturalness of the Higgs mass. This coincidence of scales advocates for the speculation of a common origin of these two seemingly unrelated phenomena. This motivates to consider the Composite Higgs (CH) paradigm [158], and, in particular, the models where fermion masses are generated via the Partial Compositeness (PC) mechanism [159], as we have done in [3].

In fact, recently there has been a lot of effort invested in analyzing the B-meson anomalies within this framework [65, 99, 95, 100, 96, 94, 101], all of which, however, focus on specific models. A novel feature of our study in [3] has been instead to carry out the analysis in the EFT language, emphasizing the correlations among the various observables. In particular, the goal has been to identify the key features that these models should possess in order to satisfy the experimental data, independently of the concrete realization of PC and thus with results expected to be quite generic. In the following Sections, the analysis of [3] is shown.

4.7.1 Two site Lagrangian

Here, there is a brief description of the minimal Composite Higgs construction, that was deeply analyzed in the original paper [160] and in the reviews [161, 162].

The global symmetry breaking pattern is taken as follows:

$$\text{MCHM} : \mathrm{U(1)_X \times SU(3) \times SO(5) \to U(1)_X \times SU(3) \times SU(2)_L \times SU(2)_R}. \tag{4.7.1}$$

The phenomenology is studied within an effective field theory approach, using the so-called two site model [163]. The model consists of two sectors; one of which consists in elementary particles, the other in composite fields. The composite sector is invariant under $G_{co} = SO(5) \times SU(3) \times U(1)_X$ and the elementary one under $G_{el} = SU(2)_L \times SU(3) \times U(1)_Y$. The latter thus is analogous to the SM for the symmetry structure and, as we will see, also for the group representations of fields: the boson and fermion content is the same apart from the Higgs. The Standard Model gauge symmetry is identified with the (gauged) diagonal subgroup of $G_{co}^{SM} \times G_{el}$, where G_{co}^{SM} is the $SU(2)_L \times SU(3) \times U(1)_Y$ subgroup of the total global symmetry G_{co} of the composite sector. The diagonal subgroup is defined as the one generated by $T_{co}^{SM} + T_{el}$, where T_{co}^{SM} and T_{el} are generators of G_{co}^{SM} and G_{el} respectively. The *composite hypercharge* generator is defined as follows

$$T_Y = T_X + T_R^3 \,. \tag{4.7.2}$$

The Higgs boson appears as the Goldstone boson of the spontaneous global symmetry breaking $SO(5) \to SO(4)$. The CCWZ formalism [164, 165] is used to parametrize the non linearly realized symmetry $SO(5)/SO(4)$ for the composite sector. Following closely the notations of [166], the Higgs boson appears inside the usual Goldstone boson matrix $U = e^{i\Pi(x)} = e^{i\sqrt{2}T^{\hat{a}}\pi^{\hat{a}}(x)/f}$, where $T^{\hat{a}}$ ($\hat{a} = 1, 2, 3, 4$) are the broken generators of $SO(5) \to SO(4)$, $\pi^{\hat{a}}(x)$ are the NG bosons living in the coset $SO(5)/SO(4)$ and transforming as a **4** of $SO(4)$ (equivalently

as a $(\mathbf{2},\mathbf{2})$ of $SU(2)\times SU(2))$, f is the scale of the global symmetry breaking. In the unitary gauge, in which $\pi^{\hat{a}}(x)=0$ for $\hat{a}=1,2,3$ and $\pi^{\hat{4}}(x)=h(x)$, U is equal to:

$$U=e^{i\Pi(x)}=\begin{pmatrix}\mathbb{1}_{3\times 3} & 0 & 0\\ 0 & \cos\frac{h(x)}{f} & \sin\frac{h(x)}{f}\\ 0 & -\sin\frac{h(x)}{f} & \cos\frac{h(x)}{f}\end{pmatrix}, \tag{4.7.3}$$

where $h(x)$ is the real scalar physical Higgs boson.
Under global $g\in SO(5)\times SU(3)\times U(1)_X$ transformation, U behaves as

$$U(\Pi)\to gU(\Pi)h^\dagger(\Pi,g) \tag{4.7.4}$$

where $h^\dagger(\Pi,g)$ contains only unbroken generators of the preserved $\mathcal{H}=SO(4)\times SU(3)\times U(1)_X$ and depends on the considered $\Pi(x)$. It is customary to define two Maurer-Cartan 1-forms d_μ and E_μ in the following way

$$-iU^\dagger\partial_\mu U=d_\mu^{\hat{a}}T^{\hat{a}}+E_\mu^a T^a=d_\mu+E_\mu \tag{4.7.5}$$

decomposing the U derivative along the broken $T^{\hat{a}}$ and unbroken T^a generators of the composite sector group. Therefore, it turns out that under G_{co} the transformations of d_μ and E_μ are

$$d_\mu(\Pi)\to \quad h(\Pi,g)d_\mu(\Pi)h^\dagger(\Pi,g) \tag{4.7.6}$$

$$E_\mu(\Pi)\to \quad h(\Pi,g)E_\mu(\Pi)h^\dagger(\Pi,g)-ih(\Pi,g)\partial_\mu h^\dagger(\Pi,g) \tag{4.7.7}$$

which is to say that they transform under local $\mathcal{H}$ behaving respectively as a field in the adjoint representation (d_μ) and as a gauge field (E_μ).

Gauging a subgroup $\mathcal{H}'\in SO(5)\times SU(3)\times U(1)_X$, the derivative $\partial_\mu U$ in Eq. (4.7.5) is substituted by the covariant derivative $D_\mu U=\partial_\mu U+iA_\mu U-iUA_\mu^R$, where $A_\mu=A_\mu^{\hat{a}}T^{\hat{a}}+A_\mu^aT^a$ and $A_\mu^R=-A_\mu^{\hat{a}}T^{\hat{a}}+A_\mu^aT^a$ trasform as gauge fields under $\mathcal{H}'$. One obtains

$$-iU^\dagger D_\mu U=d_\mu^{\hat{a}}T^{\hat{a}}+E_\mu^aT^a=d_\mu+E_\mu\,. \tag{4.7.8}$$

In the case under analysis, the gauging is internal to the preserved $\mathcal{H}=SO(4)\times SU(3)\times U(1)_X$ subgroup and involves the $SU(2)_L\times U(1)_Y$ subgroup of $SO(4)\times U(1)_X$, where the generator of $U(1)_Y$ is a linear combination of the one of the abelian $U(1)_X$ and of the third generator of $SU(2)_R$ (see Eq. (4.7.2)), while the other $SU(2)\subset SO(4)$ is completely gauged. Thus, we have $A_\mu=A_\mu^R$. In particular, as previously seen, what is gauged is the diagonal subgroup of the product between the elementary symmetry group and this $SU(2)_L\times U(1)_Y$ subgroup of composite $SO(4)\times U(1)_X$. Then, one obtains $A_\mu=A_\mu^R=gT_L^aW_{L\mu}^a+g'B_{Y\mu}Y$, where $W_{L\mu}^a$ and $B_{Y\mu}$ are the SM $SU(2)_L$ and $U(1)_Y$ gauge fields, g and g' are the corresponding couplings and T^a are $SU(2)$ generators.

The leading most general non constant Lagrangian for the Nambu Goldoston bosons, i.e. for the Composite Higgs, that is invariant under $SO(5)$ is given by

$$\frac{f^2}{4}Tr\left((D_\mu U)^\dagger D^\mu U)\right). \tag{4.7.9}$$

Indeed, $Tr(U^\dagger U)$ is a constant and, as a consequence, a NG potential is forbidden and the leading NG interactions are $O(p^2)$, in the limit of exact $SO(5)$ only spontaneously broken to $SO(4)$. However, the gauging of $SU(2)_L \times U(1)_Y$ explicitly breaks $\mathcal{H}$: a potential for U and its couplings to fermions are generated at quantum level and lead to EW SSB.

The Higgs kinetic term and the gauge bosons mass terms come from the two derivative piece of the chiral Lagrangian in Eq. (4.7.9):

$$\frac{f^2}{4} Tr(d_\mu d^\mu) = \frac{1}{2}(\partial_\mu h)^2 + \frac{1}{2}\left(2m_W^2 W_\mu^+ W_\mu^- + m_Z^2 Z_\mu Z^\mu\right) \sin^2 \frac{h}{f} \tag{4.7.10}$$

where $m_W^2 = \frac{g^2}{2} f^2 \sin^2 \frac{v}{f}$ and $m_Z^2 = m_W^2 \frac{g^2+g'^2}{g^2}$, in which v is the h VEV.

Fermion sector

Here, the fermion mass generation through Partial Compositeness mechanism is explained. In MCHM5 model [160], in particular, the composite fields appear as a fiveplets of SO(5), namely in the fundamental representation of this global symmetry. In any case, the results depend only mildly on this assumption and practically do not change for the other fermion embeddings.

The elementary sector has exactly the same symmetry structure and field content of the Standard Model, apart from the absence of the Higgs boson. Therefore, the fermion representations under $G_{el} \cong G_{SM}$ and their multiplicity are as in the SM. On the other hand, the composite sector is invariant under a broader group and thus the multiplet type and variety are not the same, with the key difference in the $SU(2)_L \leftrightarrow SO(5)$ subgroups. For each elementary $SU(2)_L$ doublet, there are two composite $SO(5)$ fiveplets with different $U(1)_X$ charges and same $SU(3)_c$ properties. Thus, there is a $SO(5)$ fundamental representation for each one of the fields that are present in the broken phase of SM, i.e. one for each one of the $SU(2)_L$ singlets plus neutrinos: as will be explained, the two different fiveplets generate mass terms for the two SM fields associated to the different components of the $SU(2)_L$ doublet.

In the composite sector, the fivepletes after the $SO(5) \to SO(4)$ breaking can be decomposed as a fourplet and a singlet of $SO(4)$. Then, a one to one correspondence appears between composite $SO(4)$ singlets and elementary $SU(2)_L$ ones plus right handed neutrinos, if they are present. The fourplet of $SO(4) \cong SU(2)_L \times SU(2)_R$, on the other hand, contains in its turn two $SU(2)_L$ doublets. One has the Standard Model quantum numbers, namely the same charges as the elementary doublet under the $SU(3) \times SU(2)_L \times U(1)_Y$ subgroup of G_{co}, and is denoted as $\tilde{\mathcal{O}}_{\mathbf{SM}}$. It is the one that can display bilinear coupling with an elementary fermion doublet. The other one is called $\tilde{\mathcal{O}}_{\mathbf{EX}}$ and is related to the previous doublet via $SU(2)_R$ transformations. The singlet composite operators are denoted as $\tilde{\mathcal{O}}_{u,d,e}$, while elementary multiplets as $\tilde{q}_L$, $\tilde{l}_L$, $\tilde{u}_R$, $\tilde{d}_R$, $\tilde{e}_R$, and the full spectrum is the following

	$SU(3)^{co}$	$SU(2)^{co}_L$	$SU(2)^{co}_R$	$U(1)^{co}_X$
$\tilde{\mathcal{O}}_{q_1}$	**3**	**2**	**2**	2/3
$\tilde{\mathcal{O}}_{q_2}$	**3**	**2**	**2**	$-1/3$
$\tilde{\mathcal{O}}_u$	**3**	**1**	**1**	2/3
$\tilde{\mathcal{O}}_d$	**3**	**1**	**1**	$-1/3$
$\tilde{\mathcal{O}}_{\ell_1}$	**1**	**2**	**2**	0
$\tilde{\mathcal{O}}_{\ell_2}$	**1**	**2**	**2**	-1
$\tilde{\mathcal{O}}_e$	**1**	**1**	**1**	-1

	$SU(3)^{\text{el}}$	$SU(2)^{\text{el}}_L$	$U(1)_Y{}^{\text{el}}$
$\tilde{q}_L$	**3**	**2**	1/6
$\tilde{u}_R$	**3**	**1**	2/3
$\tilde{d}_R$	**3**	**1**	$-1/3$
$\tilde{\ell}_L$	**1**	**2**	$-1/2$
$\tilde{e}_R$	**1**	**1**	-1
$\tilde{\nu}_R$	**1**	**1**	0

Table 4.3: Group representations and charges of the fermion composite resonances and elementary fields.

$$\tilde{\mathcal{O}}_{q_1} = \left(\tilde{\mathcal{O}}^{q_1}_{\mathbf{EX}}\, \tilde{\mathcal{O}}^{q_1}_{\mathbf{SM}}\right), \qquad \tilde{\mathcal{O}}^{q_1}_{\mathbf{SM}} = \begin{pmatrix} U \\ D \end{pmatrix}, \qquad \tilde{\mathcal{O}}^{q_1}_{\mathbf{EX}} = \begin{pmatrix} \chi_{5/3} \\ \chi_{2/3} \end{pmatrix}$$

$$\text{5-plet} \quad \Psi_{q_1} = \left(\tilde{\mathcal{O}}_{q_1}, \tilde{\mathcal{O}}_u\right) \tag{4.7.11}$$

$$\tilde{\mathcal{O}}_{q_2} = \left(\tilde{\mathcal{O}}^{q_2}_{\mathbf{SM}}\, \tilde{\mathcal{O}}^{q_2}_{\mathbf{EX}}\right), \qquad \tilde{\mathcal{O}}^{q_2}_{\mathbf{SM}} = \begin{pmatrix} U' \\ D' \end{pmatrix}, \qquad \tilde{\mathcal{O}}^{q_2}_{\mathbf{EX}} = \begin{pmatrix} \chi_{-1/3} \\ \chi_{-4/3} \end{pmatrix} \tag{4.7.12}$$

$$\text{5-plet} \quad \Psi_{q_2} = \left(\tilde{\mathcal{O}}_{q_2}, \tilde{\mathcal{O}}_d\right) \tag{4.7.13}$$

$$\tilde{\mathcal{O}}_{\ell_1} = \left(\tilde{\mathcal{O}}^{\ell_1}_{\mathbf{EX}}\, \tilde{\mathcal{O}}^{\ell_1}_{\mathbf{SM}}\right), \qquad \tilde{\mathcal{O}}^{\ell_1}_{\mathbf{SM}} = \begin{pmatrix} N \\ E \end{pmatrix}, \qquad \tilde{\mathcal{O}}^{\ell_1}_{\mathbf{EX}} = \begin{pmatrix} \chi_{+1} \\ \chi_0 \end{pmatrix} \tag{4.7.14}$$

$$\text{5-plet} \quad \Psi_{l_1} = \left(\tilde{\mathcal{O}}_{l_1}, \tilde{\mathcal{O}}_N\right)$$

$$\tilde{\mathcal{O}}_{\ell_2} = \left(\tilde{\mathcal{O}}^{\ell_2}_{\mathbf{SM}}\, \tilde{\mathcal{O}}^{\ell_2}_{\mathbf{EX}}\right), \qquad \tilde{\mathcal{O}}^{\ell_2}_{\mathbf{SM}} = \begin{pmatrix} N' \\ E' \end{pmatrix}, \qquad \tilde{\mathcal{O}}^{\ell_2}_{\mathbf{EX}} = \begin{pmatrix} \chi_{-1} \\ \chi_{-2} \end{pmatrix}$$

$$\text{5-plet} \quad \Psi_{l_2} = \left(\tilde{\mathcal{O}}_{l_2}, \tilde{\mathcal{O}}_e\right) \tag{4.7.15}$$

where the charges of the components of $\tilde{\mathcal{O}}_1$ and $\tilde{\mathcal{O}}_2$ within a $SU(2)_R$ doublet $\tilde{\mathcal{O}} = \left(\tilde{\mathcal{O}}_1, \tilde{\mathcal{O}}_2\right)$ under T^3_R are equal to $+\frac{1}{2}$ and $-\frac{1}{2}$ respectively. Each field is a 3-vector in the flavor generation space and the subscript of χ field, inside the *exotic* doublets $\mathcal{O}_{\mathbf{EX}}$, indicates its electric charge.

The group representations and charges of the fermion states are depicted in Table 4.3. Note, as discussed, that we have two composite doublets $\tilde{\mathcal{O}}^{q_1}_{\mathbf{SM}}$ and $\tilde{\mathcal{O}}^{q_2}_{\mathbf{SM}}$ which have the same quantum numbers under the SM gauge group; similarly for the leptons.

The symmetries of the composite sector are broken explicitly to the G^{SM}_{co} subgroup, isomorphic to the SM group, and then to the diagonal subgroup of $G^{SM}_{co} \times G_{el}$, described above, by

the mixing with the elementary sector. In $SO(5)$ notation this mixing has the following form:

$$\mathcal{L}_{flavor} = \lambda_q M_* \overline{\tilde{q}}_L U(h)\Psi_{q_1} + \tilde{\lambda}_q M_* \overline{\tilde{q}}_L U(h)\Psi_{q_2} + \lambda_u M_* \overline{\tilde{u}}_R U(h)\Psi_{q_1} + \lambda_d M_* \overline{\tilde{d}}_R U(h)\Psi_{q_2} \\ + \lambda_l M_* \overline{\tilde{l}}_L U(h)\Psi_{l_1} + \tilde{\lambda}_l M_* \overline{\tilde{l}}_L U(h)\Psi_{l_2} + \lambda_e M_* \overline{\tilde{e}}_R U(h)\Psi_{l_2} \quad (4.7.16)$$

where $U(h)$ is defined as in Eq. (4.7.3). Above, the elementary $SU(2)_L$ doublets, $\tilde{q}_L$ and $\tilde{l}_L$, are embedded in incomplete fiveplets of SO(5). For example, in the q quark case we have:

$$\lambda_q \tilde{q}_L \equiv \lambda_q \left[(0, q_L), 0\right] \\ \tilde{\lambda}_q \tilde{q}_L \equiv \tilde{\lambda}_q \left[(q_L, 0), 0\right], \quad (4.7.17)$$

where zeros have been put in all the missing components and $(q_L, 0)$ singles out the $SO(4)$ fourplet. Note also that the residual symmetries of the model after $SO(5) \to SO(4)$ breaking allow us to further split λ_q mixing into two independent parameters $\lambda_q^{(4)}$ and $\lambda_q^{(1)}$ defined as

$$\lambda_q \overline{\tilde{q}}_L U(h)\Psi_{q_1} \to \begin{cases} \left[\lambda_q^{(4)} \overline{\tilde{q}}_L\right]_I U(h)_{Ii} \left[\mathcal{O}_{q_1}\right]_i, \text{ where } I = 1, ...5, \quad i = 1, ...4 \\ \left[\lambda_q^{(1)} \overline{\tilde{q}}_L\right]_I U(h)_{I5} \mathcal{O}_u \end{cases}, \quad (4.7.18)$$

where the sum over repeating indices is understood.
Then, if we take $U(h)$ equal to identity, the mixing is allowed between the elementary multiplets and the G_{co}^{SM} representations, embedded in $SO(4)$ multiplets, having the same $SU(3)_c \times SU(2)_L \times U(1)_Y$ quantum numbers of the elementary fields. Thus, only the $SO(4)$ singlets $\tilde{\mathcal{O}}_{u,d,e}$ and the $SU(2)_L$ doublets $\tilde{\mathcal{O}}_{\mathbf{SM}}$, not the $\tilde{\mathcal{O}}_{\mathbf{EX}}$ ones, end up having non zero couplings with elementary fermions:

$$\mathcal{L}_{flavor} = \lambda_q^{(4)} M_* \overline{\tilde{q}}_L \tilde{\mathcal{O}}_{\mathbf{SM}}^{q_1} + \tilde{\lambda}_q^{(4)} M_* \overline{\tilde{q}}_L \tilde{\mathcal{O}}_{\mathbf{SM}}^{q_2} + \lambda_u^{(1)} M_* \overline{\tilde{u}}_R \tilde{\mathcal{O}}_u + \lambda_d^{(1)} M_* \overline{\tilde{d}}_R \tilde{\mathcal{O}}_d \\ + \lambda_l^{(4)} M_* \overline{\tilde{l}}_L \tilde{\mathcal{O}}_{\mathbf{SM}}^{l_1} + \tilde{\lambda}_l^{(4)} M_* \overline{\tilde{l}}_L \tilde{\mathcal{O}}_{\mathbf{SM}}^{l_2} + \lambda_e^{(1)} M_* \overline{\tilde{e}}_R \tilde{\mathcal{O}}_e \,. \quad (4.7.19)$$

Let us look at the fermion spectrum, before EW SSB. We consider the bi-dimensional space generated by one elementary field multiplet ($\tilde{\psi}$) and one composite resonance G_{co}^{SM} representation ($\tilde{\mathcal{O}}$), taking $U(h) \sim \mathbf{1}$. Due to the composite-elementary mixing λ, there is one massless state and one heavy field with mass $M_*(1+\lambda)/\sqrt{1+\lambda^2}$, which becomes M_* in the limit $\lambda \ll 1$. They are organized in representation of the residual symmetry, which, as seen, coincides with the SM group. The massless eigenstates ψ' are identified with the Standard Model fermion fields that, thus, contain also a composite component: this is what we call *Partial Compositeness* (PC). Mass eigenstates $\mathcal{O}$ are obtained through a change of basis in the space spanned by $\tilde{\psi}$ and $\tilde{\mathcal{O}}$, that can be described as a rotation of angle θ_ψ

$$\begin{pmatrix} \tilde{\psi} \\ \tilde{\mathcal{O}} \end{pmatrix} = \begin{pmatrix} \cos\theta_\psi & -\sin\theta_\psi \\ \sin\theta_\psi & \cos\theta_\psi \end{pmatrix} \begin{pmatrix} \psi' \\ \mathcal{O} \end{pmatrix} \quad (4.7.20)$$

with

$$\sin\theta_\psi \equiv \hat{s} = \frac{\lambda}{\sqrt{1+\lambda^2}}, \qquad \cos\theta_\psi \equiv \hat{c} = \frac{1}{\sqrt{1+\lambda^2}}, \quad (4.7.21)$$

where $\hat{s}$ and $\hat{c}$ are matrices in the flavor space.
The angle θ_ψ parametrizes the elementary component of the SM massless field ψ' and the composite component of the heavy mass eigenstate $\mathcal{O}$. The latter are the ones that are integrated out in order to obtain the SMEFT. A soft mixing is assumed, with the entries of $\hat{s}$ much smaller than the ones of $\hat{c}$: the Standard Model fields are more elementary than composite and the vice versa holds for the heavy fermions.

Elementary fermions are not coupled to the Higgs boson, that lives in the composite sector. In the phase with unbroken $G_{co}^{SM} \times G_{el}$, which is to say before elementary-composite mixing of Eq. (4.7.16), only $\tilde{\mathcal{O}}$ multiplets have Yukawa interactions. In particular, the up-type singlet $\tilde{\mathcal{O}}_u$ couples only with $\tilde{\mathcal{O}}_{q_1}$, while the down-type singlet $\tilde{\mathcal{O}}_d$ only with $\tilde{\mathcal{O}}_{q_2}$, in order to guarantee invariance under $U(1)_X \subset G_{co}$. Similarly, the charged lepton singlet $\tilde{\mathcal{O}}_e$ has Yukawa coupling only with $\tilde{\mathcal{O}}_{l_2}$.

Then, the SM Yukawa couplings are due to the composite components of the Standard Model fermion multiplets ψ', quantified by θ_ψ angles, one for the left handed fermion doublet and one for the right handed singlet. For example, in the quark case

$$y_{u,d} \sim \frac{s_{q_{1,2}} s_{u,d} M_*}{f}. \tag{4.7.22}$$

Up-type Yukawas depend only on the $\tilde{q}_L$ compositeness with respect to $\tilde{\mathcal{O}}_{q_1}$ and not $\tilde{\mathcal{O}}_{q_2}$. Since the top mass is larger than the bottom one, one can assume that the mixing of the elementary quark doublet $\tilde{q}_L$ with the up-type $SU(2)_L$ composite doublet $\tilde{\mathcal{O}}_{q_1}$ is much larger than the one with $\tilde{\mathcal{O}}_{q_2}$, that will be neglected in the following.

Vector sector

In this work, the interest is in the interactions between the Standard Model fermions, which are external fields of $b \to c\tau\nu$ and $b \to s\mu\mu$ processes, and the composite vector fields, that provide the new physics contribution in these semileptonic b decays.

The vector formalism [166] (see for example [167] for the comparison of various formalisms) is followed for spin-1 fields. In the composite sector they, called here $\tilde{\rho}_\mu$, are introduced through a gauging of the $\mathcal{H}$ unbroken subgroup; thus, they transform non homogeneously under $\mathcal{H}$, as gauge bosons

$$\tilde{\rho}_\mu \to \mathcal{H}\tilde{\rho}_\mu\mathcal{H}^\dagger - \frac{i}{g^*}\mathcal{H}\partial_\mu\mathcal{H}^\dagger\,. \tag{4.7.23}$$

Then, the following pure composite boson interactions, for each simple subgroup of the unbroken (gauged) $\mathcal{H} \subset G_{co}$, are allowed by the CCWZ symmetries:

$$\mathcal{L}_{co}^{vec} = -\frac{1}{4}\tilde{\rho}^a_{\mu\nu}\tilde{\rho}^{\mu\nu}_a + \frac{M_*^2}{2}(\tilde{\rho}^a_\mu - E^a_\mu)^2 + ... \tag{4.7.24}$$

where higher derivative terms have been ignored. M_* is the mass scale of composite vectors, that can be in principle different for any simple subgroup of $\mathcal{H}$ and does not necessarily coincide

with the one of Eq. (4.7.16). E_μ is the covariant derivative defined in Eq. (4.7.8), associated to the generators that are unbroken in $SO(5) \to SO(4)$, whose gauging is related to the presence of the $\tilde{\rho}_\mu$ vectors.

The Lagrangian Eq. (4.7.24) in the limit of vanishing Higgs VEV reduces to the covariant kinetic term and to the M_* mass term for the composite vectors:

$$-\frac{1}{4}\tilde{\rho}^a_{\mu\nu}\tilde{\rho}^{\mu\nu}_a + \frac{M_*^2}{2}\tilde{\rho}^a_\mu\tilde{\rho}^\mu_a \,. \tag{4.7.25}$$

Then, also in the vector sector Partial Compositeness is realized introducing a mixing between composite resonances $\tilde{\rho}^\mu_a$ and elementary fields A^μ_a. The latter are associated to the gauging of the symmetry G_{el} of the elementary sector, under which they transform non homogeneously:

$$A_\mu \to U_{el} A_\mu U^\dagger_{el} - \frac{i}{g_{el}} U_{el}\partial_\mu U^\dagger_{el} \,, \;\; U_{el} \in G_{el} \,. \tag{4.7.26}$$

Since $G_{el} = SU(3) \times SU(2)_L \times U(1)_Y$, a mixing preserving SM gauge group is possible only for composite vectors associated to the G^{SM}_{co} subgroup of $\mathcal{H}$. As in the fermion sector, this leads to the breaking pattern $G_{co} \times G_{el} \to \left(G^{SM}_{co} \times G_{el}\right)|_{diag}$. Then, the total pure vector Lagrangian, for any simple subgroup of $SU(3) \times SU(2)_L \times U(1)_Y$, is

$$\mathcal{L}^{vec} = -\frac{1}{4}\tilde{\rho}^a_{\mu\nu}\tilde{\rho}^{\mu\nu}_a - \frac{1}{4}A^a_{\mu\nu}A^{\mu\nu}_a + \frac{M_*^2}{2}\tilde{\rho}^a_\mu\tilde{\rho}^\mu_a - M_*^2\frac{g_{el}}{g_*}\tilde{\rho}^a_\mu A^\mu_a + \frac{M_*^2}{2}\frac{g_{el}^2}{g_*^2}A^a_\mu A^\mu_a, \tag{4.7.27}$$

where g_* and g_{el} are the coupling constants of a given simple subgroup of G^{SM}_{co} and G_{el} respectively. The composite sector has in general stronger couplings with respect to the elementary sector, which is to say $g_* \gg g_{el}$. One can notice that the mixing is suppressed by a factor $\frac{g_{el}}{g_*}$ with respect to the $\tilde{\rho}_\mu$ squared mass.

In order to get mass eigenstates vectors, one should diagonalize the matrix of masses and mixing of A_μ and $\tilde{\rho}_\mu$, that can be deduced from Eq. (4.7.27):

$$\begin{pmatrix} A_\mu \\ \tilde{\rho}_\mu \end{pmatrix} \to \begin{pmatrix} \cos\theta & -\sin\theta \\ \sin\theta & \cos\theta \end{pmatrix} \begin{pmatrix} A^{SM}_\mu \\ \rho_\mu \end{pmatrix} , \qquad \cos\theta = \frac{g_*}{\sqrt{g_*^2 + g_{el}^2}} \tag{4.7.28}$$

where ρ_μ is an eigenstate with mass of $M_*\sqrt{1 + g_{el}^2/g_*^2}$ and the orthogonal A^{SM}_μ is the massless state, that is identified with the SM gauge boson. Indeed, under the action of $\left(G^{SM}_{co} \times G_{el}\right)|_{diag}$, the vector field $A^{SM}_\mu = \cos\theta\, A_\mu + \sin\theta\, \tilde{\rho}_\mu$ transforms in the following way

$$A^{SM}_\mu \to U A^{SM}_\mu U^{-1} - \frac{i}{\frac{g_{el}g_*}{\sqrt{g_{el}^2+g_*^2}}} U\partial_\mu U^{-1} \tag{4.7.29}$$

from which one can read the SM coupling as a function of the elementary and composite ones. The residual symmetry group is actually a preserved gauge symmetry, since no mass terms for A^{SM}_μ are present. This analysis holds for each simple subgroup of $SU(3) \times SU(2)_L \times U(1)_Y$, that can have different coupling constants.

Now we set the focus on the interactions between vector bosons and fermions, starting from the composite sector. The coupling between $\tilde{\rho}_\mu$ and a composite fermion $\tilde{\mathcal{O}}$ comes from the covariant kinetic term of the latter

$$\mathcal{L}^{ferm} = \bar{\tilde{\mathcal{O}}} \gamma^\mu \left(i\partial_\mu + g_* \tilde{\rho}_\mu \right) \tilde{\mathcal{O}}, \tag{4.7.30}$$

where $\tilde{\rho}_\mu = \tilde{\rho}^a_\mu T^{co}_a$and T^{co}_a are the generators of the global symmetry group of the composite sector. Again, one can have different values of g_* for $SU(3)$, $SO(4)$ and $U(1)_X$ subgroups.

Rotating to the mass eigenstate basis both for vectors and fermions, one can extract the interaction between the Standard Model fermions ψ' and the heavy mass eigenstates vectors ρ_μ, which is to say the ones that are integrated out in order to get the low energy EFT.
We end up with

$$\bar{\psi'}_i \left[\sqrt{g_*^2 - g^2} \left[\hat{s}^\dagger T^{co}_a \hat{s} \right]^i_j - \frac{g^2}{\sqrt{g_*^2 - g^2}} \left[\hat{c}^\dagger T^{\rm el}_a \hat{c} \right]^i_j \right] \gamma^\mu \psi'^j \rho^a_\mu \,, \tag{4.7.31}$$

where g is the SM coupling $\frac{g_{el} g_*}{\sqrt{g_{el}^2 + g_*^2}}$ and $\hat{s}$ and $\hat{c}$ are defined as in Eq. (4.7.21).

In the expression above, the first term comes from the mixing of the elementary and composite fermions and the second term corresponds to the mixing between composite and elementary vector bosons (Eq. (4.7.28)).

Here, the main interest is on the flavor non universal and flavor violating effects, so the contribution of the last term can be neglected, even if $|\hat{s}| \ll |\hat{c}|$. In fact, $g_* \gg g$ and the non universal piece in $\hat{c} \sim 1 - \hat{s}^2/2$ arises at second order in $\hat{s}$ and thus has an extra $\hat{s} \ll \hat{c}$ suppression.

Note that the Eq. (4.7.31) is a generic prediction of the Partial Compositeness and various fermion embeddings lead only to different actions of T^a_{co} on fermions.

4.7.2 $R_{D^{(*)}}$ from the composite electroweak resonances

The goal is the analysis of flavor observables, described through dimension 6 four fermion operators, within this framework of Composite Higgs and Partial Compositeness. These operators are generated integrating out the heavy vector resonances ρ_μ, defined in Eq. (4.7.28), that are exchanged at tree-level in a process with four fermion external states and two of the vertices shown in Eq. (4.7.31). Assuming $g_* \gg g$ and being interested in flavor non universal effects, in the coupling between heavy vectors and SM fermion currents one can take into account the $\sqrt{g_*^2 - g^2}\, \bar{\psi'}\, \hat{s}^\dagger T^{co}_a \hat{s}\, \gamma^\mu \psi'\, \rho^a_\mu$ contribution only; then, the induced dimension 6 four fermion operators take the form

$$\frac{g_*^2}{M_*^2} \left[\bar{\psi'}\, \hat{s}^\dagger T^{co}_a \hat{s}\, \gamma^\mu \psi' \right] \left[\bar{\psi'}\, \hat{s}^\dagger T^{co}_a \hat{s}\, \gamma_\mu \psi' \right] . \tag{4.7.32}$$

Above, ψ' is the vector of all different fermion multiplets, in flavor basis; they, thus, can be different between the first and second parentheses. The 3×3 matrices $\hat{s}$, as previously defined,

represent the composite components of the SM fermions ψ'. Eq. (4.7.32) provides a set of SMEFT operators, according to the choice of fermion representations and of the specific simple G_{co}^{SM} subgroup generated by T_a^{co}. For examples, considering the term associated to $SU(2)_L$ and taking ψ' equal to ℓ'_L and q'_L in the first and second parentheses respectively, one gets $\mathcal{O}_{lq}^{(3)}$.

The aim would now be to understand the correlations among the flavor changing $\Delta F = 2$ operators and those that contribute to $R_{D^{(*)}}$ anomalies, which can be both obtained from the four fermion interaction of Eq. (4.7.32).

The $\Delta F = 2$ transitions are generated by tree-level exchange of neutral heavy vectors. In order to analyze the $\bar{K}$-K, $\bar{B}_d$-B_d and $\bar{B}_s$-B_s mixings in correlation with charged current flavor anomalies, left handed down-type quark currents are taken into account. Then, this effective $\Delta F = 2$ Lagrangian can be written as

$$\mathcal{L}_{\Delta F=2} = -\text{const} \times \frac{g_*^2}{M_*^2} \left(\bar{d}_{i\,L} \left[V_L^{d\dagger} \hat{s}_q^\dagger \hat{s}_q V_L^d \right]^i{}_j \gamma^\mu d_{j\,L} \right)^2 , \tag{4.7.33}$$

where V_L^d is the rotation matrix for the left handed quarks defined in Eq. (4.5.14); it is associated to the change from the basis of d'_L flavor eigenstates, considered in the unbroken phase with massless fermions, to the basis of mass eigenstates. The constant in front, for this MCHM5 and Partial Compositeness framework, is equal to

$$\text{const} = \frac{M_*^2}{2g_*^2} \left(\frac{1}{3} \frac{g_{*3}^2}{M_{*3}^2} + \frac{1}{2} \frac{g_{*2}^2}{M_{*2}^2} + \frac{4}{9} \frac{g_{*X}^2}{M_{*X}^2} \right) . \tag{4.7.34}$$

The first term inside the parenthesis corresponds to the contribution of the composite gluon, the second to the $\mathrm{SU(2)_{L,R}}$ triplets and the third to $\mathrm{U(1)_X}$ vector bosons. The number 4/9 is fixed by the $U(1)_X$ charge assignment of the up-like $SU(2)_L$ doublet $\tilde{O}_{q_1}$ (see Table 4.3); indeed, as anticipated, the mixing of $\tilde{q}_L$ with the down-type $\tilde{O}_{q_2}$ is neglected. Thus, in effective Lagrangian above $\hat{s}_q$ is the matrix, in flavor space, of the $\tilde{O}_{q_1}$ component inside q'_L.

Here, there is the assumption that only one $\Delta F = 2$ operator is generated, the operator Q_1 in the basis of [168]. In principle, other operator(s) may also be generated at the matching scale, and cancel part of the contribution from Q_1. However, unless large accidental cancellations arise, the following results should always hold.

Given what stated above, experimental data on $\bar{K}$-K, $\bar{B}_d$-B_d and $\bar{B}_s$-B_s mixings give the following constraints

$$\left| \left[V_L^{d\dagger} \hat{s}_q^\dagger \hat{s}_q V_L^d \right]^i{}_j \right| \lesssim \frac{(M_*/\text{TeV})}{g_* \sqrt{\text{const}}} \begin{cases} 10^{-3} \text{ , from } \bar{K}\text{-}K \text{ mixing, i.e., } i=1, j=2 \text{ [168]} \\ 1.1 \times 10^{-3} \text{ , from } \bar{B}_d\text{-}B_d \text{ mixing, i.e., } i=1, j=3 \text{ [169]} \\ 4 \times 10^{-3} \text{ , from } \bar{B}_s\text{-}B_s \text{ mixing, i.e., } i=2, j=3 \text{ [169]} \end{cases} , \tag{4.7.35}$$

where the numerical values are obtained by running the couplings to the scale M_*.

Keeping the above constraints from $\Delta F = 2$ processes in mind, one can look at the $b \to c\tau\nu$ transitions, described through the four fermion operator of Eq. (4.7.32). It is assumed that the NP contribution arises from the exchange of a heavy vector field which is a triplet of $SU(2)_L$.

This generates the effective dimension 6 Lagrangian

$$\mathcal{L}_{b\to c\,\tau\,\nu} = -\frac{g_{*2}^2}{2M_{*2}^2}\left(\bar{\tau}_L\left[V_L^{e\dagger}\hat{s}_l{}^\dagger\hat{s}_l V_L^{\nu\dagger}\right]^3{}_3\,\gamma^\mu\,\nu_{\tau L}\right)\left(\bar{c}_L\left[V_L^{u\dagger}\hat{s}_q{}^\dagger\hat{s}_q V_L^{d}\right]^2{}_3\,\gamma^\mu\,b_L\right) \tag{4.7.36}$$

$$= -\frac{g_{*}^2}{2M_{*}^2}\left(\bar{\tau}_L\left[V_L^{e\dagger}\hat{s}_l{}^\dagger\hat{s}_l V_L^{\nu}\right]^3{}_3\,\gamma^\mu\,\nu_{\tau L}\right)\left(\bar{c}_L\left[V_{\rm CKM}V_L^{d\dagger}\hat{s}_q{}^\dagger\hat{s}_q V_L^{d}\right]^2{}_3\,\gamma^\mu\,b_L\right), \tag{4.7.37}$$

where we have assumed $g_{*2} = g_*, M_{*2} = M_*$ and the matrices $V_L^{u,d}$ for the change of basis are defined in Eq. (4.5.14). In the second line, the $V_{\rm CKM}$ has been explicitly indicated.
Even remaining agnostic about the leptonic sector, one can still use the loose upper bound

$$\left|\left[V_L^{e\dagger}\hat{s}_l{}^\dagger\hat{s}_l V_L^{\nu}\right]^3{}_3\right| \leqslant 1 \tag{4.7.38}$$

which is satisfied even for maximal possible τ compositeness. Thus, the explanation of R_D and R_{D^*} anomalies at $1\,\sigma$ level translates into the following lower bound, on the involved $(2,3)$ matrix element for the given combination of V and $\hat{s}_q$ matrices:

$$\left[V_{\rm CKM}V_L^{d\dagger}\hat{s}_q{}^\dagger\hat{s}_q V_L^{d}\right]^2{}_3 \gtrsim 0.2\left(\frac{M_*/g_*}{\rm TeV}\right)^2, \tag{4.7.39}$$

where the numerical factor 0.2 corresponds to $\Delta C_{\rm VL}^\tau = -\Delta C_{\rm AL}^\tau = 0.08$ (see Fig. 4.3).

Expanding Eq. (4.7.39) on $V_{\rm CKM}$ matrix elements, one gets

$$V_{cd}\left[V_L^{d\dagger}\hat{s}_q{}^\dagger\hat{s}_q V_L^{d}\right]^1{}_3 + V_{cs}\left[V_L^{d\dagger}\hat{s}_q{}^\dagger\hat{s}_q V_L^{d}\right]^2{}_3 + V_{cb}\left[V_L^{d\dagger}\hat{s}_q{}^\dagger\hat{s}_q V_L^{d}\right]^3{}_3 \gtrsim 0.2\left(\frac{M_*/g_*}{\rm TeV}\right)^2$$

$$\implies |V_{cd}|\left|\left[V_L^{d\dagger}\hat{s}_q{}^\dagger\hat{s}_q V_L^{d}\right]^1{}_3\right| + |V_{cs}|\left|\left[V_L^{d\dagger}\hat{s}_q{}^\dagger\hat{s}_q V_L^{d}\right]^2{}_3\right| + |V_{cb}|\left|\left[V_L^{d\dagger}\hat{s}_q{}^\dagger\hat{s}_q V_L^{d}\right]^3{}_3\right| \gtrsim 0.2\left(\frac{M_*/g_*}{\rm TeV}\right)^2.$$

Using the upper bounds on $\left|\left[V_L^{d\dagger}\hat{s}_q{}^\dagger\hat{s}_q V_L^{d}\right]^1{}_3\right|$ and $\left|\left[V_L^{d\dagger}\hat{s}_q{}^\dagger\hat{s}_q V_L^{d}\right]^2{}_3\right|$ from Eq. (4.7.35) and the trivial inequality $\left|\left[V^{d\dagger}\hat{s}_q{}^\dagger\hat{s}_q V^{d}\right]^3{}_3\right| \leqslant 1$, we have

$$1.1\times10^{-3}\,|V_{cd}|\,\frac{(M_*/\text{TeV})}{g_*\sqrt{\text{const}}} + 4\times10^{-3}\,|V_{cs}|\,\frac{(M_*/\text{TeV})}{g_*\sqrt{\text{const}}} + |V_{cb}| \gtrsim 0.2\left(\frac{M_*/\text{TeV}}{g_*}\right)^2. \tag{4.7.40}$$

As the first two terms are negligibly small compared to the third one, for small enough $(M_*/\text{TeV})/g_*$, we finally get

$$M_*/g_* \lesssim\ 0.45\,\text{TeV}\,. \tag{4.7.41}$$

Note that Partial Compositeness automatically selects the scenario (II) (see discussion after Eq. (4.5.48)) for fitting the charged current flavor anomalies $R_{D^{(*)}}$, namely the dominant NP contribution to $b\to cl\nu$ transition is proportional to the V_{cb} element of CKM matrix. This solution, as mentioned in Section 4.5.4, requires the presence of additional UV contributions to protect $g_L^{\tau,\nu}$ couplings of the Z boson.

One of the advantages of this MCHM5 and PC model, indeed, is that it can provide protection for some of the g_Z^τ, g_Z^b, g_Z^ν couplings. In fact, discrete P_{LR} symmetry [170] avoids NP modifications to g_Z^τ, but it cannot protect simultaneously also both g_Z^ν and g_W^τ. Indeed let us consider the mass and kinetic terms for composite leptons together with the part of the Lagrangian in Eq. (4.7.16) that involves the lepton doublet $\tilde{l}_L$ and allow the splitting of the mixing parameters defined in the Eq. (4.7.18):

$$\begin{aligned}\mathcal{L} &= i\overline{\tilde{\mathcal{O}}}_{l_1}\left(\not{D}+i\not{E}\right)\tilde{\mathcal{O}}_{l_1}+i\overline{\tilde{\mathcal{O}}}_{l_2}\left(\not{D}+i\not{E}\right)\mathcal{O}_{l_2}+\left(ic_1\overline{\tilde{\mathcal{O}}}^i_{l_1}\not{d}_i\tilde{\mathcal{O}}_N+ic_2\overline{\tilde{\mathcal{O}}}^i_{l_2}\not{d}_i\tilde{\mathcal{O}}_e+h.c.\right)+\\ &- m_1^{(4)}\overline{\tilde{\mathcal{O}}}_{l_1}\tilde{\mathcal{O}}_{l_1}-m_2^{(4)}\overline{\tilde{\mathcal{O}}}_{l_2}\tilde{\mathcal{O}}_{l_2}-m_e^{(1)}\overline{\tilde{\mathcal{O}}}_e\tilde{\mathcal{O}}_e-m_N^{(1)}\overline{\tilde{\mathcal{O}}}_N\tilde{\mathcal{O}}_N+\\ &+ \lambda_l^{(4)}\bar{\tilde{l}}_L U(h)_{Ii}\mathcal{O}_{l_1}+\lambda_l^{(1)}\bar{\tilde{l}}_L U(h)_{I5}\mathcal{O}_N+\tilde{\lambda}_l^{(4)}\bar{\tilde{l}}_L U(h)_{Ii}\mathcal{O}_{l_2}+\tilde{\lambda}_l^{(1)}\bar{\tilde{l}}_L U(h)_{I5}\mathcal{O}_e\,. \end{aligned} \tag{4.7.42}$$

Following the analysis of [171, 172], where analogous discussion was applied to the top quark, one can derive the modifications to g_Z^τ, g_Z^ν, namely the Z coupling to τ lepton and neutrino:

$$\delta g_Z^\tau=-\frac{v^2}{4f^2}\frac{M_*^2\left[\left(\tilde{\lambda}_l^{(4)}m_e^{(1)}\right)^2+\left(\tilde{\lambda}_l^{(1)}m_2^{(4)}\right)^2-2\sqrt{2}c_2\tilde{\lambda}_l^{(4)}\tilde{\lambda}_l^{(1)}m_e^{(1)}m_2^{(4)}\right]}{\left(m_e^{(1)}\right)^2\left(\left(m_2^{(4)}\right)^2+\left(\tilde{\lambda}_l^{(4)}M_*\right)^2\right)}\,, \tag{4.7.43}$$

$$\delta g_Z^\nu=-\frac{v^2}{4f^2}\frac{M_*^2\left[\left(\lambda_l^{(4)}m_N^{(1)}\right)^2+\left(\lambda_l^{(1)}m_1^{(4)}\right)^2-2\sqrt{2}c_1\lambda_l^{(4)}\lambda_l^{(1)}m_N^{(1)}m_1^{(4)}\right]}{\left(m_N^{(1)}\right)^2\left(\left(m_1^{(4)}\right)^2+\left(\lambda_l^{(4)}M_*\right)^2\right)}\,. \tag{4.7.44}$$

We can see that P_{LR} symmetry forces the δg_Z^τ to depend only on $\tilde{\lambda}_l^{(1,4)}$ and δg_Z^ν only on $\lambda_l^{(1,4)}$, which is to say that only $\tilde{\mathcal{O}}_{l_2}$ mediates the interaction with charged leptons and only $\tilde{\mathcal{O}}_{l_1}$ the one with neutrinos.

Since the bound on g_Z^τ is a bit stronger, it is natural to assume that $\lambda_l > \tilde{\lambda}_l$, in order to have negligible δg_Z^τ. Then, the contribution to $R_{D^{(*)}}$ is dominated by λ_l: in this way it is possible to enhance $b\to cl\nu$ and explain charged current flavor anomalies without having too large modification to the $Z\tau\tau$ vertex. Note that this λ_l coupling does not enter the leading expression of the τ mass which scales as

$$m_\tau \propto \lambda_e\tilde{\lambda}_l^{(1,4)}\,. \tag{4.7.45}$$

Indeed, similarly to the quark case of Eq. (4.7.22), the SM Yukawas for charged leptons arise from coupling involving $\tilde{\mathcal{O}}_{l_2}$ and $\tilde{\mathcal{O}}_e$ and thus depend only on the compositeness of l'_L with respect to the doublet that has $U(1)_X$ charge equal to the electric charge of the considered SM field. In this way, one can enlarge the new physics contribution to $b\to cl\nu$ without spoiling the size of the τ lepton mass.

Thus, it is possible to fit simultaneously g_Z^τ and $R_{D^{(*)}}$ in this framework with Composite Higgs and Partial Compositeness, with the only simple assumption that one SM lepton doublet mixing, with $\tilde{\mathcal{O}}_{l_1}$, is much larger than the other, with $\tilde{\mathcal{O}}_{l_2}$. Then in order to pass also the constraints from g_Z^ν, it is necessary to tune additionally the parameter c_1 as was suggested in [65].

Interestingly, if one assumes, as already done, that the composite components of l'_L and q'_L come dominantly from the up-type doublets $\tilde{\mathcal{O}}_{SM}^{l_1}$ and $\tilde{\mathcal{O}}_{SM}^{q_1}$ respectively, the $SO(4)$ structure of the model leads to a cancellation of the NP contribution to $b \to s\nu\nu$: the generated four fermions operators automatically satisfy also the condition of scenario (I). Indeed, there is a cancellation between the diagrams with tree-level exchange of the neutral vector corresponding to the third generators of $SU(2)_L$ and $SU(2)_R$ and the $U(1)_X$ boson has vanishing coupling with $\tilde{\mathcal{O}}_{l_1}$; it corresponds to a cancellation between the contributions of the four fermion operators $\mathcal{O}_{lq}^{(3)}$ and $\mathcal{O}_{lq}^{(1)}$, generated integrating out the $SU(2)_L$ and $SU(2)_R$ vectors respectively.

We make now a few comments regarding the robustness of this result and its applicability to the various models employing Partial Compositeness. The only assumption that has been made in deriving the Eq. (4.7.41) is that the charged current operator (see Eq. (4.7.36)) is generated by a vector field, which is a triplet of electroweak $SU(2)_L$. The rest of the discussion is completely model independent and applies to various embeddings of the SM fermions into the composite multiplets and to various choices of the elementary-composite mixing parameters $\hat{s}$, and is practically independent from the mass of the composite gluon and the mass of the $U(1)_X$ vector, due to the conservative approximations made in Eq. (4.7.40). It should also be emphasized that we have been completely agnostic about the dynamics that allows the model under consideration to satisfy the constraints from $\Delta F = 2$ processes, namely those given in Eq. (4.7.35). For example, in anarchic Partial Compositeness, where the left handed quark mixing parameters scale as the CKM matrix elements, namely $[\hat{s}_q]_i \sim V_{ti}$, these bounds are roughly $M_* \gtrsim 10 - 20$ TeV [173, 174], with the strongest constraint coming in this case from the ϵ_K bound. It would be a too large scale to explain the R_D and R_{D^*} anomalies. However the scale of the compositeness can be lowered and made consistent with the $R_{D^{(*)}}$ anomalies by invoking additional flavor symmetries, for example $U(2)$ [175, 176, 92]. Interestingly, the bounds from the direct searches (see Section 4.3) at the LHC [177, 178] on the composite partners of the top quarks are still in the range of $M_* \gtrsim 1.2$ TeV, making them rather consistent with the requirement of Eq. (4.7.41).

The constraint in Eq. (4.7.41), in general, can pose serious difficulties with the electroweak precision observables and measurement of Higgs's couplings to electroweak vector bosons. Indeed the constraints from electroweak precision tests [179, 180, 181] require the scale of compositeness to be $\gtrsim 1.2$ TeV in order to satisfy the data at 2σ level. At the same time the mass of the vector resonance is related to the scale of compositeness, f, as

$$M_*^2 = a_\rho g_*^2 f^2, \tag{4.7.46}$$

where a_ρ is a number of $\mathcal{O}(1)$. In an explicit two site construction, $a_\rho = 1/\sqrt{2}$ (see for example [162]) so that the $R_{D^{(*)}}$ upper bound on M_* induces on compositeness scale the constraint

$$f \lesssim 0.64\,\text{TeV}. \tag{4.7.47}$$

This is incompatible with the bound from electroweak precision measurements mentioned above. It may however be possible to accommodate the electroweak precision observables by additional UV contributions providing appropriate cancellations in them, see for example, [182, 171, 183].

Depending on the strength of the coupling g_*, Eq. (4.7.41) might provide a quite strict upper bound on the mass M_* of the heavy mediators and this can create some tensions with the bounds from high-p_T data and direct searches, briefly described in Section 4.3.

The tension with meson mixing data makes it interesting to think of other possibilities of enhancing the contributions to R_D and R_{D^*} without modifying the $\Delta F = 2$ observables considerably. This can be partially achieved in scenarios with composite vector leptoquarks which will be discussed in the next Section.

4.7.3 $R_{D^{(*)}}$ with additional vector leptoquark contribution

The composite vector leptoquark scenario in connection to the B-meson anomalies was first proposed in [92, 95, 65]. In this construction, the global symmetry of the composite sector is extended from $SO(5) \times SU(3) \times U(1)_X$ (where SU(3) is weakly gauged later and becomes the SU(3) of QCD) to the group

$$SO(5) \times SU(4) \times U(1)_X. \tag{4.7.48}$$

The composite gluon, which is an octet of SU(3), lies inside the **15** dimensional adjoint of SU(4) and is accompanied by two SU(3) triplets $\mathbf{3} + \bar{\mathbf{3}}$ ($U_{1_{(3,1)_{\frac{2}{3}}}} + U^*_{1_{(\bar{3},1)_{-\frac{2}{3}}}}$) and a singlet ($\tilde{B}_{(1,1)_0}$), where the subscripts of vectors indicate the representations under the $SU(3) \times SU(2)_L \times U(1)_Y$ subgroup. The hypercharge is given by the following combination of group generators:

$$Y = \sqrt{\frac{2}{3}} T_{15} + T^3_R + X \tag{4.7.49}$$

where $T_{15} = \mathrm{diag}(1, 1, 1, -3)/\sqrt{24}$ is a diagonal $SU(4)$ generator.

The Lagrangian is the same as in Section 4.7.1, apart from the presence of $U_{1_{(3,1)_{\frac{2}{3}}}}$ and $\tilde{B}_{(1,1)_0}$ vector bosons. In particular, in the composite sector, leptoquarks couple to fermion currents in which there are quark and lepton resonances. Indeed, from Eq. (4.7.30) one gets also the interaction

$$\frac{g_*}{\sqrt{2}} U_{1\mu} \overline{\tilde{\mathcal{O}}}^q_{SM} \gamma^\mu \tilde{\mathcal{O}}^l_{SM} \tag{4.7.50}$$

where g_* is the strong coupling for the $SU(4)$ of the composite sector. Invariance under $G^{SM}_{co} = SU(3) \times SU(2)_L \times U(1)_Y$ is guaranteed if the two composite fermions are: $\overline{\tilde{\mathcal{O}}}^{q_{1,2}}_{SM} \tilde{\mathcal{O}}^{l_{1,2}}_{SM}$, $\overline{\tilde{\mathcal{O}}}_u \tilde{\mathcal{O}}_N$ or $\overline{\tilde{\mathcal{O}}}_d \tilde{\mathcal{O}}_e$, where $\overline{\tilde{\mathcal{O}}}^{q_{1,2}}_{SM} \tilde{\mathcal{O}}^{l_{2,1}}_{SM}$ terms could not be generated from a $SO(4)$ invariant Lagrangian. This interaction, after integrating out the heavy fermions, reduces to the following vector leptoquark coupling to SM fermions

$$\frac{g_*}{\sqrt{2}} \bar{\psi}'_q \left[\hat{s}_q{}^\dagger \hat{s}_l\right] \gamma^\mu \psi'_l U_{1\mu} \,. \tag{4.7.51}$$

The relevant interaction term for charged current anomalies is

$$\mathcal{L}_{LQ} = -g_* \left(\bar{q}'_{L\,i} \left[\hat{s}_q^\dagger \hat{s}_l \right]^i{}_j \gamma_\mu \, l'_{L\,j} \right) U_1^\mu \,. \tag{4.7.52}$$

Then, integrating out the heavy vector leptoquark, one gets a contribution to the effective Lagrangian for the $b \to c\,\tau\,\nu$ processes, that in the SM fermion mass basis can be expressed as

$$\mathcal{L}_{b\to c\,\tau\,\nu} = -\frac{g_*^2}{2M_*^2} \left(\bar{c}_L \left[V_{\rm CKM} V_L^{d\dagger} \hat{s}_q{}^\dagger \hat{s}_l V_L^\nu \right]^2_{\ 3} \gamma^\mu \, \nu_{\tau L} \right) \left(\bar{\tau}_L \left[V_L^{e\dagger} \hat{s}_l{}^\dagger \hat{s}_q V_L^d \right]^3_{\ 3} \gamma^\mu \, b_L \right) \tag{4.7.53}$$

$$\overset{\text{Fierz}}{=} -\frac{g_*^2}{2M_*^2} \left[V_{\rm CKM} V_L^{d\dagger} \hat{s}_q{}^\dagger \hat{s}_l V_L^\nu \right]^2_{\ 3} \left[V_L^{e\dagger} \hat{s}_l{}^\dagger \hat{s}_q V_L^d \right]^3_{\ 3} \left(\bar{c}_L \, \gamma^\mu \, b_L \right) \left(\bar{\tau}_L \, \gamma^\mu \, \nu_{\tau L} \right) \,. \tag{4.7.54}$$

where in the second line Fierz transformations have been used to obtain a pure quark current and a pure lepton current and get $\mathcal{O}_{lq}^{(3)}$ effective operator, in the same basis as above.

In order to find the upper bound on the coefficient of the operator $\left(\bar{c}_L \, \gamma^\mu \, b_L \right) \left(\bar{\tau}_L \, \gamma^\mu \, \nu_{\tau L} \right)$, it is necessary to find an upper bound on $\left[V_{\rm CKM} V_L^{d\dagger} \hat{s}_q{}^\dagger \hat{s}_l V_L^\nu \right]^2_{\ 3}$ consistent with the data on B-meson mixing. As before, a trivial inequality $\left[V_L^{e\dagger} \hat{s}_l{}^\dagger \hat{s}_q V_L^d \right]^3_{\ 3} \leqslant 1$ is used.

Without loss of generality, one can go to the basis of elementary and composite fields in which the lepton compositeness matrix has the following form:

$$\hat{s}_l = \begin{pmatrix} * & 0 & 0 \\ * & * & 0 \\ * & * & * \end{pmatrix} \,, \tag{4.7.55}$$

where $*$ stands for non zero entry.
In the analysis of the leptoquark contribution to $b \to cl\nu$, some assumption on the flavor structure of the fermion compositeness is necessary in order to study the correlation with $\Delta F = 2$ processes. In particular, we assume here that only the third family of leptons has a strong mixing with the composite sector, i.e. only $(\hat{s}_l)_{33}$ is ~ 1 and the rest of the elements are much smaller. In this case, the WC in Eq. (4.7.54) is controlled by

$$\left[V_{\rm CKM} V_L^{d\dagger} \hat{s}_q{}^\dagger \right]^2_{\ 3} = V_{cd} [V_L^{d\dagger} \hat{s}_q{}^\dagger]^1_{\ 3} + V_{cs} [V_L^{d\dagger} \hat{s}_q{}^\dagger]^2_{\ 3} + V_{cb} [V_L^{d\dagger} \hat{s}_q{}^\dagger]^3_{\ 3} \,. \tag{4.7.56}$$

The aim now is to understand how big $\left[V_{\rm CKM} V_L^{d\dagger} \hat{s}_q{}^\dagger \right]^2_{\ 3}$ can be, consistently with an almost diagonal $\left[V_L^{d\dagger} \hat{s}_q{}^\dagger \hat{s}_q V_L^d \right]$ (as the off-diagonal elements are constrained to be $\lesssim 10^{-3}$, as shown in Eq. (4.7.35)). This latter WC comes only from the contributions of the colorless bosons, described in the previous Section, since the leptoquarks do not mediate $\Delta F = 2$ processes at tree-level. Similarly to the leptonic elementary-composite mixing matrix $\hat{s}_l$, also $\hat{s}_q$ can be made triangular by suitable field redefinitions of the elementary (massless) fields. Thus, without loss of generality, one can write

$$\hat{s}_q = \begin{pmatrix} s_{11} & 0 & 0 \\ s_{21} & s_{22} & 0 \\ s_{31} & s_{32} & s_{33} \end{pmatrix} \,. \tag{4.7.57}$$

As in the lepton case, let us now consider the special case where only the third generation quark mixes strongly with the composite sector so that

$$s_{33} \gg s_{ij}, \quad i \text{ or } j \neq 3\,, \tag{4.7.58}$$

In this case, while $[V_L^{d\dagger}\hat{s_q}^\dagger]^3{}_3$ can be close to unity, the other terms in Eq. (4.7.56), in order to be consistent with a diagonal $\left[V_L^{d\dagger}\hat{s_q}^\dagger\hat{s_q}V_L^d\right]$, must scale as

$$[V_L^{d\dagger}\hat{s_q}^\dagger]^1{}_3 \sim \frac{s_{31}(s_{ij})^2}{(s_{33})^2}, \quad [V_L^{d\dagger}\hat{s_q}^\dagger]^2{}_3 \sim \frac{s_{32}(s_{ij})^2}{(s_{33})^2}\,. \tag{4.7.59}$$

It can be noticed that these elements have an additional suppression of (s_{ij}/s_{33}) compared to the naive expectation. This renders the contributions of the first two terms of Eq. (4.7.56) subdominant: again, we are in a scenario in which the leading piece of $b \to cl\nu$ amplitude is proportional to V_{cb}. Thus, adding the contribution of the electroweak triplet from Eq. (4.7.40), for the explanation of $R_{D^{(*)}}$ anomalies at the $1\,\sigma$ level, one must have

$$\begin{aligned} 2V_{cb} &\gtrsim 0.2\left(\frac{M_*/g_*}{\text{TeV}}\right)^2 \\ \implies M_*/g_* &\lesssim 0.63\,\text{TeV}\,, \end{aligned} \tag{4.7.60}$$

where it has been assumed that the electroweak triplet and the leptoquarks have the same mass and coupling. Hence, the role of U_1 leptoquark is just to double the contribution to $b \to cl\nu$ transition without worsening the other low energy observables. This increase of the upper bound on the scale of compositeness by a factor of $\sqrt{2}$ helps ameliorate the constraints from S and T parameters which are now in agreement at almost $2\,\sigma$ level. Note, however, that assuming $\frac{g_{*4}}{M_{*4}} > \frac{g_{*2}}{M_{*2}}$, namely taking masses of the $SU(4)$ resonances smaller than those of the $SO(4)$ fields, one can be in the situation where the composite leptoquark contribution dominates in $R_{D^{(*)}}$ and the tension with electroweak precision observables can be relaxed even further.

It is worth emphasizing that the result of Eq. (4.7.60) was derived assuming the hierarchical nature (see Eq. (4.7.58)) of the mixing matrix $\hat{s}_q$ and the constraint can be relaxed if this assumption is not valid. For example, if we assume that the matrix $\hat{s_q}$ is not hierarchical but unitary, then also $\left[V_L^{d\dagger}\hat{s_q}^\dagger\right]$ is unitary and $\left[V_L^{d\dagger}\hat{s_q}^\dagger\hat{s_q}V_L^d\right]$ is automatically diagonal. However, this implies that

$$\left(\left[V_L^{d\dagger}\hat{s_q}^\dagger\right]^1{}_3\right)^2 + \left(\left[V_L^{d\dagger}\hat{s_q}^\dagger\right]^2{}_3\right)^2 + \left(\left[V_L^{d\dagger}\hat{s_q}^\dagger\right]^3{}_3\right)^2 = 1\,. \tag{4.7.61}$$

Then, choosing $\left[V_L^{d\dagger}\hat{s_q}^\dagger\right]^2{}_3 \sim 1$, in order to maximize the effects on $R_{D^{(*)}}$, and the other two elements very small, one gets from Eq. (4.7.56) that $\left[V_{\text{CKM}}V_L^{d\dagger}\hat{s_q}^\dagger\right]^2{}_3 \sim 1$. In this case, Eq. (4.7.60) gets modified to

$$\begin{aligned} (1+V_{cb}) &\gtrsim 0.2\left(\frac{M_*/g_*}{\text{TeV}}\right)^2 \\ \to M_*/g_* &\lesssim 2.28\,\text{TeV}\,. \end{aligned} \tag{4.7.62}$$

This very conspired scenario could be realized in $U(3)$ symmetric models [176, 184] where $\hat{s}_q \propto \mathbb{1}_{3\times3}$. However in this case [176] we have to face the constraints from the modification of the Z decays to hadrons requiring (see Table 4 of [176])

$$M_* \gtrsim 6\sqrt{g_*}\text{TeV}, \tag{4.7.63}$$

for the composite fermions masses. Assuming the vector fields are at the same scale, fitting the anomalies becomes practically impossible.

4.7.4 $R_{K^{(*)}}$ anomalies

In this Section, we investigate very briefly whether the $R_{K^{(*)}}$ anomalies can be explained within this Composite Higgs framework (see [93, 94, 95, 96, 97, 65, 99, 100, 101, 67, 185] for related discussion).

It is known that the discrepancy of the experimental data on R_K and R_{K^*} with respect to the SM expectations can be alleviated by the following WET four fermion operator [186, 187]

$$\mathcal{L}_{b\to s\mu\mu} = -\frac{1}{\Lambda^2}\,(\bar{s}\gamma_\mu P_L\, b)(\bar{\mu}\gamma^\mu P_L\,\mu)\,, \tag{4.7.64}$$

with $1/\Lambda^2 \gtrsim 1/(38\,\text{TeV})^2$ at the $1\,\sigma$ level. Thus, the requirements on new physics scale are much milder than the ones needed to explain charged current flavor anomalies. As a consequence, the compatibility of the anomaly explanation with other low energy observables (see Section 4.2) and with high-p_T data and direct searches (see Section 4.3) is easier to obtain.

In models with Partial Compositeness, such an operator can be generated by the exchange of either a neutral Z' vector boson or a vector leptoquark. In the following, there is an analysis of the flavor structures of these two cases and an identification of the features that can explain the data.

Z' contribution

Following the analysis of Section 4.7.2, neutral colorless composite bosons $\rho^3_{L,R}$, corresponding to the third generators of $SU(2)_{L,R}$, generate

$$\frac{g_{*2}^2}{2M_{*2}^2}\left(\bar{s}\,[V_L^{d\,\dagger}\hat{s}_q^\dagger\hat{s}_q V_L^d]^2{}_3\gamma_\mu P_L\, b\right)\left(\bar{\mu}\,[V_L^{e\,\dagger}\hat{s}_l^\dagger\hat{s}_l V_L^e]^2{}_2\gamma^\mu P_L\,\mu\right) \tag{4.7.65}$$

where $g_{*,2} = g_*$, $M_{*,2} = M_*$, if one assumes that for all simple subgroups of the composite sector symmetry the couplings and boson masses are the same. In principle, also ρ_X, associated to $U(1)_X$, is a Z' vector; however its coupling to SM lepton doublets is negligible if the elementary l'_L dominantly mixes with the composite doublet $\mathcal{O}^{\ell_1}_{SM}$, which is the one that does not enter in the generation of SM charged lepton masses.
Assuming $V_L^e = \mathbb{1}$ and diagonal $\hat{s}_l$, after implementing the $\bar{B}_s$ - B_s mixing constraints from Eq. (4.7.35), the explanation of $R_{K^{(*)}}$ with the effective operator above implies

$$\frac{g_*}{(M_*/\text{TeV})}\frac{1}{\sqrt{\text{const}}}\,s_\mu^2 \gtrsim 0.35\,, \tag{4.7.66}$$

where 'const' is defined in Eq. (4.7.33). This inevitably requires large muon compositeness.

Constraints from $\Delta F = 2$ processes require an almost diagonal $\left[V_L^{d\dagger}\hat{s}^\dagger\hat{s}V_L^d\right]$ matrix, which forces the operator in Eq. (4.7.65) to be small as well. However, note that if $\left[V_L^{d\dagger}\hat{s}^\dagger\hat{s}V_L^d\right]_{23} = \epsilon$, where ϵ is some small parameter, then $\Delta F = 2$ observables scale as ϵ^2 and R_K as ϵ. It is precisely this extra power of ϵ suppression that can make the explanation for the two measurements consistent [95].

U_1 vector leptoquark contribution

The flavor structure in this case is different from the Z' contribution and the relevant operator inducing $b \to s\mu\mu$ is given by

$$\frac{g_*^2}{M_*^2}\left(\bar{s}\,[V_L^{d\,\dagger}\hat{s}_q^\dagger\hat{s}_l V_L^e]^2{}_2\gamma_\mu P_L\,\mu\right)\left(\bar{\mu}\,[V_L^{e\,\dagger}\hat{s}_l^\dagger\hat{s}_q V_L^d]^2{}_3\gamma^\mu P_L\,b\right)\,. \tag{4.7.67}$$

In this case correlations with the other low energy measurements are less strict and as an illustration one can consider the two following extreme scenarios. For simplicity diagonal $\hat{s}_{l,q}$ compositeness matrices will be assumed (MFV).

- **Flavor trivial lepton sector**

  In this case $V_L^e = \mathbb{1}$ is taken and this obviously evades all the constraints from LFV processes like $\tau \to 3\mu$. In such a scenario, the main constraint comes from the combination of K - $\bar{K}$ (Eq. (4.7.35)) and D_0 -$\bar{D}_0$ mixings.
  The latter is described by the four fermion operator

$$-\,\text{const}\times\frac{g_*^2}{M_*^2}\left(\bar{u}_L\left[V_L^{u\dagger}\hat{s}_q^\dagger\hat{s}_q V_L^u\right]^1{}_2\,\gamma^\mu\,c_L\right)^2 \tag{4.7.68}$$

  where the constant in front is the same as in Eq. (4.7.34).
  The upper bounds on D_0 - $\bar{D}_0$ mixing implies

$$\left|\left[V_L^{u\dagger}\hat{s}_q^\dagger\hat{s}_q V_L^u\right]^1{}_2\right| \leqslant 10^{-3}\frac{M_*/\text{TeV}}{g_*\sqrt{\text{const}}}\,. \tag{4.7.69}$$

  Then, using $V_{CKM} = V_L^{u\dagger}V_L^d$ matrix, one can correlate this up-quark sector mixing with the ones in the down-quark sector, involved in K-$\bar{K}$ and in $R_{K^{(*)}}$. Indeed, we have

$$\left[V_L^{u\dagger}\hat{s}_q^\dagger\hat{s}_q V_L^u\right]^1{}_2 = \left[V_{CKM}V_L^{d\dagger}\hat{s}_q^\dagger\hat{s}_q V_L^d V_{CKM}^\dagger\right]^1{}_2 = \tag{4.7.70}$$

$$= V_{ud}\left[V_L^{d\dagger}\hat{s}_q^\dagger\hat{s}_q V_L^d\right]^1{}_2 V_{cs}^* + V_{ud}\left[V_L^{d\dagger}\hat{s}_q^\dagger\hat{s}_q V_L^d\right]^1{}_1 V_{us}^* + V_{us}\left[V_L^{d\dagger}\hat{s}_q^\dagger\hat{s}_q V_L^d\right]^2{}_2 V_{cs}^* \sim \tag{4.7.71}$$

$$\sim 0.94\left[V_L^{d\dagger}\hat{s}_q^\dagger\hat{s}_q V_L^d\right]^1{}_2 + 0.22\left(\left[V_L^{d\dagger}\hat{s}_q^\dagger\hat{s}_q V_L^d\right]^1{}_1 + \left[V_L^{d\dagger}\hat{s}_q^\dagger\hat{s}_q V_L^d\right]^2{}_2\right)\,. \tag{4.7.72}$$

The first term, because of the constraints on it coming from K - $\bar{K}$ mixing (see Eq. (4.7.35)), is $\left|\left[V_L^{d\dagger}\hat{s}_q^\dagger\hat{s}_q V_L^d\right]^1_{\ 2}\right| \leqslant 10^{-3}\frac{M_*/\text{TeV}}{g_*\sqrt{\text{const}}}$, namely there is an upper bound of the same size as the one on the total $\left|\left[V_L^{u\dagger}\hat{s}_q^\dagger\hat{s}_q V_L^u\right]^1_{\ 2}\right|$ (see Eq. (4.7.69)).
Therefore, a conservative bound can be set on the second term of Eq. (4.7.72)

$$\left(\left[V_L^{d\dagger}\hat{s}_q^\dagger\hat{s}_q V_L^d\right]^1_{\ 1} + \left[V_L^{d\dagger}\hat{s}_q^\dagger\hat{s}_q V_L^d\right]^2_{\ 2}\right) \leqslant 8.8\times 10^{-3}\frac{M_*/\text{TeV}}{g_*\sqrt{\text{const}}}\,. \tag{4.7.73}$$

Furthermore, the diagonal elements of $\left[V_L^{d\dagger}\hat{s}_q^\dagger\hat{s}_q V_L^d\right]$ are positive definite, since $\left[V_L^{d\dagger}\hat{s}_q^\dagger\hat{s}_q V_L^d\right]^i_{\ i} = \sum_j |\left[\hat{s}_q V_L^d\right]^j_{\ i}|^2$. Each one of the terms of this sum is non negative and, thus, the constraint of Eq. (4.7.73) translates into a conservative upper bound on each one of the $|\left[\hat{s}_q V_L^d\right]^j_{\ i}|$ contributions:

$$|\left[\hat{s}_q V_L^d\right]^j_{1,2}| \leqslant 0.09\sqrt{\frac{M_*/\text{TeV}}{g_*\sqrt{\text{const}}}}\,. \tag{4.7.74}$$

Inserting this into the Z' and U_1 contributions to $b\to s\mu\mu$ of Eq. (4.7.65) and Eq. (4.7.67), the $R_{K^{(*)}}$ constraints gives the following lower bound on the muon compositeness

$$s_\mu \geqslant 0.08(\text{const})^{1/8}\left(\frac{M_*/\text{TeV}}{g_*}\right)^{3/4}\,. \tag{4.7.75}$$

Interestingly, the bound becomes less strict compared to the one obtained with the Z' contribution only (see Eq. (4.7.66)), even if probably also because they are derived in a very conservative way. However, the scale of the muon compositeness must still be quite high.

- **Flavor trivial down quark sector [65]**

  Assuming $V_L^d = \mathbb{1}$, $R_{K^{(*)}}$ can be generated solely by the leptoquark contribution and Z' mediated diagrams vanish. Interestingly, we can correlate the $R_{K^{(*)}}$ with the flavor violating τ decay $\tau\to 3\mu$ arising from the operator:

$$\text{const}\times\frac{g_*^2}{M_*^2}\left(\bar{\tau}\left[V_L^{e\dagger}\hat{s}_l^\dagger\hat{s}_l V_L^e\right]^3_{\ 2}\gamma_\mu P_L\mu\right)\left(\bar{\mu}\left[V_L^{e\dagger}\hat{s}_l^\dagger\hat{s}_l V_L^e\right]^2_{\ 2}\gamma_\mu P_L\mu\right) \tag{4.7.76}$$

  where now

$$\text{const} = \frac{1}{2}\frac{M_*^2}{g_*^2}\left(\frac{g_{*2}^2}{2M_{*2}^2}+\frac{3g_{*3}^2}{8M_{*3}^2}\right) \tag{4.7.77}$$

  comes from the contributions of the ρ_L^3, ρ_R^3 and $\rho_{T_{15}}$, under the assumption, used also above, that the elementary $SU(2)_L$ doublet $\tilde{l}_L$ mixes dominantly with the composite doublet $\tilde{O}_{l_1}$ with $U(1)_X$ charge equal to zero. Assuming that the mixing with the first generation is small, one can focus on the $\mu-\tau$ rotations only, described with the mixing angle θ. The experimental bound on $\tau\to 3\mu$ [54] gives

$$\frac{\text{const}}{2}\frac{g_*^2}{M_*^2}s_\tau^2\sin 2\theta\left[\cos^2\theta\, s_\mu^2+\sin^2\theta\, s_\tau^2\right] \leqslant \frac{4\times 10^{-3}}{\text{TeV}^2}\,. \tag{4.7.78}$$

If the angle θ is small, say $\theta \sim s_\mu/s_\tau \ll 1$, then the upper bound on the muon compositeness becomes

$$s_\mu s_\tau^{1/3} \leqslant 0.1\,(\text{const})^{-1/3} \left(\frac{M_*/\text{TeV}}{g_*}\right)^{2/3} . \tag{4.7.79}$$

On the other hand, the lower bound on the new physics contribution to $b \to s\mu\mu$ implies

$$s_s s_b s_\mu s_\tau \sin 2\theta \geqslant 10^{-3} \left(\frac{M_*/\text{TeV}}{g_*}\right)^{2} \tag{4.7.80}$$

If $s_b \sim 1$ and $s_\tau \sim 1$, one can see that there is no tension between the $R_{K^{(*)}}$ observed values and the $\tau \to 3\mu$ data; in fact Eq. (4.7.79) translates into a bound on the compositeness scale of the strange quark

$$s_s \geqslant 0.02 \left(\frac{M_*/\text{TeV}}{g_*}\right)^{2/3} , \tag{4.7.81}$$

which is similar to the naive expectations for the left handed s quark compositeness $s_s \sim V_{ts}$.

Thus, we can conclude that it is possible to fit neutral current flavor anomalies as well, together with $R_{D^{(*)}}$, within the considered Partial Compositeness paradigm.

Chapter 5

Conclusions

The present thesis is an extract of the work done during my PhD at SISSA, which has been devoted to the study of various searches of physics Beyond the Standard Model. In particular, I have analyzed the possibility to observe hints of new physics in an indirect way, as deviation from Standard Model predictions in precision measurements. Two different directions have been followed. The first one is focused on the study of anomalous Triple Gauge Couplings at LHC (or future colliders) in the high energy regime. The second one is associated to the so-called flavor anomalies, which is to say to the discrepancy, with respect to SM, that has been observed in semileptonic B-meson decay, by Belle, BaBar and LHCb experiments.

In Chapter 3, an analysis of the diboson production has been performed. In particular, following the discussion of [2], we have considered $pp \to WZ$ and $pp \to W\gamma$ processes at NLO QCD order in the presence of the dimension 6 operators $\mathcal{O}_{3W}$ and $\mathcal{O}_{3\tilde{W}}$, paying special attention to the effects related to the interference between the SM and BSM contributions to the cross section. Indeed, the Wilson Coefficients of these operators, or equivalently the aTGCs λ_Z and $\tilde{\lambda}_Z$, were considered to be particularly difficult to test at hadron colliders, because interference effects are suppressed by a helicity selection rule. This issue can be solved by taking into account particular differential distributions.

It turns out that NLO QCD effects mildly affects the results of the analogous LO analysis, that we performed in [1], since the helicity selections rules do not apply at NLO. For both the $pp \to WZ$ and $pp \to W\gamma$ processes, the observables related to the azimuthal angles lead to an enhancement of the interference providing a better sensitivity to the new physics interactions. In order to estimate the LHC possibilities on measuring these interactions, available experimental studies of diboson production [34, 33] have been closely followed.

Interestingly, it has been found that some of the kinematic selection cuts, needed to suppress the reducible backgrounds in realistic analyses, are partially performing an azimuthal angular bin selection. This effect turns out to be particularly important for the $pp \to W\gamma$ processes where the strong cut on the M_W^T forces the azimuthal angle to be close to $\pi/2$, making a further binning in the azimuthal angle ϕ_W less important with respect to what is naively expected.

The prospects of the bounds at the HL and HE phases of the LHC have been presented. This leads to a sensitivity $\sim 10^{-3}$ on the Triple Gauge Couplings λ_Z and $\tilde{\lambda}_Z$ at HL-LHC, where the normalization is such that $O_{\lambda_Z} = \lambda_Z \frac{ig}{m_W^2} W^{+\mu_2}_{\mu_1} W^{-\mu_3}_{\mu_2} W^{3\mu_1}_{\mu_3}$, and analogously for $\tilde{\lambda}_Z$. The HE phase of the CERN machine can further improve the bounds by factor of $\sim 2-5$. These results are summarized in Table 5.1.

Channel	Energy	Luminosity	λ_Z [$\times 10^{-3}$]		$\tilde{\lambda}_Z$ [$\times 10^{-3}$]	
			68%	95%	68%	95%
$\boldsymbol{WZ}$	14 TeV	3 ab^{-1}	[-2.1, 1.2]	[-2.9, 1.7]	[-1.7, 1.7]	[-2.4, 2.4]
	27 TeV	3 ab^{-1}	[-1.4, 0.7]	[-2.2, 1.2]	[-1.5, 1.3]	[-2.0, 1.8]
		15 ab^{-1}	[-0.7, 0.4]	[-1.2, 0.6]	[-0.9, 0.8]	[-1.3, 1.2]
$\boldsymbol{W\gamma}$	14 TeV	3 ab^{-1}	[-1.2, 0.9]	[-2.0, 1.6]	[-2.2, 2.1]	[-3.0, 2.9]
	27 TeV	3 ab^{-1}	[-0.7, 0.4]	[-1.2 0.8]	[-1.8, 1.7]	[-2.5, 2.4]
		15 ab^{-1}	[-0.4, 0.2]	[-0.6, 0.3]	[-1.3, 1.2]	[-1.7, 1.5]

Table 5.1: Summary of the results for the various channels in terms of the CP-even and CP-odd anomalous Triple Gauge Couplings. Only events with $m^T_{WZ,W\gamma} < 1.5$ TeV are used.

In Chapter 4, various aspects of the R_D and R_{D^*} anomalies have been studied, following our analysis in [3]. The main objective has been to understand potential correlations of $R_{D^{(*)}}$ with other $\Delta F = 1$ and $\Delta F = 2$ processes, which give rise to constraints on the new physics explanations for the experimental discrepancy, thus allowing to identify the desired properties of the underlying UV theory.

A model independent analysis of possible solutions for these charged current flavor anomalies has been performed, at first in the context of Weak Effective Theory (Section 4.1) and then within a SMEFT (Section 4.5), in which linearly realized $SU(2)_L \times U(1)_Y$ symmetry gives rise to correlations with other well measured $\Delta F = 1$ processes, e.g. $B \to K^* \nu\nu$, $B \to \pi \nu\nu$, $B \to \tau\nu$, and couplings like $Z\tau\tau$, $Z\nu\nu$ and $W\tau\nu$. This poses in serious difficulties the explanation of the $R_{D^{(*)}}$ observed values together with other low energy observables.

Then, the analysis is extended to Composite Higgs paradigm, with Partial Compositeness mechanism to generate the fermion masses. In this case, because of the structure of the model and the corresponding power counting rules, the $\Delta F = 2$ processes, namely K, B_d and B_s mixing measurements, turn out to be extremely constraining. Generically, the models with Partial Compositeness can offer an explanation of these flavor anomalies only if the scale of compositeness is below 0.90 (0.64) TeV for scenarios with (without) the U_1 vector leptoquark. While the requirement of such a low scale is favored by the solution of the electroweak hierarchy problem, it has problematic compatibility with direct searches, and also indirect electroweak precision measurements, unless some additional cancellations are involved.

Finally, it has been shown that it is possible to perform a combined explanation of the analyzed $R_{D^{(*)}}$ with the neutral current B-meson anomalies R_K and R_{K^*}, in this framework.

As charged current flavor anomalies require a NP scale which is rather low ($\sim$ TeV), they might as well be the hints of new physics at the TeV scale. It is thus important to critically examine the models that can provide simultaneous solutions to different problems at the TeV scale. At this point, it seems that the manifestation of new physics, if any, in the dynamics of these flavor transition processes is likely to be quite non generic and subtle; as a consequence, the interpretation of any NP signal would require a large amount of data with a high precision. It is encouraging that such a large amount of data are expected to come from both the LHCb and Belle-II in the near future.

Appendix A

Detailed results of the preliminary LO analysis of $\mathcal{O}_{3W}$

In this Appendix, more complete results are shown for the analysis of $\mathcal{O}_{3W}$ TGC operator at LO, described in Section 3.6.4.

In Table A.1, there is a comparison of the bounds on the Wilson Coefficient obtained with the three different methods described in Section 3.5. The first, is the so-called *leakage* method, used also in analysis discussed in Second 3.6.4; then there is the second, more conservative, method discussed in Section 3.5 in Eq. (3.5.7) and (3.5.8); finally, we have the last method used in [11] and shown in Eq. (3.5.11). One can see that all methods lead to results in the same ball park; even though the method of Eq. (3.5.8) does not make any assumption on the nature of UV completion, the sensitivity to the interference term is a bit worse than in the other two methods.

In Table A.2, there is a comparison of results obtained with one single differential distribution each time. Bounds are extracted with the *leakage* method used also in Table 3.2, which is to say with a m^T_{WZ} upper bound. *No* ϕ_Z *binning* stands for the presence of binning only on p^T_j and *No* p^T_j *binning* corresponds to the case in which only the information for $p^T_j \in [0; 100]$GeV is used and the angular binning is applied. As anticipated in Section 3.6.4, both the differential distributions, in p^T_j and ϕ_Z, bring an increase of sensitivity to the interference term, but the latter has a stronger effect. Indeed, the azimuthal binning reduces the confidence intervals by $\sim 20\%$ while the distribution in the transverse momentum of an extra hard jet only by $\sim 10\%$; furthermore the former provides the major contribution to bounds in the case in which only the c_{3W} linear term in the EFT expansion is considered.

	Lumi. 300 fb^{-1}		Lumi. 3000 fb^{-1}		Q [TeV]
	95% CL	68% CL	95% CL	68% CL	
Same as Table 3.2	[-1.06,1.11]	[-0.59,0.61]	[-0.44,0.45]	[-0.23,0.23]	
Use of (3.5.8)	[-1.59,1.55]	[-1.05,1.01]	[-1.17,1.06]	[-0.72,0.66]	1
Method of [11]	[-0.88,0.88]	[-0.50,0.50]	[-0.41,0.40]	[-0.22,0.22]	
Same as Table 3.2	[-0.69,0.78]	[-0.39,0.45]	[-0.31,0.35]	[-0.17,0.18]	
Use of (3.5.8)	[-0.74,0.79]	[-0.48,0.50]	[-0.51,0.52]	[-0.34,0.30]	1.5
Method of [11]	[-0.55,0.60]	[-0.32,0.35]	[-0.26,0.29]	[-0.15,0.16]	
Same as Table 3.2	[-0.47,0.54]	[-0.27,0.31]	[-0.22,0.26]	[-0.12,0.14]	
Use of (3.5.8)	[-0.49,0.53]	[-0.30,0.34]	[-0.30,0.33]	[-0.20,0.20]	2
Method of [11]	[-0.43,0.47]	[-0.24,0.27]	[-0.20,0.23]	[-0.12,0.13]	

Table A.1: Comparison of different methods.

	Lumi. 300 fb^{-1}		Lumi. 3000 fb^{-1}		Q [TeV]
	95% CL	68% CL	95% CL	68% CL	
Excl.	[-1.06,1.11]	[-0.59,0.61]	[-0.44,0.45]	[-0.23,0.23]	1
Excl., linear	[-1.50,1.49]	[-0.76,0.76]	[-0.48,0.48]	[-0.24,0.24]	
No ϕ_Z binning	[-1.19,1.20]	[-0.69,0.70]	[-0.57,0.57]	[-0.32,0.31]	
No ϕ_Z binning, linear	[-2.28,2.22]	[-1.15,1.14]	[-0.74,0.73]	[-0.38,0.38]	
No p_j^T binning	[-1.14,1.17]	[-0.64,0.67]	[-0.50,0.51]	[-0.27,0.27]	
No p_j^T binning, linear	[-1.80,1.81]	[-0.91,0.92]	[-0.57,0.57]	[-0.29,0.29]	
Incl.	[-1.29,1.27]	[-0.77,0.76]	[-0.69,0.67]	[-0.40,0.39]	
Incl., linear	[-4.27,4.27]	[-2.17,2.17]	[-1.37,1.37]	[-0.70,0.70]	
Excl.	[-0.69,0.78]	[-0.39,0.45]	[-0.31,0.35]	[-0.17,0.18]	1.5
Excl., linear	[-1.22,1.19]	[-0.61,0.61]	[-0.39,0.39]	[-0.20,0.20]	
No ϕ_Z binning	[-0.75,0.82]	[-0.43,0.49]	[-0.37,0.43]	[-0.21,0.25]	
No ϕ_Z binning, linear	[-2.02,1.95]	[-1.02,1.00]	[-0.65,0.64]	[-0.33,0.33]	
No p_j^T binning	[-0.73,0.80]	[-0.41,0.49]	[-0.34,0.38]	[-0.19,0.20]	
No ϕ_Z binning., linear	[-1.43,1.40]	[-0.72,0.71]	[-0.45,0.45]	[-0.23,0.23]	
Incl.	[-0.79,0.85]	[-0.46,0.52]	[-0.41,0.47]	[-0.24,0.29]	
Incl., linear	[-3.97,3.92]	[-2.01,2.00]	[-1.27,1.26]	[-0.64,0.64]	
Excl.	[-0.47,0.54]	[-0.27,0.31]	[-0.22,0.26]	[-0.12,0.14]	2
Excl., linear	[-1.03,0.99]	[-0.52,0.51]	[-0.33,0.32]	[-0.17,0.17]	
No ϕ_Z binning	[-0.50,0.56]	[-0.28,0.34]	[-0.25,0.30]	[-0.14,0.18]	
No ϕ_Z binning, linear	[-1.84,1.73]	[-0.92,0.89]	[-0.59,0.58]	[-0.30,0.30]	
No p_j^T binning	[-0.49,0.55]	[-0.28,0.32]	[-0.23,0.27]	[-0.13,0.15]	
No p_j^T binning, linear	[-1.18,1.12]	[-0.60,0.58]	[-0.37,0.37]	[-0.19,0.19]	
Incl.	[-0.52,0.57]	[-0.30,0.34]	[-0.27,0.31]	[-0.15,0.19]	
Incl., linear	[-3.55,3.41]	[-1.79,1.75]	[-1.12,1.11]	[-0.57,0.57]	

Table A.2: Bounds on $c_{3W}/\Lambda^2 \times \text{TeV}^2$. The total leakage in the various bins of m_{WZ}^T is $\lesssim 5\%$.

Appendix B

From the gauge to the mass eigenstates

$\boxed{[C_{lq}^{(3)}]'_{p'r's't'}\left(\bar{l'}_{p'}\gamma_\mu\sigma^I l'_{r'}\right)\left(\bar{q'}_{s'}\gamma^\mu\sigma^I q'_{t'}\right)}$:

Using Eq. (4.5.11) and the definitions from Eq. (4.5.13), we get,

$$
\begin{aligned}
&\sum_{p',r',s',t'}\left[[C_{lq}^{(3)}]'_{p'r's't'}\left(\bar{l'}_{p'}\gamma_\mu\sigma^I l'_{r'}\right)\left(\bar{q'}_{s'}\gamma^\mu\sigma^I q'_{t'}\right)\right]\\
&=\sum_{p,r,s,t}\Bigg[\sum_{p',r',s',t'}[C_{lq}^{(3)}]'_{p'r's't'}\Big[(V_L^\nu)^\dagger_{pp'}(V_L^\nu)_{r'r}(V_L^u)^\dagger_{ss'}(V_L^u)_{t't}\left(\bar{\nu}_p\gamma^\mu P_L\nu_r\right)\left(\bar{u}_s\gamma_\mu P_L u_t\right)\\
&\qquad+(V_L^e)^\dagger_{pp'}(V_L^e)_{r'r}(V_L^d)^\dagger_{ss'}(V_L^d)_{t't}\left(\bar{e}_p\gamma^\mu P_L e_r\right)\left(\bar{d}_s\gamma_\mu P_L d_t\right)\\
&\qquad-(V_L^e)^\dagger_{pp'}(V_L^e)_{r'r}(V_L^u)^\dagger_{ss'}(V_L^u)_{t't}\left(\bar{e}_p\gamma^\mu P_L e_r\right)\left(\bar{u}_s\gamma_\mu P_L u_t\right)\\
&\qquad-(V_L^\nu)^\dagger_{pp'}(V_L^\nu)_{r'r}(V_L^d)^\dagger_{ss'}(V_L^d)_{t't}\left(\bar{\nu}_p\gamma^\mu P_L\nu_r\right)\left(\bar{d}_s\gamma_\mu P_L d_t\right)\\
&\qquad+2(V_L^\nu)^\dagger_{pp'}(V_L^e)_{r'r}(V_L^d)^\dagger_{ss'}(V_L^u)_{t't}\left(\bar{\nu}_p\gamma^\mu P_L e_r\right)\left(\bar{d}_s\gamma_\mu P_L u_t\right)\\
&\qquad+2(V_L^e)^\dagger_{pp'}(V_L^\nu)_{r'r}(V_L^u)^\dagger_{ss'}(V_L^d)_{t't}\left(\bar{e}_p\gamma^\mu P_L\nu_r\right)\left(\bar{u}_s\gamma_\mu P_L d_t\right)\Big]\Bigg]\\
&=\sum_{p,r,s,t}\Bigg[[\tilde{C}_{lq}^{(3)\nu\nu uu}]_{prst}\left(\bar{\nu}_p\gamma^\mu P_L\nu_r\right)\left(\bar{u}_s\gamma_\mu P_L u_t\right)+[\tilde{C}_{lq}^{(3)eedd}]_{prst}\left(\bar{e}_p\gamma^\mu P_L e_r\right)\left(\bar{d}_s\gamma_\mu P_L d_t\right)\\
&-\ [\tilde{C}_{lq}^{(3)eeuu}]_{prst}\left(\bar{e}_p\gamma^\mu P_L e_r\right)\left(\bar{u}_s\gamma_\mu P_L u_t\right)-[\tilde{C}_{lq}^{(3)\nu\nu dd}]_{prst}\left(\bar{\nu}_p\gamma^\mu P_L\nu_r\right)\left(\bar{d}_s\gamma_\mu P_L d_t\right)\\
&+2[\tilde{C}_{lq}^{(3)\nu edu}]_{prst}\left(\bar{\nu}_p\gamma^\mu P_L e_r\right)\left(\bar{d}_s\gamma_\mu P_L u_t\right)+2[\tilde{C}_{lq}^{(3)e\nu ud}]_{prst}\left(\bar{e}_p\gamma^\mu P_L\nu_r\right)\left(\bar{u}_s\gamma_\mu P_L d_t\right)\Bigg],
\end{aligned}
\tag{B.0.1}
$$

where

$$
\begin{aligned}
\sum_{p',r',s',t'} [C_{lq}^{(3)}]'_{p'r's't'} (V_L^{\nu})^{\dagger}_{pp'} (V_L^{\nu})_{r'r} (V_L^{u})^{\dagger}_{ss'} (V_L^{u})_{t't} &\equiv [\tilde{C}_{lq}^{(3)\nu\nu uu}]_{prst} \\
\sum_{p',r',s',t'} [C_{lq}^{(3)}]'_{p'r's't'} (V_L^{e})^{\dagger}_{pp'} (V_L^{e})_{r'r} (V_L^{d})^{\dagger}_{ss'} (V_L^{d})_{t't} &\equiv [\tilde{C}_{lq}^{(3)eedd}]_{prst} \\
\sum_{p',r',s',t'} [C_{lq}^{(3)}]'_{p'r's't'} (V_L^{e})^{\dagger}_{pp'} (V_L^{e})_{r'r} (V_L^{u})^{\dagger}_{ss'} (V_L^{u})_{t't} &\equiv [\tilde{C}_{lq}^{(3)eeuu}]_{prst} \\
\sum_{p',r',s',t'} [C_{lq}^{(3)}]'_{p'r's't'} (V_L^{\nu})^{\dagger}_{pp'} (V_L^{\nu})_{r'r} (V_L^{d})^{\dagger}_{ss'} (V_L^{d})_{t't} &\equiv [\tilde{C}_{lq}^{(3)\nu\nu dd}]_{prst} \\
\sum_{p',r',s',t'} [C_{lq}^{(3)}]'_{p'r's't'} (V_L^{\nu})^{\dagger}_{pp'} (V_L^{e})_{r'r} (V_L^{d})^{\dagger}_{ss'} (V_L^{u})_{t't} &\equiv [\tilde{C}_{lq}^{(3)\nu edu}]_{prst} \\
\sum_{p',r',s',t'} [C_{lq}^{(3)}]'_{p'r's't'} (V_L^{e})^{\dagger}_{pp'} (V_L^{\nu})_{r'r} (V_L^{u})^{\dagger}_{ss'} (V_L^{d})_{t't} &\equiv [\tilde{C}_{lq}^{(3)e\nu ud}]_{prst}
\end{aligned}
\tag{B.0.2}
$$

$\boxed{[C_{\phi l}^{(3)}]'_{p'r'} \left(\phi^{\dagger} i \overleftrightarrow{D}^{I}_{\mu} \phi\right) \left(\bar{l}'_{p'} \sigma^{I} \gamma^{\mu} l'_{r'}\right)}$:

$$
\begin{aligned}
& \sum_{p',r'} [C_{\phi l}^{(3)}]'_{p'r'} \left(\phi^{\dagger} i \overleftrightarrow{D}^{I}_{\mu} \phi\right) \left(\bar{l}'_{p'} \sigma^{I} \gamma^{\mu} l'_{r'}\right) \\
= \; & \left(v^2 + 2vh + h^2\right) \sum_{p,r} \Bigg[\sum_{p',r'} [C_{\phi l}^{(3)}]'_{p'r'} \Bigg[- \frac{1}{2} \frac{g_2}{\cos\theta_W} (V_L^{\nu})^{\dagger}_{pp'} (V_L^{\nu})_{r'r} Z_{\mu} \left(\overline{\nu}_p \gamma^{\mu} P_L \nu_r\right) \\
+ \; & \frac{1}{2} \frac{g_2}{\cos\theta_W} (V_L^{e})^{\dagger}_{pp'} (V_L^{e})_{r'r} Z_{\mu} \left(\overline{e}_p \gamma^{\mu} P_L e_r\right) - \frac{g_2}{\sqrt{2}} (V_L^{\nu})^{\dagger}_{pp'} (V_L^{e})_{r'r} W_{\mu}^{+} \left(\overline{\nu}_p \gamma^{\mu} P_L e_r\right) \\
- \; & \frac{g_2}{\sqrt{2}} (V_L^{e})^{\dagger}_{pp'} (V_L^{\nu})_{r'r} W_{\mu}^{-} \left(\overline{e}_p \gamma^{\mu} P_L \nu_r\right) \Bigg] \Bigg] \\
= \; & \left(v^2 + 2vh + h^2\right) \sum_{p,r} \Bigg[- \frac{1}{2} \frac{g_2}{\cos\theta_W} [\tilde{C}_{\phi l}^{(3)\nu\nu}]_{pr} Z_{\mu} \left(\overline{\nu}_p \gamma^{\mu} P_L \nu_r\right) \\
+ \; & \frac{1}{2} \frac{g_2}{\cos\theta_W} [\tilde{C}_{\phi l}^{(3)ee}]_{pr} Z_{\mu} \left(\overline{e}_p \gamma^{\mu} P_L e_r\right) - \frac{g_2}{\sqrt{2}} [\tilde{C}_{\phi l}^{(3)\nu e}]_{pr} W_{\mu}^{+} \left(\overline{\nu}_p \gamma^{\mu} P_L e_r\right) \\
- \; & \frac{g_2}{\sqrt{2}} [\tilde{C}_{\phi l}^{(3)e\nu}]_{pr} W_{\mu}^{-} \left(\overline{e}_p \gamma^{\mu} P_L \nu_r\right) \Bigg],
\end{aligned}
\tag{B.0.3}
$$

where

$$\begin{aligned}
\sum_{p',r'}[C^{(3)}_{\phi l}]'_{p'r'}(V^{\nu}_L)^{\dagger}_{pp'}(V^{\nu}_L)_{r'r} &= [\tilde{C}^{(3)\nu\nu}_{\phi l}]_{pr} \\
\sum_{p',r'}[C^{(3)}_{\phi l}]'_{p'r'}(V^{e}_L)^{\dagger}_{pp'}(V^{e}_L)_{r'r} &= [\tilde{C}^{(3)ee}_{\phi l}]_{pr} \\
\sum_{p',r'}[C^{(3)}_{\phi l}]'_{p'r'}(V^{\nu}_L)^{\dagger}_{pp'}(V^{e}_L)_{r'r} &= [\tilde{C}^{(3)\nu e}_{\phi l}]_{pr} \\
\sum_{p',r'}[C^{(3)}_{\phi l}]'_{p'r'}(V^{e}_L)^{\dagger}_{pp'}(V^{\nu}_L)_{r'r} &= [\tilde{C}^{(3)e\nu}_{\phi l}]_{pr} \qquad \text{(B.0.4)}
\end{aligned}$$

$\boxed{[C_{ledq}]'_{p'r's't'}\left(\bar{l}'^{j}_{p'}e'_{r'}\right)\left(\bar{d}'_{s'}q'^{j}_{t'}\right)}$ **:**

$$\begin{aligned}
&\sum_{p',r',s',t'}[C_{ledq}]'_{p'r's't'}\left(\bar{l}'^{j}_{p'}e'_{r'}\right)\left(\bar{d}'_{s'}q'^{j}_{t'}\right) \\
&= \sum_{p,r,s,t}\Bigg[\sum_{p',r',s',t'}[C_{ledq}]'_{p'r's't'}\Bigg[(V^{\nu}_L)^{\dagger}_{pp'}(V^{e}_R)_{r'r}(V^{d}_R)^{\dagger}_{ss'}(V^{u}_L)_{t't}\left(\bar{\nu}_p P_R e_r\right)\left(\bar{d}_s P_L u_t\right) \\
&+ \ (V^{e}_L)^{\dagger}_{pp'}(V^{e}_R)_{r'r}(V^{d}_R)^{\dagger}_{ss'}(V^{d}_L)_{t't}\left(\bar{e}_p P_R e_r\right)\left(\bar{d}_s P_L d_t\right)\Bigg]\Bigg] \\
&= \sum_{p,r,s,t}\Bigg[[\tilde{C}^{\nu edu}_{ledq}]_{prst}\left(\bar{\nu}_p P_R e_r\right)\left(\bar{d}_s P_L u_t\right) + [\tilde{C}^{eedd}_{ledq}]_{prst}\left(\bar{e}_p P_R e_r\right)\left(\bar{d}_s P_L d_t\right)\Bigg], \qquad \text{(B.0.5)}
\end{aligned}$$

where

$$\begin{aligned}
\sum_{p',r',s',t'}[C_{ledq}]'_{p'r's't'}(V^{\nu}_L)^{\dagger}_{pp'}(V^{e}_R)_{r'r}(V^{d}_R)^{\dagger}_{ss'}(V^{u}_L)_{t't} &= [\tilde{C}^{\nu edu}_{ledq}]_{prst} \\
\sum_{p',r',s',t'}[C_{ledq}]'_{p'r's't'}(V^{e}_L)^{\dagger}_{pp'}(V^{e}_R)_{r'r}(V^{d}_R)^{\dagger}_{ss'}(V^{d}_L)_{t't} &= [\tilde{C}^{eedd}_{ledq}]_{prst} \qquad \text{(B.0.6)}
\end{aligned}$$

$\boxed{[C^{(1)}_{lequ}]'_{p'r's't'}\left(\bar{l'}^j_{\ p'}e'_{r'}\right)\epsilon_{jk}\left(\bar{q'}^k_{\ s'}u'_{t'}\right)}$:

$$
\begin{aligned}
&\sum_{p',r',s',t'}[C^{(1)}_{lequ}]'_{p'r's't'}\left(\bar{l'}^j_{\ p'}e'_{r'}\right)\epsilon_{jk}\left(\bar{q'}^k_{\ s'}u'_{t'}\right)\\
&= \sum_{p,r,s,t}\left[\sum_{p',r',s',t'}[C^{(1)}_{lequ}]'_{p'r's't'}\left[(V_L^{\nu})^{\dagger}_{pp'}(V_R^{e})_{r'r}(V_L^{d})^{\dagger}_{ss'}(V_R^{u})_{t't}\left(\bar{\nu}_p P_R e_r\right)\left(\bar{d}_s P_R u_t\right)\right.\right.\\
&- \left.\left.(V_L^{e})^{\dagger}_{pp'}(V_R^{e})_{r'r}(V_L^{u})^{\dagger}_{ss'}(V_R^{u})_{t't}\left(\bar{e}_p P_R e_r\right)\left(\bar{u}_s P_R u_t\right)\right]\right]\\
&= \sum_{p,r,s,t}\left[[\tilde{C}^{(1)\nu edu}_{lequ}]_{prst}\left(\bar{\nu}_p P_R e_r\right)\left(\bar{d}_s P_R u_t\right) - [\tilde{C}^{(1)eedu}_{lequ}]_{prst}\left(\bar{e}_p P_R e_r\right)\left(\bar{u}_s P_R u_t\right)\right], \qquad \text{(B.0.7)}
\end{aligned}
$$

where

$$
\begin{aligned}
\sum_{p',r',s',t'}[C^{(1)}_{lequ}]'_{p'r's't'}(V_L^{\nu})^{\dagger}_{pp'}(V_R^{e})_{r'r}(V_L^{d})^{\dagger}_{ss'}(V_R^{u})_{t't} &= [\tilde{C}^{(1)\nu edu}_{lequ}]_{prst}\\
\sum_{p',r',s',t'}[C^{(1)}_{lequ}]'_{p'r's't'}(V_L^{e})^{\dagger}_{pp'}(V_R^{e})_{r'r}(V_L^{u})^{\dagger}_{ss'}(V_R^{u})_{t't} &= [\tilde{C}^{(1)eedu}_{lequ}]_{prst} \qquad \text{(B.0.8)}
\end{aligned}
$$

Thus,

$$
\Delta C^{cb\tau\nu_3}_{\rm SL} = \frac{1}{2}\frac{\Lambda^2_{\rm SM}}{\Lambda^2}\left([\tilde{C}^{\nu edu}_{ledq}]_{3332} + [\tilde{C}^{(1)\nu edu}_{lequ}]_{3332}\right)^*, \qquad \text{(B.0.9)}
$$

$$
\Delta C^{cb\tau\nu_3}_{\rm PL} = \frac{1}{2}\frac{\Lambda^2_{\rm SM}}{\Lambda^2}\left([\tilde{C}^{\nu edu}_{ledq}]_{3332} - [\tilde{C}^{(1)\nu edu}_{lequ}]_{3332}\right)^*. \qquad \text{(B.0.10)}
$$

$\boxed{[C^{(3)}_{lequ}]'_{p'r's't'}\left(\bar{l'}^j_{\ p'}\sigma^{\mu\nu}e'_{r'}\right)\epsilon_{jk}\left(\bar{q'}^k_{\ s'}\sigma_{\mu\nu}u'_{t'}\right)}$:

$$
\begin{aligned}
&\sum_{p',r',s',t'}[C^{(3)}_{lequ}]'_{p'r's't'}\left(\bar{l'}^j_{\ p'}\sigma^{\mu\nu}e'_{r'}\right)\epsilon_{jk}\left(\bar{q'}^k_{\ s'}\sigma_{\mu\nu}u'_{t'}\right)\\
&= \sum_{p,r,s,t}\left[\sum_{p',r',s',t'}[C^{(3)}_{lequ}]'_{p'r's't'}\left[(V_L^{\nu})^{\dagger}_{pp'}(V_R^{e})_{r'r}(V_L^{d})^{\dagger}_{ss'}(V_R^{u})_{t't}\left(\bar{\nu}_p\sigma^{\mu\nu} P_R e_r\right)\left(\bar{d}_s\sigma_{\mu\nu} P_R u_t\right)\right.\right.\\
&- \left.\left.(V_L^{e})^{\dagger}_{pp'}(V_R^{e})_{r'r}(V_L^{u})^{\dagger}_{ss'}(V_R^{u})_{t't}\left(\bar{e}_p\sigma^{\mu\nu} P_R e_r\right)\left(\bar{u}_s\sigma_{\mu\nu} P_R u_t\right)\right]\right]\\
&= \sum_{p,r,s,t}\left[[\tilde{C}^{(3)\nu edu}_{lequ}]_{prst}\left(\bar{\nu}_p\sigma^{\mu\nu} P_R e_r\right)\left(\bar{d}_s\sigma_{\mu\nu} P_R u_t\right) - [\tilde{C}^{(3)eedu}_{lequ}]_{prst}\left(\bar{e}_p\sigma^{\mu\nu} P_R e_r\right)\left(\bar{u}_s\sigma_{\mu\nu} P_R u_t\right)\right], \qquad \text{(B.0.11)}
\end{aligned}
$$

where

$$\begin{aligned}
\sum_{p',r',s',t'} [C^{(3)}_{lequ}]'_{p'r's't'} (V_L^{\nu})^{\dagger}_{pp'} (V_R^{e})_{r'r} (V_L^{d})^{\dagger}_{ss'} (V_R^{u})_{t't} &= [\tilde{C}^{(3)\nu edu}_{lequ}]_{prst} \\
\sum_{p',r',s',t'} [C^{(3)}_{lequ}]'_{p'r's't'} (V_L^{e})^{\dagger}_{pp'} (V_R^{e})_{r'r} (V_L^{u})^{\dagger}_{ss'} (V_R^{u})_{t't} &= [\tilde{C}^{(3)eedu}_{lequ}]_{prst} \qquad \text{(B.0.12)}
\end{aligned}$$

Thus,

$$\Delta C_{\mathrm{TL}}^{cb\tau\nu_3} = \frac{1}{2} \frac{\Lambda_{\mathrm{SM}}^2}{\Lambda^2} \left([\tilde{C}^{(3)\nu edu}_{lequ}]_{3332} \right)^* . \qquad \text{(B.0.13)}$$

Bibliography

[1] A. Azatov, J. Elias-Miro, Y. Reyimuaji and E. Venturini, *Novel measurements of anomalous triple gauge couplings for the LHC*, *JHEP* **10** (2017) 027, [1707.08060].

[2] A. Azatov, D. Barducci and E. Venturini, *Precision diboson measurements at hadron colliders*, *JHEP* **04** (2019) 075, [1901.04821].

[3] A. Azatov, D. Bardhan, D. Ghosh, F. Sgarlata and E. Venturini, *Anatomy of $b \to c\tau\nu$ anomalies*, *JHEP* **11** (2018) 187, [1805.03209].

[4] R. Contino, A. Falkowski, F. Goertz, C. Grojean and F. Riva, *On the Validity of the Effective Field Theory Approach to SM Precision Tests*, *JHEP* **07** (2016) 144, [1604.06444].

[5] W. Buchmuller and D. Wyler, *Effective Lagrangian Analysis of New Interactions and Flavor Conservation*, *Nucl. Phys.* **B268** (1986) 621–653.

[6] B. Grzadkowski, M. Iskrzynski, M. Misiak and J. Rosiek, *Dimension-Six Terms in the Standard Model Lagrangian*, *JHEP* **10** (2010) 085, [1008.4884].

[7] K. J. F. Gaemers and G. J. Gounaris, *Polarization Amplitudes for e+ e- —¿ W+ W- and e+ e- —¿ Z Z*, *Z. Phys.* **C1** (1979) 259.

[8] U. Baur, T. Han and J. Ohnemus, *WZ production at hadron colliders: Effects of nonstandard WWZ couplings and QCD corrections*, *Phys. Rev.* **D51** (1995) 3381–3407, [hep-ph/9410266].

[9] U. Baur, T. Han and J. Ohnemus, *Amplitude zeros in W+- Z production*, *Phys. Rev. Lett.* **72** (1994) 3941–3944, [hep-ph/9403248].

[10] A. Falkowski and F. Riva, *Model-independent precision constraints on dimension-6 operators*, *JHEP* **02** (2015) 039, [1411.0669].

[11] A. Falkowski, M. Gonzalez-Alonso, A. Greljo, D. Marzocca and M. Son, *Anomalous Triple Gauge Couplings in the Effective Field Theory Approach at the LHC*, *JHEP* **02** (2017) 115, [1609.06312].

[12] R. Roth, F. Campanario, S. Sapeta and D. Zeppenfeld, *Anomalous couplings in WZ production beyond NLO QCD*, *PoS* **LHCP2016** (2016) 141, [1612.03577].

[13] L. Berthier, M. Bjorn and M. Trott, *Incorporating doubly resonant $W^{\pm}$ data in a global fit of SMEFT parameters to lift flat directions*, *JHEP* **09** (2016) 157, [1606.06693].

[14] L. Berthier and M. Trott, *Consistent constraints on the Standard Model Effective Field Theory*, *JHEP* **02** (2016) 069, [1508.05060].

[15] A. Butter, O. J. P. Eboli, J. Gonzalez-Fraile, M. C. Gonzalez-Garcia, T. Plehn and M. Rauch, *The Gauge-Higgs Legacy of the LHC Run I*, *JHEP* **07** (2016) 152, [1604.03105].

[16] B. Dumont, S. Fichet and G. von Gersdorff, *A Bayesian view of the Higgs sector with higher dimensional operators*, *JHEP* **07** (2013) 065, [1304.3369].

[17] J. Ellis, V. Sanz and T. You, *Complete Higgs Sector Constraints on Dimension-6 Operators*, *JHEP* **07** (2014) 036, [1404.3667].

[18] B. M. Gavela, E. E. Jenkins, A. V. Manohar and L. Merlo, *Analysis of General Power Counting Rules in Effective Field Theory*, *Eur. Phys. J.* **C76** (2016) 485, [1601.07551].

[19] ALEPH, DELPHI, L3, OPAL, LEP Electroweak collaboration, S. Schael et al., *Electroweak Measurements in Electron-Positron Collisions at W-Boson-Pair Energies at LEP*, *Phys. Rept.* **532** (2013) 119–244, [1302.3415].

[20] J. Elias-Miro, J. R. Espinosa, E. Masso and A. Pomarol, *Higgs windows to new physics through d=6 operators: constraints and one-loop anomalous dimensions*, *JHEP* **11** (2013) 066, [1308.1879].

[21] A. Pomarol and F. Riva, *Towards the Ultimate SM Fit to Close in on Higgs Physics*, *JHEP* **01** (2014) 151, [1308.2803].

[22] C. Grojean, M. Montull and M. Riembau, *Diboson at the LHC vs LEP*, *JHEP* **03** (2019) 020, [1810.05149].

[23] G. F. Giudice, C. Grojean, A. Pomarol and R. Rattazzi, *The Strongly-Interacting Light Higgs*, *JHEP* **06** (2007) 045, [hep-ph/0703164].

[24] S. Banerjee, R. S. Gupta, J. Y. Reiness and M. Spannowsky, *Resolving the tensor structure of the Higgs coupling to Z-bosons via Higgs-strahlung*, 1905.02728.

[25] A. Azatov, R. Contino, C. S. Machado and F. Riva, *Helicity selection rules and noninterference for BSM amplitudes*, *Phys. Rev.* **D95** (2017) 065014, [1607.05236].

[26] L. J. Dixon and Y. Shadmi, *Testing gluon selfinteractions in three jet events at hadron colliders*, *Nucl. Phys.* **B423** (1994) 3–32, [hep-ph/9312363]. [Erratum: Nucl. Phys.B452,724(1995)].

[27] L. J. Dixon, *Calculating scattering amplitudes efficiently*, in *QCD and beyond. Proceedings, Theoretical Advanced Study Institute in Elementary Particle Physics, TASI-95, Boulder, USA, June 4-30, 1995*, pp. 539–584, 1996. hep-ph/9601359.

[28] G. D'Ambrosio, G. F. Giudice, G. Isidori and A. Strumia, *Minimal flavor violation: An Effective field theory approach*, *Nucl. Phys.* **B645** (2002) 155–187, [hep-ph/0207036].

[29] R. Barbieri, A. Pomarol, R. Rattazzi and A. Strumia, *Electroweak symmetry breaking after LEP-1 and LEP-2*, *Nucl. Phys.* **B703** (2004) 127–146, [hep-ph/0405040].

[30] C. Arzt, M. B. Einhorn and J. Wudka, *Patterns of deviation from the standard model*, *Nucl. Phys.* **B433** (1995) 41–66, [hep-ph/9405214].

[31] D. Liu, A. Pomarol, R. Rattazzi and F. Riva, *Patterns of Strong Coupling for LHC Searches*, *JHEP* **11** (2016) 141, [1603.03064].

[32] G. Panico, F. Riva and A. Wulzer, *Diboson Interference Resurrection*, *Phys. Lett.* **B776** (2018) 473–480, [1708.07823].

[33] ATLAS collaboration, T. A. collaboration, *Measurement of $W^{\pm}Z$ production cross sections and gauge boson polarisation in pp collisions at $\sqrt{s} = 13$ TeV with the ATLAS detector*, *ATLAS-CONF-2018-034* (2018) .

[34] CMS collaboration, S. Chatrchyan et al., *Measurement of the $W\gamma$ and $Z\gamma$ inclusive cross sections in pp collisions at $\sqrt{s} = 7$??TeV and limits on anomalous triple gauge boson couplings*, *Phys. Rev.* **D89** (2014) 092005, [1308.6832].

[35] CMS collaboration, A. M. Sirunyan et al., *Search for anomalous couplings in boosted* $\mathrm{WW/WZ} \to \ell\nu\mathrm{q\bar{q}}$ *production in proton-proton collisions at $\sqrt{s} = 8$ TeV*, *Phys. Lett.* **B772** (2017) 21–42, [1703.06095].

[36] D. Racco, A. Wulzer and F. Zwirner, *Robust collider limits on heavy-mediator Dark Matter*, *JHEP* **05** (2015) 009, [1502.04701].

[37] ATLAS collaboration, G. Aad et al., *Measurements of $W^{\pm}Z$ production cross sections in pp collisions at $\sqrt{s} = 8$ TeV with the ATLAS detector and limits on anomalous gauge boson self-couplings*, *Phys. Rev.* **D93** (2016) 092004, [1603.02151].

[38] J. Alwall, R. Frederix, S. Frixione, V. Hirschi, F. Maltoni, O. Mattelaer et al., *The automated computation of tree-level and next-to-leading order differential cross sections, and their matching to parton shower simulations*, *JHEP* **07** (2014) 079, [1405.0301].

[39] A. Alloul, N. D. Christensen, C. Degrande, C. Duhr and B. Fuks, *FeynRules 2.0 - A complete toolbox for tree-level phenomenology*, *Comput. Phys. Commun.* **185** (2014) 2250–2300, [1310.1921].

[40] C. Degrande, C. Duhr, B. Fuks, D. Grellscheid, O. Mattelaer and T. Reiter, *UFO - The Universal FeynRules Output*, *Comput. Phys. Commun.* **183** (2012) 1201–1214, [1108.2040].

[41] C. Degrande, B. Fuks, K. Mawatari, K. Mimasu and V. Sanz, *Electroweak Higgs boson production in the standard model effective field theory beyond leading order in QCD*, *Eur. Phys. J.* **C77** (2017) 262, [1609.04833].

[42] T. Sjostrand, S. Mrenna and P. Z. Skands, *A Brief Introduction to PYTHIA 8.1*, *Comput. Phys. Commun.* **178** (2008) 852–867, [0710.3820].

[43] R. Frederix and S. Frixione, *Merging meets matching in MC@NLO*, *JHEP* **12** (2012) 061, [1209.6215].

[44] M. Cacciari, G. P. Salam and G. Soyez, *The anti-k_t jet clustering algorithm*, *JHEP* **04** (2008) 063, [0802.1189].

[45] E. Conte, B. Fuks and G. Serret, *MadAnalysis 5, A User-Friendly Framework for Collider Phenomenology*, *Comput. Phys. Commun.* **184** (2013) 222–256, [1206.1599].

[46] DELPHES 3 collaboration, J. de Favereau, C. Delaere, P. Demin, A. Giammanco, V. Lemaitre, A. Mertens et al., *DELPHES 3, A modular framework for fast simulation of a generic collider experiment*, *JHEP* **02** (2014) 057, [1307.6346].

[47] M. Grazzini, S. Kallweit, D. Rathlev and M. Wiesemann, *$W^{\pm}Z$ production at the LHC: fiducial cross sections and distributions in NNLO QCD*, *JHEP* **05** (2017) 139, [1703.09065].

[48] M. Chiesa, A. Denner and J.-N. Lang, *Anomalous triple-gauge-boson interactions in vector-boson pair production with RECOLA2*, *Eur. Phys. J.* **C78** (2018) 467, [1804.01477].

[49] A. Helset and M. Trott, *On interference and non-interference in the SMEFT*, *JHEP* **04** (2018) 038, [1711.07954].

[50] C. Degrande, N. Greiner, W. Kilian, O. Mattelaer, H. Mebane, T. Stelzer et al., *Effective Field Theory: A Modern Approach to Anomalous Couplings*, *Annals Phys.* **335** (2013) 21–32, [1205.4231].

[51] F. Boudjema, K. Hagiwara, C. Hamzaoui and K. Numata, *Anomalous moments of quarks and leptons from nonstandard W W gamma couplings*, *Phys. Rev.* **D43** (1991) 2223–2232.

[52] B. Gripaios and D. Sutherland, *Searches for CP-violating dimension-6 electroweak gauge boson operators*, *Phys. Rev.* **D89** (2014) 076004, [1309.7822].

[53] C. Dib, A. Faessler, T. Gutsche, S. Kovalenko, J. Kuckei, V. E. Lyubovitskij et al., *The Neutron electric dipole form-factor in the perturbative chiral quark model*, *J. Phys.* **G32** (2006) 547–564, [hep-ph/0601144].

[54] Particle Data Group collaboration, C. Patrignani et al., *Review of Particle Physics*, *Chin. Phys.* **C40** (2016) 100001.

[55] X. Cid Vidal et al., *Beyond the Standard Model Physics at the HL-LHC and HE-LHC*, 1812.07831.

[56] Belle collaboration, A. Abdesselam et al., *Measurement of $\mathcal{R}(D)$ and $\mathcal{R}(D^*)$ with a semileptonic tagging method*, 1904.08794.

[57] LHCb Collaboration collaboration, R. Aaij et al., *Measurement of the ratio of branching fractions $\mathcal{B}(B_c^+ \to j/\psi\tau^+\nu_\tau)/\mathcal{B}(B_c^+ \to j/\psi\mu^+\nu_\mu)$*, *Phys. Rev. Lett.* **120** (Mar, 2018) 121801.

[58] Belle collaboration, A. Abdesselam et al., *Measurement of the D^{*-} polarization in the decay $B^0 \to D^{*-}\tau^+\nu_\tau$*, in *10th International Workshop on the CKM Unitarity Triangle (CKM 2018) Heidelberg, Germany, September 17-21, 2018*, 2019. 1903.03102.

[59] Belle Collaboration collaboration, S. Hirose et al., *Measurement of the τ lepton polarization and $r(D^*)$ in the decay $\overline{B} \to D^* \tau^- \overline{\nu}_\tau$*, *Phys. Rev. Lett.* **118** (May, 2017) 211801.

[60] LHCb collaboration, R. Aaij et al., *Angular analysis of the $B^0 \to K^{*0} \mu^+ \mu^-$ decay using 3 fb^{-1} of integrated luminosity*, *JHEP* **02** (2016) 104, [1512.04442].

[61] LHCb collaboration, R. Aaij et al., *Measurement of the $B_s^0 \to \mu^+ \mu^-$ branching fraction and effective lifetime and search for $B^0 \to \mu^+ \mu^-$ decays*, *Phys. Rev. Lett.* **118** (2017) 191801, [1703.05747].

[62] ATLAS collaboration, M. Aaboud et al., *Study of the rare decays of B_s^0 and B^0 mesons into muon pairs using data collected during 2015 and 2016 with the ATLAS detector*, *JHEP* **04** (2019) 098, [1812.03017].

[63] D. Buttazzo, A. Greljo, G. Isidori and D. Marzocca, *B-physics anomalies: a guide to combined explanations*, *JHEP* **11** (2017) 044, [1706.07808].

[64] M. Bordone, C. Cornella, J. Fuentes-Martin and G. Isidori, *A three-site gauge model for flavor hierarchies and flavor anomalies*, *Phys. Lett.* **B779** (2018) 317–323, [1712.01368].

[65] R. Barbieri and A. Tesi, *B-decay anomalies in Pati-Salam SU(4)*, 1712.06844.

[66] A. Greljo and B. A. Stefanek, *Third family quark?lepton unification at the TeV scale*, *Phys. Lett.* **B782** (2018) 131–138, [1802.04274].

[67] D. Marzocca, *Addressing the B-physics anomalies in a fundamental Composite Higgs Model*, 1803.10972.

[68] M. Bordone, C. Cornella, J. Fuentes-Martin and G. Isidori, *Low-energy signatures of the* PS^3 *model: from B-physics anomalies to LFV*, *JHEP* **10** (2018) 148, [1805.09328].

[69] D. Becirevic, I. Dorsner, S. Fajfer, N. Kosnik, D. A. Faroughy and O. Sumensari, *Scalar leptoquarks from grand unified theories to accommodate the B-physics anomalies*, *Phys. Rev.* **D98** (2018) 055003, [1806.05689].

[70] L. Di Luzio, J. Fuentes-Martin, A. Greljo, M. Nardecchia and S. Renner, *Maximal Flavour Violation: a Cabibbo mechanism for leptoquarks*, *JHEP* **11** (2018) 081, [1808.00942].

[71] C. Cornella, J. Fuentes-Martin and G. Isidori, *Revisiting the vector leptoquark explanation of the B-physics anomalies*, 1903.11517.

[72] Y. Amhis et al., *Averages of b-hadron, c-hadron, and τ-lepton properties as of summer 2016,* Online update at *http://www.slac.stanford.edu/xorg/hflav/semi/fpcp17/RDRDs.html*, 1612.07233.

[73] Y. Amhis et al., *Averages of b-hadron, c-hadron, and τ-lepton properties as of summer 2016,* Online update at *https://hflav-eos.web.cern.ch/hflav-eos/semi/spring19/main.shtml*, 1612.07233.

[74] S. Aoki et al., *Review of lattice results concerning low-energy particle physics*, *Eur. Phys. J.* **C77** (2017) 112, [1607.00299].

[75] HPQCD collaboration, H. Na, C. M. Bouchard, G. P. Lepage, C. Monahan and J. Shigemitsu, *$B \to D l \nu$ form factors at nonzero recoil and extraction of $|V_{cb}|$*, *Phys. Rev.* **D92** (2015) 054510, [1505.03925]. [Erratum: Phys. Rev.D93,no.11,119906(2016)].

[76] D. Bigi and P. Gambino, *Revisiting $B \to D \ell \nu$*, *Phys. Rev.* **D94** (2016) 094008, [1606.08030].

[77] S. Fajfer, J. F. Kamenik and I. Nisandzic, *On the $B \to D^* \tau \bar{\nu}_\tau$ Sensitivity to New Physics*, *Phys. Rev.* **D85** (2012) 094025, [1203.2654].

[78] D. Bigi, P. Gambino and S. Schacht, *$R(D^*)$, $|V_{cb}|$, and the Heavy Quark Symmetry relations between form factors*, *JHEP* **11** (2017) 061, [1707.09509].

[79] Belle collaboration, S. Hirose et al., *Measurement of the τ lepton polarization and $R(D^*)$ in the decay $\bar{B} \to D^* \tau^- \bar{\nu}_\tau$*, *Phys. Rev. Lett.* **118** (2017) 211801, [1612.00529].

[80] Belle collaboration, S. Hirose et al., *Measurement of the τ lepton polarization and $R(D^*)$ in the decay $\bar{B} \to D^* \tau^- \bar{\nu}_\tau$ with one-prong hadronic τ decays at Belle*, 1709.00129.

[81] Z.-R. Huang, Y. Li, C.-D. Lu, M. A. Paracha and C. Wang, *Footprints of New Physics in $b \to c\tau\nu$ Transitions*, *Phys. Rev.* **D98** (2018) 095018, [1808.03565].

[82] S. Bhattacharya, S. Nandi and S. Kumar Patra, *$b \to c\tau\nu_\tau$ Decays: a catalogue to compare, constrain, and correlate new physics effects*, *Eur. Phys. J.* **C79** (2019) 268, [1805.08222].

[83] LHCb collaboration, R. Aaij et al., *Measurement of the ratio of branching fractions $\mathcal{B}(B_c^+ \to J/\psi\tau^+\nu_\tau)/\mathcal{B}(B_c^+ \to J/\psi\mu^+\nu_\mu)$*, 1711.05623.

[84] BaBar collaboration, J. P. Lees et al., *Evidence for an excess of $\bar{B} \to D^{(*)}\tau^-\bar{\nu}_\tau$ decays*, *Phys. Rev. Lett.* **109** (2012) 101802, [1205.5442].

[85] BaBar collaboration, J. P. Lees et al., *Measurement of an Excess of $\bar{B} \to D^{(*)}\tau^-\bar{\nu}_\tau$ Decays and Implications for Charged Higgs Bosons*, *Phys. Rev.* **D88** (2013) 072012, [1303.0571].

[86] Belle collaboration, M. Huschle et al., *Measurement of the branching ratio of $\bar{B} \to D^{(*)}\tau^-\bar{\nu}_\tau$ relative to $\bar{B} \to D^{(*)}\ell^-\bar{\nu}_\ell$ decays with hadronic tagging at Belle*, *Phys. Rev.* **D92** (2015) 072014, [1507.03233].

[87] LHCb collaboration, R. Aaij et al., *Measurement of the ratio of branching fractions $\mathcal{B}(\bar{B}^0 \to D^{*+}\tau^-\bar{\nu}_\tau)/\mathcal{B}(\bar{B}^0 \to D^{*+}\mu^-\bar{\nu}_\mu)$*, *Phys. Rev. Lett.* **115** (2015) 111803, [1506.08614]. [Erratum: Phys. Rev. Lett.115,no.15,159901(2015)].

[88] Belle collaboration, Y. Sato et al., *Measurement of the branching ratio of $\bar{B}^0 \to D^{*+}\tau^-\bar{\nu}_\tau$ relative to $\bar{B}^0 \to D^{*+}\ell^-\bar{\nu}_\ell$ decays with a semileptonic tagging method*, *Phys. Rev.* **D94** (2016) 072007, [1607.07923].

[89] A. Raphael. https://indico.cern.ch/event/586719/contributions/2531261/attachments/1470695/2275576/2_fpcp_talk_wormser.pdf, Talk given at FPCP Conference, June 5 2017, Prague.

[90] W.-F. Wang, Y.-Y. Fan and Z.-J. Xiao, *Semileptonic decays $B_c \to (\eta_c, J/\Psi) l\nu$ in the perturbative QCD approach*, *Chin. Phys.* **C37** (2013) 093102, [1212.5903].

[91] Y. Amhis et al., *Averages of b-hadron, c-hadron, and τ-lepton properties as of summer 2016,* Online update at *https://hflav-eos.web.cern.ch/hflav-eos/semi/summer18/RDRDs.html*, 1612.07233.

[92] R. Barbieri, G. Isidori, A. Pattori and F. Senia, *Anomalies in B-decays and $U(2)$ flavour symmetry*, *Eur. Phys. J.* **C76** (2016) 67, [1512.01560].

[93] B. Gripaios, M. Nardecchia and S. A. Renner, *Composite leptoquarks and anomalies in B-meson decays*, *JHEP* **05** (2015) 006, [1412.1791].

[94] C. Niehoff, P. Stangl and D. M. Straub, *Direct and indirect signals of natural composite Higgs models*, *JHEP* **01** (2016) 119, [1508.00569].

[95] R. Barbieri, C. W. Murphy and F. Senia, *B-decay Anomalies in a Composite Leptoquark Model*, *Eur. Phys. J.* **C77** (2017) 8, [1611.04930].

[96] C. Niehoff, P. Stangl and D. M. Straub, *Electroweak symmetry breaking and collider signatures in the next-to-minimal composite Higgs model*, *JHEP* **04** (2017) 117, [1611.09356].

[97] E. Megias, G. Panico, O. Pujolas and M. Quiros, *A Natural origin for the LHCb anomalies*, *JHEP* **09** (2016) 118, [1608.02362].

[98] D. Buttazzo, A. Greljo, G. Isidori and D. Marzocca, *Toward a coherent solution of diphoton and flavor anomalies*, *JHEP* **08** (2016) 035, [1604.03940].

[99] G. D'Ambrosio and A. M. Iyer, *Flavour issues in warped custodial models: B anomalies and rare K decays*, 1712.08122.

[100] F. Sannino, P. Stangl, D. M. Straub and A. E. Thomsen, *Flavor Physics and Flavor Anomalies in Minimal Fundamental Partial Compositeness*, 1712.07646.

[101] A. Carmona and F. Goertz, *Recent **B** Physics Anomalies - a First Hint for Compositeness?*, 1712.02536.

[102] P. Asadi, M. R. Buckley and D. Shih, *It's all right(-handed neutrinos): a new W' model for the $R_{D^{(*)}}$ anomaly*, 1804.04135.

[103] A. Greljo, D. J. Robinson, B. Shakya and J. Zupan, *$R(D^{(*)})$ from W' and right-handed neutrinos*, 1804.04642.

[104] A. Azatov, D. Barducci, D. Ghosh, D. Marzocca and L. Ubaldi, *Combined explanations of B-physics anomalies: the sterile neutrino solution*, *JHEP* **10** (2018) 092, [1807.10745].

[105] R. Alonso, B. Grinstein and J. Martin Camalich, *The lifetime of the B_c^- meson and the anomalies in $B \to D^{(*)}\tau\nu$*, *Phys. Rev. Lett.* **118** (2017) 081802, [1611.06676].

[106] A. G. Akeroyd and C.-H. Chen, *Constraint on the branching ratio of $B_c \to \tau\bar{\nu}$ from LEP1 and consequences for $R(D^{(*)})$ anomaly*, *Phys. Rev.* **D96** (2017) 075011, [1708.04072].

[107] HPQCD collaboration, B. Colquhoun, C. T. H. Davies, R. J. Dowdall, J. Kettle, J. Koponen, G. P. Lepage et al., *B-meson decay constants: a more complete picture from full lattice QCD*, *Phys. Rev.* **D91** (2015) 114509, [1503.05762].

[108] LHCb collaboration, R. Aaij et al., *Test of lepton universality using $B^+ \to K^+\ell^+\ell^-$ decays*, *Phys. Rev. Lett.* **113** (2014) 151601, [1406.6482].

[109] LHCb collaboration, R. Aaij et al., *Search for lepton-universality violation in $B^+ \to K^+\ell^+\ell^-$ decays*, *Phys. Rev. Lett.* **122** (2019) 191801, [1903.09252].

[110] LHCb collaboration, R. Aaij et al., *Test of lepton universality with $B^0 \to K^{*0}\ell^+\ell^-$ decays*, *JHEP* **08** (2017) 055, [1705.05802].

[111] Belle collaboration, A. Abdesselam et al., *Test of lepton flavor universality in $B \to K^*\ell^+\ell^-$ decays at Belle*, 1904.02440.

[112] D. A. Faroughy, A. Greljo and J. F. Kamenik, *Confronting lepton flavor universality violation in B decays with high-p_T tau lepton searches at LHC*, *Phys. Lett.* **B764** (2017) 126–134, [1609.07138].

[113] A. Greljo and D. Marzocca, *High-p_T dilepton tails and flavor physics*, *Eur. Phys. J.* **C77** (2017) 548, [1704.09015].

[114] I. Dorsner, S. Fajfer and A. Greljo, *Cornering Scalar Leptoquarks at LHC*, *JHEP* **10** (2014) 154, [1406.4831].

[115] M. J. Baker, J. Fuentes-Martin, G. Isidori and M. Koenig, *High- p_T signatures in vector?leptoquark models*, *Eur. Phys. J.* **C79** (2019) 334, [1901.10480].

[116] A. Datta, M. Duraisamy and D. Ghosh, *Diagnosing New Physics in $b \to c\,\tau\,\nu_\tau$ decays in the light of the recent BaBar result*, *Phys. Rev.* **D86** (2012) 034027, [1206.3760].

[117] M. Tanaka and R. Watanabe, *New physics in the weak interaction of $\bar{B} \to D^{(*)}\tau\bar{\nu}$*, *Phys. Rev.* **D87** (2013) 034028, [1212.1878].

[118] D. Choudhury, D. K. Ghosh and A. Kundu, *B decay anomalies in an effective theory*, *Phys. Rev.* **D86** (2012) 114037, [1210.5076].

[119] Y. Sakaki, M. Tanaka, A. Tayduganov and R. Watanabe, *Testing leptoquark models in $\bar{B} \to D^{(*)}\tau\bar{\nu}$*, *Phys. Rev.* **D88** (2013) 094012, [1309.0301].

[120] B. Bhattacharya, A. Datta, D. London and S. Shivashankara, *Simultaneous Explanation of the R_K and $R(D^{(*)})$ Puzzles*, *Phys. Lett.* **B742** (2015) 370–374, [1412.7164].

[121] O. Cata and M. Jung, *Signatures of a nonstandard Higgs boson from flavor physics*, *Phys. Rev.* **D92** (2015) 055018, [1505.05804].

[122] M. Freytsis, Z. Ligeti and J. T. Ruderman, *Flavor models for $\bar{B} \to D^{(*)}\tau\bar{\nu}$*, *Phys. Rev.* **D92** (2015) 054018, [1506.08896].

[123] D. Choudhury, A. Kundu, S. Nandi and S. K. Patra, *Unified resolution of the $R(D)$ and $R(D^*)$ anomalies and the lepton flavor violating decay $h \to \mu\tau$*, *Phys. Rev.* **D95** (2017) 035021, [1612.03517].

[124] A. Celis, M. Jung, X.-Q. Li and A. Pich, *Scalar contributions to $b \to c(u)\tau\nu$ transitions*, *Phys. Lett.* **B771** (2017) 168–179, [1612.07757].

[125] D. Choudhury, A. Kundu, R. Mandal and R. Sinha, *Minimal unified resolution to $R_{K^{(*)}}$ and $R(D^{(*)})$ anomalies with lepton mixing*, *Phys. Rev. Lett.* **119** (2017) 151801, [1706.08437].

[126] A. Crivellin, D. Muller and T. Ota, *Simultaneous explanation of $R(D^{(?)})$ and $b?s?^+$ $?^?$: the last scalar leptoquarks standing*, *JHEP* **09** (2017) 040, [1703.09226].

[127] P. Colangelo and F. De Fazio, *Scrutinizing $\bar{B} \to D^*(D\pi)\ell^-\bar{\nu}_\ell$ and $\bar{B} \to D^*(D\gamma)\ell^-\bar{\nu}_\ell$ in search of new physics footprints*, 1801.10468.

[128] C. Murgui, A. Penuelas, M. Jung and A. Pich, *Global fit to $b \to c\tau\nu$ transitions*, 1904.09311.

[129] D. Bardhan, P. Byakti and D. Ghosh, *A closer look at the R_D and R_{D^*} anomalies*, *JHEP* **01** (2017) 125, [1610.03038].

[130] R. Alonso, E. E. Jenkins, A. V. Manohar and M. Trott, *Renormalization Group Evolution of the Standard Model Dimension Six Operators III: Gauge Coupling Dependence and Phenomenology*, *JHEP* **04** (2014) 159, [1312.2014].

[131] I. Dorsner, S. Fajfer, N. Kosnik and I. Nisandzic, *Minimally flavored colored scalar in $\bar{B} \to D^{(*)}\tau\bar{\nu}$ and the mass matrices constraints*, *JHEP* **11** (2013) 084, [1306.6493].

[132] U. Nierste, S. Trine and S. Westhoff, *Charged-Higgs effects in a new $B \to D\tau\nu$ differential decay distribution*, *Phys. Rev.* **D78** (2008) 015006, [0801.4938].

[133] M. Duraisamy and A. Datta, *The Full $B \to D^*\tau^-\bar{\nu}_\tau$ Angular Distribution and CP violating Triple Products*, *JHEP* **09** (2013) 059, [1302.7031].

[134] Z. Ligeti, M. Papucci and D. J. Robinson, *New Physics in the Visible Final States of $B \to D^{(*)}\tau\nu$*, *JHEP* **01** (2017) 083, [1610.02045].

[135] R. Alonso, A. Kobach and J. Martin Camalich, *New physics in the kinematic distributions of $\bar{B} \to D^{(*)}\tau^-(\to \ell^-\bar{\nu}_\ell\nu_\tau)\bar{\nu}_\tau$*, *Phys. Rev.* **D94** (2016) 094021, [1602.07671].

[136] A. K. Alok, D. Kumar, S. Kumbhakar and S. U. Sankar, *D^* polarization as a probe to discriminate new physics in $\bar{B} \to D^*\tau\bar{\nu}$*, *Phys. Rev.* **D95** (2017) 115038, [1606.03164].

[137] DELPHI, OPAL, ALEPH, LEP Electroweak Working Group, L3 collaboration, *A Combination of preliminary electroweak measurements and constraints on the standard model*, hep-ex/0511027.

[138] A. Pich, *Precision Tau Physics*, *Prog. Part. Nucl. Phys.* **75** (2014) 41–85, [1310.7922].

[139] SLD Electroweak Group, DELPHI, ALEPH, SLD, SLD Heavy Flavour Group, OPAL, LEP Electroweak Working Group, L3 collaboration, S. Schael et al., *Precision electroweak measurements on the Z resonance*, *Phys. Rept.* **427** (2006) 257–454, [hep-ex/0509008].

[140] Belle collaboration, J. Grygier et al., *Search for $B \to h\nu\bar{\nu}$ decays with semileptonic tagging at Belle*, *Phys. Rev.* **D96** (2017) 091101, [1702.03224].

[141] C. Hambrock, A. Khodjamirian and A. Rusov, *Hadronic effects and observables in $B \to \pi\ell^+\ell^-$ decay at large recoil*, *Phys. Rev.* **D92** (2015) 074020, [1506.07760].

[142] Belle II collaboration, E. Manoni, *Studies of missing energy decays of B meson at Belle II*, *PoS* **EPS-HEP2017** (2017) 226.

[143] A. J. Buras, J. Girrbach-Noe, C. Niehoff and D. M. Straub, *$B \to K^{(*)}\nu\overline{\nu}$ decays in the Standard Model and beyond*, *JHEP* **02** (2015) 184, [1409.4557].

[144] B. Capdevila, A. Crivellin, S. Descotes-Genon, L. Hofer and J. Matias, *Searching for New Physics with $b \to s\tau^+\tau^-$ processes*, 1712.01919.

[145] F. Feruglio, P. Paradisi and A. Pattori, *Revisiting Lepton Flavor Universality in B Decays*, *Phys. Rev. Lett.* **118** (2017) 011801, [1606.00524].

[146] F. Feruglio, P. Paradisi and A. Pattori, *On the Importance of Electroweak Corrections for B Anomalies*, *JHEP* **09** (2017) 061, [1705.00929].

[147] C. Bobeth and U. Haisch, *New Physics in Γ_{12}^s: $(\bar{s}b)(\bar{\tau}\tau)$ Operators*, *Acta Phys. Polon.* **B44** (2013) 127–176, [1109.1826].

[148] A. Dighe and D. Ghosh, *How large can the branching ratio of $B_s \to \tau^+\tau^-$ be ?*, *Phys. Rev.* **D86** (2012) 054023, [1207.1324].

[149] E. E. Jenkins, A. V. Manohar and M. Trott, *Renormalization Group Evolution of the Standard Model Dimension Six Operators II: Yukawa Dependence*, *JHEP* **01** (2014) 035, [1310.4838].

[150] M. Tanaka and R. Watanabe, *Tau longitudinal polarization in $B \to D\tau\nu$ and its role in the search for charged Higgs boson*, *Phys. Rev.* **D82** (2010) 034027, [1005.4306].

[151] S. Fajfer, J. F. Kamenik, I. Nisandzic and J. Zupan, *Implications of Lepton Flavor Universality Violations in B Decays*, *Phys. Rev. Lett.* **109** (2012) 161801, [1206.1872].

[152] A. Crivellin, C. Greub and A. Kokulu, *Explaining $B \to D\tau\nu$, $B \to D^*\tau\nu$ and $B \to \tau\nu$ in a 2HDM of type III*, *Phys. Rev.* **D86** (2012) 054014, [1206.2634].

[153] X.-G. He and G. Valencia, *B decays with τ leptons in nonuniversal left-right models*, *Phys. Rev.* **D87** (2013) 014014, [1211.0348].

[154] S. M. Boucenna, A. Celis, J. Fuentes-Martin, A. Vicente and J. Virto, *Phenomenology of an $SU(2) \times SU(2) \times U(1)$ model with lepton-flavour non-universality*, *JHEP* **12** (2016) 059, [1608.01349].

[155] A. Greljo, G. Isidori and D. Marzocca, *On the breaking of Lepton Flavor Universality in B decays*, *JHEP* **07** (2015) 142, [1506.01705].

[156] I. Dorsner, S. Fajfer, A. Greljo, J. F. Kamenik and N. Kosnik, *Physics of leptoquarks in precision experiments and at particle colliders*, *Phys. Rept.* **641** (2016) 1–68, [1603.04993].

[157] J. C. Pati and A. Salam, *Lepton Number as the Fourth Color*, *Phys. Rev.* **D10** (1974) 275–289. [Erratum: Phys. Rev.D11,703(1975)].

[158] D. B. Kaplan and H. Georgi, *SU(2) x U(1) Breaking by Vacuum Misalignment*, *Phys. Lett.* **136B** (1984) 183–186.

[159] D. B. Kaplan, *Flavor at SSC energies: A New mechanism for dynamically generated fermion masses*, *Nucl. Phys.* **B365** (1991) 259–278.

[160] R. Contino, Y. Nomura and A. Pomarol, *Higgs as a holographic pseudoGoldstone boson*, *Nucl. Phys.* **B671** (2003) 148–174, [hep-ph/0306259].

[161] R. Contino, *The Higgs as a Composite Nambu-Goldstone Boson*, in *Physics of the large and the small, TASI 09, proceedings of the Theoretical Advanced Study Institute in Elementary Particle Physics, Boulder, Colorado, USA, 1-26 June 2009*, pp. 235–306, 2011. 1005.4269. DOI.

[162] G. Panico and A. Wulzer, *The Composite Nambu-Goldstone Higgs*, *Lect. Notes Phys.* **913** (2016) pp.1–316, [1506.01961].

[163] R. Contino, T. Kramer, M. Son and R. Sundrum, *Warped/composite phenomenology simplified*, *JHEP* **05** (2007) 074, [hep-ph/0612180].

[164] S. R. Coleman, J. Wess and B. Zumino, *Structure of phenomenological Lagrangians. 1.*, *Phys. Rev.* **177** (1969) 2239–2247.

[165] C. G. Callan, Jr., S. R. Coleman, J. Wess and B. Zumino, *Structure of phenomenological Lagrangians. 2.*, *Phys. Rev.* **177** (1969) 2247–2250.

[166] R. Contino, D. Marzocca, D. Pappadopulo and R. Rattazzi, *On the effect of resonances in composite Higgs phenomenology*, *JHEP* **10** (2011) 081, [1109.1570].

[167] G. Ecker, J. Gasser, H. Leutwyler, A. Pich and E. de Rafael, *Chiral Lagrangians for Massive Spin 1 Fields*, *Phys. Lett.* **B223** (1989) 425–432.

[168] UTfit collaboration, M. Bona et al., *Model-independent constraints on $\Delta F = 2$ operators and the scale of new physics*, *JHEP* **03** (2008) 049, [0707.0636].

[169] ETM collaboration, N. Carrasco et al., *B-physics from $N_f = 2$ tmQCD: the Standard Model and beyond*, *JHEP* **03** (2014) 016, [1308.1851].

[170] K. Agashe, R. Contino, L. Da Rold and A. Pomarol, *A Custodial symmetry for $Zb\bar{b}$*, *Phys. Lett.* **B641** (2006) 62–66, [hep-ph/0605341].

[171] C. Grojean, O. Matsedonskyi and G. Panico, *Light top partners and precision physics*, *JHEP* **10** (2013) 160, [1306.4655].

[172] A. Azatov, C. Grojean, A. Paul and E. Salvioni, *Resolving gluon fusion loops at current and future hadron colliders*, *JHEP* **09** (2016) 123, [1608.00977].

[173] C. Csaki, A. Falkowski and A. Weiler, *The Flavor of the Composite Pseudo-Goldstone Higgs*, *JHEP* **09** (2008) 008, [0804.1954].

[174] K. Agashe, A. Azatov and L. Zhu, *Flavor Violation Tests of Warped/Composite SM in the Two-Site Approach*, *Phys. Rev.* **D79** (2009) 056006, [0810.1016].

[175] R. Barbieri, G. Isidori, J. Jones-Perez, P. Lodone and D. M. Straub, *$U(2)$ and Minimal Flavour Violation in Supersymmetry*, *Eur. Phys. J.* **C71** (2011) 1725, [1105.2296].

[176] R. Barbieri, D. Buttazzo, F. Sala, D. M. Straub and A. Tesi, *A 125 GeV composite Higgs boson versus flavour and electroweak precision tests*, *JHEP* **05** (2013) 069, [1211.5085].

[177] CMS collaboration, A. M. Sirunyan et al., *Search for vector-like T and B quark pairs in final states with leptons at $\sqrt{s} = 13$ TeV*, *JHEP* **08** (2018) 177, [1805.04758].

[178] ATLAS collaboration, M. Aaboud et al., *Combination of the searches for pair-produced vector-like partners of the third-generation quarks at $\sqrt{s} = 13$ TeV with the ATLAS detector*, *Phys. Rev. Lett.* **121** (2018) 211801, [1808.02343].

[179] M. Ciuchini, E. Franco, S. Mishima and L. Silvestrini, *Electroweak Precision Observables, New Physics and the Nature of a 126 GeV Higgs Boson*, *JHEP* **08** (2013) 106, [1306.4644].

[180] Gfitter Group collaboration, M. Baak, J. Cuth, J. Haller, A. Hoecker, R. Kogler, K. Monig et al., *The global electroweak fit at NNLO and prospects for the LHC and ILC*, *Eur. Phys. J.* **C74** (2014) 3046, [1407.3792].

[181] J. de Blas, M. Ciuchini, E. Franco, S. Mishima, M. Pierini, L. Reina et al., *Electroweak precision observables and Higgs-boson signal strengths in the Standard Model and beyond: present and future*, *JHEP* **12** (2016) 135, [1608.01509].

[182] A. Azatov, R. Contino, A. Di Iura and J. Galloway, *New Prospects for Higgs Compositeness in $h \to Z\gamma$*, *Phys. Rev.* **D88** (2013) 075019, [1308.2676].

[183] D. Ghosh, M. Salvarezza and F. Senia, *Extending the Analysis of Electroweak Precision Constraints in Composite Higgs Models*, *Nucl. Phys.* **B914** (2017) 346–387, [1511.08235].

[184] M. Redi and A. Weiler, *Flavor and CP Invariant Composite Higgs Models*, *JHEP* **11** (2011) 108, [1106.6357].

[185] M. Chala and M. Spannowsky, *On the behaviour of composite resonances breaking lepton flavour universality*, 1803.02364.

[186] G. D'Amico, M. Nardecchia, P. Panci, F. Sannino, A. Strumia, R. Torre et al., *Flavour anomalies after the R_{K^*} measurement*, *JHEP* **09** (2017) 010, [1704.05438].

[187] D. Ghosh, *Explaining the R_K and R_{K^*} anomalies*, *Eur. Phys. J.* **C77** (2017) 694, [1704.06240].

Acknowledgements

I would like to express my gratitude to my advisors Prof. Aleksandr Azatov and Prof. Andrea Romanino for their really important guidance and support. I am really thankful also to all my collaborators: Joan Elias-Miró, Reyimuaji Yakefu, Francesco Sgarlata, Diptimoy Ghosh, Daniele Barducci, David Marzocca and Valerio Gherardi. Furthermore, I wish to acknowledge all the professors for the very useful and complete classes.

Special thanks go to my classmates and friends at SISSA, among which Carlos has been my office mate for the longest period; they all made my days there very enjoyable. But I would like to remember also all the other friends met during these years in Trieste, in particular Serena, that has been always so close despite the current geographic distance between us.

I would like to sincerely acknowledge my family, in particular my mother Stefania and my father Sandro, that have always supported me, and my cousin Miriam, that is like a sister to me.

Finally, I wish to thank all my little gymnasts, all my coaching companions and my dance teacher Liuba, who have made my days in Trieste so pleasant and full of gratifications.